



MONASH University

Cyclic D/L Peptide Nanotubes

Mitchell Ramesh Silk

B.Pharm.Sci. (Hons)

A thesis submitted for the degree of Doctor of Philosophy at
Monash University in 2019
Department of Medicinal Chemistry

Copyright notice

© Mitchell R. Silk 2019.

I certify that I have made all reasonable efforts to secure copyright permissions for third-party content included in this thesis and have not knowingly added copyright content to my work without the owner's permission.

Table of contents

Abstract.....	iv
Declaration.....	v
Acknowledgements.....	vii
Chapter 1 – Introduction	1
1. Rational design of functional proteins.....	1
1.1. Directing self-assembly.....	2
2. Nanotubes	3
2.1. Carbon nanotubes	3
2.2. Inorganic nanotubes	5
2.3. Organic nanotubes	5
3. Cyclic D/L peptide nanotubes.....	7
3.1. Backbone <i>N</i> -methylation of CPs.....	9
3.2. Internal functionalisation	10
3.3. External functionalisation.....	12
3.4. CPNs as transmembrane channels	16
3.5. Covalent tethering.....	17
3.6. Techniques to study CPNs	19
3.7. Limitations of CPN structure and analysis	24
4. Hypothesis and aims	26
5. References	28
Chapter 2 – Using ionic interactions to direct the assembly of well-ordered cyclic D/L peptide nanotubes	39
Journal article	41
Appendix.....	45
Chapter 3 – Controlled construction of cyclic D/L peptide nanorods	53
Journal article	55
Appendix.....	61
Chapter 4 – Studies of cyclic D/L peptide nanotube stability.....	87
Manuscript	89
Appendix.....	101
Chapter 5 – Developing the structure, stability and function of tethered CP nanorods	103
Manuscript	105
Appendix.....	115
Chapter 6 – Conclusions	143

Abstract

Cyclic peptides composed of alternating D- and L- amino acids (CPs) self-assemble into nanotubes (CPNs) with great potential for applications in biomedicine as synthetic protein-like structures. The chemical and physical properties of CPNs are directly controlled by their amino acid composition, allowing for customisation of the CP to suit different situations. However, difficult structural characterisation and poor control over the self-assembly process limits the complexity of the structures that can be built from CPs, hindering their development into functional materials.

We explored methods to direct the self-assembly of CPNs involving the use of reversible and irreversible interactions, in order to develop heterogeneous CPN material of controlled composition. Reversible interactions such as charge-charge or hydrophobic interactions were studied in an effort to control the relative alignment of CPs and stabilise inter-CP interactions. Irreversible interactions by covalent tethering of the amino acid side-chains were applied to control the direct arrangement of CPs within heterogeneous CPNs and control their relative alignments to one-another.

Charge-charge interactions were initially found to induce the formation of highly-ordered CPN materials. CPNs formed bundles with one-another through a network of inter-side-chain ionic interactions. Crystalline material was grown from the ordered structures and studied by X-ray diffraction, yielding the first ever crystal structures of continuously H-bonded CPNs.

We developed novel CP tetramers by tethering CPs together through the amino acid side-chains. The coupling chemistry was orthogonal to acidic and basic side-chains, enabling the tethering of deprotected CP subunits. Fibrous structures were identified for some of the tetramers, revealing that tethering did not interfere with the self-assembly process. NMR spectroscopy was used to confirm the formation of highly-ordered material, although some instability was present in the structures.

We then investigated the interactions crucial to the stability of CPNs using combined experimental and theoretical analyses. Hydrophobic interactions were found to provide highly-stable CPN systems while charge-charge interactions could stabilise or destabilise a system depending on alignment of like or opposing charges. In addition, the various hydrogen bond networks generated through the different residue-alignments were significantly important to CPN stability.

To combine our tethering and stability studies, we synthesised and analysed a series of CP tetramers. The modular design of our CP tetramers allowed for different combinations of peptide subunits to be explored, resulting in the formation of a range of tetramers with distinctly different stabilities and behaviour. Experimental analysis revealed well-ordered analogues with stable hydrogen bond configurations identified by MD simulations.

Ultimately, we have developed substantial control over the order and arrangement of CPs within assembled CPN structures. Using specific combinations of amino acids, one can generate structures with their stability engineered to promote or destabilise specific hydrogen bond interfaces. Conjugation of bioactive compounds, fluorophores, chromophores and more to our tethered CPN structures could provide CPNs of diverse functionality with potential applications throughout biomedicine.

Thesis including published works declaration

I hereby declare that this thesis contains no material which has been accepted for the award of any other degree or diploma at any university or equivalent institution and that, to the best of my knowledge and belief, this thesis contains no material previously published or written by another person, except where due reference is made in the text of the thesis.

This thesis includes 2 original papers published in peer reviewed journals and 2 unpublished manuscripts. The core theme of the thesis is cyclic peptide nanotubes. The ideas, development and writing up of all the papers in the thesis were the principal responsibility of myself, the student, working within the Faculty of Pharmacy & Pharmaceutical Sciences under the supervision of David K. Chalmers and Philip E. Thompson.

In the case of *Chapters 2-5* my contribution to the work involved the following:

Thesis Chapter	Publication Title	Status	Nature and % of student contribution	Co-author name(s) Nature and % of Co-author's contribution	Co-author(s), Monash student
2	Parallel and antiparallel cyclic D/L peptide nanotubes	Published	70%, developing methodology, compound synthesis and analysis, crystallisation, analysing data, writing manuscript.	J. Newman (crystallisation, 5%), J. Ratcliffe & J. White (assistance with cryo-EM, 5%), T. Caradoc-Davies & J. Price (X-ray crystallography, 10%), S. Perrier, D. Chalmers & P. Thompson (experimental design, manuscript preparation, 10%)	No
3	Controlled construction of cyclic D/L peptide nanorods	Published	75%, developing methodology, compound synthesis and analysis, analysing data, writing manuscript.	B. Mohanty & M. Scanlon (NMR analysis 10%), J. Sampson (synthesis, 5%), D. Chalmers & P. Thompson (experimental design, manuscript preparation, 10%)	No
4	Studies of cyclic D/L peptide nanotube stability by crystallography, NMR and molecular dynamics	Not submitted	80%, developing methodology, compound synthesis and NMR analysis, crystallisation, X-ray crystallography, MD studies, analysing data, writing manuscript.	J. Price (X-ray crystallography 5%), B. Mohanty & M. Scanlon (NMR analysis 5%), D. Chalmers & P. Thompson (experimental design, manuscript preparation, 10%)	No

5	Developing the stability and function of modular nanorods built from tetramers of cyclic octapeptides	Not submitted	80%, developing methodology, compound synthesis and NMR analysis, MD studies, analysing data, writing manuscript.	B. Mohanty & M. Scanlon (NMR analysis 5%), J. Rho, S. Ellacott & S. Perrier (compound synthesis, analysing data 5%), D. Chalmers & P. Thompson (experimental design, manuscript preparation, 10%)	No
---	---	---------------	---	---	----

I have not renumbered sections of submitted or published papers in order to generate a consistent presentation within the thesis.

Student name: Mitchell Silk

Student signature:

Date: 09/11/2019

I hereby certify that the above declaration correctly reflects the nature and extent of the student's and co-authors' contributions to this work. In instances where I am not the responsible author I have consulted with the responsible author to agree on the respective contributions of the authors.

Main Supervisor name: David Chalmers

Main Supervisor signature:

Date: 09/11/2019

Acknowledgements

First and foremost I would like to thank my supervisors, David and Phil. David was regularly inventing fresh schemes for potential tube-based exploits, and I am grateful for all our discussions. Phil always seemed to know the answer to any and every peptide question I may have had. Both of you supported me from beginning to end in every aspect of the project and my time at Monash, and I am truly thankful.

Thanks to the wide range of researchers who have taught me along the way as we explored any and every avenue in our pursuit of the perfect tube. Particular thanks goes to Simon for his chemistry advice, instrument knowledge and general know-how of all that is lab-based. A special thanks to Jo who not only doubled the size of tube team, but taught me that literally everything in Australia is exciting if you are from Bristol.

For all discussions both productive and unproductive, I thank my desk-neighbours of the past (Trayder, Tamir, Matt, Estelle) and desk-neighbours of the present (Amanda, Sanju, Shane, Amali, Billy). All of you helped me maintain a degree of sanity throughout my time here, in your own way.

To my cohort from undergraduate studies through to the end of our PhDs, thanks for such a wonderful journey together. From MedChem; Cass, Hanson, Jisook and Matt, and from D4; Andrew, Chris, Dimmi and Tara.

Lastly, thanks to Leigh for seeing me through this journey and supporting me all the way.

This research was supported by a Research Training Program (RTP) scholarship from the Australian Government.

Chapter 1

Introduction

1. Rational design of functional proteins

Proteins designed and developed by Nature are among the most functionally-diverse biological macromolecules, performing an array of complex processes in efficient ways.¹ Proteins are increasingly being employed as therapeutic agents and can be tailored for the treatment of a range of diseases.^{2, 3} The rational design of proteins has emerged as an approach to customising or tuning protein structure and function, and has greatly improved our understanding of protein structure and stability.⁴ Further chemical and functional diversity can be achieved by exploring unnatural or pseudo-protein space.⁵ These protein-like structures have the potential to yield novel architectures and functions for unique applications in biomedicine that would be otherwise unattainable. This project will focus on cyclic peptide nanotubes, an exciting class of organic nanotube, using their structural diversity and biological compatibility to develop functional nanomaterials.

Synthetic proteins are often designed around known structural motifs of natural proteins such as α -helices and β -sheets. Novel structures can be developed by incorporating stable portions of an existing protein and modifying the non-essential residues to invoke novel or specific function.⁶ This approach can be extended to engineer specific quaternary structures from tertiary-structured synthetic proteins using polar and non-polar interactions. Computational tools such as HBNet from the Baker group have enabled the prediction of hydrogen bond (H-bond) networks in the design of *de novo* protein-oligomer structures (**Figure 1a**).⁷ However, non-ideal and non-canonical structural elements are considered critical in novel, stable, synthetic proteins and protein-like structures, but the process is often limited by the imagination of the designer. Better mimics of the natural evolutionary design process can be computationally modelled, such as the SEWING approach developed by Kuhlman and co-workers (**Figure 1b**).⁸ Full *de novo* protein channels have been developed through ground-up design and synthesis by the Woolfson group, utilising α -helix motifs to create coiled-coil proteins with tunable design and function (**Figure 1c**).⁹

Synthetic protein channels are of particular interest in the biomedical and bioengineering fields as they have the potential to transport potent therapeutic agents across membranes to hard-to-reach targets. However, due to the high complexity of naturally-developed proteins and channels, the stability of their tertiary or quaternary structures and specificity of their function are difficult features to replicate synthetically and complex to engineer biologically.

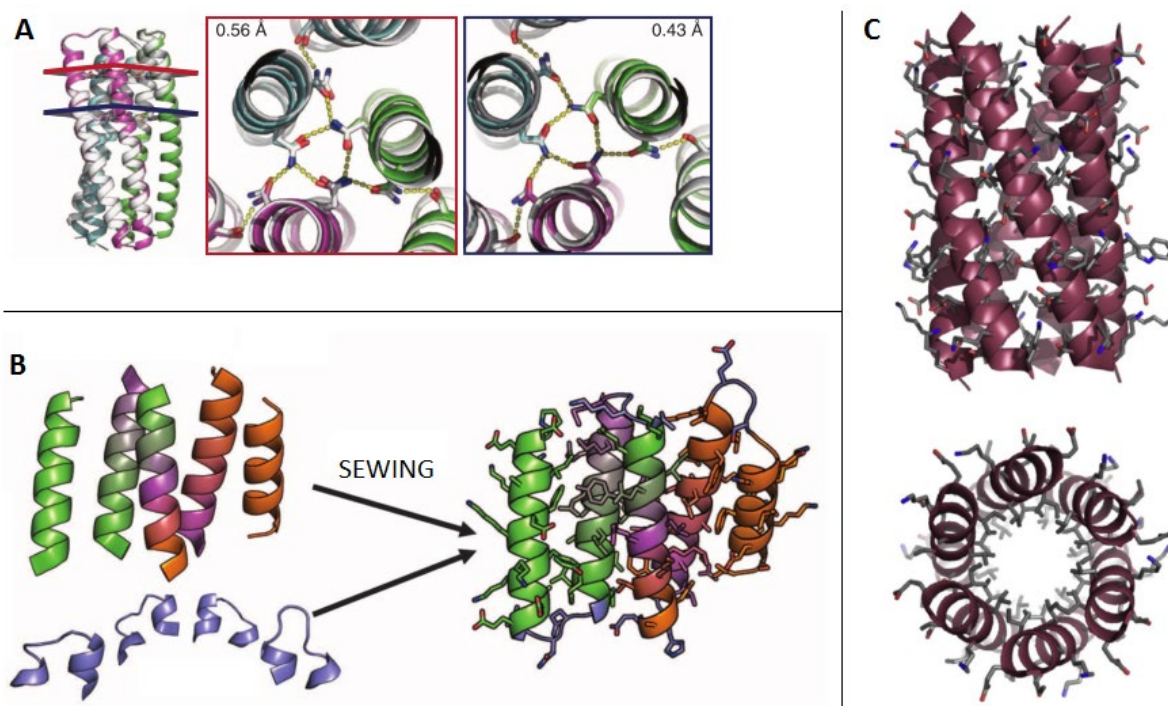


Figure 1. Synthetic protein design can be approached through a range of different methods which often take advantage of computational predictive techniques. A) HBNet from the Baker group is used to engineer a network of polar contacts to drive intermolecular assembly. B) The Kuhlman group use SEWING to combine stable tertiary structure components from natural proteins into novel synthetic structures. C) A *de novo* coiled-coil hexamer developed by the Woolfson group beginning with computational design and ratified through synthesis and x-ray crystallography. Figure adapted from ^{7, 8} and ⁹.

1.1. Directing self-assembly

Designing and developing synthetic proteins and pseudo-proteins requires methods to direct or modulate the self-assembly of smaller subunits into the desired functional structure. Reversible charge-charge interactions and covalent bonds are among some of the tools for organising molecular assembly.

Charge-charge interactions between amino acid side chains can be designed to direct the self-assembly process in specific ways. These interactions are commonly encountered in nature and studies of the biological trend show that these ionic side-chain interactions logically favour length-matching of paired charge interactions.¹⁰

Self-sorting covalent cages are an entirely synthetic example of directed self-assembly in action (**Figure 2**). Cages are derived from organic small-molecules which form reversible covalent bonds with one-another upon changes in temperature or solvent composition. Heterogeneous mixtures of the cage components will selectively self-organise to form a range of cage morphologies for molecular encapsulation and release.¹¹

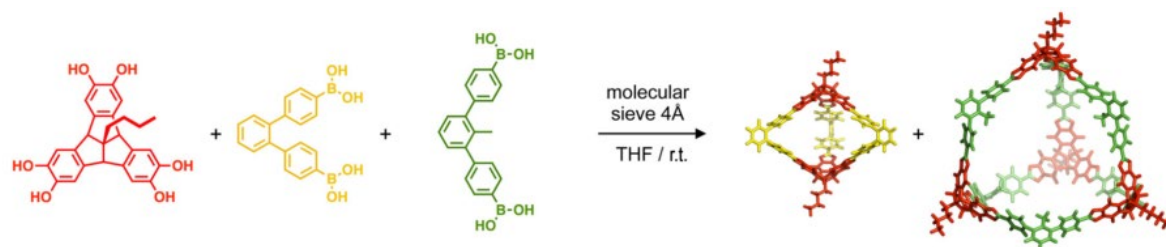


Figure 2. The organised, reversible self-assembly of cage-like nanostructures from organic small molecules. Figure adapted from ¹¹.

The oligomerisation process of self-assembling structures can be modelled computationally and further ratified with experimental data. A recent example involves *N6,N9*-Dimethyladenine molecules which undergo reversible stacking in solution to form stacked oligomers.¹² This study demonstrates that assembly processes and oligomerisation can be effectively modelled and the key interactions explained, facilitating regular improvements in our understanding of the mechanisms involved in biological self-assembly processes.

2. Nanotubes

Nanotubes are a form of molecular structure characterized by hollow rods, bearing applications in energy-transfer and molecular transport. They can be considered as three distinct classes; carbon, inorganic and organic, which vary in properties and potential applications. Carbon nanotubes possess properties such as high tensile strength and electrical conductivity, proving useful in electronics, energy storage and water filtration.^{13, 14} Metal oxides and sulfides form the components of inorganic nanotubes, which show similar properties to carbon nanotubes yet are not as strong under tensile stress.^{13, 15} However, they are stronger under compression making them viable for use in bullet proof vests and other impact-resistant applications.¹⁵ Organic nanotubes have a higher degree of biological compatibility than their carbon and inorganic counterparts due to their biodegradable composition and reversible binding interactions.¹⁶ In addition, organic nanotubes are highly tunable for internal selectivity and external functionality, encouraging a diverse range of biomedical and bioengineering applications.^{17, 18} With the right control and design, these structures could be developed into functional protein-like structures and biological macromolecules.

2.1. Carbon nanotubes

Carbon-based nanomaterials are among the most diverse classes of nanomaterial and are comprised of carbon allotropes that range from spherical fullerenes¹⁹ to multi-layered sheets of graphene.²⁰ These carbon-based structures can be further functionalised using carbon-carbon chemistry and addition of various moieties to their exterior.²¹

Among its numerous allotropes, carbon can be arranged into elongated, porous nanotubes. These carbon nanotubes (CNTs) are formed through covalent carbon-carbon bonds similar to those of graphene or fullerene and can exist with single¹⁴ or multiple walls¹³ layering a hollow core (**Figure 3**). The covalent-based assembly contributes to very high stability and a versatile array of properties from electrical and heat conductivity to compression and compact force resistance, making them ideal subjects for materials science and materials engineering.²² Their unique electronic and structural properties have also been exploited to develop energy-storage applications.²³

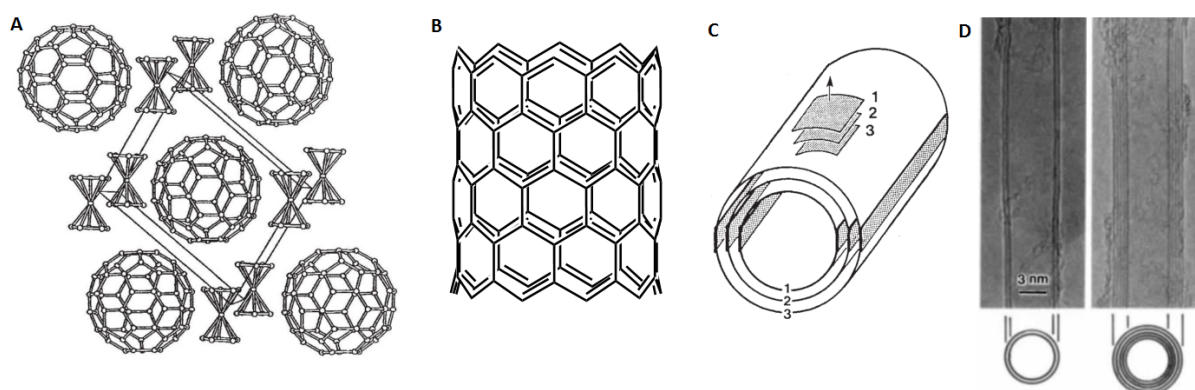


Figure 3. A) C_{60} fullerenes,²⁰ B) single-walled and C) multi-walled carbon nanotubes.¹³ D) EM images of MWCNTs depicting various numbers of wall layers.¹³ Figure adapted from ¹³ and ²⁰.

Toxicity concerns initially prevented CNTs from being explored in the biomedical setting. However, these concerns have been somewhat mitigated thanks to shielding and concealment of the structures by PEGylation of the CNT exterior^{24, 25} or dispersion with polyethyleneglycol (PEG) materials.^{26, 27} Conjugation of hexahistidine tags to the CNT exterior (**Figure 4**) has been shown to improve aqueous solubility and allow the formation of complex nanotube networks and structures through nickel complexes.²⁸ Functionalisation of the CNT interior is possible, but can detract from the stability of the overall structure as the conjugation of functional groups can interfere with the precise network of conjugated covalent bonds required in the CNT structure.

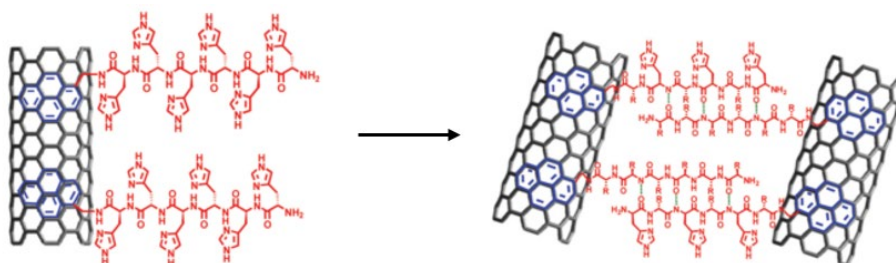


Figure 4. CNTs can be functionalised with peptides, polymers or other moieties to invoke function. Figure adapted from ²⁸.

2.2. Inorganic nanotubes

Coordination complexes between metal oxides,²⁹⁻³¹ metal sulfides³⁰⁻³⁷ and other non-metals^{30, 38} of particular atomic geometry can, under appropriate environmental and chemical conditions, self-assemble into inorganic nanotubes. Self-assembling nanotubes benefit from relatively simple synthetic approaches, particularly with regards to inorganic nanotubes. Inorganic nanotubes such as multi-layered WS₂ nanotubes (**Figure 5**) can encapsulate atoms and small molecules within their capillaries.³⁴ Inorganic nanotubes have demonstrated electron conductivity³⁷ and have been developed as hydrogen storage materials of completely inorganic composition³⁵ as well as from multi-layered organic-inorganic composite nanotubes.³⁸ The properties of inorganic nanotubes can be further modulated by combining them with organic material, such as polymers to reduce aggregation³² or small-molecules to induce hydrogelation.³¹ Self-assembly can even occur in the gas-phase,³⁰ highlighting the diversity and highly-coordinated process involved in the self-assembly of inorganic nanostructures. Inorganic nanotubes (such as those assembled from WS₂) can have relatively low cytotoxicity, indicating their potential application as biomedical devices or formulations.³⁶

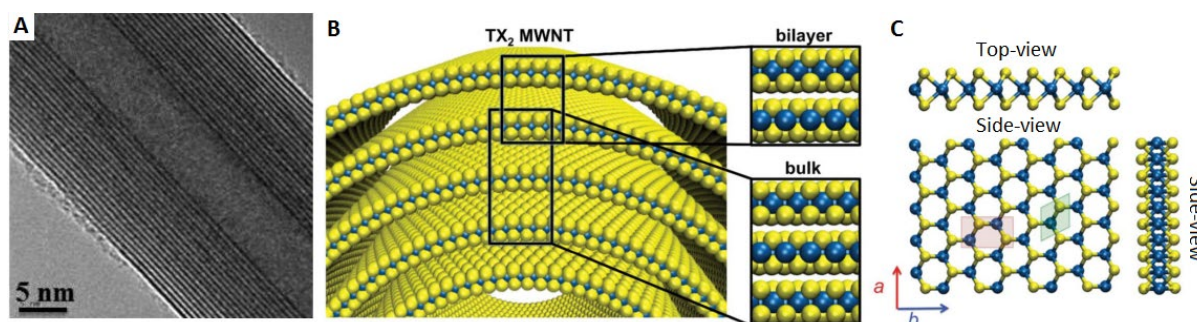


Figure 5. A) EM of a WS₂ inorganic nanotube with striations indicating the multiple-layered walls encasing a hollow channel.³⁶ B) Representation of a multi-walled inorganic nanotube of TX₂ composition, where T is a group IV transition metal and X is a chalcogen atom.³⁷ C) Crystal structure of WS₂ showing the atomic configuration where blue = tungsten, yellow = sulfur, red indicates the unit cell and green indicates the asymmetric unit of the crystal. Figure adapted from ³⁶ and ³⁷.

2.3. Organic nanotubes

Organic nanotubes have proven to be useful tools in the medical and pharmaceutical science fields and show the greatest promise for synthetic protein design. They can form synthetic membranes,³⁹ drug-delivery vehicles,³⁹ have been shown to embed into membranes,^{40, 41} act as synthetic transport channels for ions^{42, 43} and show promise as bio-optics and optoelectronics.^{44, 45} Organic nanotubes have been constructed from a range of different components, such as lipid-based or peptidic components.^{46, 47}

Organic lipid nanotubes occur in nature such as the membrane tethers formed by lipid bilayers,⁴⁸ but they have also been prepared synthetically from lipid-based subunits such as the nickel-based lipid subunit DOGS-NTA-Ni (**Figure 6a**) with a variety of applications.^{49, 50}

Soybean lecithin lipid nanotubes have been used to create an artificial model of the processes involved in neuronal exocytosis.⁵⁰ A stable form of the liposome-lipid nanotube was produced that provided structural and mechanical information regarding the exocytosis of lipid-based vesicles.⁵⁰ Lipid-metal complexes have been demonstrated to aid in the crystallisation of protein complexes. Existing as metal-stabilised organic nanotubes (**Figure 6b**), the structures were found to promote helical structures in proteins and encourage their crystallization.⁴⁹

Peptide-based nanotubes can self-assemble from a range of subunits, such as diphenylalanine or Phe-Trp.⁵¹ A study of diphenylalanine found it to be the structural motif of β -Amyloid that gives rise to its fibrous, tubular structure. Further studies on the diphenylalanine dipeptide produced crystal structures depicting the mechanisms involved in the assembly of these nanotube structures (**Figure 6c**).⁵² The nanotubes are the result of a combination of β -sheet H-bonding between peptide backbones and π -stacking between aromatic phenyl rings.⁵²⁻⁵⁴ Organic Phe-Phe nanotubes have been used to template the formation of inorganic, metal nanowires within the tubes. The reduction of silver triggered the formation of thin nanowires within the Phe-Phe tubes before enzymatic degradation of the peptide cast.⁵¹ The significant chemical and thermal stability of diphenylalanine peptide nanotubes suggests uses in microelectronics and microelectromechanical processes, serving as the subject of much research.⁵²⁻⁵⁴ Incorporation of the self-assembling Phe-Phe motif into larger peptides has produced novel self-assembling organic nanomaterials, such as AAKLVFF. This heptapeptide self-assembles into water-soluble nanotubes and triggers the formation of a nematic phase at high concentrations.⁵⁵

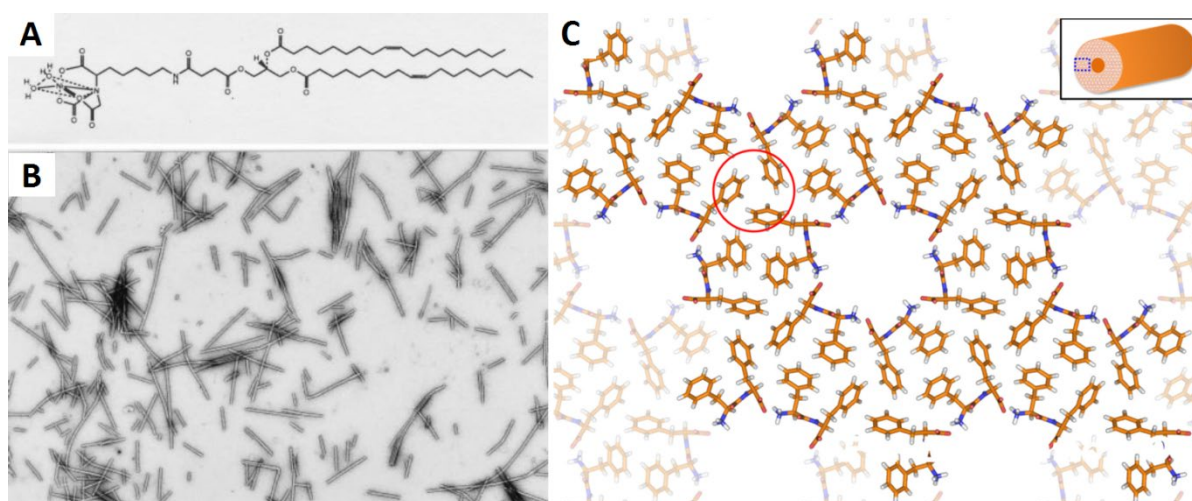


Figure 6. Images and diagrams of organic nanotubes, both lipid and peptide based. A) The chemical structure of a nickel-complexed lipid.⁴⁹ B) Organic nanotubes at x7,600 magnification that have self-assembled from the nickel-functionalised lipids of panel A.⁴⁹ C) Crystal structure of organic nanotubes formed from diphenylalanine. Red circle indicates aromatic interactions between phenyl rings. Figure adapted from ⁴⁹ and ⁵⁶.

Other organic building blocks can be driven into a variety of nanomaterials under the right conditions. 1,4-bis(1,2':6',1''-bis(3-butyl-1H-3,4,5-triazolyl)pyridin-4'-yl)benzene self-assembles into rhombus-shaped 2D nanosheets in organic solvent and can be driven into 1D nanotubes and 0D nanorings through variations in solvent composition and an ultrasound-assisted shape-shifting strategy (**Figure 7**).⁵⁷

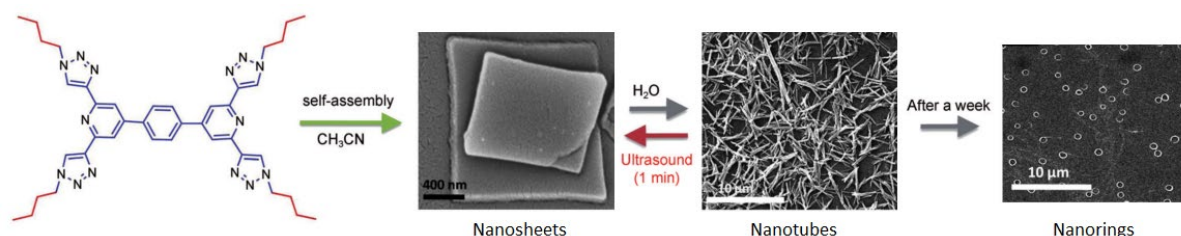


Figure 7. 1,4-bis(1,2':6',1''-bis(3-butyl-1H-3,4,5-triazolyl)pyridin-4'-yl)benzene self-assembles into 2D nanosheets in ACN and can be transformed between 1D nanotubes and 0D nanorings using different solvents and ultrasound assistance. Figure adapted from ⁵⁷.

3. Cyclic D/L peptide nanotubes

Cyclic peptide nanotubes (CPNs) are a class of organic nanotube comprised of self-assembling peptide rings with alternating D- and L- amino acids. CPNs are highly tunable, biologically compatible, porous structures that are promising candidates for developing novel, functional biomolecules, including synthetic proteins.

Cyclic D/L- α peptides (CPs) were first envisaged through computational studies of peptide conformations by Santis *et al* in 1973.⁵⁸ Whilst initially investigating linear α -peptides, Santis *et al* theorised that head-to-tail cyclic peptides with alternating D- and L- α -amino acid configurations would adopt planar conformations and form β -sheet-like H-bonding of the peptide backbones. Further studies into linear⁵⁹ and cyclic⁶⁰ D/L peptides by the Lorenzi group produced crystal-structure evidence of the flat conformation adopted by CPs but these lacked any inter-CP interactions.⁶¹ M. R. Ghadiri and coworkers in 1993 found that cyclic peptides with an even number of alternating D- and L- amino acids adopted a planar conformation (**Figure 8**) allowing the peptides to self-assemble into organic nanotubes by intermolecular H-bonding between the backbone amides.⁶² The original cyclic peptide that Ghadiri developed was *cyclo*[(L-Glu-D-Ala-L-Gln-D-Ala)₂], containing ionisable glutamic acid side chains. By using controlled acidification, the peptides were driven into nanotube self-assembly. The glutamic acid side-chains are ionised in alkaline solutions and are believed to repel one-another, disfavoured self-assembly and promoting dissolution. Upon acidification, the glutamate acid side-chains are protonated and unionised, forming favourable H-bonds with one-another and promoting the formation of rod-shaped crystals.⁶² Analysis of the crystals by transmission electron microscopy and electron diffraction revealed bundles of hundreds of nanotubes within each crystal, with a unit cell of dimensions $a = 4.73 \text{ \AA}$ and $b = c = 15.1 \text{ \AA}$. Although many

conformations are possible for a CP, the authors report only a single conformation to fit the unit cell; a flat, disk-like conformation where all side chains project outwards in the plane of the disk. The authors deduced that antiparallel β -sheet-like stacking of the CPs provided the most favourable H-bond interactions, although an antiparallel stacked structure would have axial-spacing of 9.5 Å rather than 4.73 Å. Further analysis by Fourier-transform infrared spectroscopy (FT-IR) supported the formation of an antiparallel β -sheet-like structure and the unit cell discrepancy was attributed to the low resolution of the electron diffraction data.

The self-assembly process of CPNs tolerates a broad variety of amino acids and is not hindered by sterically bulky or charged side-chains. In particular, Ghadiri *et al* investigated the effect of different sequence variants on nanotube structure and stability.⁶³ They studied *cyclo*[(L-Gln-D-Ala)₄], *cyclo*[(L-Gln-D-Leu)₄], *cyclo*[(L-Gln-D-Phe)₄] and *cyclo*[(L-Gln-D-Val)₄] and found that Ala, Leu, Phe and Val all produce cyclic peptide nanotubes of similar strength. *Cyclo*[(L-Gln-D-Val)₄] produced smaller, less-ordered fibres but the nanotubes displayed the same degree of stability.⁶³ Even minimally functionalised CPs of *cyclo*[(L-Ala-D-Ala)₄] assemble into nanotubes and bundles of nanotubes up to 10 μm in length.⁶⁴ Aromatic amino acids such as tryptophan and phenylalanine have been employed in some CP sequences as they can form favourable π - π stacking interactions, contributing to improved stability. Further control of the functional groups expressed on the exterior and even interior of cyclic peptide nanotubes greatly enhances their utility and diversity. This external and internal modification can offer greater control of hydrophilicity and charge state throughout the nanotube and be used to encourage or discourage membrane interaction, depending on the desired application.

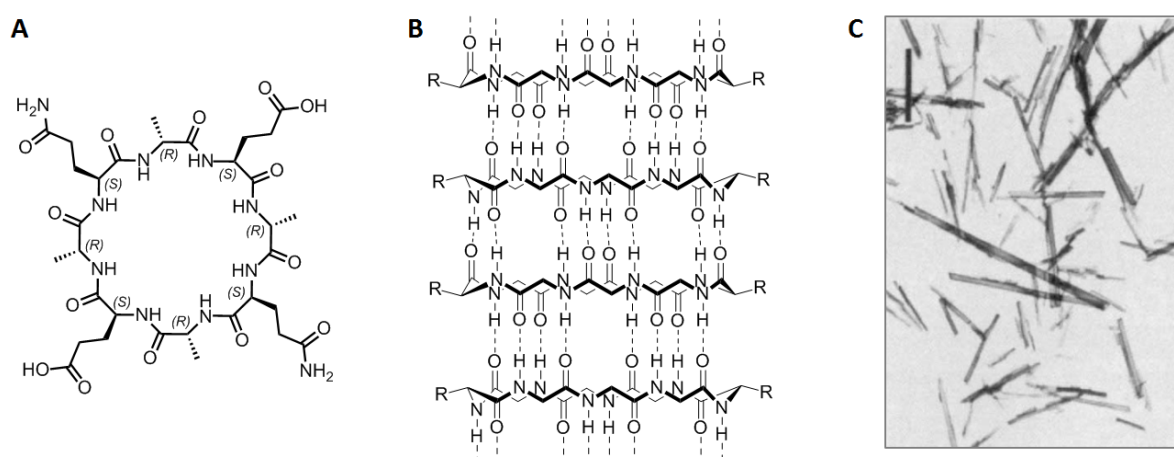


Figure 8. A) Structure of *cyclo*[(L-Glu-D-Ala-L-Gln-D-Ala)₂] and B) representation of the intermolecular interactions driving self-assembly into the nanotube, where dotted lines represent hydrogen bonds. C) Low-magnification electron microscopy image of nanotube suspension adsorbed on carbon support film (scale bar, 1 μm). EM adapted from ⁶².

3.1. Backbone *N*-methylation of CPs

Selective *N*-alkylation of the CP backbone restricts CPN-formation to blocked dimers, providing some modulation of the self-assembly process and a potential means of end-capping nanotubes.⁶⁵ *N*-methylation of an amino acid amide in a CP removes its ability to form H-bonds with the carbonyls of other CP backbones. By selectively removing the H-bonding capabilities from only one face of the cyclic peptide, the self-assembly process is restricted to the production of antiparallel CP dimers only. Backbone *N*-methylation has proven to be particularly useful for investigating nanotube structure and the self-assembly process.^{65, 66} Initially, the only successful X-ray crystallography studies of D/L cyclic peptides have been through the use of blocked *N*-methyl dimers.⁶⁵⁻⁷⁰ Non-*N*-methylated cyclic peptides are difficult to crystallise as they can self-assemble into polymorphic nanotubes of varying lengths, sizes and orientations, preventing the formation of well-ordered crystal lattices. The successful crystallography studies by Saviano *et al* of an *N*-methylated hexapeptide⁷⁰ and by Ghadiri *et al* of the *N*-methylated octapeptide *cyclo*[(L-Phe-D-*N*-MeAla)₄]⁶⁵ (**Figure 9**) provided extensive structural information. The structure of *cyclo*[(L-Phe-D-*N*-MeAla)₄] revealed π -stacking interactions between aromatic Phe side-chains in addition to the backbone H-bonding between cyclic peptides.⁶⁵

A CP with only L or only D-amino acid *N*-methylations can only form a backbone H-bonded CP dimer in the antiparallel configuration. By synthesising a CP and its mirror image (one with L-AA *N*-methylations and the other with D-AA *N*-methylations), the two CPs interact to form a parallel H-bonded dimer and allow the relative stabilities to be studied.⁷¹ Dimerisation association constants for *cyclo*[(NMe-L-Ala-D-Phe)₄] and its mirror image *cyclo*[(NMe-D-Ala-L-Phe)₄] were derived by ¹H NMR spectroscopy for the individual antiparallel H-bonded dimers and the parallel dimer obtained through combining the mirror images.⁷¹ The antiparallel configuration was found to be 4-fold more stable than the parallel H-bonded configuration, with little influence from the aromatic Phe side-chains but possible influence from the nature of the solvent. However, backbone *N*-methylation is widely used to induce turns in peptide secondary structure and similarly can cause twisting within CPs as an unwanted side-effect.⁷²

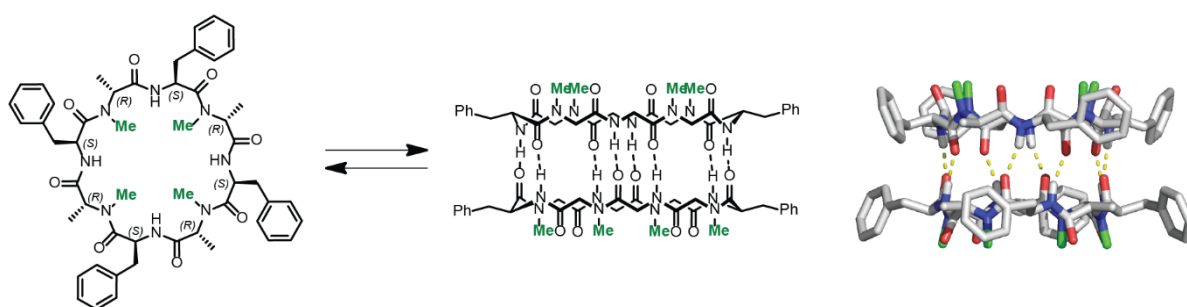


Figure 9. *N*-methylated CP; *cyclo*[(L-Phe-D-*N*-MeAla)₄], and crystal structure of the peptide dimer,⁶⁵ where dashed lines indicate H-bonding. Note the methyl groups (green) preventing further H-bonding on exterior faces of the CPs.

3.2. Internal functionalisation

Decoration of the nanotube interior with functional groups enables the design of interiors selective to molecules or ions of interest and aids the development of CPNs as synthetic transport channels. The internal dimensions of CPNs are directly controlled by the number of residues within the CP.^{73, 74} Functionalisation and modification of the interior cavity of CPNs is possible with the addition of carbocycles and heterocycles to the cyclic peptide backbone (**Figure 10**).^{75, 76} Such α,γ -CPs were initially developed with (1*R*,3*S*)-3-aminocyclohexanoic acid (γ -Ach) alternating with a D- α -amino acid in hexapeptide^{67, 77} and octapeptide^{69, 77} designs, but have also been derived entirely from paired γ -Ach enantiomers.⁷⁸ *N*-methylation of one face of the α,γ -CP backbone enabled crystallisation of CP dimers (**Figure 11**), revealing antiparallel H-bond assemblies similar to those of D/L- α -CPs with internal pore van der Waals diameters of approximately 5.4 and 7 Å for the hexapeptide and octapeptide respectively.^{67, 69, 77} Further exploration has resulted in the development of α,γ -CPs with 4, 6, 8, 10 and 12 α/γ amino acids with internal diameters of 1, 7, 10, 13 and 17 Å respectively, although α,γ -CPs with >10 amino acids appear more disordered due to increased backbone flexibility.⁷⁹ α,γ -CPs built with (1*R*,3*S*)-3-aminocyclopentanoic acid (γ -Acp) still enable functional group projection within the CPN pore, but additionally favour heterodimerisation with γ -Ach containing CPs rather than their respective homodimerisations.^{77, 80} However, the self-assembly process can be quite sensitive to α,γ -CP systems with CPs twisting into intramolecularly-folded H-bonded aggregates when not strictly alternating α - γ amino acids within the backbone⁷² or adding rigidity to the γ -Acp subunits.⁸¹

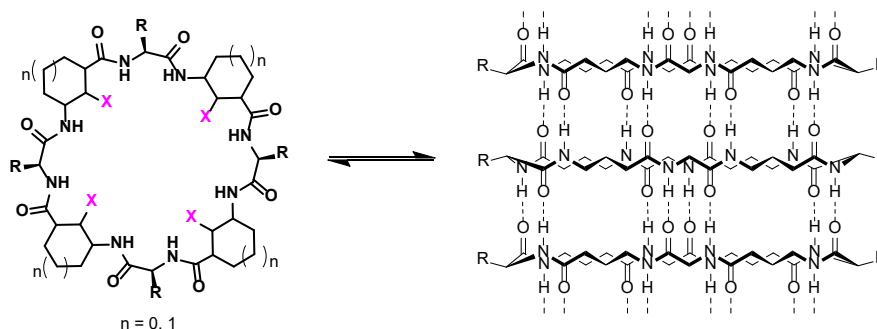


Figure 10. A cyclic peptide that contains 3-aminocyclopentanoic acid ($n = 0$) or 3-aminocyclohexanoic acid ($n = 1$) residues and the resulting nanotube. Rings in the peptide backbone enable the incorporation of functional groups on the interior of the nanotube pore, indicated by 'x'.

Molecular transport of specific targets by CPNs requires a pore diameter large enough to incorporate functional groups whilst still maintaining room for the guest molecules. A cyclic octapeptide with no interior modification has a pore size of ~ 7.6 Å which is large enough to house a variety of ions and small para-substituted aromatic compounds. However, a larger cavity is required when considering larger guest molecules or decorated CPN interiors. One

such α,γ -CP dimer system has been shown to bind platinum (II) within the internal pore of a decapeptide.⁸² The key features of the CP dimer include a carboxylic acid decorated on one of the γ -Ach residues projecting within the pore to act as the metal recognition site, backbone *N*-methylation to restrict dimer formation and external conjugation of a PEG polymer to aid solubility and cellular delivery of the complex. The α,γ -CP-Pt(II) complex was less active than cisplatin when tested against a range of cancer cell lines, but retained activity against cisplatin-resistant cancer and demonstrated no cytotoxicity against non-tumour cell lines.⁸²

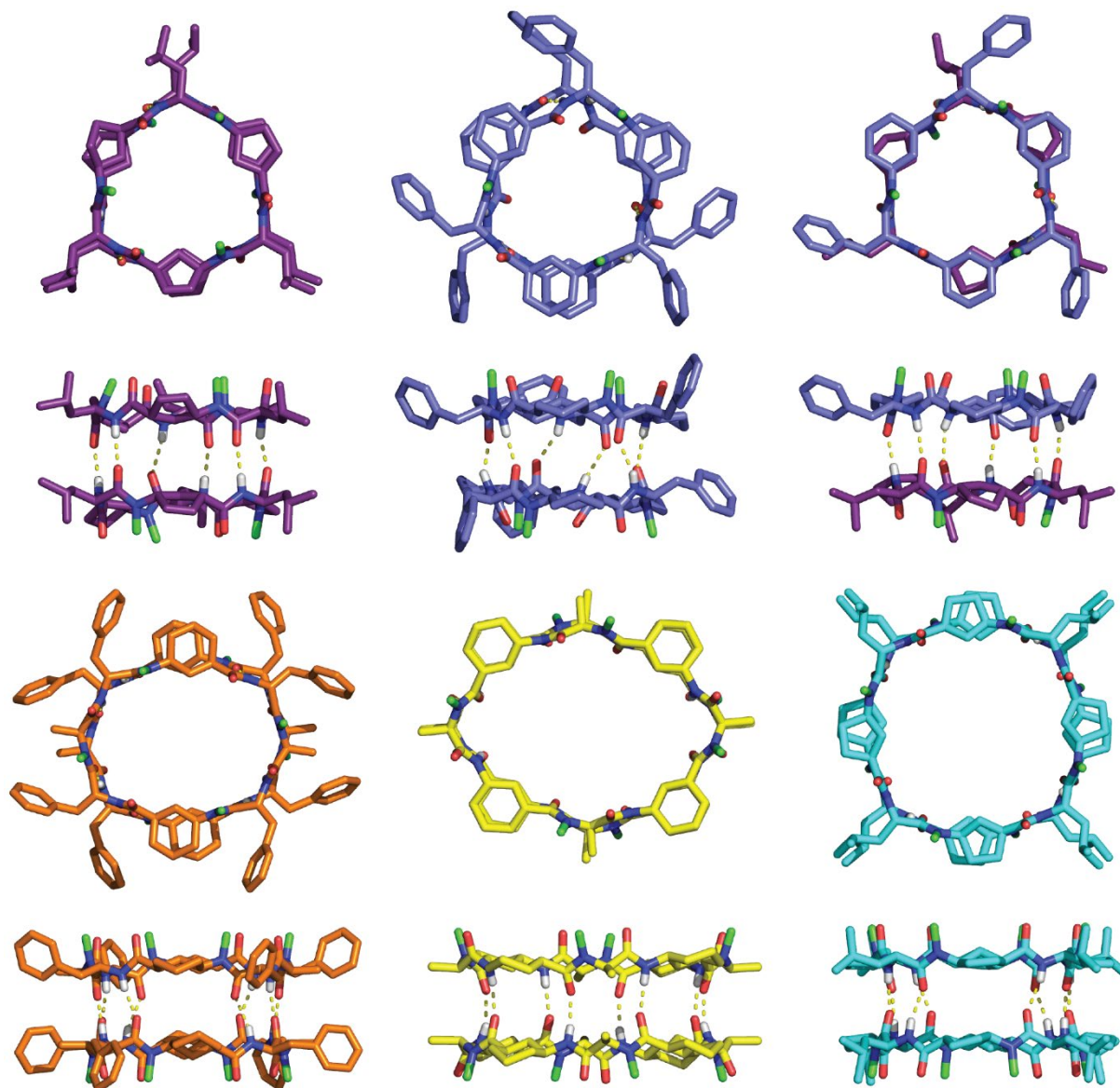


Figure 11. A selection of *N*-methylated α,γ -CP crystal structures (top and side views). Dashed lines represent H-bonding and green indicates methylation of the peptide backbone. Hexapeptide homodimers have been reported for γ -Acp-containing CPs (purple)⁷⁷ and γ -Ach-containing CPs (navy)⁶⁷ and heterodimer⁷⁷ between γ -Ach and γ -Acp-containing CPs. Octapeptide homodimers have been reported for CPs containing two γ -Ach residues (orange),⁷² four γ -Ach residues (yellow)⁶⁹ or four γ -Acp residues (aqua)⁷⁹ within the α,γ -CP backbone.

3.3. External functionalisation

The major contribution to the chemical and physical properties of CPNs are the amino acid side chains as they project outwards from the nanotube centre and effectively coat the surface area of the nanotube exterior.⁸³ The function of CPNs is therefore controlled through amino acid composition of the CPs themselves, which are not limited to natural amino acids alone and thereby increasing the accessibility to different external functional groups and potential properties or applications.⁸⁴

CPNs are electrically insulating and can conduct electrons^{85, 86} or protons,⁸⁶ making them suitable for applications in optics or electrochemistry. The coupling of amino acid side chains with moieties of high aromaticity to the exterior of cyclic peptide nanotubes (**Figure 11**) can further modulate and enhance charge-transfer properties.^{87, 88} Manipulation and control of this conductive property could provide organic nanotubes with applications in electronics.

Fluorescent tags can be conjugated to the exterior of CP nanotube systems in order to study the underlying mechanisms of the self-assembly process and the behaviour of CPNs with lipid bilayer systems (**Figure 12**).⁸⁹ Rho *et al* conjugated complementary FRET dyes to separate CPs and induced their respective self-assembly in water. Homogeneous CPNs were mixed with one-another and produced an instantaneous reduction in FRET signal, indicating close proximity between the acceptor and donor CPs and providing strong evidence to the highly-dynamic nature of CP systems. Similar reduction of FRET signal was observed whether the CPs were assembled or disassembled upon mixing. Dilution of either system would result in a rise in FRET signal as dilution induced the disassembly of the mixed CPN systems into their individual, fluorescent CP components. The dynamic self-assembly between distinct CPs was present even within a cellular environment, highlighting the robustness of the CPN systems and their applicability for biomedical applications.⁸⁹

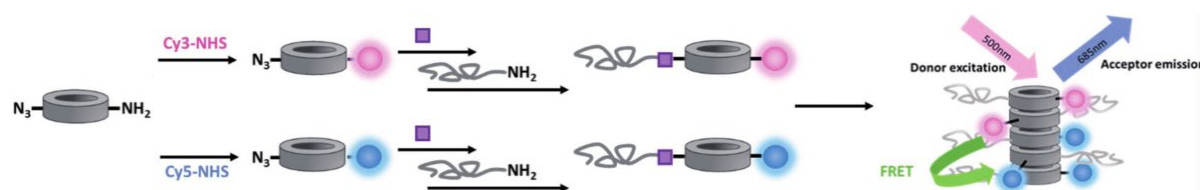


Figure 12. A schematic representation of the FRET occurring between different PEG-functionalised CPs containing Cy3 donor and Cy5 acceptor groups. Figure adapted from ⁸⁹.

3.3.1. Complex amino acids

A highly diverse selection of unnatural amino acids are readily obtainable both synthetically and commercially, allowing for substantial control over CPN surface chemistry. CPs with amino acid side chains bearing aromatic groups can form π -stacking interactions and encourage inter-CP alignment in the assembled nanotubes.^{87, 88} Charge-transfer properties

can be introduced to CPNs when CP subunits bear complex, conjugated ring systems such as 1,4,5,8-naphthalenetetracarboxylic acid diimide (NDI) as demonstrated by Horne *et al.*⁸⁷ Up to four NDI substituents were incorporated into cyclic D/L octapeptides via modification of Lys residues (**Figure 13**). Self-assembly into CPNs was triggered by the reversible reduction of the NDI side chains in an aqueous environment, providing an alternate method for modulating the assembly behaviour of CPNs.⁸⁸ A simpler charge-transfer CPN system has been achieved through a glutamic acid and lysine-containing pair of peptides, encouraging alignment of opposing charges and facilitating charge transfer as measured by electrodes.⁸⁵ Incorporating ionisable amino acid side-chains into CP structures can have additional benefits such as modulating aqueous solubility or pH-triggered self-assembly.⁹⁰

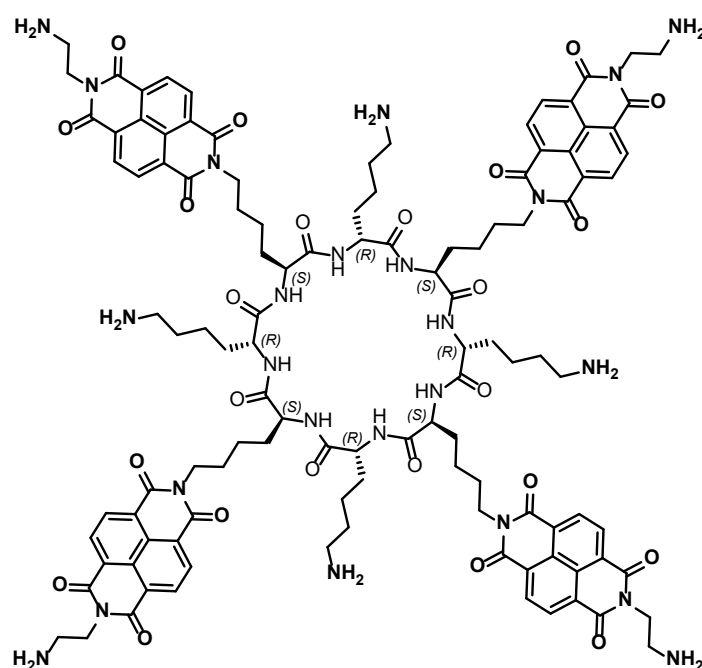


Figure 13. Cyclic peptide bearing NDI side-chains. Nanotubes arise through H-bonding and alignment of aromatic NDI side-chains, granting charge-transfer properties.⁸⁷

3.3.2. Polymer conjugation

The surface chemistry of CPNs can be modulated after peptide synthesis by conjugating polymers, biomolecules and labels to reactive handles of amino acid side-chains. This can be performed selectively in the presence of other amino acids such as Lys or Asp, using chemoselective conjugation reactions.

Conjugating polymers to the surface of a CPN core allows one to tune the properties of assembled CP nanotubes according to the nature of the polymer attached, including aggregation or solubility. Surrounding the CPN in a polymeric shell reduces both lateral and longitudinal aggregation (**Figure 14**), creating discrete nanotubes with lengths of 100-300 nm.^{90, 91} Additionally, the polymeric shell has been found to shield the CP backbone from

potential disruption of the H-bonding network critical to their self-assembly and improve their stability at low dilution in a range of solvents. Perrier *et al* demonstrated that hybrid CP-polymer nanotubes with high graft density could be synthesised with up to four conjugated polymers per cyclo-octapeptide. Alkyne-functionalised hydroxy ethyl acrylate (HEA) polymers were prepared by reversible addition fragmentation chain transfer (RAFT) polymerisation and grafted to azide-functionalised CP side-chains through copper-activated azide-alkyne cycloaddition (CuAAC) 'click' chemistry.⁹² Conjugation efficiency was highly dependent on the size of the polymer and the number of conjugation sites per CP, and as such only low molecular weight polymers could be grafted to all four sites of the CP simultaneously.^{92, 93} Notably, CP-polymer conjugates with high graft density were not inhibited from the self-assembly process of the peptide core. By using a standard CP scaffold and varying the polymer, a range of different CP-polymer materials can be developed rapidly through a combinatorial approach.⁹⁴ Reducing the number of polymer conjugation sites from four to two allows for more efficient grafting of larger molecular weight polymers in which nanotube length and function can be modulated by polymer size and type.⁹⁴

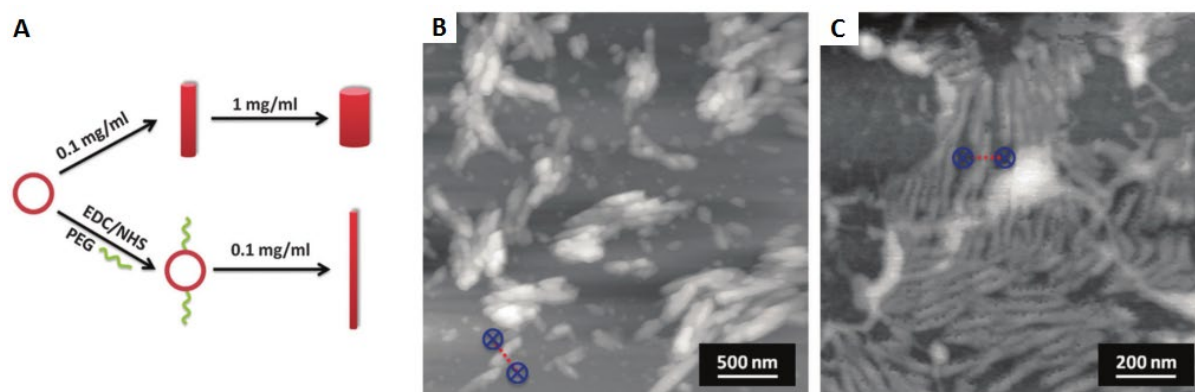


Figure 14. A) Outline of the effect of polymer-CP conjugation on nanotube aggregation, where PEGylation can significantly reduce aggregation of assembled nanotubes. B) AFM image of *cyclo*[(Gln-D-Ala-Glu-D-Ala)₂] nanotubes at 0.1 mg/mL with ~100 nm diameter. C) AFM image of PEG-conjugated *cyclo*[(Gln-D-Ala-Glu-D-Ala)₂] nanotubes at 0.1 mg/mL with ~20 nm diameter, demonstrating the reduction in lateral aggregation as a result of PEGylation. Figure adapted from ⁹⁰.

Multi-functional copolymers can be incorporated into the polymeric shell of hybrid CP-polymer systems to create nanotubes of greater complexity and diversity. Perrier *et al* developed multi-shell nanotubes comprised of a hydrophobic inner polymeric shell (polyisoprene) and a hydrophilic external polymeric shell (poly(acrylic acid)) surrounding the internal core of a CPN.⁹⁵ The poly(acrylic acid) shell could be maintained in a hydrophobic state with tert-butyl protecting groups or deprotected to expose the acrylic acid moieties as a hydrophilic shell, enabling tunable solubility. In the deprotected state, acrylic acid polymers introduce pH-responsive aqueous solubility to CP-polymer systems.⁹³ In addition, acrylic acid sites could be cross-linked between polymers by addition of toluene diisocyanate, effectively stabilising the

assembled nanotube to the effects of dilution or solvents that would normally trigger disassembly.⁹⁵

Distinctly different polymers can be coupled to the same CP to produce CP-polymer hybrids with dual functionality.⁹⁶ Perrier *et al* used orthogonal coupling strategies to allow the selective conjugation of distinct polymers to the same CP. An azide-functionalised amino acid was used to couple one polymer through CuAAC chemistry while another polymer was coupled to an alkene-functionalised amino acid via thiol-ene chemistry. The thiol-ene and CuAAC reactions are orthogonal to one-another and to most amino acid side-chains, allowing for selective conjugation of each polymer to the side-chain deprotected CP. Perrier *et al* conjugated non-miscible polymers (polystyrene; PS and poly(*n*-butyl acrylate); PBA) to opposite sides of the same CP in order to drive a microphase separation in DMSO and create CP-polymer nanotubes with distinct faces (a 'demixed' corona nanotube). This arrangement would then invert upon exposure to large unilamellar vesicles such that the hydrophobic polymers were exposed to the lipid bilayer (**Figure 15**). CPs were also grafted with chemically distinct but miscible polymers (PS and poly(cyclohexyl acrylate); PCHA) to study mixed corona CPN-polymer hybrids.⁹⁶

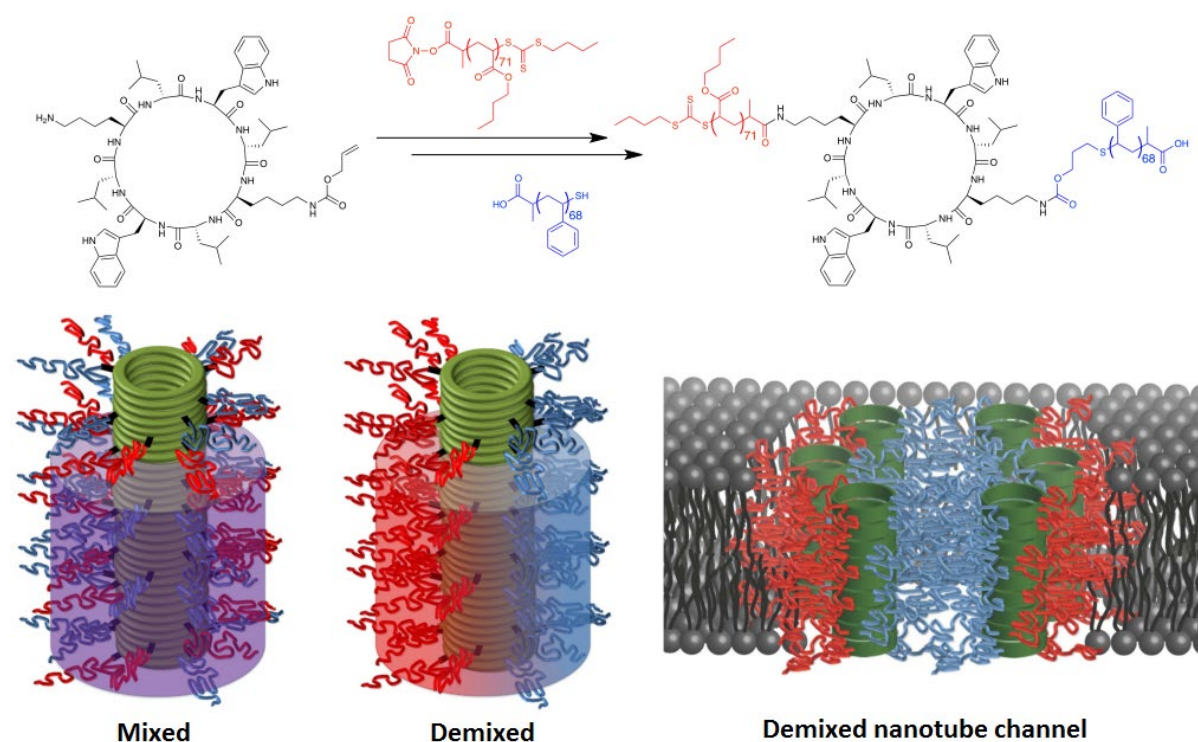


Figure 15. CPs conjugated with non-miscible polymers create polymer-CP nanotubes of a 'demixed' corona with the ability to form macropores within phospholipid bilayers. 'Mixed' corona nanotubes can be generated when miscible polymers are conjugated to the same CP. Figure adapted from ⁹⁶.

Polymerisation reactions can be performed directly onto a linear peptide both on resin^{97, 98} and in-solution,⁹⁹ where initiator sites can be incorporated onto amino acid side-chains or the N-

terminus of the peptide. By a similar principle, atom-transfer radical polymerisation (ATRP) can be performed directly onto the surface of self-assembled CPN systems rather than conjugating a previously synthesised polymer to the CP or CPN.¹⁰⁰⁻¹⁰² Biesalski *et al* modified the Lys side-chains of a resin-bound linear peptide to act as initiation sites for controlled free-radical polymerisation by ATRP. After synthesising the CP, self-assembly was induced and a polymerisation reaction of *N*-isopropylacrylamide (NIPAM) was performed directly onto the assembled CPNs (**Figure 16**). AFM analysis of the CP-PNIPAM conjugates revealed homogeneous coating of the CPN core by the polymeric shell and demonstrated the versatility of CPs in conjugation and exterior modification.¹⁰⁰ Controlling the polymerisation time allowed for precise control of the outer diameter of CP-PNIPAM nanotubes as the molar mass of the polymeric shell is directly modulated by polymerisation time. In addition, the molar mass of the grafted polymers directly influenced the length of CP-PNIPAM nanotubes including the disassembly of nanotubes at the longer polymerisation times.^{101, 103}

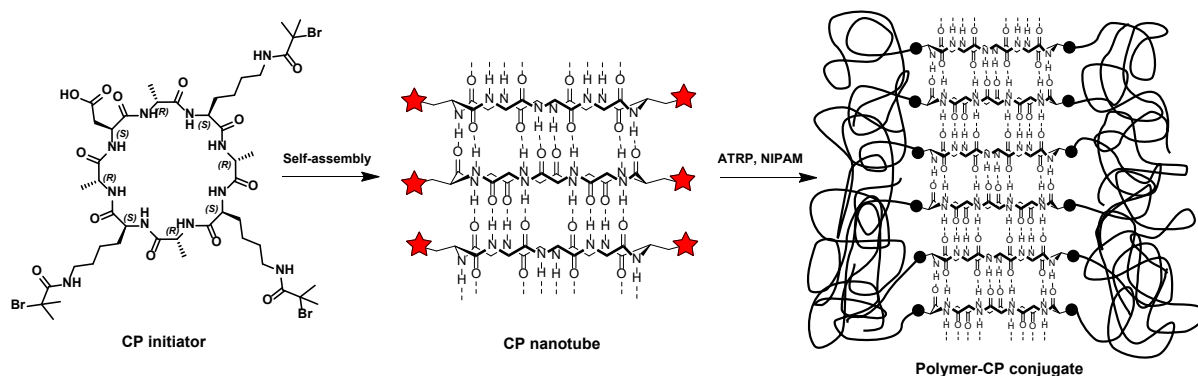


Figure 16. A CP with modified Lys side-chains to act as initiator sites for ATRP self-assembles into CPNs before polymerisation is performed directly on the nanotube, resulting in a polymer-coated CPN.¹⁰¹

3.4. CPNs as transmembrane channels

The porous, tubular nature of cyclic D/L peptide nanotubes makes them ideal candidates for synthetic ion channels and molecular transport vehicles.^{40, 42, 43, 74, 82, 104-110} The external properties of CPNs can be tuned to target specific regions or membranes of interest, while the internal properties of the channel can be customised using functionalised γ -Ach and γ -Acp residues.

Computational methods have been widely used to predict, measure and design the molecular and ion transport properties of a range of CPNs.^{40, 42, 43, 105-109} In particular, amphiphilic D/L cyclic octapeptides have demonstrated membrane interactions experimentally and have been shown to possess antiviral properties.⁴¹ Their ability to interact with and self-assemble in lipid membranes (**Figure 17**) causes an increase in the porosity of membranes, resulting in an increase in ion permeability. This causes a collapse of the transmembrane ion-potential ultimately resulting in cell death. Due to the differences in membrane physiology between

mammalian cells and viruses, the composition of cyclic peptides can be manipulated to be selective for non-mammalian cells. *Cyclo(wLwSeNsk)* is an amphiphilic cyclic D/L octapeptide with anti-hepatitis C virus activity that is selective for viral cells.⁴¹

Antibacterial CPs have been developed following a combinatorial approach to the synthesis of a library of D/L- α -cyclic octapeptides¹¹¹ and hexapeptides.¹¹² Despite high sensitivity of activity to minor sequence changes within the hexapeptides, the study identified both broad spectrum and highly selective biocidal hexapeptides which included those active against methicillin-resistant bacterial strains.¹¹²

Many of the biomedical applications of CPNs relies on the transport of ions or disruption of cell bilayer potentials rather than the transport of therapeutic agents. However, the transport of the antitumour drug 5-fluorouracil demonstrates that larger, medicinal compounds can potentially be delivered to specific targets and difficult-to-reach sites of action.¹⁰⁶

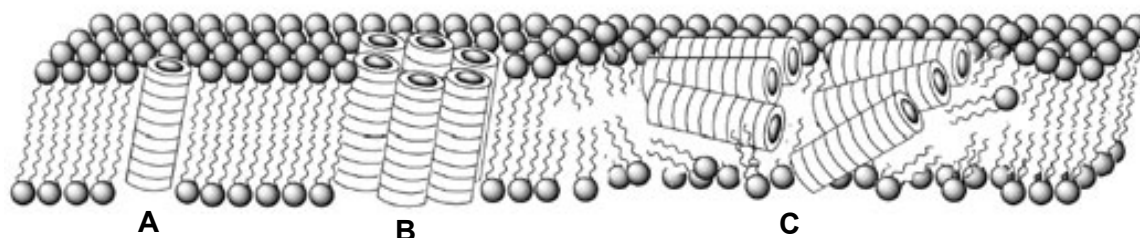


Figure 17. The different types of interactions that D/L cyclic peptide nanotubes can form with phospholipid membranes. A) Intramolecular pore; B) barrel stave; and C) carpet-like, where the nanotube orients hydrophilic side-chains to the surface of the membrane. Figure adapted from ¹¹¹.

3.5. Covalent tethering

Covalently-tethering CPs to one-another allows for potential control over the relative orientation and alignment of CPs within self-assembled CPNs. Attachment can be performed through the amino acid side chains¹¹³⁻¹¹⁸ or directly to the peptide backbone amides.^{110, 119} Initial approaches to CP tethering involved the alkene-metathesis of CP side chains and their subsequent reduction to generate CPs joined by two saturated hydrocarbon linkers (**Figure 18**).¹¹³ This tethered CP dimer demonstrated the 'covalent capture' of a singular H-bond configuration in an *N*-methyl-capped H-bonded CP dimer. Based on this design, Clark *et al* replaced the alkenes with thiols and performed intermolecular disulfide tethering of CPs to generate a reversibly-tethered CP dimer.¹¹⁴ Natural amino acids such as glutamic acid and lysine have also been used to create amide tethers between CP subunits and selectively generate CP heterodimers.¹¹⁷

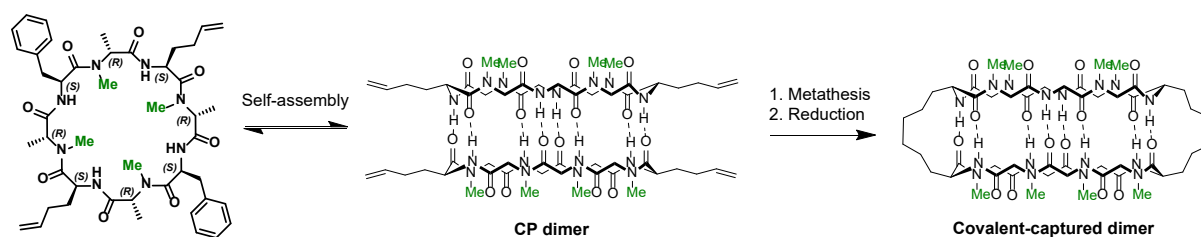


Figure 18. Metathesis of an alkene-functionalised CP will covalently trap a CP dimer in a particular configuration.¹¹⁴

A more complex approach to tethering is the use of an azobenzene linker between CP side-chains (**Figure 19**). The azobenzene moiety acts as a photo-switchable linker which converts between *trans* and *cis* configurations under UV irradiation, providing reversible modulation of the self-assembly process by encouraging and inhibiting CP alignment.^{115, 116} Longer tethers such as cross-linked polymers can also be conjugated to CP side-chains in order to covalently link CPs. Polymer tethering has been shown to modulate the length of the self-assembled conjugates to approximately 100 nm regardless of the mass of polymer attached.¹¹⁸

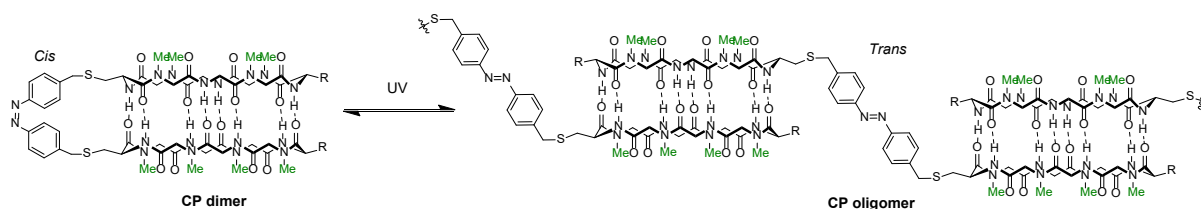


Figure 19. A photoswitchable azobenzene tether between CPs allows for reversible aggregation.¹¹⁵

Tethering can also be performed directly between the CP backbone amides, leaving the side-chains available for customising other CP properties. Encapsulation devices have been built from backbone tethered CP dimer units that undergo further dimerization to produce a 4-subunit structure (**Figure 20**). The structure was comprised of a γ -Acp-containing CP tethered to a zinc-binding ligand via the CP backbone amides using hydrazine-aldehyde click chemistry.¹¹⁰



Figure 20. Encapsulation device constructed from a γ -Acp-containing CP tethered to a zinc-binding moiety through the backbone amides. The covalently-tethered dimer undergoes further dimerisation through backbone-backbone H-bonding to form the encapsulation device. Figure adapted from ¹¹⁰.

CP self-assembly is highly dynamic and requires methods to direct and control the assembly,⁸⁹ such as covalent tethering within CPN-based systems to develop nanostructures.¹¹⁰ Multiple methods for directing the self-assembly process can be incorporated into a CPN structure to

create precisely designed systems. Covalent tethering and γ -Ach-Acp complimentary association have been combined to develop CPNs of moderately controlled length and composition (**Figure 21**). In these systems, CuAAC-tethered peptides and γ -Ach-Acp interactions drive the self-assembly of heterogeneous CP nanotube structures of 15-50 Å in length.¹¹⁹

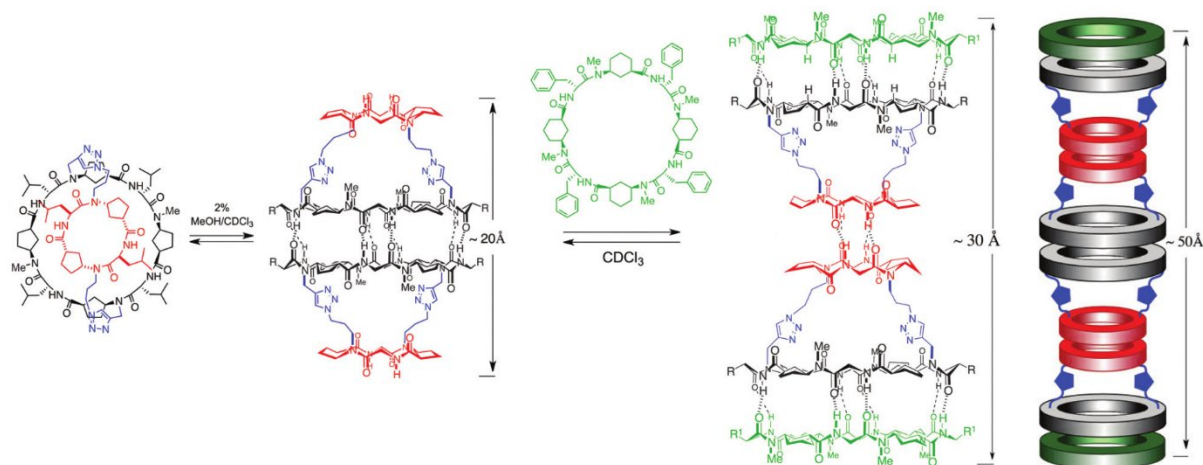


Figure 21. Schematic of the various sized oligomers produced from the reversible self-assembly of a heterogeneous CP mixture. The green CP contains backbone *N*-methylations to act as a capping peptide to terminate the CP assembly at shorter structures. Figure adapted from ¹¹⁹.

3.6. Techniques to study CPNs

The complexity of CPNs has required researchers to explore many different techniques to characterise CPN structure and function. Experimental analysis has been performed in the solid-state and in-solution, while theoretical computational analysis has been performed by energy calculations and molecular dynamics (MD) simulations. Each experimental or theoretical analytical technique has unique advantages, but no method alone can sufficiently characterise all features of CPNs and indeed a complementary combination of techniques is required in the study of CPNs.

3.6.1. Experimental methods for CPN analysis

CPNs have been studied in the solid-state by FT-IR spectroscopy, atomic force microscopy (AFM), electron microscopy (EM) and X-ray crystallography, or in-solution by light scattering (DLS and SLS), cryo-EM and NMR spectroscopy. Most of these techniques provide a more general overview of the size and morphology of CPN aggregates while crystallography and NMR spectroscopy can examine the finer details of CPN structure.

FT-IR, light scattering and microscopy have been used to analyse general structural features such as peptide secondary structure, aggregation and morphology. FT-IR has long been used to characterise secondary structure and conformation in proteins and peptides.¹²⁰ In their initial studies, Ghadiri *et al.* used FT-IR to identify the formation of β -sheet-like structures consistent

with the predicted stacking of CPs into H-bonded nanotubes.^{62, 63} FT-IR has been useful in characterising peptide secondary structure for complex materials such as polymer-conjugated CPNs.^{91, 92, 94, 100} Dynamic and static light scattering (DLS and SLS) have been used to estimate the sizes of CPN assemblies in-solution.^{91, 94} However, light scattering techniques only provide a broad overview of the average species in the sample. Microscopy techniques such as EM, AFM and SEM have been useful tools for characterising CPN morphology and providing evidence towards the formation of nanotubes.^{91, 92, 94} Although, due to inter-CPN aggregation, singular nanotubes have only been isolated and viewed by microscopy when conjugated to polymers.^{94, 100} Furthermore, limitations in current microscopy technology (although rapidly improving) have prevented imaging of individual CP subunits within larger assemblies.

X-ray crystallography provides structural information of peptides and proteins on the atomic level, although structures cannot be acquired without highly-ordered, crystalline material. Ordered, crystalline material suitable for X-ray diffraction studies are difficult to obtain for extended CPNs due to aggregation and the formation of amorphous (non-crystalline) assemblies. Backbone *N*-methylation has been used to generate crystal structures from D/L- α -CPs^{65, 70} and α,γ -CPs^{67, 69, 72} as these materials have less aggregation and disorder than non-*N*-methylated CPs, assisting the formation of crystalline material. The structures acquired from *N*-methylated dimers provide useful insight into the backbone H-bonding networks which can be related to extended CPNs.

NMR spectroscopy provides detailed information into the behaviour, structure and function of CPs in-solution. 1D ¹H NMR spectroscopy has been used to characterise the concentration-dependent assembly behaviour of CPNs^{66, 87} and association constants for CP-dimerization in different solvents,^{65, 87} although significantly-sized molecular assemblies are difficult to detect by NMR spectroscopy. Kobayashi *et al.* used 1D and 2D NMR spectroscopy studies of *N*-methylated CPs to further support the preference of CPN assembly for antiparallel H-bonding over parallel.⁷¹ CPs have been studied by 2D [¹H, ¹H]-NOESY spectroscopy to identify structural features such as the relative orientations of CPs within assembled structures^{82, 113} and function by confirming the internalisation of guest-molecules within CPN cavities.^{82, 110}

3.6.2. Theoretical analysis of CPNs

CPNs were first envisaged theoretically through predictions of the 3D structure created from the alternating D/L configuration. Since then, computational methods have been used prior to CPN synthesis to design and predict their structure and stability, or after synthesis to provide explanations and interpretations of experimentally acquired data. Both approaches benefit from relating the theoretical findings to experimental data and improve our understanding of

the mechanisms governing CP and CPN interactions, aiding in the development of functional CPN material. Molecular dynamics is particularly useful for studying CPNs due to the complexity of the interactions governing their stability. MD has been used to study CPN structure (such as CP composition and CPN size) and CPN function, particularly regarding the transport of molecules across membranes.

3.6.2.1. Molecular dynamics

Molecular dynamics simulations model the behaviour of atoms and molecules over time, granting insight into their behaviour on the atomic scale.¹²¹ MD simulations rely on force-fields to calculate the forces affecting each atom while additional computational algorithms determine other parameters of the system such as temperature and pressure. MD simulations of biological systems are built in aqueous conditions and allow for control over the pH by setting the protonation states, salt content, temperature and pressure. However, the behaviour of water is significantly complex despite its small size, and a range of models have been developed to better predict water behaviour in MD simulations.

During an MD simulation, the positions and velocities of atoms are updated according to the forces exerted and new atomic positions are recalculated by the MD software. This process is repeated many times to create multiple snapshots of the molecular behaviour on nanosecond to millisecond timescales,¹²² depending on the computational resources available.¹²³ Atomic positions are typically performed every 1 to 5 femtoseconds, where increasing the frequency of the calculations (timestep) can improve the accuracy of the simulation at the expense of resources (i.e. CPU time).

MD simulations are almost always used as a small-scale model of larger experimental environments as it is not computationally feasible to simulate a whole sample, even for a picolitre of solution. Algorithms are applied to control the temperature and pressure throughout the cell and periodic boundary conditions (PBC) are used to avoid any artefacts that would arise near to the boundaries of cell. These algorithms work in combination to ensure the MD simulation models the bulk solution as accurately as possible (**Figure 22**).

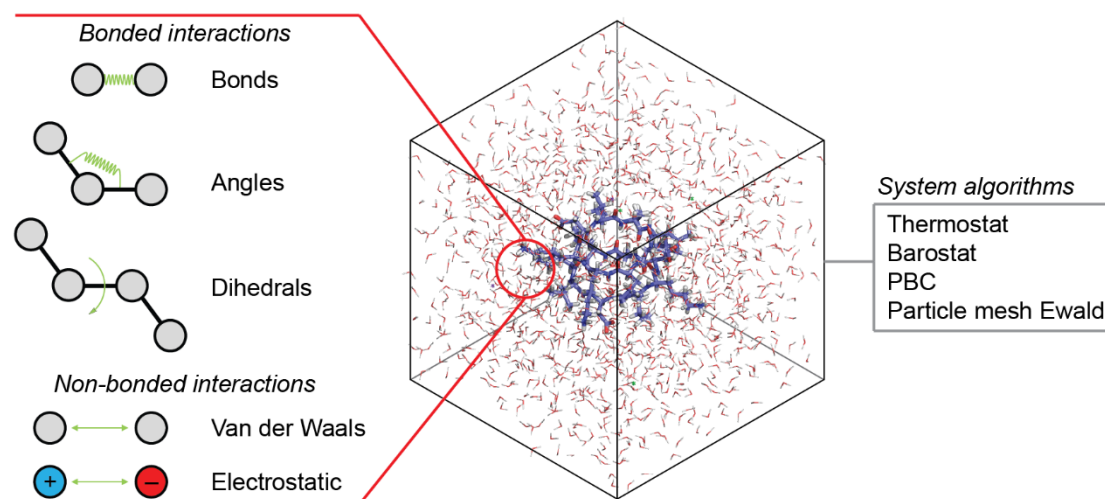


Figure 22. A typical system prepared for molecular dynamics simulation. The force-field describes the forces applied and exerted by atoms as bonded and non-bonded interactions. Additional algorithms control the system parameters, such as pressure (barostat), temperature (thermostat), periodic boundary conditions (PBC) and long-range electrostatic interactions using the particle mesh Ewald method.^{124, 125}

The critical component of an MD simulation is the force-field, which describes all the forces applied and exerted by atoms within the system (**Figure 22**) and governs the reliability of the predictions generated by MD and computational analysis. Force-fields are regularly being updated based on experimentally-determined properties for atoms and molecules in a system. In our group we have explored a range of different force-fields, although only the OPLS force-field^{126, 127} will be discussed in the work presented in later chapters. The OPLS force-field is a general force-field suitable for studying organic molecules such as peptides.¹²⁸ In the case of most force-fields, atomistic interactions are categorized by bonded or non-bonded interactions. As the terms suggest, bonded interactions refer to the angles and distances of covalent bonds while non-bonded interactions include electrostatic and van der Waals interactions. Bonded interactions are limited to the molecules of a particular system while non-bonded interactions extend not only throughout the cell but infinitely through the neighbouring cells of the system. Electrostatic interactions have long-range effects on the behaviour of a system and require a specific algorithm to determine their impact, which is most often determined by the particle mesh Ewald method.^{124, 125}

All of these computational calculations, algorithms, models and parameters are required in combination to manage the properties of MD systems and to ensure they accurately model real or experimental data.

3.6.2.2. CPN structure

Molecular dynamics has been used to study the structural features of CPNs, including internal CP diameter and overall length of CPNs.

The CP diameter is dictated by the number of residues within the CP backbone. Fewer residues increases the rigidity and stability of CPNs although it reduces the available space within the nanotube channel.^{74, 107} CPN stability is directly proportionate to CPN length, where more CPs within an assembled CPN grants greater overall stability.¹²⁹ Furthermore, CPs within the core of a nanotube are significantly more stable than those at the nanotube termini.⁸³ The terminal CPs have significantly more surface-area exposed to the solvent than core-CPs which can interfere with their conformation and disrupt the interactions between CPs and the CPN. However, CPs within the nanotube core are packed between other CPs which encourages their planar, H-bonded conformations and promotes the stability of the CPN core.

3.6.2.3. CPN function

Detailed molecular models of CPN systems act as *in silico* filters to ensure the CPN designed is the most suitable for the purpose, prior to synthesis and experimental analysis. This is particularly useful when engineering CPN function, such as molecular transport across membranes (**Figure 23**). CPN-mediated transport of a number of different ions, water and small-molecule compounds across membranes has been studied by MD.

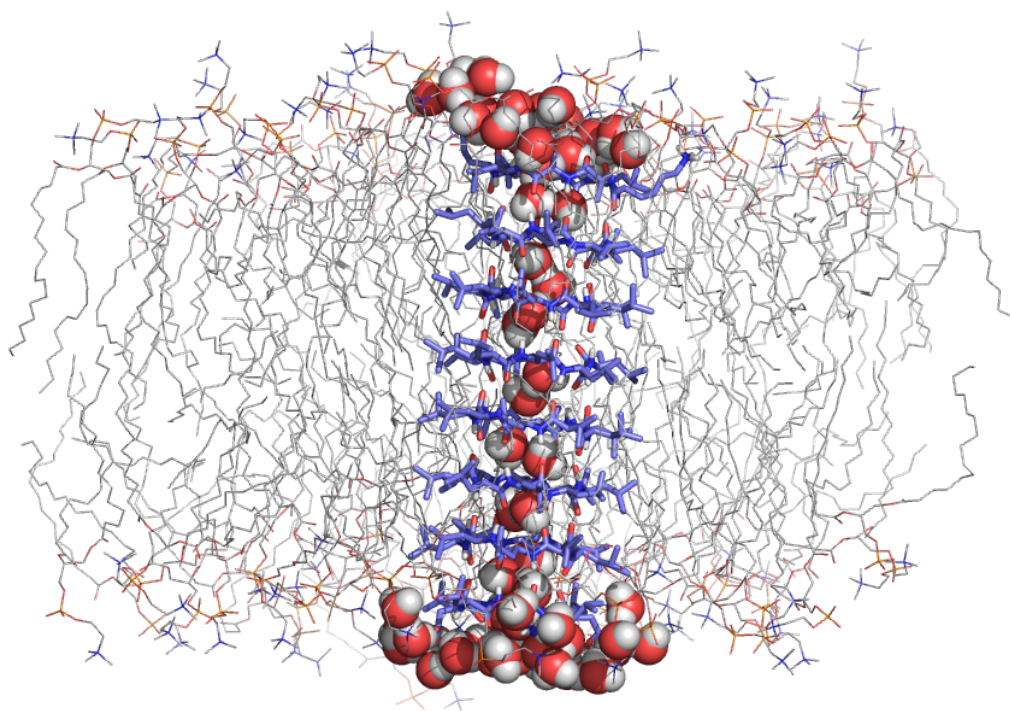


Figure 23. A system prepared for simulation by MD containing a CPN (blue) embedded in a membrane (grey) with internalised waters shown (red) and other waters hidden. CPN interactions with membranes can be studied by MD, including the transport of water, ions and organic compounds.

CPNs as transmembrane channels can aid in the delivery of drug-like molecules to their cellular targets. This is particularly useful for compounds that have difficulty reaching their targets, as Liu *et al* have demonstrated with the transport of the antitumour drug 5-fluorouracil (5-FU).¹⁰⁶ Liu *et al* combined theoretical MD analysis with experimental studies of liposomes

to demonstrate the efficient transport of 5-FU across lipid bilayers. The diffusion of 5-FU involved alternating polar and non-polar interactions as it travelled the length of the nanotube, a feature that could only be identified through MD analysis.

The diffusion of water through CPN channels follows a similar phenomenon as a result of the antiparallel nature of the CPN. Several groups have shown that CPNs of different internal diameters accommodate different quantities of water which in turn affects the interactions between waters or with the CPN interior.¹⁰⁷ In smaller CPN channels (6-8 AA CPs), most waters alternate between interactions with each-other and to the polar atoms of the CPN backbone.¹⁰⁷ However, the antiparallel stacking of CPs creates alternating interfaces of subtly different properties which restrict the passive diffusion of water through the CPN channel.⁷⁴¹⁰⁵ In most cases, a driving force is required for water to diffuse through a CPN channel.

3.7. Limitations of CPN structure and analysis

Despite the customisable, highly versatile and widely-applicable nature of CPs they are not without their flaws. With increasing complexity in nanomaterial composition and design comes greater difficulties in controlling the structure and properties of the final material. The major complications for CPs hindering their development into functional biomedical tools are a lack of control over the self-assembly process and difficulties in precise structural characterisation.

3.7.1. Uncontrolled self-assembly

The self-assembly process for CPs into CPNs is spontaneous and highly dynamic, which makes production of nanotubes quite straight-forward but lacks efficient means for directing or controlling the precise mechanisms involved in self-assembly. The vast majority of studied and reported CPNs are of a homogeneous CP composition and only a limited number of examples exist for heterogeneous and more complex CPN systems. In addition, there has been little success in controlling CPN length beyond *N*-methylated dimers or < 100 nm fibres. However, terminal CPs are the least stable within a CPN and this phenomenon is exacerbated in shorter CPNs of only a few subunits.¹²⁹ In order to restrict assembly to shorter nanotubes of 4 to 8 CP subunits, the stability of these smaller constructs would also need to be addressed. These factors combined significantly limit the potential nanostructures that can be achieved from CP subunits.

3.7.2. Difficult characterisation of CP-CP interactions

Characterising CPN structures is mostly achieved by analysing the general structure of the aggregates and nanostructure assemblies. Due to multiple conformational states or the size of the aggregates it is often difficult to determine the precise structural features within CPNs and the key interactions involved in their assembly and stability. *N*-methylation of the CP

backbone has yielded numerous crystal structures of CP dimers as a result of removing their potential for assembly, and has provided insight into the backbone H-bond network. However, prior to this work, X-ray crystallography or cryo-EM studies of continuously H-bonded CPNs had been unsuccessful and had not yielded any structures.

4. Hypotheses and Aims

4.1. Hypotheses

Cyclic peptide nanotubes show great promise for the development of novel, synthetic protein-like structures and bionanomaterials. The self-assembly of cyclic D/L peptides into nanotubes has advantages from being spontaneous and reversible, but there is much room for improvements in CP analysis, structure and function. To date, there are few reported methods that effectively manage and direct the assembly process and the complexity of CPN systems makes characterisation of CP interactions substantially difficult. These factors in combination are hindering the development of CPs into functional materials. We propose that the use of ionic interactions and covalent links between peptide subunits could allow for the order and arrangement of peptides within subsequent nanotubes to be guided and a level of control to be introduced to CPN assembly. We hypothesise that the use of amino acid side-chain interactions between cyclic D/L peptides and covalent links between peptide monomers could allow for the development of novel, discrete, protein-like structures and other functional bionanomaterials. Charged amino acid side-chains could be used to direct the packing arrangements of nanotube bundles to form ionically-coordinated crystal lattices. The use of covalent links between cyclic peptide monomers could allow for controlled self-assembly and direct the formation of discrete, modular nanorods with protein-like properties and behaviour.

4.2. Aims

The overall aims of this thesis are to understand the factors that govern CPN stability and assembly and to develop novel nanotube architectures. Furthermore, this work aims to demonstrate the controlled assembly of CP-based nanomaterials and to develop CP-nanorods of controlled composition. These aims will be achieved through a number of sub-aims:

- To design and synthesise a range of charged cyclic D/L peptides by solid-phase peptide synthesis techniques.
- To use cyclic D/L peptides with charged amino acid side-chains in the production of ionically-coordinated nanotube crystal lattices to investigate their ability to direct the packing arrangements of nanotube bundles.
- To use molecular dynamics to study the different factors contributing to CPN stability.
- To design and synthesise protein-like nanorods by covalently linking peptide monomers through disulfide and triazole bonds.
- To characterize secondary structure of the nanorods through a range of analytical methods (DLS, NMR spectroscopy, X-ray crystallography).

- To study the structure-stability relationship for synthesised nanorods experimentally and computationally through molecular dynamics.

Ultimately, the purpose of this PhD project is to explore methods for controlling the self-assembly process of cyclic peptide nanotubes in order to produce more complex CPNs of controlled composition and specialised biological function.

5. References

1. Black, D. L. Protein Diversity from Alternative Splicing: A Challenge for Bioinformatics and Post-Genome Biology. *Cell* **2000**, 103, 367-370.
2. Leader, B.; Baca, Q. J.; Golan, D. E. Protein therapeutics: a summary and pharmacological classification. *Nat. Rev. Drug Discov.* **2008**, 7, 21.
3. Dimitrov, D. S. Therapeutic proteins. *Methods in Molecular Biology* **2012**, 899, 1-26.
4. Wilson, C. J. Rational protein design: developing next-generation biological therapeutics and nanobiotechnological tools. *WIREs Nanomed. Nanobiotechnol.* **2015**, 7, 330-341.
5. Kent, S. Novel forms of chemical protein diversity — in nature and in the laboratory. *Current Opinion in Biotechnology* **2004**, 15, 607-614.
6. Kohler, V. Protein Design: Methods and Applications. *Methods in Molecular Biology* **2014**.
7. Boyken, S. E.; Chen, Z.; Groves, B.; Langan, R. A.; Oberdorfer, G.; Ford, A.; Gilmore, J. M.; Xu, C.; DiMaio, F.; Pereira, J. H.; Sankaran, B.; Seelig, G.; Zwart, P. H.; Baker, D. De novo design of protein homo-oligomers with modular hydrogen-bond network-mediated specificity. *Science* **2016**, 352, 680-687.
8. Jacobs, T. M.; Williams, B.; Williams, T.; Xu, X.; Eletsky, A.; Federizon, J. F.; Szyperki, T.; Kuhlman, B. Design of structurally distinct proteins using strategies inspired by evolution. *Science* **2016**, 352, 687-690.
9. Woolfson, D. N.; Bartlett, G. J.; Burton, A. J.; Heal, J. W.; Niitsu, A.; Thomson, A. R.; Wood, C. W. De novo protein design: how do we expand into the universe of possible protein structures? *Curr. Opin. Struct. Biol.* **2015**, 33, 16-26.
10. Kuo, H. T.; Fang, C. J.; Tsai, H. Y.; Yang, M. F.; Chang, H. C.; Liu, S. L.; Kuo, L. H.; Wang, W. R.; Yang, P. A.; Huang, S. J.; Huang, S. L.; Cheng, R. P. Effect of charged amino acid side chain length on lateral cross-strand interactions between carboxylate-containing residues and lysine analogues in a beta-hairpin. *Biochemistry* **2013**, 52, 9212-22.
11. Beuerle, F.; Klotzbach, S.; Dhara, A. Let's Sort It Out: Self-Sorting of Covalent Organic Cage Compounds. *Synlett* **2016**, 27, 1133-1138.
12. Zeller, F.; Zacharias, M. Thermodynamics and Kinetics of Nucleobase Stacking Oligomerization Revealed by Molecular Dynamics Simulations. *J. Chem. Theory Comput.* **2017**.
13. Iijima, S. Helical Microtubules of Graphitic Carbon. *Nature* **1991**, 354, 56-58.
14. Seraphin, S.; Zhou, D. Single-walled carbon nanotubes produced at high yield by mixed catalysts. *Applied Physics Letters* **1994**, 64, 2087-2089.

15. Chhowalla, M.; Amaratunga, G. A. J. Thin films of fullerene-like MoS₂ nanoparticles with ultra-low friction and wear. *Nature* **2000**, 407, 164-167.
16. Martin, C. R.; Kohli, P. The emerging field of nanotube biotechnology. *Nat. Rev. Drug Discov.* **2003**, 2, 29-37.
17. Hamley, I. W. Peptide nanotubes. *Angew. Chem. Int. Ed.* **2014**, 53, 6866-81.
18. Shimizu, T.; Minamikawa, H.; Kogiso, M.; Aoyagi, M.; Kameta, N.; Ding, W.; Masuda, M. Self-organized nanotube materials and their application in bioengineering. *Polymer Journal* **2014**, 46, 831-858.
19. Kroto, H. W.; Heath, J. R.; O'Brien, S. C.; Curl, R. F.; Smalley, R. E. C60: Buckminsterfullerene. *Nature* **1985**, 318, 162-163.
20. Taylor, R.; Walton, D. R. M. The chemistry of fullerenes. *Nature* **1993**, 363, 685-693.
21. Hirsch, A. The Chemistry of the Fullerenes: An Overview. *Angew. Chem. Int. Ed.* **1993**, 32, 1138-1141.
22. Rao, C. N. R.; Satishkumar, B. C.; Govindaraj, A.; Nath, M. Nanotubes. *ChemPhysChem* **2001**, 2, 78-105.
23. Tang, B.; Wang, Y.; Qiu, M.; Zhang, S. A full-band sunlight-driven carbon nanotube/PEG/SiO₂ composites for solar energy storage. *Solar Energy Materials and Solar Cells* **2014**, 123, 7-12.
24. Bhirde, A. A.; Patel, S.; Sousa, A. A.; Patel, V.; Molinolo, A. A.; Ji, Y.; Leapman, R. D.; Gutkind, J. S.; Rusling, J. F. Distribution and clearance of PEG-single-walled carbon nanotube cancer drug delivery vehicles in mice. *Nanomedicine* **2010**, 5, 1535-1546.
25. Han, B.; Zhang, M.; Tang, T.; Zheng, Q.; Wang, K.; Li, L.; Chen, W. The Long-Term Fate and Toxicity of PEG-Modified Single-Walled Carbon Nanotube Isoliquiritigenin Delivery Vehicles in Rats. *Journal of Nanomaterials* **2014**, 2014, 1-8.
26. Wang, S.; Liu, Y.; Huang, S.; Wu, H.; Li, Y.; Tian, Z.; Jiang, Z. Pebax-PEG-MWCNT hybrid membranes with enhanced CO₂ capture properties. *Journal of Membrane Science* **2014**, 460, 62-70.
27. Di Meo, E. M.; Di Crescenzo, A.; Velluto, D.; O'Neil, C. P.; Demurtas, D.; Hubbell, J. A.; Fontana, A. Assessing the Role of Poly(ethylene glycol-bl-propylene sulfide) (PEG-PPS) Block Copolymers in the Preparation of Carbon Nanotube Biocompatible Dispersions. *Macromolecules* **2010**, 43, 3429-3437.
28. Baati, R.; Ihiawakrim, D.; Mafouana, R. R.; Ersen, O.; Dietlin, C.; Duportail, G. Hexahistidine-Tagged Single-Walled Carbon Nanotubes (His₆-tagSWNTs): A Multifunctional Hard Template for Hierarchical Directed Self-Assembly and Nanocomposite Construction. *Adv. Funct. Mat.* **2012**, 22, 4009-4015.

29. Chen, T.; Qiu, L.; Kia, H. G.; Yang, Z.; Peng, H. Designing aligned inorganic nanotubes at the electrode interface: towards highly efficient photovoltaic wires. *Adv. Mater.* **2012**, *24*, 4623-8.
30. Deepak, F.; Tenne, R. Gas-phase synthesis of inorganic fullerene-like structures and inorganic nanotubes. *Open Chemistry* **2008**, *6*.
31. Qiao, Y.; Lin, Y.; Zhang, S.; Huang, J. Lanthanide-containing photoluminescent materials: from hybrid hydrogel to inorganic nanotubes. *Chemistry* **2011**, *17*, 5180-7.
32. Naffakh, M.; Remškar, M.; Marco, C.; Gómez-Fatou, M. A.; Jiménez, I. Towards a new generation of polymer nanocomposites based on inorganic nanotubes. *Journal of Materials Chemistry* **2011**, *21*, 3574.
33. Kreizman, R.; Enyashin, A. N.; Deepak, F. L.; Albu-Yaron, A.; Popovitz-Biro, R.; Seifert, G.; Tenne, R. Synthesis of Core-Shell Inorganic Nanotubes. *Adv. Funct. Mat.* **2010**, *20*, 2459-2468.
34. Hong, S. Y.; Popovitz-Biro, R.; Tobias, G.; Ballesteros, B.; Davis, B. G.; Green, M. L. H.; Tenne, R. Synthesis and characterization of WS₂ inorganic nanotubes with encapsulated/intercalated Csl. *Nano Research* **2010**, *3*, 170-173.
35. Laikhtman, A.; Michaelson, S.; Hoffman, A.; Kim, T. K.; Moon, H. R.; Zak, A. Using hydrogen activated by microwave plasma vs. molecular hydrogen for hydrogen storage in tungsten disulfide inorganic nanotubes. *International Journal of Hydrogen Energy* **2014**, *39*, 9837-9841.
36. Pardo, M.; Shuster-Meiseles, T.; Levin-Zaidman, S.; Rudich, A.; Rudich, Y. Low cytotoxicity of inorganic nanotubes and fullerene-like nanostructures in human bronchial epithelial cells: relation to inflammatory gene induction and antioxidant response. *Environ. Sci. Technol.* **2014**, *48*, 3457-66.
37. Ghorbani-Asl, M.; Zibouche, N.; Wahiduzzaman, M.; Oliveira, A. F.; Kuc, A.; Heine, T. Electromechanics in MoS₂ and WS₂: nanotubes vs. monolayers. *Sci. Rep.* **2013**, *3*, 2961.
38. Attia, N. F.; Menemparabath, M. M.; Arepalli, S.; Geckeler, K. E. Inorganic nanotube composites based on polyaniline: Potential room-temperature hydrogen storage materials. *International Journal of Hydrogen Energy* **2013**, *38*, 9251-9262.
39. Scanlon, S.; Aggeli, A. Self-assembling peptide nanotubes. *Nano Today* **2008**, *3*, 22-30.
40. Asthagiri, D.; Bashford, D. Continuum and Atomistic Modeling of Ion Partitioning into a Peptide Nanotube. *Biophysical Journal* **2002**, *82*, 1176-1189.
41. Montero, A.; Gastaminza, P.; Law, M.; Cheng, G.; Chisari, F. V.; Ghadiri, M. R. Self-assembling peptide nanotubes with antiviral activity against hepatitis C virus. *Chem. Biol.* **2011**, *18*, 1453-62.

42. Montenegro, J.; Ghadiri, M. R.; Granja, J. R. Ion Channel Models Based on Self-Assembling Cyclic Peptide Nanotubes. *Accounts of Chemical Research* **2013**, 46, 2955-2965.
43. Hwang, H.; Schatz, G. C.; Ratner, M. A. Ion Current Calculations Based on Three Dimensional Poisson-Nernst-Planck Theory for a Cyclic Peptide Nanotube. *J. Phys. Chem. B* **2006**, 110, 6999-7008.
44. Lopez, J. L.; Perez, E. M.; Viruela, P. M.; Viruela, R.; Orti, E.; Martin, N. Controlled Self-Assembly of Electron Donor Nanotubes. *Org. Lett.* **2009**, 11, 4524-4527.
45. Gauthier, D.; Baillargeon, P.; Drouin, M.; Dory, Y. L. Self-Assembly of Cyclic Peptides into Nanotubes and then into Highly Anisotropic Crystalline Materials. *Angew. Chem. Int. Ed.* **2001**, 40, 4635-4638.
46. Bong, D. T.; Clark, T. D.; Granja, J. R.; Ghadiri, M. R. Self-Assembling Organic Nanotubes. *Angew. Chem. Int. Ed.* **2001**, 40, 988-1011.
47. Ishihara, Y.; Kimura, S. Four-peptide-nanotube bundle formation by self-assembling of cyclic tetra-beta-peptide using G-quartet motif. *Biopolymers* **2013**, 100, 141-7.
48. Baoukina, S.; Marrink, S. J.; Tieleman, D. P. Molecular structure of membrane tethers. *Biophysical journal* **2012**, 102, 1866-71.
49. Wilson-Kubalek, E. M.; Brown, R. E.; Celia, H.; Milligan, R. A. Lipid Nanotubes as Substrates for Helical Crystallization of Macromolecules. *PNAS* **1998**, 95, 8040-8045.
50. Cans, A. S.; Wittenberg, N.; Karlsson, R.; Sombers, L.; Karlsson, M.; Orwar, O.; Ewing, A. Artificial cells: unique insights into exocytosis using liposomes and lipid nanotubes. *PNAS* **2003**, 100, 400-4.
51. Reches, M.; Gazit, E. Casting metal nanowires within discrete self-assembled peptide nanotubes. *Science* **2003**, 300.
52. Kol, N.; Adler-Abramovich, L.; Barlam, D.; Shneck, R. Z.; Gazit, E.; Rousso, I. Self-Assembled Peptide Nanotubes are Uniquely Rigid Bioinspired Supramolecular Structures. *Nano Lett.* **2005**, 5, 1345-1356.
53. Adler-Abramovich, L.; Reches, M.; Sedman, V. L.; Allen, S.; Tendler, S. J. B.; Gazit, E. Thermal and chemical stability of diphenylalanine peptide nanotubes: implications for nanotechnological applications. *Langmuir* **2006**, 22, 1313-1320.
54. Reches, M.; Gazit, E. Controlled patterning of aligned self-assembled peptide nanotubes. *Nat. Nanotech.* **2006**, 1, 195-200.
55. Krysmann, M. J.; Castelletto, V.; McKendrick, J. E.; Clifton, L. A.; Hamley, I. W. Self-Assembly of Peptide Nanotubes in an Organic Solvent. *Langmuir* **2008**, 24.
56. Jeon, J.; Mills, C. E.; Shell, M. S. Molecular insights into diphenylalanine nanotube assembly: all-atom simulations of oligomerization. *J. Phys. Chem. B* **2013**, 117, 3935-3943.

57. Chandrasekhar, N.; Chandrasekar, R. Reversibly shape-shifting organic optical waveguides: formation of organic nanorings, nanotubes, and nanosheets. *Angew. Chem. Int. Ed.* **2012**, 51, 3556-61.
58. Santis, P. D.; Morosetti, S.; Rizzo, R. Conformational Analysis of Regular Enantiomeric Sequences. *Macromolecules* **1973**, 7, 52-58.
59. Tomasic, L.; Stefani, A.; Lorenzi, G. P. Linear Stereo-co-oligopeptides with Alternating D- and L-Residues: Synthesis and Mass Spectrometric Behaviour of the Members of a Series with Valine Residues. *Helvetica Chimica Acta* **1980**, 63, 2000-2004.
60. Tomasic, L.; Lorenzi, G. P. Some Cyclic Oligopeptides with S_{2n} Symmetry. *Helvetica Chimica Acta* **1987**, 70, 1012 - 1016.
61. Pavone, V.; Benedetti, Ettore; Di Blasio, B.; Lombardi, A.; Pedone, C.; Tomasich, L.; Lorenzi, G. P. Regularly Alternating L,D-Peptides. III. Hexacyclic Peptides from Valine or Phenylalanine. *Biopolymers* **1989**, 28, 215-223.
62. Ghadiri, M. R.; Granja, J. R.; Milligan, R. A.; McRee, D. E.; Khazanovich, N. Self-assembling organic nanotubes based on a cyclic peptide architecture. *Nature* **1993**, 366, 324-327.
63. Hartgerink, J. D.; Granja, J. R.; Milligan, R. A.; Ghadiri, M. R. Self-Assembling Peptide Nanotubes. *J. Am. Chem. Soc.* **1996**, 118, 43-50.
64. Cheng, J.; Zhu, J.; Liu, B.; Liao, Z.; Lai, Z. Structure of a self-assembled single nanotube of cyclo[(-d-Ala-l-Ala)₄]. *Molecular Simulation* **2009**, 35, 625-630.
65. Ghadiri, M. R.; Kobayashi, K.; Granja, J. R.; Chadha, R. K.; McRee, D. E. The Structural and Thermodynamic Basis of the Formation of Self-Assembled Peptide Nanotubes. *Angew. Chem. Int. Ed.* **1995**, 34, 93-95.
66. Sun, X.; Lorenzi, G. P. On the Stacking of β -Rings: The Solution Self-Association Behaviour of Two Partially N-Methylated Cyclo(hexaleucines). *Helvetica Chimica Acta* **1994**, 77, 1520-1526.
67. Amarin, M.; Castedo, L.; Granja, J. R. New Cyclic Peptide Assemblies with Hydrophobic Cavities: The Structural and Thermodynamic Basis of a New Class of Peptide Nanotubes. *J. Am. Chem. Soc.* **2003**, 125, 2844-2845.
68. Horne, W. S.; Stout, C. D.; Ghadiri, M. R. A Heterocyclic Peptide Nanotube. *J. Am. Chem. Soc.* **2003**, 125, 9372-9376.
69. Amarin, M.; Castedo, L.; Granja, J. R. Self-assembled peptide tubelets with 7 A pores. *Chemistry* **2005**, 11, 6543-51.
70. Saviano, M.; Zaccaro, L.; Lombardi, A.; Pedone, C.; Blasio, B. D.; Sun, X.; Lorenzi, G. P. A Structural Two-Ring Version of a Tubular Stack of β -Rings in Crystals of a Cyclic D,L-Hexapeptide. *J. Inc. Phen. and Mol. Rec. in Chem* **1994**, 18, 27-36.

71. Kobayashi, K.; Granja, J. R.; Ghadiri, M. R. β -Sheet Peptide Architecture: Measuring the Relative Stability of Parallel vs. Antiparallel β -Sheets. *Angew. Chem. Int. Ed.* **1995**, 34, 95-98.
72. Amorin, M.; Castedo, L.; Granja, J. R. Folding control in cyclic peptides through N-methylation pattern selection: formation of antiparallel beta-sheet dimers, double reverse turns and supramolecular helices by 3 α , γ cyclic peptides. *Chemistry* **2008**, 14, 2100-11.
73. Cortez-Diaz, M. D.; d'Orlye, F.; Gutierrez-Granados, S.; de Leon-Rodriguez, L. M.; Varenne, A. Design, synthesis, and characterization of new cyclic d,l-alpha-alternate amino acid peptides by capillary electrophoresis coupled to electrospray ionization mass spectrometry. *Analytical biochemistry* **2016**, 502, 8-15.
74. Zhu, J.; Cheng, J.; Liao, Z.; Lai, Z.; Liu, B. Investigation of structures and properties of cyclic peptide nanotubes by experiment and molecular dynamics. *J. Comput. Aided Mol. Des.* **2008**, 22, 773-81.
75. Hourani, R.; Zhang, C.; van der Weegen, R.; Ruiz, L.; Li, C.; Keten, S.; Helms, B. A.; Xu, T. Processable cyclic peptide nanotubes with tunable interiors. *J. Am. Chem. Soc.* **2011**, 133, 15296-9.
76. Rodriguez-Vazquez, N.; Amorin, M.; Granja, J. R. Recent advances in controlling the internal and external properties of self-assembling cyclic peptide nanotubes and dimers. *Org. Biomol. Chem.* **2017**.
77. Brea, R. J.; Amorin, M.; Castedo, L.; Granja, J. R. Methyl-blocked dimeric alpha, γ -peptide nanotube segments: formation of a peptide heterodimer through backbone-backbone interactions. *Angew. Chem. Int. Ed.* **2005**, 44, 5710-3.
78. Li, L.; Zhan, H.; Duan, P.; Liao, J.; Quan, J.; Hu, Y.; Chen, Z.; Zhu, J.; Liu, M.; Wu, Y.-D.; Deng, J. Self-Assembling Nanotubes Consisting of Rigid Cyclic γ -Peptides. *Adv. Funct. Mat.* **2012**, 22, 3051-3056.
79. Brea, R. J.; Castedo, L.; Granja, J. R. Large-diameter self-assembled dimers of alpha, γ -cyclic peptides, with the nanotubular solid-state structure of cyclo-[(L-Leu-D-(Me)N- γ -Acp)₄].4CHCl₂COOH. *Chem. Commun.* **2007**, 3267-9.
80. Garcia-Fandino, R.; Castedo, L.; Granja, J. R.; Vazquez, S. A. Interaction and Dimerization Energies in Methyl-Blocked α , γ -Peptide Nanotube Segments. *J. Phys. Chem. B* **2010**, 114, 4973-4983.
81. Reiriz, C.; Castedo, L.; Granja, J. R. New alpha, γ -cyclic peptides-nanotube molecular caps using alpha,alpha-dialkylated alpha-amino acids. *J. Pept. Sci.* **2008**, 14, 241-9.

82. Rodriguez-Vazquez, N.; Garcia-Fandino, R.; Aldegunde, M. J.; Brea, J.; Loza, M. I.; Amorin, M.; Granja, J. R. cis-Platinum Complex Encapsulated in Self-Assembling Cyclic Peptide Dimers. *Org. Lett.* **2017**.
83. Vijayaraj, R.; Van Damme, S.; Bultinck, P.; Subramanian, V. Molecular dynamics and umbrella sampling study of stabilizing factors in cyclic peptide-based nanotubes. *J. Phys. Chem. B* **2012**, 116, 9922-33.
84. Chapman, R.; Danial, M.; Koh, M. L.; Jolliffe, K. A.; Perrier, S. Design and properties of functional nanotubes from the self-assembly of cyclic peptide templates. *Chem. Soc. Rev.* **2012**, 41, 6023-41.
85. Mizrahi, M.; Zakrassov, A.; Lerner-Yardeni, J.; Ashkenasy, N. Charge transport in vertically aligned, self-assembled peptide nanotube junctions. *Nanoscale* **2012**, 4, 518-24.
86. Lerner Yardeni, J.; Amit, M.; Ashkenasy, G.; Ashkenasy, N. Sequence dependent proton conduction in self-assembled peptide nanostructures. *Nanoscale* **2016**, 8, 2358-66.
87. Horne, W. S.; Ashkenasy, N.; Ghadiri, M. R. Modulating charge transfer through cyclic D,L-alpha-peptide self-assembly. *Chem. Eur. J.* **2005**, 11, 1137-1144.
88. Ashkenasy, N.; Horne, W. S.; Ghadiri, M. R. Design of self-assembling peptide nanotubes with delocalized electronic states. *Small* **2006**, 2, 99-102.
89. Rho, J. Y.; Brendel, J. C.; MacFarlane, L. R.; Mansfield, E. D. H.; Peltier, R.; Rogers, S.; Hartlieb, M.; Perrier, S. Probing the Dynamic Nature of Self-Assembling Cyclic Peptide-Polymer Nanotubes in Solution and in Mammalian Cells. *Adv. Funct. Mat.* **2018**, 28, 1704569.
90. Sun, L.; Fan, Z.; Wang, Y.; Huang, Y.; Schmidt, M.; Zhang, M. Tunable synthesis of self-assembled cyclic peptide nanotubes and nanoparticles. *Soft matter* **2015**, 11, 3822-32.
91. ten Cate, M.; Severin, N.; Borner, H. Self-Assembling Peptide-Polymer Conjugates Comprising (D-alt-L)-Cyclopeptides as Aggregator Domains. *Macromolecules* **2006**, 39, 7831-7838.
92. Chapman, R.; Jolliffe, K. A.; Perrier, S. Synthesis of Self-assembling Cyclic Peptide-polymer Conjugates using Click Chemistry. *Aust. J. Chem.* **2010**, 63, 1169-1172.
93. Chapman, R.; Warr, G. G.; Perrier, S.; Jolliffe, K. A. Water-soluble and pH-responsive polymeric nanotubes from cyclic peptide templates. *Chemistry* **2013**, 19, 1955-61.
94. Chapman, R.; Jolliffe, K. A.; Perrier, S. Modular design for the controlled production of polymeric nanotubes from polymer/peptide conjugates. *Polymer Chemistry* **2011**, 2, 1956.

95. Chapman, R.; Jolliffe, K. A.; Perrier, S. Multi-shell soft nanotubes from cyclic peptide templates. *Adv. Mater.* **2013**, *25*, 1170-2.
96. Danial, M.; Tran, C. M.; Young, P. G.; Perrier, S.; Jolliffe, K. A. Janus cyclic peptide-polymer nanotubes. *Nat. Commun.* **2013**, *4*, 2780.
97. Becker, M. L.; Liu, J.; Wooley, K. L. Peptide-polymer bioconjugates: hybrid block copolymers generated via living radical polymerizations from resin-supported peptides. *Chem. Commun.* **2003**, 180-181.
98. Mei, Y.; Beers, K. L.; Byrd, H. C. M.; VanderHart, D. L.; Washburn, N. R. Solid-Phase ATRP Synthesis of Peptide-Polymer Hybrids. *J. Am. Chem. Soc.* **2004**, *126*, 3472-3476.
99. Rettig, H.; Krause, E.; Börner, H. G. Atom Transfer Radical Polymerization with Polypeptide Initiators: A General Approach to Block Copolymers of Sequence-Defined Polypeptides and Synthetic Polymers. *Macromol. Rapid Commun.* **2004**, *25*, 1251-1256.
100. Couet, J.; Samuel, J. D.; Kopyshov, A.; Santer, S.; Biesalski, M. Peptide-Polymer Hybrid Nanotubes. *Angew. Chem. Int. Ed.* **2005**, *44*, 3297-3301.
101. Couet, J.; Biesalski, M. Surface-Initiated ATRP of *N*-Isopropylacrylamide from Initiator-Modified Self-Assembled Peptide Nanotubes. *Macromolecules* **2006**, *39*, 7258-7268.
102. Loschonsky, S.; Couet, J.; Biesalski, M. Synthesis of Peptide/Polymer Conjugates by Solution ATRP of Butylacrylate Using an Initiator-Modified Cyclic D-alt-L-Peptide. *Macromol. Rapid Commun.* **2008**, *29*, 309-315.
103. Couet, J.; Biesalski, M. Polymer-Wrapped Peptide Nanotubes: Peptide-Grafted Polymer Mass Impacts Length and Diameter. *Small* **2008**, *4*, 1008-1016.
104. Motesharei, K.; Ghadiri, M. R. Diffusion-Limited Size-Selective Ion Sensing Based on SAM-Supported Peptide Nanotubes. *J. Am. Chem. Soc.* **1997**, *119*, 11306-11312.
105. Garcia-Fandino, R.; Granja, J. R.; D'Abramo, M.; Orozco, M. Theoretical Characterization of the Dynamical Behaviour and Transport Properties of α,γ -peptide Nanotubes in Solution. *J. Am. Chem. Soc.* **2009**, *131*, 15678-15686.
106. Liu, H.; Chen, J.; Shen, Q.; Fu, W.; Wu, W. Molecular Insights on the Cyclic Peptide Nanotube-Mediated Transportation of Antitumor Drug 5-Fluorouracil. *Molecular Pharmaceutics* **2010**, *7*, 1985-1994.
107. Liu, J.; Fan, J.; Tang, M.; Cen, M.; Yan, J.; Liu, Z.; Zhou, W. Water Diffusion Behaviours and Transportation Properties in Transmembrane Cyclic Hexa-, Octa and Decapeptide Nanotubes. *J. Phys. Chem. B* **2010**, *114*, 12183-12192.

108. Li, R.; Fan, J.; Li, H.; Yan, X.; Yu, Y. Exploring the dynamic behaviors and transport properties of gas molecules in a transmembrane cyclic peptide nanotube. *J. Phys. Chem. B* **2013**, *117*, 14916-27.
109. Alsina, M. A.; Gaillard, J. F.; Keten, S. Conformational changes during permeation of Na⁺ through a modified cyclic peptide nanotube promote energy landscape roughness. *Phys. Chem. Chem. Phys.* **2016**, *18*, 31698-31710.
110. Ozores, H. L.; Amorin, M.; Granja, J. R. Self-Assembling Molecular Capsules Based on alpha,gamma-Cyclic Peptides. *J. Am. Chem. Soc.* **2017**.
111. Fernandez-Lopez, S.; Kim, H.-S.; Choi, E. C.; Delgado, M.; Granja, J. R.; Khasanov, A.; Kraehenbuehl, K.; Long, G.; Weinberger, D. A.; Wilcoxon, K. M.; Ghadiri, M. R. Antibacterial agents based on the cyclic D,L- α peptide architecture. *Nature* **2001**, *412*, 452-455.
112. Fletcher, J. T.; Finlay, J. A.; Callow, M. E.; Callow, J. A.; Ghadiri, M. R. A combinatorial approach to the discovery of biocidal six-residue cyclic D,L-alpha-peptides against the bacteria methicillin-resistant *Staphylococcus aureus* (MRSA) and *E. coli* and the biofouling algae *Ulva linza* and *Navicula perminuta*. *Chemistry* **2007**, *13*, 4008-13.
113. Clark, T. D.; Ghadiri, M. R. Supramolecular Design by Covalent Capture. Design of a Peptide Cylinder via Hydrogen-Bond-Promoted Intermolecular Olefin Metathesis. *J. Am. Chem. Soc.* **1995**, *117*, 12364-12365.
114. Clark, T. D.; Kobayashi, K.; Ghadiri, M. R. Covalent capture and stabilization of cylindrical beta-sheet peptide assemblies. *Chem. Eur. J.* **1999**, *5*, 782-792.
115. Steinem, C.; Janshoff, A.; Vollmer, M. S.; Ghadiri, M. R. Reversible Photoisomerization of Self-Organized Cylindrical Peptide Assemblies at Air-Water and Solid Interfaces. *Langmuir* **1999**, *15*, 3956-3964.
116. Vollmer, M. S.; Clark, T. D.; Steinem, C.; Ghadiri, M. R. Photoswitchable Hydrogen-Bonding in Self-Organized Cylindrical Peptide Systems. *Angew. Chem. Int. Ed.* **1999**, *38*, 1598-1601.
117. Maarseveen, J. H. V.; Horne, W. S.; Ghadiri, M. R. Efficient Route to C₂ Symmetric Heterocyclic Backbone Modified Cyclic Peptides. *Org. Lett.* **2005**, *7*, 4503-4506.
118. Gokhale, R.; Couet, J.; Biesalski, M. In situ cross-linking of the shell of self-assembled peptide nanotubes. *Phys. Status Solidi A* **2010**, *207*, 878-883.
119. Fuertes, A.; Ozores, H. L.; Amorin, M.; Granja, J. R. Self-assembling Venturi-like peptide nanotubes. *Nanoscale* **2017**, *9*, 748-753.
120. Krimm, S.; Bandekar, J. Vibrational Spectroscopy and Conformation of Peptides, Polypeptides, and Proteins. **1986**, *38*, 181-364.

121. Karplus, M. Molecular Dynamics Simulations of Biomolecules. *Accounts of Chemical Research* **2002**, 35, 321-323.
122. Shaw, D. E.; Dror, R. O.; Salmon, J. K.; Grossman, J. P.; Mackenzie, K. M.; Bank, J. A.; Young, C.; Deneroff, M. M.; Batson, B.; Bowers, K. J.; Chow, E.; Eastwood, M. P.; Lerardi, D. J.; Klepeis, J. L.; Kuskin, J. S.; Larson, R. H.; Lindorff-Larsen, K.; Maragakis, P.; Moraes, M. A.; Piana, S.; Shan, Y.; Towles, B. Millisecond-scale molecular dynamics simulations on Anton. In 2009; pp 1-11.
123. Shaw, D. E.; Chao, J. C.; Eastwood, M. P.; Gagliardo, J.; Grossman, J. P.; Ho, C. R.; Lerardi, D. J.; Kolossváry, I.; Klepeis, J. L.; Layman, T.; McLeavey, C.; Deneroff, M. M.; Moraes, M. A.; Mueller, R.; Priest, E. C.; Shan, Y.; Spengler, J.; Theobald, M.; Towles, B.; Wang, S. C.; Dror, R. O.; Kuskin, J. S.; Larson, R. H.; Salmon, J. K.; Young, C.; Batson, B.; Bowers, K. J. Anton, a special-purpose machine for molecular dynamics simulation. *Communications of the ACM* **2008**, 51, 91.
124. Essmann, U.; Perera, L.; Berkowitz, M. L.; Darden, T.; Lee, H.; Pedersen, L. G. A smooth particle mesh Ewald method. *The Journal of Chemical Physics* **1995**, 103, 8577-8593.
125. Shan, Y.; Klepeis, J. L.; Eastwood, M. P.; Dror, R. O.; Shaw, D. E. Gaussian split Ewald: A fast Ewald mesh method for molecular simulation. *The Journal of Chemical Physics* **2005**, 122.
126. Jorgensen, W. L.; Maxwell, D. S.; Tirado-Rives, J. Development and Testing of the OPLS All-Atom Force Field on Conformational Energetics and Properties of Organic Liquids. *Journal of the American Chemical Society* **1996**, 118, 11225-11236.
127. Kaminski, G. A.; Friesner, R. A.; Tirado-Rives, J.; Jorgensen, W. L. Evaluation and Reparametrization of the OPLS-AA Force Field for Proteins via Comparison with Accurate Quantum Chemical Calculations on Peptides. *The Journal of Physical Chemistry B* **2001**, 105, 6474-6487.
128. Tzanov, A. T.; Cuendet, M. A.; Tuckerman, M. E. How Accurately Do Current Force Fields Predict Experimental Peptide Conformations? An Adiabatic Free Energy Dynamics Study. *The Journal of Physical Chemistry B* **2014**, 118, 6539-6552.
129. Vijayaraj, R.; Raman, S. S.; Kumar, R. M.; Subramanian, V. Studies on the Structure and Stability of Cyclic Peptide Based Nanotubes Using Oligomeric Approach: A Computational Chemistry Investigation. *J. Phys. Chem. B* **2010**, 114, 16574-16583.

Chapter 2

Using ionic interactions to direct the assembly of well-ordered cyclic D/L peptide nanotubes

CPs self-assemble through backbone H-bonding interactions to form CPNs of a diverse range of sizes. However, the spontaneous, dynamic nature of CP self-assembly renders it difficult to precisely control CPN composition and hinders the development of CPNs into functional nanomaterials. The use of charge-charge interactions could coordinate the self-assembly process and introduce a high degree of order within the assembled CPNs. Additionally, combining CPs with oppositely charged side-chains could direct the assembly of heterogeneous CPNs composed of different CPs.

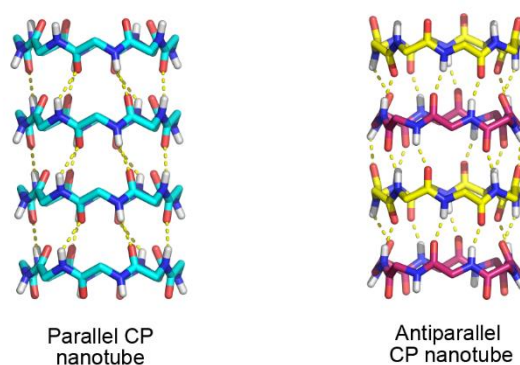


Figure i. CP backbones from the crystal structures of *cyclo*[(Asp-D-Ala-Lys-D-Ala)₂] and *cyclo*[(Asp-D-Leu-Lys-D-Leu)₂] with parallel and antiparallel H-bonding respectively. These are the first crystal structures of continuously H-bonded CP nanotubes.

A selection of ionisable CPs were synthesised by Fmoc-based solid-phase peptide synthesis methodology and studied by X-ray crystallography, FT-IR and DLS. Remarkably, *cyclo*[(Asp-D-Ala-Lys-D-Ala)₂] (CP **1**) and *cyclo*[(Asp-D-Leu-Lys-D-Leu)₂] (CP **2**) crystallised as continuously H-bonded nanotubes. CP **1** crystallised with parallel H-bonding while CP **2** crystallised with antiparallel H-bonding (**Figure i**). Both crystal structures involve a network of charge-charge interactions which stabilize the structures and promote the highly-ordered arrangements. While we were unable to generate heterogeneous material, ionic interactions were effective in coordinating the assembly process and CP alignment within and between nanotubes. Until now, the only published crystal-structures of CP-based material were of backbone *N*-methylated CP dimers and there were no structures for extended CPNs. The work presented in this chapter represents a significant advancement in CPN characterisation, providing atomic-resolution evidence of both antiparallel and parallel H-bonding networks within extended CP nanotubes. Furthermore, it ratifies the use of ionic interactions in

generating well-ordered CPN materials and may provide a means for further control over CPN structure by directing CP orientation and arrangement.

This chapter is the published article: M. R. Silk, J. Newman, J. C. Ratcliffe, J. F. White, T. Caradoc-Davies, J. R. Price, S. Perrier, P. E. Thompson, D. K. Chalmers, *Chem. Commun.* **2017**, 53, 6613-6616. Supplementary information is included after the article and contains detailed experimental methods for the synthesis and crystallisation of CPs.

Cite this: *Chem. Commun.*, 2017, 53, 6613Received 1st February 2017,
Accepted 30th May 2017

DOI: 10.1039/c7cc00846e

rsc.li/chemcomm

Parallel and antiparallel cyclic D/L peptide nanotubes†

 Mitchell R. Silk,^a Janet Newman,^b Julian C. Ratcliffe,^c Jacinta F. White,^c
 Tom Caradoc-Davies,^d Jason R. Price,^{b,d} Sébastien Perrier,^{b,ef}
 Philip E. Thompson^{b,a} and David K. Chalmers^{b,*a}

Nanotubes made from H-bonded cyclic D/L peptide (CP) subunits have great potential for the construction of nanomaterials of wide chemical and structural diversity but, to date, difficulties in structural characterisation have restricted development of these materials. We present the first crystal structures of continuous CP nanotubes with antiparallel and parallel stacking arrangements, assembled separately from two peptides; *cyclo*[(Asp-D-Leu-Lys-D-Leu)₂] and *cyclo*[(Asp-D-Ala-Lys-D-Ala)₂].

Self-assembling cyclic peptide (CP) nanotubes made from H-bonded cyclic D/L peptide subunits are exciting materials that promise extensive chemical and structural diversity through simple variation of the amino acid composition. Incorporation of natural and non-natural amino acids into the CPs allows for innumerable structural possibilities and fine control of the properties of the resultant nanotubes. CP nanotubes can be tailored for a range of applications including charge-transfer for materials science,^{1–3} synthetic protein channels with biological applications⁴ and have demonstrated anti-viral⁵ and anti-bacterial⁶ activity through membrane interactions.

Nanotubes composed of cyclic D/L peptide monomers were first described by Ghadiri *et al.* in 1993.⁷ Acidification of a solution of *cyclo*[(D-Ala-Glu-D-Ala-Gln)₂] produced very small crystals that could be analysed by electron diffraction, revealing a regularly packed structure with a unit cell of dimensions;

$a = 9.5 \text{ \AA}$, $b = c = 15.1 \text{ \AA}$, $\alpha = 90^\circ$, $\beta = \gamma = 99^\circ$. Based on these data, Ghadiri and co-workers proposed a nanotube structure formed from antiparallel stacking of peptide monomers with β -sheet-like hydrogen bonding between peptides (Fig. 1). Nanotube formation in the solid state is supported by FT-IR spectra that are indicative of β -sheet-like structures^{4,7–17} and electron microscopy showing fibrous supramolecular assemblies.^{1,7,9–12,14–18} A computational study¹⁴ has proposed that antiparallel stacking is more stable than parallel stacking (Fig. 1).

Subsequent to the original report, a wide variety of D/L CP nanotubes have been described, including structures built from peptides having 6, 8, 10 and 12 amino acids^{6,17,19} structures containing β - and γ -amino acids that enable modification of the pore^{8,15,16,19–24} and tubes with external functionalisation.^{1–4,9–11,16,18} Although crystallisation of D/L CP nanotubes has not been reported

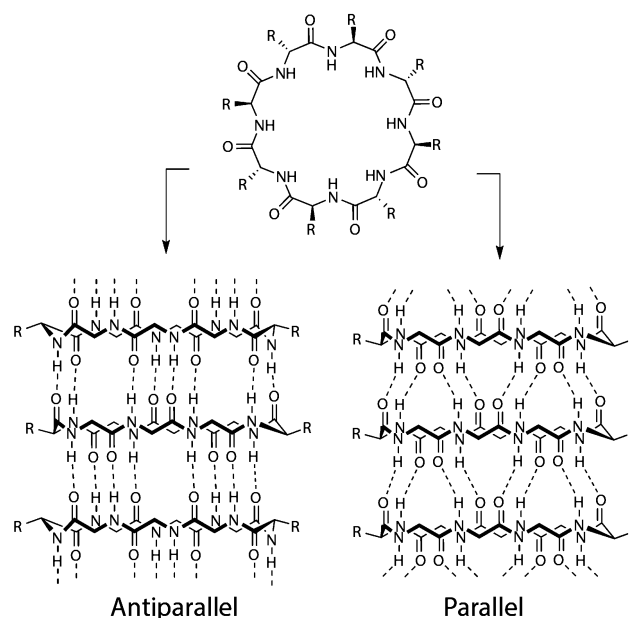


Fig. 1 Cyclic octapeptides with alternating D and L amino acids can potentially stack to form antiparallel or parallel nanotubes.

^a Medicinal Chemistry, Monash Institute of Pharmaceutical Sciences, Monash University, 381 Royal Parade, Parkville, Victoria 3052, Australia. E-mail: david.chalmers@monash.edu

^b Biomedical Program, CSIRO, 343 Royal Parade, Parkville, Victoria, 3052, Australia

^c CSIRO manufacturing, CSIRO, Research Way, Clayton, Victoria, 3168, Australia

^d Australian Synchrotron, 800 Blackburn Rd, Clayton, Victoria, 3168, Australia

^e Drug Delivery, Disposition and Dynamics, Monash Institute of Pharmaceutical Sciences, Monash University, 381 Royal Parade, Parkville, Victoria 3052, Australia

^f Department of Chemistry, The University of Warwick, Coventry CV4 7AL, UK

† Electronic supplementary information (ESI) available: Experimental procedures and results for peptide synthesis, crystallisation and crystallography. CCDC 1520675 and 1520676. For ESI and crystallographic data in CIF or other electronic format see DOI: 10.1039/c7cc00846e

to date, support for the formation of antiparallel-stacked nanotubes has been provided by crystal structures of D/L cyclopeptide dimers that have the hydrogen bonding on one face blocked by methylation of the amide nitrogen atoms.^{2,8,13,14,16,24} In the solution state, evidence of nanotube formation is more ambiguous than in the solid state with the exception of polymer functionalised CPs developed by Perrier and coworkers that assemble in solution^{4,9–11,18} to form soluble rods that can be characterised by SANS.¹¹

Although most reports in the literature propose that the nanostructures formed by D/L CPs are antiparallel, in principle, similar nanotubes can be formed by either parallel or antiparallel stacking, and the evidence that a particular nanotube is formed from antiparallel stacked peptides is circumstantial. Computational models show that an antiparallel arrangement creates the best alignment between backbone amide NH and carbonyl groups^{12,25,26} but parallel stacked peptide nanotubes still allow regular H-bonding although with less favourable inter-strand hydrogen bonding geometries.¹⁴

In a study of the factors that drive nanotube formation, we investigated the crystallisation of a variety of water-soluble cyclooctapeptides, including compounds **1** and **2**, as individual compounds or as peptide mixtures. Intriguingly, and despite the relatively minor structural differences between compounds, peptides **1** and **2** crystallise in distinctly different arrangements as continuous antiparallel and parallel nanotubes (Fig. 2).

Crystallographic screens of CPs were conducted using sitting drop vapour diffusion in aqueous solution using the diverse conditions of the 'shotgun' screen²⁷ at 20 °C. Conditions that provided initial crystal hits were selected for further optimisation using the Hampton Additive Screen HT mixed with the original hit condition (90 : 10 v/v original condition : additive).

Peptide **1** was crystallised as small needles from a 1 : 1 mixture of **1** and *cyclo*[(His-D-Leu-Lys-D-Leu)₂] (**3**) which had been used in an attempt to produce heterogenous nanotubes. Despite the presence of two peptides in the crystallisation experiment, the solved structure consisted only of peptide **1** arranged in continuous β -sheet-like nanotubes with extensive H-bonding interactions with two neighbouring peptides (Fig. 2a). Within each nanotube, the peptides are assembled in antiparallel fashion with like-residues aligned along the length of the nanotubes, although there is a small rotational offset between adjacent peptides. Two conformations of peptide **1** are present within the unit cell, differing slightly in backbone conformation and also in side chain rotamers. Some disorder is present in the amide carbonyls of the aspartic acid residues and the side chains of aspartic acid and lysine. The positively charged Lys side chains of each nanotube make a continuous network of intermolecular ionic interactions with the negatively charged Asp side chains of an adjacent tube. Adjacent nanotubes run antiparallel to one-another. Stacking of the peptides produces a continuous central pore and the interstitial space between nanotubes creates a second pore of a different chemical nature.

In contrast to peptide **1**, the crystal structure of peptide **2** (Fig. 2b) consists of sheets of parallel nanotubes, separated by layers of hexafluoroisopropanol (HFIP). Along the nanotube,

each peptide is in register with the neighbouring peptides, meaning that the amide carbonyl and NH groups are nearly directly aligned and the hydrogen bonding between peptide chains is offset. Despite this offset, the CO HN distances are similar to those found in the antiparallel crystal structure. The short Ala side chains allow the tubes to pack closely together and each peptide makes two ionic interactions with neighbouring peptides. The lower steric constraints imparted by the Ala residues in **2** increases the flexibility of the peptide backbone, which is evident in disorder of all backbone amide carbonyl groups, and a more oval pore shape than for **1**.

This remarkable observation of both antiparallel and parallel stacking in CPs with similar peptide sequences shows that, contrary to the assumptions that have been made to date, D/L CPs do not necessarily adopt an antiparallel arrangement in the solid state. Rather, the relationship of the CP rings is controlled by the packing geometry; particularly by side chain interactions between adjacent nanotubes, which clearly can overwhelm any energetic differences between parallel and antiparallel CP arrangements. These observations in the solid state suggest that similar considerations need to be made in solution.

The FT-IR spectra of a freeze-dried powder of **1** revealed amide I, I secondary and II bands at 1628, 1667 and 1528 cm⁻¹, characteristic of a β -sheet-like structure. The amide A band at 3271 cm⁻¹ is consistent with the originally reported frequency of 3277 cm⁻¹ for N-H stretching of *cyclo*[(D-Ala-Glu-D-Ala-Gln)₂],⁷ and is strongly indicative of a tight network of backbone-backbone H-bonds.²⁸ Peptide **2** yielded similar results, with amide I, I secondary, II and A bands at 1626, 1670, 1537 and 3275 cm⁻¹ respectively.

The behaviour of peptides **1** and **2** in solution was investigated. At 10 mg mL⁻¹, a solution of peptide **1** is visibly glossy while peptide **2** is clear at the same concentration. Dynamic light scattering (DLS) in water (Fig. 3) shows concentration-dependent aggregate formation, although sizing by DLS makes assumptions about the nature of the particles (*i.e.* that the particle is spherical) and the measured aggregate sizes should be regarded as nominal. In the concentration range 2–10 mg mL⁻¹, peptide **1** forms aggregates with nominal average diameters ranging from 20 to 1100 nm. At all concentrations a larger aggregate, with nominal diameter ~6500 nm is also present, accounting for the glossy appearance. Peptide **2** has a similar concentration-dependent behaviour, but with larger average diameters and tighter size distributions. Solutions of both peptides are reasonably stable over time, with the aggregation of peptide **1** being largely unchanged after 7 days while peptide **2** forms a precipitate after two days at room temperature.

The solution behaviour of peptides **1** and **2** was further studied by cryo-transmission electron microscopy (TEM) at concentrations of 2, 5 and 10 mg mL⁻¹ in water. Peptide **1** was found to form rod-like structures of up to 130 nm in length at 5 mg mL⁻¹ and up to 170 nm at 10 mg mL⁻¹ with a thickness of ~10 nm (Fig. 4a), suggesting the formation of nanotube bundles since a single CP nanotube has a diameter of ~1 nm. Peptide **2** formed roughly spherical aggregates of up to 200 nm in diameter at 5 mg mL⁻¹ and 500 nm at 10 mg mL⁻¹ (Fig. 4b).

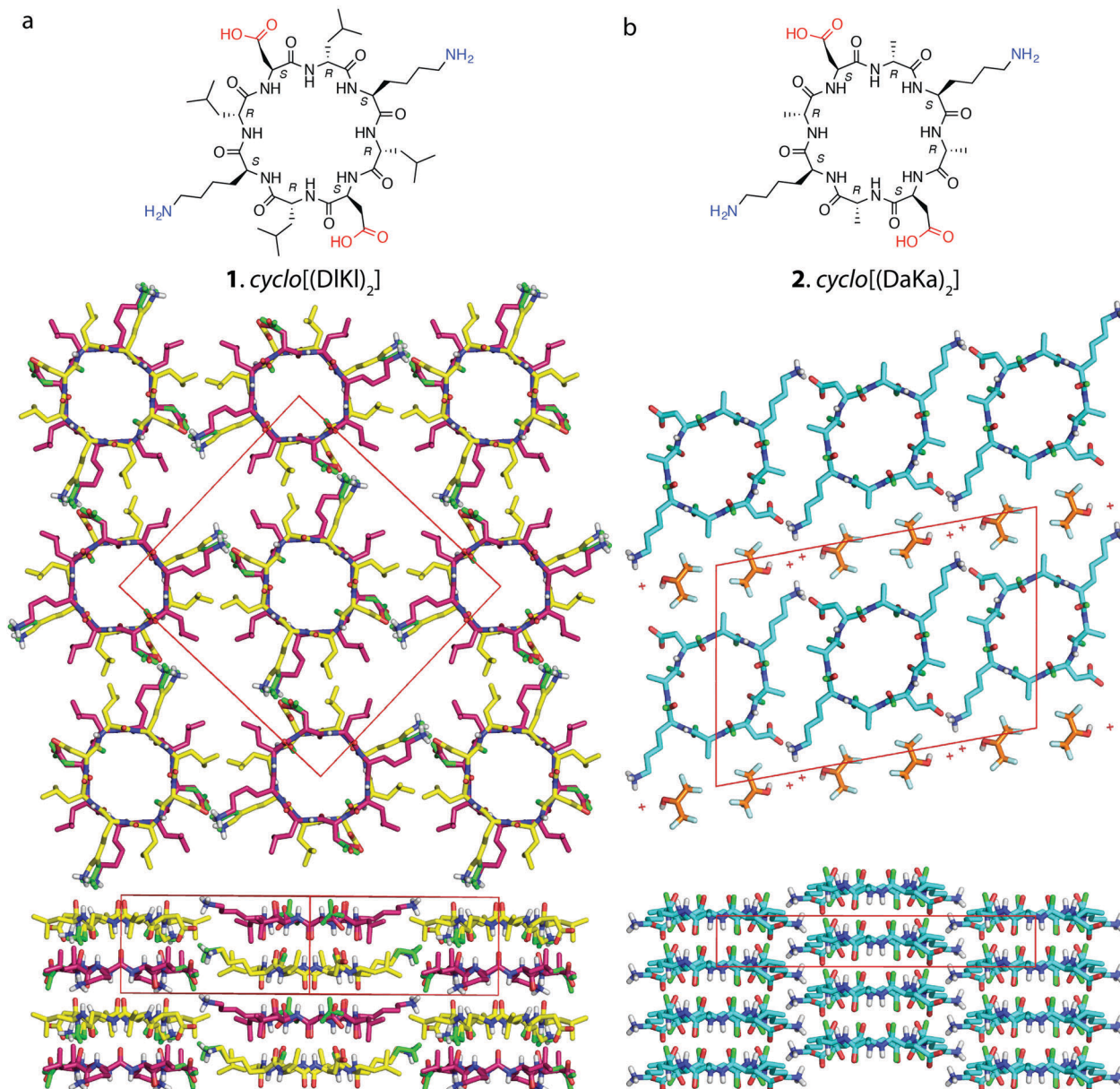


Fig. 2 X-ray crystal structures of peptide nanotubes. Unit cells are shown in red. Alternate conformations are shown in green. (a) Antiparallel nanotubes formed by peptide **1**. Two conformations of the peptide are present (pink and yellow). The view down the axis reveals continuous internal and interstitial pores, with each aspartic acid and lysine side chain making charge-reinforced hydrogen bonds to two neighbouring peptides. Adjacent nanotubes are oriented head-to-tail. (b) Parallel nanotubes of peptide **2** formed by a single peptide conformer. In this case, the short alanine side chains allow close packing of nanotubes, which facilitates the formation of two ionic interactions per pair of adjacent nanotubes. Adjacent nanotubes are parallel to one-another and form sheets separated by HFIP molecules (orange).

The aggregates appeared to consist of smaller subunits of ~ 10 nm in diameter that pack together into the larger structures. Whilst the precise nature of the spherical structures found for peptide **2** is not conclusive, the appearance of rods for peptide **1** is consistent with the formation of nanotube bundles.

The X-ray crystal structures reported here are the first atomic resolution structures of continuous cyclic *D/L* peptide nanotubes and further reveal the expected antiparallel stacking arrangement and an unexpected parallel form. The crystal

structure of peptide **1** is consistent with the antiparallel structure originally proposed by Ghadiri *et al.*⁷ (although the cell size and space group differs) while the structure of peptide **2** shows that parallel stacking is also feasible. FT-IR studies of both peptides contain amide bands that are characteristic of a tight network of backbone-backbone H-bonds, consistent with those of previously reported peptide nanotubes. Analysis of solutions of the peptides in water by DLS reveals that both peptides form large aggregates in solution at concentrations between 2 and 10 mg mL⁻¹. Further investigation by cryo-TEM reveals rod-like

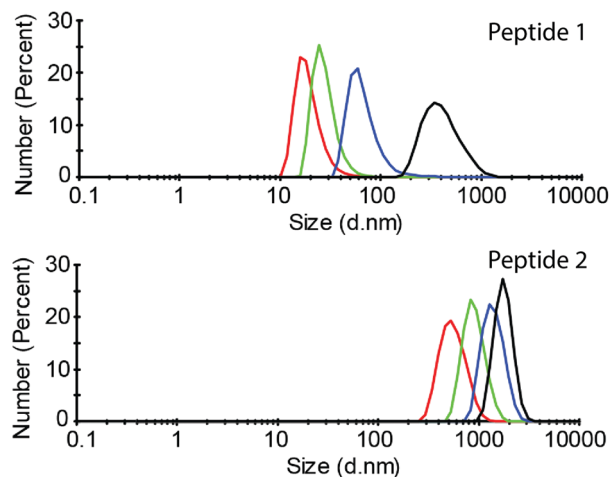


Fig. 3 Dynamic light scattering measurements of peptides **1** and **2** in water showing the concentration-dependent formation of large aggregates. Concentrations of 1, 2, 5 and 10 mg mL⁻¹ are shown as red, green, blue and black curves.

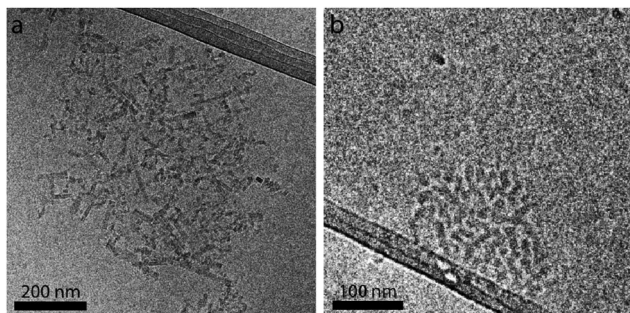


Fig. 4 Cryo-TEM images of peptides **1** and **2** at 10 mg mL⁻¹ frozen in water. The large structures in each image are the support grid. (a) Rod-like structures of peptide **1**, up to 170 × 10 nm suggesting bundles of tubes. (b) Spherical aggregate of peptide **2** with 200 nm diameter comprised of 10 nm subunits.

structures of peptide **1**, consistent with bundles of tubes up to 170 nm in length. Peptide **2** forms spherical aggregates up to 500 nm in diameter comprised of 10 nm subunits although the exact nature of the structures is not clear. Together, these observations greatly extend our understanding of this interesting class of material. Importantly, the observation of both parallel and antiparallel forms reveals that, in the solid state, intra- and inter-nanotube interactions can dictate the nature of the nanotube structure. Distinguishing between parallel and antiparallel nanotube structures using low-resolution analyses is likely to be difficult or impossible. Lastly, these crystal structures offer guidance for the design of new cyclic peptide subunits with optimised side chain interactions to direct and control the self-assembly process for the development of complex organic, functionalised nanomaterials for biomedicine or other applications.

MRS acknowledges an RTP scholarship provided by the Australian Government. SP acknowledges a Royal Society Wolfson Merit Award (WM130055), and the Monash-Warwick Alliance and the European Research Council (TUSUPO 647106) for funding. X-ray data was acquired using the MX2 beamline at the Australian Synchrotron.

References

- 1 N. Ashkenasy, W. S. Horne and M. R. Ghadiri, *Small*, 2006, **2**, 99–102.
- 2 W. S. Horne, N. Ashkenasy and M. R. Ghadiri, *Chem. – Eur. J.*, 2005, **11**, 1137–1144.
- 3 M. Mizrahi, A. Zakrassov, J. Lerner-Yardeni and N. Ashkenasy, *Nanoscale*, 2012, **4**, 518–524.
- 4 M. Danial, C. M. Tran, P. G. Young, S. Perrier and K. A. Jolliffe, *Nat. Commun.*, 2013, **4**, 2780.
- 5 A. Montero, P. Gastaminza, M. Law, G. Cheng, F. V. Chisari and M. R. Ghadiri, *Chem. Biol.*, 2011, **18**, 1453–1462.
- 6 J. T. Fletcher, J. A. Finlay, M. E. Callow, J. A. Callow and M. R. Ghadiri, *Chem. – Eur. J.*, 2007, **13**, 4008–4013.
- 7 M. R. Ghadiri, J. R. Granja, R. A. Milligan, D. E. McRee and N. Khazanovich, *Nature*, 1993, **366**, 324–327.
- 8 M. Amarin, L. Castedo and J. R. Granja, *J. Am. Chem. Soc.*, 2003, **125**, 2844–2845.
- 9 R. Chapman, K. A. Jolliffe and S. Perrier, *Aust. J. Chem.*, 2010, **63**, 1169–1172.
- 10 R. Chapman, K. A. Jolliffe and S. Perrier, *Polym. Chem.*, 2011, **2**, 1956.
- 11 R. Chapman, G. G. Warr, S. Perrier and K. A. Jolliffe, *Chem. – Eur. J.*, 2013, **19**, 1955–1961.
- 12 J. Cheng, J. Zhu, B. Liu, Z. Liao and Z. Lai, *Mol. Simul.*, 2009, **35**, 625–630.
- 13 M. R. Ghadiri, K. Kobayashi, J. R. Granja, R. K. Chadha and D. E. McRee, *Angew. Chem., Int. Ed.*, 1995, **34**, 93–95.
- 14 J. D. Hartgerink, J. R. Granja, R. A. Milligan and M. R. Ghadiri, *J. Am. Chem. Soc.*, 1996, **118**, 43–50.
- 15 R. Hourani, C. Zhang, R. van der Weegen, L. Ruiz, C. Li, S. Keten, B. A. Helms and T. Xu, *J. Am. Chem. Soc.*, 2011, **133**, 15296–15299.
- 16 L. Li, H. Zhan, P. Duan, J. Liao, J. Quan, Y. Hu, Z. Chen, J. Zhu, M. Liu, Y.-D. Wu and J. Deng, *Adv. Funct. Mater.*, 2012, **22**, 3051–3056.
- 17 J. Zhu, J. Cheng, Z. Liao, Z. Lai and B. Liu, *J. Comput.-Aided Mol. Des.*, 2008, **22**, 773–781.
- 18 R. Chapman, K. A. Jolliffe and S. Perrier, *Adv. Mater.*, 2013, **25**, 1170–1172.
- 19 R. J. Brea, L. Castedo and J. R. Granja, *Chem. Commun.*, 2007, 3267–3269.
- 20 M. Amarin, L. Castedo and J. R. Granja, *Chem. – Eur. J.*, 2005, **11**, 6543–6551.
- 21 M. Amarin, L. Castedo and J. R. Granja, *Chem. – Eur. J.*, 2008, **14**, 2100–2111.
- 22 R. J. Brea, M. Amarin, L. Castedo and J. R. Granja, *Angew. Chem., Int. Ed. Engl.*, 2005, **44**, 5710–5713.
- 23 W. S. Horne, C. D. Stout and M. R. Ghadiri, *J. Am. Chem. Soc.*, 2003, **125**, 9372–9376.
- 24 C. Reiriz, L. Castedo and J. R. Granja, *J. Pept. Sci.*, 2008, **14**, 241–249.
- 25 R. Vijayaraj, S. S. Raman, R. M. Kumar and V. Subramanian, *J. Phys. Chem. B*, 2010, **114**, 16574–16583.
- 26 R. Vijayaraj, S. Van Damme, P. Bultinck and V. Subramanian, *J. Phys. Chem. B*, 2012, **116**, 9922–9933.
- 27 V. J. Fazio, T. S. Peat and J. Newman, *Acta Crystallogr., Sect. F: Struct. Biol. Commun.*, 2014, **70**, 1303–1311.
- 28 S. Krimm and J. Bandekar, in *Advances in Protein Chemistry*, ed. C. B. Anfinsen, J. T. Edsall and F. M. Richards, 1986, vol. 38, pp. 181–364.

Chapter 2 – Appendix

Using ionic interactions to direct the assembly of well-ordered cyclic D/L peptide nanotubes – Supplementary Information

Parallel and Antiparallel Cyclic D/L Peptide Nanotubes

Mitchell R. Silk,^a Janet Newman,^c Julian C. Ratcliffe,^d Jacinta F. White,^d Tom Caradoc-Davies,^e Jason R. Price,^e Sébastien Perrier,^{b,f} Philip E. Thompson,^a David K. Chalmers^{a*}

^aMedicinal Chemistry, and ^bDrug Delivery, Disposition and Dynamics, Monash Institute of Pharmaceutical Sciences, Monash University, 381 Royal Parade, Parkville, Victoria, 3052, Australia.

^cBiomedical Program, CSIRO, 343 Royal Parade, Parkville, Victoria, 3052, Australia. ^dCSIRO manufacturing, CSIRO, Research Way, Clayton, Victoria, 3168, Australia. ^eAustralian Synchrotron, 800 Blackburn Rd, Clayton, Victoria, 3168, Australia. ^fDepartment of Chemistry, The University of Warwick, Coventry CV4 7AL, United Kingdom

Peptide synthesis

Side-chain protected linear peptides were synthesised by automated methods using Fmoc chemistry on acid-labile 2-chlorotrityl chloride resin. Head-to-tail cyclisation was performed on side chain-protected peptide over 2 days in DMF solution using PyClock/DIPEA as the coupling agent. Following side-chain deprotection, the crude peptides were purified by preparative reverse-phase HPLC.

Coupling of the first amino acid: 2-chlorotrityl chloride resin (83 mg, resin loading 1.2 mmol g⁻¹, 0.1 mmol) was swelled in 5 mL of CH₂Cl₂ for 30 minutes in a sinter-fitted syringe. The resin was then drained and treated with 1 equivalent (relative to resin capacity) of Fmoc-amino acid dissolved in CH₂Cl₂ (4 mL). To the mixture was added 6 equivalents of DIPEA relative to amino acid and the resulting mixture was agitated at room temperature overnight. The resin was drained and washed with DMF (3 x 3 mL) and treated with MeOH (2 x 3 mL) to cap any unreacted sites. The resin was then washed with DMF (3 x 3 mL) and transferred to an SPPS reaction vessel.

Automated synthesis of linear peptides: The linear peptides were prepared using an automated solid-phase peptide-synthesiser (Protein Technologies Inc. PS3). On each coupling cycle, the resin was first washed with DMF (3 x 30 s). Fmoc deprotection was achieved using 20% piperidine in DMF (2 x 5 min) followed by washing with DMF (6 x 30 s) to provide the resin-bound free amino-terminal of the peptide. Couplings used three equivalents of Fmoc amino acid and 2-(6-chloro-1H-benzotriazole-1-yl)-1,1,3,3-tetramethylammonium hexafluorophosphate (HCTU), relative to resin loading. The amino acid and HCTU was dissolved in a solution of 7% DIPEA in DMF. The solution was added to the resin which was agitated at room temperature for 1 h, drained and washed with DMF (3 x 30 s). After coupling the final amino acid, a further Fmoc deprotection was performed to obtain the resin-bound peptide with free amino terminal. The resin was transferred to a sinter-fitted syringe and washed with DMF (3 x 3 mL), MeOH (3 x 3 mL) and Et₂O (3 x 3 mL).

Peptide cleavage from resin: The resin-bound linear peptide was treated with a solution of 20% 1,1,1,3,3,3-hexafluoroisopropanol (HFIP) in CH₂Cl₂ (3 x 3 mL x 10 min) and the HFIP washings were collected by filtration. The resin was then washed with CH₂Cl₂ (3 x 3 mL). The combined HFIP and CH₂Cl₂ washings were concentrated under reduced pressure and freeze-dried from 1:1 ACN/H₂O to yield the side-chain-protected linear peptide as a white powder. A sample of the peptide was deprotected and analysed by LCMS to confirm the linear sequence.

Cyclisation: The linear peptide was added to DMF (7 mg/mL) and treated with 3 equivalents of PyClock and 6 equivalents of DIPEA. The solution was stirred at room temperature for 2 days before being concentrated under reduced pressure to yield a thick oil. The oil was freeze-dried from 1:1 ACN/H₂O to yield the crude side-chain-protected cyclic peptide as an off-white solid.

Deprotection: The side chain protecting groups of the cyclic peptide were removed by treatment with a solution of TFA/TIPS/H₂O (95:2.5:2.5 v/v, 2 mL) for 3 h. The TFA was evaporated using a stream

of N₂ gas and the remaining oil was then treated with ice-cold Et₂O to precipitate the peptide. The precipitate was collected by centrifugation and freeze-dried from 1:1 ACN/H₂O to yield the crude cyclic deprotected peptide as a white solid.

Purification: Peptides were purified by preparative reverse-phase HPLC using a Waters Associates liquid chromatography system (Model 600 Controller and Waters 486 Tunable Absorbance Detector) with a Phenomenex Luna C8(2) 100 Å, 10 µm, 250 x 21.2 mm column with 0.1% TFA/H₂O as buffer A and 0.1% TFA in 90% ACN/H₂O as buffer B with a flow rate of 15 mL/min.

Peptide 1, *cyclo*[(Asp-D-Leu-Lys-D-Leu)₂]. Purification gradient: 20-60% buffer B over 60 mins, R_T = 28.4 mins (38.9% B). Yield: 90 mg (31.2%) as a white solid on 0.3 mmol scale synthesis. ¹H NMR (400 MHz, DMSO-*d*₆) δ 12.35 (s, 1H), 8.29 (d, *J* = 6.1 Hz, 1H), 8.25 (d, *J* = 7.7 Hz, 1H), 8.02 (d, *J* = 8.1 Hz, 1H), 7.86 (d, *J* = 8.5 Hz, 1H), 7.64 (s, 3H), 4.57 (dd, *J* = 13.6, 7.2 Hz, 1H), 4.41 (dd, *J* = 11.6, 8.7 Hz, 1H), 4.36 – 4.22 (m, 2H), 2.80 – 2.56 (m, 5H), 1.68 – 1.33 (m, 12H), 1.26 (dd, *J* = 10.6, 4.3 Hz, 4H), 0.92 – 0.77 (m, 14H). HRMS (ESI) [M + Na]⁺ calculated: 961.5693, found: 961.5681, [M + H]⁺ calculated: 939.5873, found: 939.5880, [M + 2H]²⁺ calculated: 470.7973, found: 470.2983.

Peptide 2, *cyclo*[(Asp-D-Ala-Lys-D-Ala)₂]. Purification gradient: 0-30% buffer B over 60 mins, R_T = 23.8 mins (11.9% B). Yield: 25 mg (32.4%) as a white solid on 0.1 mmol scale synthesis. ¹H NMR (400 MHz, DMSO-*d*₆) δ 12.31 (s, 1H), 8.30 (d, *J* = 7.7 Hz, 1H), 8.18 (d, *J* = 7.2 Hz, 1H), 8.01 (d, *J* = 7.5 Hz, 1H), 7.90 (d, *J* = 8.5 Hz, 1H), 7.63 (s, 3H), 4.57 (dd, *J* = 14.1, 7.5 Hz, 2H), 4.44 – 4.16 (m, 4H), 2.84 – 2.61 (m, 4H), 1.62 (dt, *J* = 19.7, 6.3 Hz, 1H), 1.56 – 1.39 (m, 3H), 1.33 – 1.23 (m, 2H), 1.19 (dd, *J* = 6.7, 5.8 Hz, 6H). HRMS (ESI) [M + Na]⁺ calculated: 793.3815, found: 793.3774, [M + H]⁺ calculated: 771.3995, found: 771.3997, [M + 2H]²⁺ calculated: 386.2034, found: 386.2041.

Peptide 3, *cyclo*[(His-D-Leu-Lys-D-Leu)₂]. Purification gradient: 5-35% buffer B over 60 mins, R_T = 38.3 mins (24.1%B). Yield: 27.1 mg (27.6%) as a white solid on 0.1 mmol scale synthesis. ¹H NMR (400 MHz, DMSO-*d*₆) δ 8.91 (s, 1H), 8.41 (d, *J* = 8.8 Hz, 1H), 8.20 (d, *J* = 8.7 Hz, 1H), 8.17 (d, *J* = 8.8 Hz, 1H), 8.10 (d, *J* = 8.7 Hz, 1H), 7.60 (s, 3H), 7.26 (s, 1H), 4.78 – 4.69 (m, 1H), 4.43 (td, *J* = 9.3, 4.0 Hz, 1H), 4.39 – 4.29 (m, 2H), 2.95 (dd, *J* = 14.9, 5.4 Hz, 1H), 2.79 (dd, *J* = 15.5, 9.4 Hz, 1H), 2.69 – 2.57 (m, 2H), 1.56 – 1.02 (m, 14H), 0.84 – 0.63 (m, 12H). HRMS (ESI) [M + Na]⁺ calculated: 1005.6332, found: 1005.6344, [M + 2H]²⁺ calculated: 492.3293, found: 492.3305, [M + 3H]³⁺ calculated: 328.5553, found: 328.5566.

Peptide crystallisation

Crystal screening was performed at the CSIRO C3 crystallisation centre using sitting drop vapour-diffusion in 96 well plates with droplets of 150 nL peptide and 150 nL of reservoir solution, equilibrated against a reservoir of 50 µL. Initial screens were set up using the ‘shotgun’ screen¹ at 20°C and each well was imaged by robot 15 times over a period of 80 days. Conditions that provided initial crystal hits were selected for further additive optimisation, using the Additive Screen HT (Hampton Research, USA) mixed with the original hit condition (90:10 v/v original condition:additive). Crystals were seen after 1 day and grew to final size after 5 days. Peptides were found to crystallise best at concentrations of 5 mg/mL, as 10 mg/mL often caused precipitation and <2 mg/mL provided little to no supersaturation (precipitation or crystal growth). Peptide **1** was crystallised from a 1:1 mixture with peptide **3**; *cyclo*[(His-D-Leu-Lys-D-Leu)₂], with only peptide **1** being present in the crystal structure, from a cocktail containing 1.44 M trisodium citrate and 3% v/v 2,2,2-trifluoroethanol, producing colourless needle-like crystals ranging from 40 to 300 µm in length and 1 to 3 µm in width. Peptide **2** crystallised from a cocktail containing 3.6 M sodium formate, 4% v/v 1,1,1,3,3,3-hexafluoropropan-2-ol (HFIP) producing needles with lengths of 200 to 400 µm and widths of up to 15 µm.

Crystallography

Diffraction data was collected using the MX2 micro-focus beamline at the Australian Synchrotron on an ADSC Quantum 315r CCD detector at 100(2) K using Si(111) monochromated synchrotron-

radiation. BluIce control software² was used for data-collection and integration was carried out with XDS.³ Datasets for crystal structure 2 were merged with SADABS.⁴ Structures were solved by dual space methods using SHELXT⁵ and refined with SHELXL.⁶

Crystals of peptide **1** were mounted on 0.05 to 0.1 mm Cryoloops (CrystalCap with Copper Magnetic ALS HT, Hampton Research, USA) in the crystallisation conditions with 20% glycerol as cryoprotectant. A single needle of dimensions 1 x 2 x 300 μm was measured using Si(111) monochromated synchrotron-radiation with $\lambda = 0.71073 \text{ \AA}$, $\Theta_{\text{max}} = 23.327^\circ$. Crystal data for structure 1 is given in Table S1. Due to the low resolution of the data and extensive disorder of the solvent the SQUEEZE routine⁷ was used with a total potential solvent accessible void volume 1899.4 \AA^3 with an electron count of 714 e^- per unit cell which has been approximated as 18 water molecules per formula unit. The labile hydrogens have been assigned as best is possible but due to poor resolution data and disorder, the actual hydrogen bonding and protonation states of the amine and carboxylic acid can't be determined with confidence. The model has been assigned with the carboxylic acid completely deprotonated and all amines are protonated. There is extensive ionic intermolecular interactions between these disordered groups and while it may be expected that there would be some further hydrogen bonding solvent within the proximal void volume, nothing could be assigned from the difference map in the pre-squeezed structure.

Colourless needle-like crystals of peptide **2** were mounted on 0.05 to 0.1 mm Cryoloops (CrystalCap with Copper Magnetic ALS HT, Hampton Research, USA) in the crystallisation conditions with 20% glycerol as cryoprotectant. The crystal was measured with 90° overlapping wedges on five different locations along the length of a 2 x 4 x 350 μm^3 needle using monochromated synchrotron-radiation with $\lambda = 0.95369 \text{ \AA}$, $\Theta_{\text{max}} = 30.227^\circ$. Crystal data for structure 2 is given in Table S1. Due to the low resolution of the data and extensive disorder of the solvent within the cyclopeptide, the SQUEEZE routine⁷ was used with a total potential solvent accessible void volume 243.2 \AA^3 with an electron count of 63.9 e^- per unit cell which has been approximated as 3 water molecules per formula unit.

Crystallographic data for the structures in this paper have been deposited with the Cambridge Crystallographic Data Centre. Deposition numbers; CCDC 1520675, 1520676. This data can be obtained free of charge by application to the CCDC; fax: +44-1223-336033 or e-mail: deposit@ccdc.cam.ac.uk.

Table S1: X-ray crystallography table of data collection and refinement.

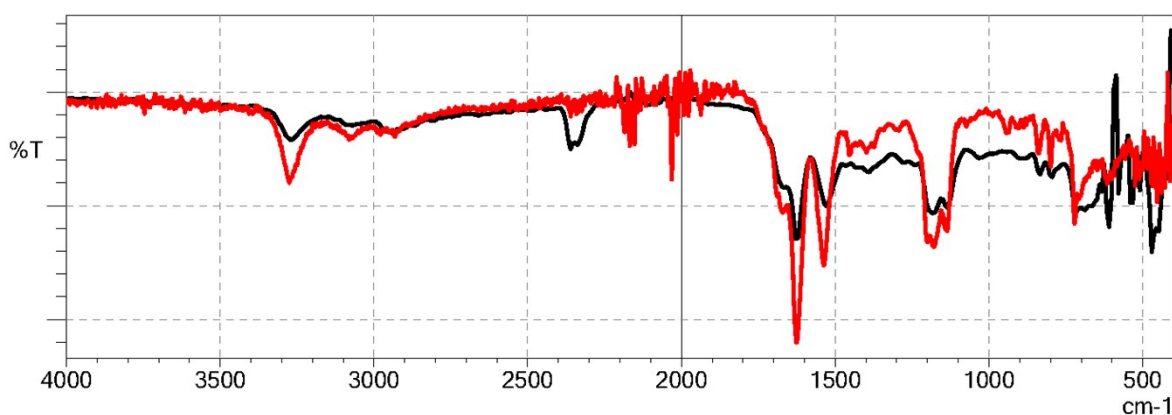
Formula	$C_{44}H_{114}N_{10}O_{30}$	$C_{38}H_{66}F_{18}N_{10}O_{15}$
Model Molecular Weight	1263.45	1245.0
Crystal System	Orthorhombic	Monoclinic
Space Group	(#18) $P2_12_12$	(#5) $C2$
a	25.256(5) Å	29.780(6) Å
b	26.729(5) Å	4.7000(9) Å
c	9.5380(19) Å	20.220(4) Å
β	-	100.38(3)°
V	6439(2) Å ³	2783.8(10) Å ³
D_c	1.303 g cm ⁻³	1.485 g cm ⁻³
Z	4	2
Crystal Size	0.3x0.002x0.001 mm	0.35x0.004x0.002 mm
Crystal Colour	Colourless	Colourless
Crystal Habit	needle	needle
Temperature	100(2) Kelvin	100(2) Kelvin
λ (synchrotron)	0.71073 Å	0.95369 Å
μ (synchrotron)	0.109 mm ⁻¹	0.321 mm ⁻¹
T (SADABS) _{min,max}	N/A	0.7616, 0.8543
$2\theta_{max}$	46.65°	60.45°
hkl range	-28 28, -29 29, -10 10	-30 30, -4 4, -21 21
N	36610	14129
N_{ind}	9053(R_{merge} 0.1257)	3194(R_{merge} 0.1269)
N_{obs}	5138($I > 2s(I)$)	2765($I > 2s(I)$)
N_{var}	672	352
GoF(all)	0.967	1.212
Residual Extrema	-0.229, 0.442 e ⁻ Å ⁻³	-0.347, 0.394 e ⁻ Å ⁻³

Dynamic Light Scattering

Dynamic light scattering was performed with a Malvern Zetasizer Nano ZS with ZEN0040 cuvettes. Peptides **1** and **2** were studied at concentrations of 1, 2, 5 and 10 mg/mL in water within 2 hours of dissolution. Peptide samples were sonicated for 30 s and centrifuged for 3 min immediately following dissolution. DLS measurements were performed in triplicates using 10 to 15 scans per sample. Measurements were performed at 25°C using a scattering angle of 173° and 60 s equilibration time between samples. Peptides **1** and **2** were freeze-dried from water as white powders for analysis by ATR-FTIR.

FT-IR

Fourier transform infrared spectroscopy was conducted using a Shimadzu IRTracer-100 with Gladiator 10 ATR. A KBr beam splitter was used to measure radiation in the MIR range of 400-4600 cm^{-1} . Peptides were analysed in the solid state as freeze-dried powders.



Peptide	Colour	Amide A (cm^{-1})	Amide I (cm^{-1})	Amide II (cm^{-1})
1: c[(Asp-D-Leu-Lys-D-Leu) ₂]	Black	3271	1667, 1628	1528
2: c[(Asp-D-Ala-Lys-D-Ala) ₂]	Red	3275	1670, 1626	1537

Figure S1: FT-IR spectra for peptides **1** and **2**, with table of wavenumbers for bands of interest.

Cryo-Transmission Electron Microscopy (cryo-TEM)

A laboratory-built humidity-controlled vitrification system was used to prepare the samples for Cryo-TEM. Humidity was kept close to 80% for all experiments, and ambient temperature was 22°C. A 3 μl aliquot of the sample were pipetted onto a 300-mesh copper grid coated with lacey formvar over a perforated carbon support (ProScitech, Thurwingowa, Australia GSCu300FL-50C). After 10 seconds adsorption time the grid was blotted manually using Whatman 541 filter paper, for approximately 2 seconds. The grid was then plunged into liquid ethane cooled by liquid nitrogen. Frozen grids were stored in liquid nitrogen until required.

The samples were examined using a Gatan 626 cryoholder (Gatan, Pleasanton, CA, USA) and Tecnai 12 Transmission Electron Microscope (FEI, Eindhoven, The Netherlands) at an operating voltage of 120KV. At all times low dose procedures were followed, using an electron dose of 8-10 electrons/ \AA^2 for all imaging. Images were recorded using a Megaview III CCD camera and AnalySIS camera control software (Olympus.)

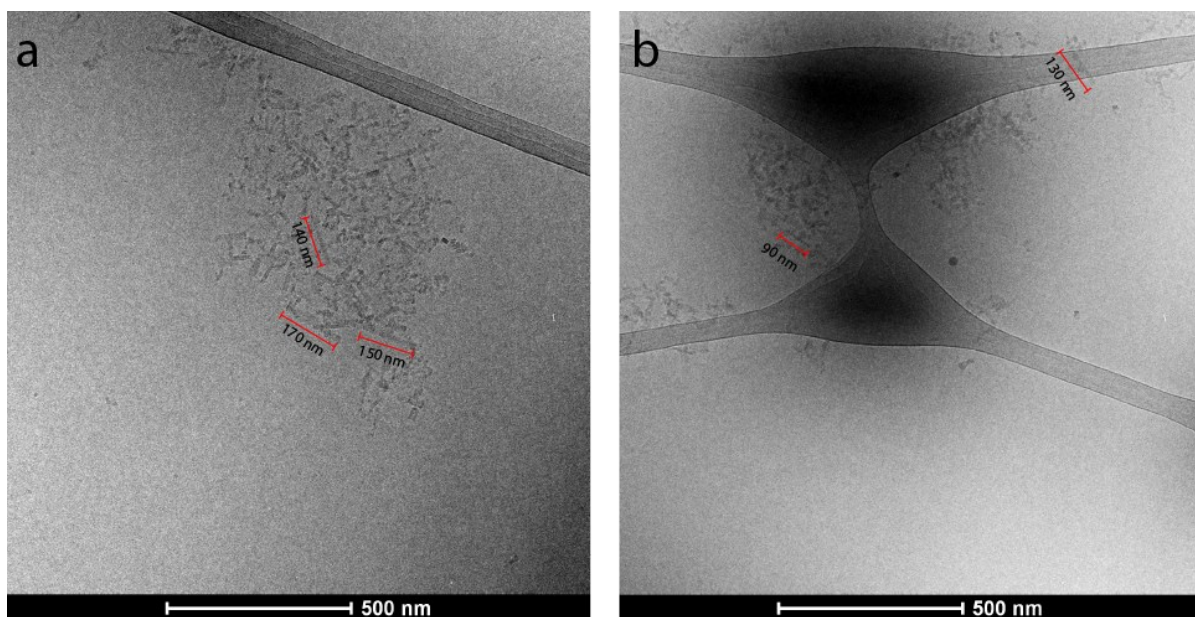


Figure S2: Cryo-TEM images of peptide 1 $\text{cyclo}[(\text{Asp-D-Leu-Lys-D-Leu})_2]$ at a) 10 mg/mL and b) 5 mg/mL.

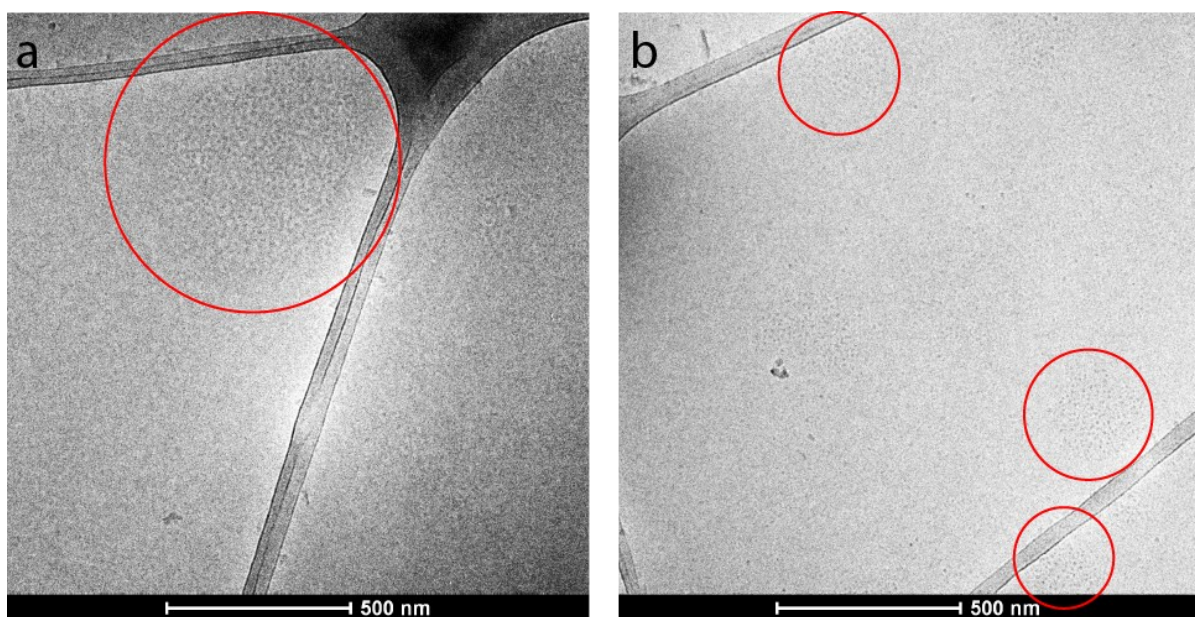


Figure S3: Cryo-TEM images of peptide 2 $\text{cyclo}[(\text{Asp-D-Ala-Lys-D-Ala})_2]$ at a) 10 mg/mL and b) 5 mg/mL. Visible structures/aggregates are circled.

HPLC and NMR

Liquid chromatographic analysis was conducted with a Phenomenex Luna C8(2) 100 Å, 3 μm, 100 x 2.0 mm reverse-phase column. Running buffer consisted of solvent A with 0.1% TFA/H₂O and solvent B with 0.1% TFA in 80% ACN/H₂O. All 1D and 2D NMR spectra were recorded at 400 MHz using a 400 MHz Bruker Avance III Nanobay spectrometer.

Supplementary References

1. V. J. Fazio, T. S. Peat and J. Newman, *Acta Crystallogr F Struct Biol Commun*, 2014, **70**, 1303-1311.
2. T. M. McPhillips, S. E. McPhillips, H. J. Chiu, A. E. Cohen, A. M. Deacon, P. J. Ellis, E. Garman, A. Gonzalez, N. K. Sauter, R. P. Phizackerley, S. M. Soltis and P. Kuhn, *J. Synchrotron Rad.*, 2002, **9**, 401-406.
3. W. Kabsch, *J. Appl. Cryst.*, 1993, **26**, 795-800.
4. G. M. Sheldrick. SDADABS. University of Göttingen, Germany., 1996.
5. G. M. Sheldrick, *Acta Cryst.*, 2015, **A71**, 3-8.
6. G. M. Sheldrick, *Acta Cryst.*, 2008, **A64**, 112-122.
7. A. L. Spek, *Acta Cryst.*, 2015, **C71**, 9-18.

Chapter 3

Controlled construction of cyclic D/L peptide nanorods

The charge-charge interactions explored in Chapter 2 enabled the development of ordered nanotube bundles as a result of inter-nanotube ionic interactions. However, these ionic interactions were insufficient in our attempts to generate heterogeneous nanotubes. Chapter 3 explores the use of side-chain tethering to construct heterogeneous CPNs and introduce short-range order. Improving our control over the self-assembly process and developing heterogeneous CPNs are essential steps to the development of functional nanomaterials.

A series of CP tetramers were synthesised by coupling CPs to one-another through the amino acid side-chains. Copper-activated azide-alkyne cycloaddition was used in addition to cysteine-oxidation to generate heterogeneous CP tetramers. The coupling chemistries were orthogonal and could be performed on the side-chain deprotected CPs (with the exception of Cys). Further self-assembly of the tetramers into extended CPNs was confirmed by cryo-EM analysis which revealed the formation of fibrous assemblies. In-solution structure and H-bonding interactions were studied by NMR and DLS, confirming the formation of ordered, folded structures with concentration-dependent behaviour. However, the CP-tetramers had different structures and degrees of stability, highlighting the need for investigation and stabilization of the interactions between CP subunits.

These tethered CP tetramers are the first of their kind, granting access to organised heterogeneous CPNs and significantly improving the potential complexity and structural diversity that can be achieved in CP-based materials.

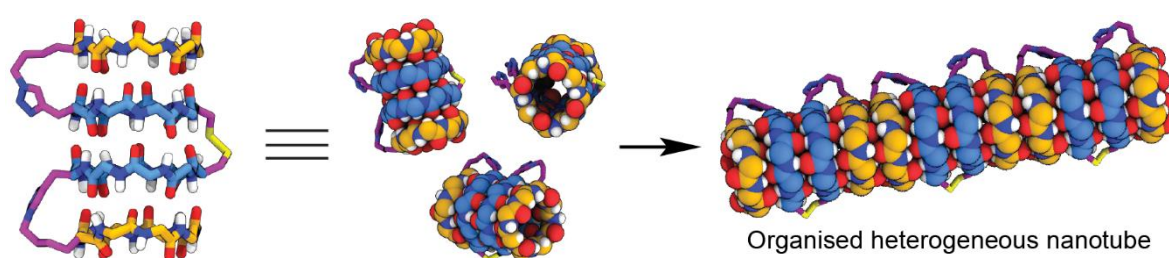


Figure i. Side-chain tethering of cyclic D/L peptides enables control over the order and arrangement of CPs within assembled nanorods and extended nanotubes, granting access to precisely-functionalised heterogeneous CP-based nanomaterial.

This chapter is the published article: M. R. Silk, B. Mohanty, J. B. Sampson, M. J. Scanlon, P. E. Thompson, D. K. Chalmers, *Angew. Chem. Int. Ed.* **2019**, *58*, 596-601. Supplementary information is included after the article and contains detailed experimental methods for the synthesis and NMR analysis of CPs.

Bionanomaterials

International Edition: DOI: 10.1002/anie.201811910
German Edition: DOI: 10.1002/ange.201811910

Controlled Construction of Cyclic D/L Peptide Nanorods

Mitchell R. Silk, Biswaranjan Mohanty, Joanne B. Sampson, Martin J. Scanlon, Philip E. Thompson, and David K. Chalmers*

Abstract: Cyclic D/L peptides (CPs) assemble spontaneously via backbone H-bonding to form extended nanostructures. These modular materials have great potential as versatile bionanomaterials. However, the useful development of CP nanomaterials requires practical methods to direct and control their assembly. In this work, we present novel, heterogeneous, covalently linked CP tetramers that achieve local control over the CP subunit order and composition through coupling of amino acid side-chains using copper-activated azide–alkyne cycloaddition and disulfide bond formation. Cryo-transmission electron microscopy revealed the formation of highly ordered, fibrous nanostructures, while NMR studies showed that these systems have strong intramolecular H-bonding in solution. The introduction of inter-CP tethers is expected to enable the development of complex nanomaterials with controllable chemical properties, facilitating the development of precisely functionalized or “decorated” peptide nanostructures.

Cyclic peptides (CPs) with alternating D and L amino acids self-assemble through β -sheet-like H-bonding of the backbone amides^[1] (Figure 1 A) and are versatile building blocks for the construction of a variety of extended nanostructures.^[2] Stable structures are reported from CPs with 6, 8, 10, and 12 residues^[3] and each possesses a central pore ranging in size from 6 Å (6 residues) to 14 Å (12 residues). CP nanostructures can incorporate a variety of unnatural α , β , or γ amino acids.^[4] A wide variety of functionalization of the nanotube exterior is possible, including decoration of the tubes with polymers that are substantially larger than the CPs themselves.^[5] A variety of model applications of CP nanotubes have been demonstrated; as structural materials with charge-transfer properties,^[4d,f,6] transporters,^[4l,5e] and as bioactive compounds.^[3,7] However, the development of complex, functional CP materials is currently limited by two main factors; 1) a lack of good methods to control the number of CP monomers that H-bond together and consequently the size of the assembled nanostructure and 2) the assembly of heterogeneous nanostructures cannot be directed.

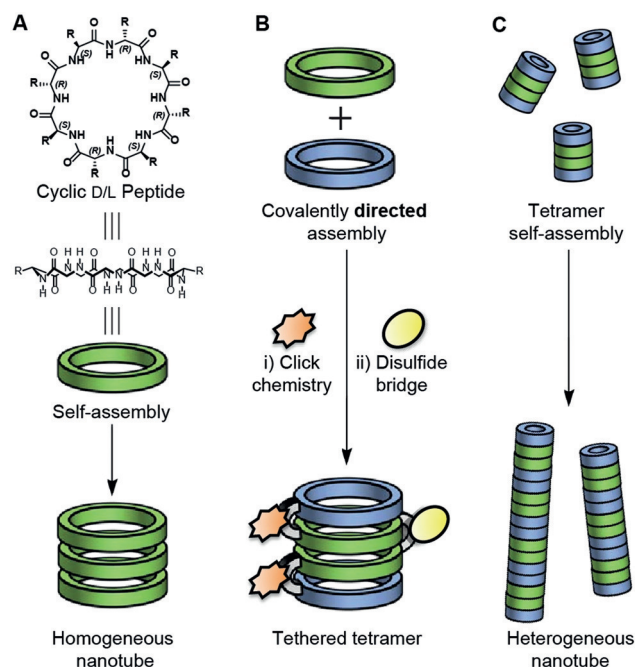


Figure 1. A) Cyclic D/L peptides (CPs) self-assemble via backbone H-bonding to form homogeneous nanotubes. B) Tethering CPs allows construction of CP multimers (such as tetramers). C) Heterogeneous nanotubes with controlled CP ordering result from the self-assembly of tetramers.

To date, most studies of CP nanotubes have focused on the construction of homogeneous self-assembled structures made from a single building block. There are only a limited number of examples of heterogeneous peptide nanotube systems^[4c,6] and there has been little investigation of methods for directing the assembly process. One apparent method to precisely direct nanotube assembly is to introduce one or more covalent linkages between CP monomers. Tethered CP homodimers have previously been produced by disulfide bond formation,^[8] metathesis of homoallylglycine containing CP monomers,^[8,9] by amide formation between Glu and Lys side chains,^[10] through photo-switchable azobenzene linkers,^[11] and by cross-linking with polymers.^[12] More recently, Fuertes et al. reported heterogeneous nanotubes assembled from CP dimers that were made using a copper-catalyzed azide–alkyne cycloaddition (CuAAC) reaction to couple reactive handles attached to peptide backbone nitrogen atoms.^[13] Herein, we describe the construction of tetrameric, heterogeneous cyclic D/L peptide subunits that provide improved control over CP nanotube composition and advance our program to develop peptide nanorods of controlled structure and length. Recently,^[14] we investigated

[*] M. R. Silk, Dr. B. Mohanty, Dr. J. B. Sampson, Prof. Dr. M. J. Scanlon, Prof. Dr. P. E. Thompson, Dr. D. K. Chalmers
Medicinal Chemistry, Monash Institute of Pharmaceutical Sciences,
Monash University
381 Royal Parade, Parkville Victoria, 3052 (Australia)
E-mail: david.chalmers@monash.edu.au

Supporting information (including detailed experimental methods for peptide synthesis, tethering, analysis, DOSY NMR, cryo-TEM, and additional NMR data) and the ORCID identification number(s) for the author(s) of this article can be found under:
<https://doi.org/10.1002/anie.201811910>.

the assembly of the water-soluble CPs cyclo[(Asp-D-Leu-Lys-D-Leu)₂] (**1**) and cyclo[(Asp-D-Ala-Lys-D-Ala)₂] (**2**). In the study, we obtained the first crystal structures of extended CP nanostructures, which revealed that CP **1** assembled in the solid state to form an antiparallel H-bonded nanotube, while CP **2** crystallized in a parallel arrangement. The design of these peptides promoted an ordered assembly between resultant nanotubes in solution, in the form of rod like (CP **1**) and spherical (CP **2**) assemblies, however the systems were homogeneous in terms of CP composition. It was envisaged that by chemoselectively tethering CP subunits to one another, the precise arrangement of CPs within assembled nanotubes could be controlled to develop heterogeneous CP

nanostructures of organized composition, without disrupting the self-assembly process.

To develop ordered, heterogeneous nanotubes of the type illustrated in Figure 1C, we designed the tethered CP tetramers **8** and **9** based on the CP monomers **1** and **2**. Each tetramer is composed of CP monomers with the general structure cyclo(dXkXdXkX), where X is a nonpolar or linker amino acid and lower case letters indicate D-chirality. Note that for convenience, we chose to use linker residues with L-chirality and, as a result, the CP monomers making up **8** and **9** have the opposite chirality to **1** and **2**, but retain the same relative stereochemistry. It was envisaged that **8** and **9** could potentially form either parallel or antiparallel H-bonded

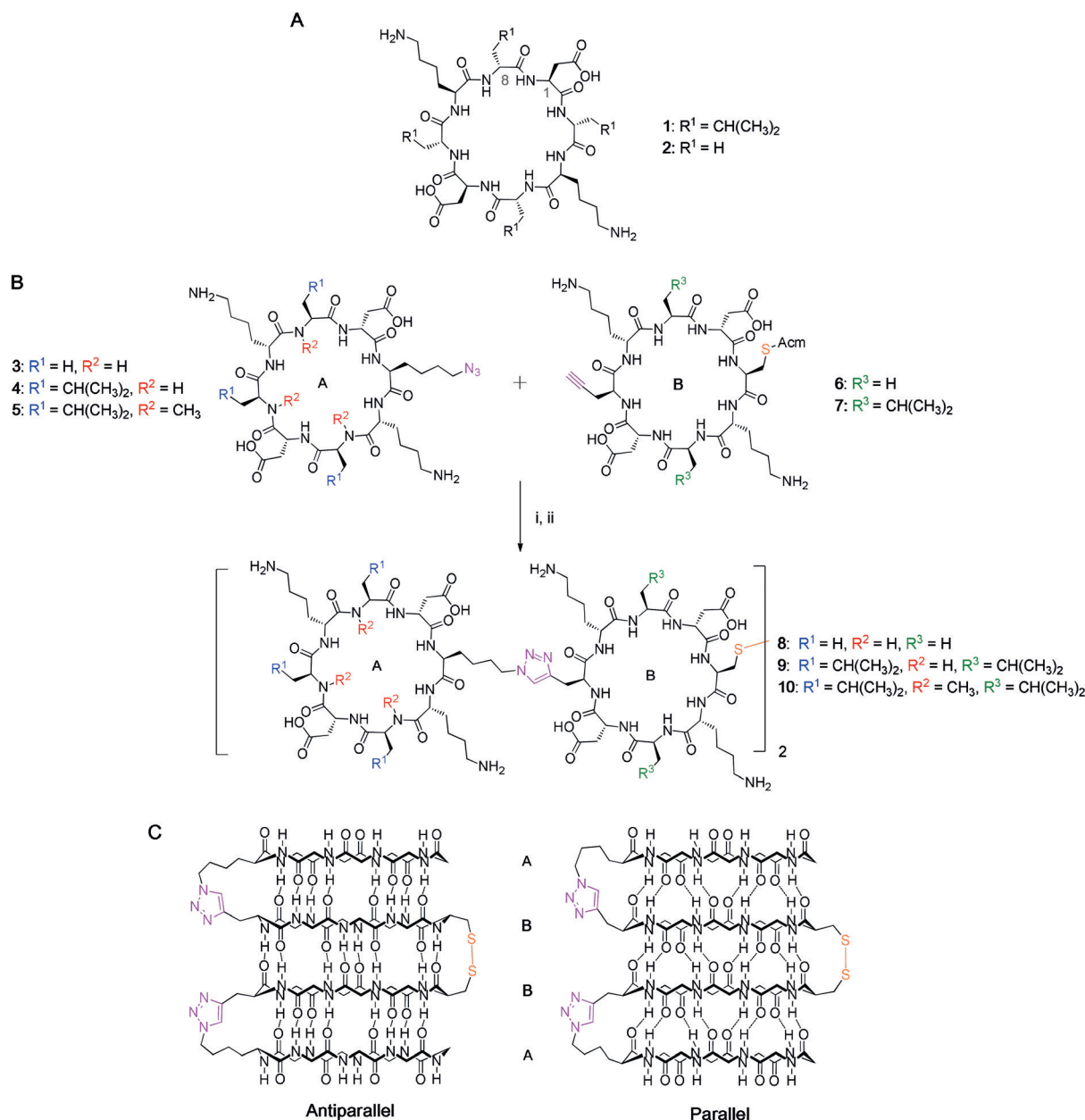


Figure 2. A) Previously reported CP monomers, **1** and **2**, which crystallize in antiparallel and parallel arrangements, respectively.^[14] B) Synthesis of covalently tethered CP tetramers **8–10**: i) 0.1 mM CuSO₄, 0.5 mM THPTA, 5 mM sodium ascorbate, 5 mM aminoguanidine, 3 h RT. ii) I₂ in glacial AcOH, 3 h under N₂. C) Possible alternative antiparallel and parallel H-bonding arrangements of tetramers **8** and **9**. In **10**, backbone N-methylation is designed to inhibit further assembly.

structures, as previously observed by crystallography.^[14] Additionally, we designed compound **10**, which incorporates *N*-Me-L-Leu residues in monomer A to inhibit H-bonding between tetramers and prevent the formation of extended rods. Note that antiparallel H-bonding creates a tetramer that is C_2 symmetric, while the parallel arrangement creates an asymmetric structure.

The CP monomers were prepared using Fmoc solid-phase synthesis with solution-phase cyclisation, as described previously.^[14] Tetramers were synthesized using a two-step procedure using orthogonal coupling chemistries (Figure 2). The chemically distinct peptide monomers (denoted A & B), containing azide and alkyne functionalized side chains, were first linked to form a heterodimer (AB) by CuAAC coupling of the azidolysine and propargylglycine residues. Acetamidomethyl (Acm) protection of the Cys residues was used to prevent interference of unprotected Cys thiol groups with the CuAAC reaction. The AB heterodimers were purified by HPLC with yields of 50–60% before use in the subsequent coupling reaction. Simultaneous deprotection and oxidation of cysteine residues afforded the disulfide-bridged ABBA CP tetramers. High peptide concentrations in glacial AcOH (10 mg mL^{-1}) facilitate intermolecular coupling and prevent over-oxidation (that is, production of sulfonic acids). The final CP tetramers were obtained in overall yields of 25–36% over the two tethering and purification steps. The identity of the products was confirmed by NMR and mass spectrometry (Supporting Information, Figures S1–S15).

The potential for supramolecular assembly of the tetramers was investigated by cryo-transmission electron microscopy (cryo-TEM) (Figure 3, top). Compounds were dissolved in

water at a concentration of 2 mM, the samples were mounted on copper-supported holey carbon grids and were frozen within 30 min of dissolution. Under the cryo-TEM conditions, the Ala tetramer (**8**) was observed to assemble into a highly ordered nanomaterial with regular striations approximately 4 nm thick throughout the sample. The striations are extensive and appear as a single layer, suggesting that the compound may have assembled into sheets of fibers at the air-liquid interface. Exhibiting a different form, the Leu tetramer (**9**) makes fibrous assemblies of up to $5 \text{ nm} \times 75 \text{ nm}$. The dimensions of the fibers suggest bundles of CP rods, as a singular backbone H-bonded tetramer is approximately $2 \text{ nm} \times 2 \text{ nm}$. The capped tetramer (**10**) produced irregular and diverse aggregates, but did not provide any evidence of extended nanostructures. Dynamic light scattering (DLS) studies further support the solution aggregation of the tetramers (Figure 3, bottom). Compound **9** formed the largest structures with nominal average diameters of approximately 33 nm. We note that particle sizing by DLS makes assumptions that the particle is spherical and the reported aggregate sizes of elongated structures, such as nanotubes, should be regarded as nominal.

The folding of individual tetramers in solution was investigated by NMR using 1D and 2D ^1H spectroscopy (90:10 $\text{H}_2\text{O}/\text{D}_2\text{O}$), diffusion-ordered spectroscopy (DOSY), and by ^1H -D exchange experiments in D_2O . The 1D ^1H spectra for **1**, **8**, and **9** are sharp with well-dispersed amide resonances, suggesting that they form well-organized, folded structures that undergo concentration-dependent assembly (Supporting Information, Figure S2). Heteronuclear correlation NMR provides further insight into tetramer structure. Although we can only partially assign the individual amide resonances with current data (see Supporting Information, Figure S7), the spectrum of the Ala tetramer **8** (Figure 4A) contains 21 distinct amide signals, which is fewer than the total number of residues (32), implying that the tetramer adopts conformation that is not entirely symmetrical or occupies multiple conformational states (or both). Two triazole proton signals are present in the ^1H spectrum (Supporting Information, Figure S2). In contrast, the spectrum of tetramer **9** (Figure 4B) has 16 amide signals and a single triazole proton signal, indicating that the 32-residue peptide adopts a symmetrical conformation (assignments in Figure S8 in the Supporting Information). Spectra of compound **10** (Supporting Information, Figure S15) contain more than 15 resonances showing that the incorporation of the *N*-Me-L-Leu residues perturbs the symmetrical structure of **9**. Reduction of the disulfide bridge in compounds **8** and **9** causes large changes in the spectra suggesting that the bridge organizes the structures (Supporting Information, Figures S9–S15), while DOSY NMR indicates that the tetramers behave primarily as individual subunits (Supporting Information Figures S16, S17, and Table S1).

The internal H-bonding of the nanostructures was studied using ^1H -D exchange measurements. Figure 5A plots the decay of individual amide H^N resonances in CP **1** on exchange with D_2O . Significantly, Leu-4,8 and Leu-2,6 have half-lives of 24 and 20 min, respectively, while the Asp and Lys residues have half-lives of 2.0 and 2.3 min, respectively. Figure 5B

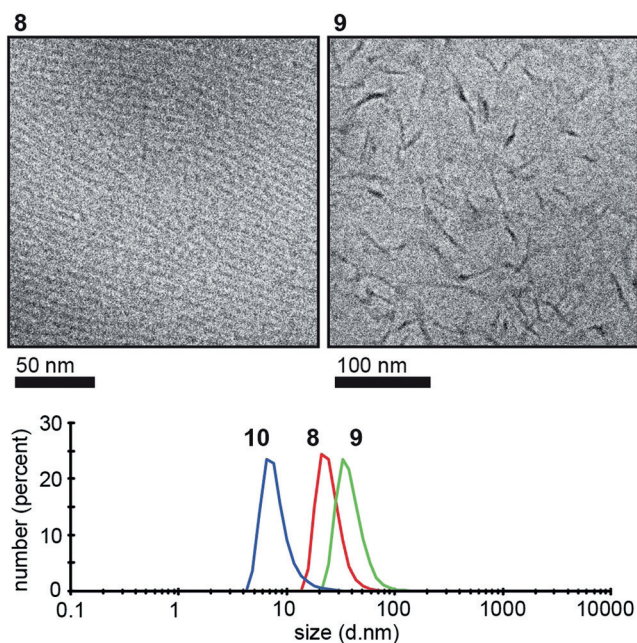


Figure 3. Cryo-TEM images of CP tetramers frozen in water at 10 mg mL^{-1} . Ala tetramer **8** forms a highly ordered fibrous network with a fiber thickness of approximately 4 nm. Leu tetramer **9** forms fibrous structures of approximately $5 \times 75 \text{ nm}$. DLS provides qualitative comparison of average assembly size in solution.

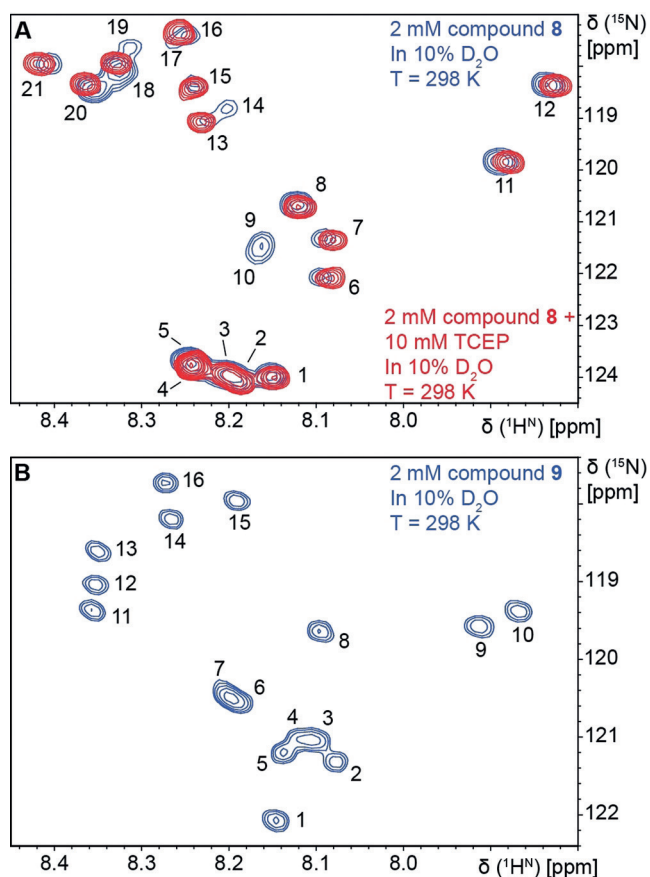


Figure 4. 2D SOFAST [^{15}N , ^1H] HMQC spectra with peak counts. A) Compound **8** before (blue) and after (red) disulfide reduction with TCEP. There are more than 16 resonances prior to reduction, suggesting multiple conformational states are present. B) Compound **9**. 16 amide environments are observed, consistent with a symmetrical antiparallel configuration. Reduction of compound **9** results in gross broadening (Supporting Information, Figures S10 and S13).

plots total amide integrals for all compounds in which the exchange of individual residues cannot be quantitated due to convolution of signals. It is clear from the faster signal decay that the backbone of **8** is more solvent accessible, whilst those of **9** and **10** contain residues that are significantly shielded from the solvent.

Taken together, the NMR studies provide an image of the CP materials in bulk solution. First, considering CP **1**: the NMR spectra show that this peptide adopts a symmetrical conformation with the Leu amides protected from the solvent. This is consistent with CP **1** forming an antiparallel dimer with association occurring via the Leu backbone amides and with the Asp and Lys amides projecting into the solvent, as shown in Figure 6A. The diffusion measurements are also consistent with the dominant form in solution being a dimer with some higher order assembly. Second, the NMR spectra of tetramers **8** and **9** are consistent with the formation of monomeric nanostructures in solution. The ^1H -D exchange experiments show that, in the Leu tetramer **9**, some backbone H^{N} groups are protected from exchange, consistent with the formation of long-lived intramolecular H-bonds. Based on the H-bond information obtained for **1**, we expect that more-

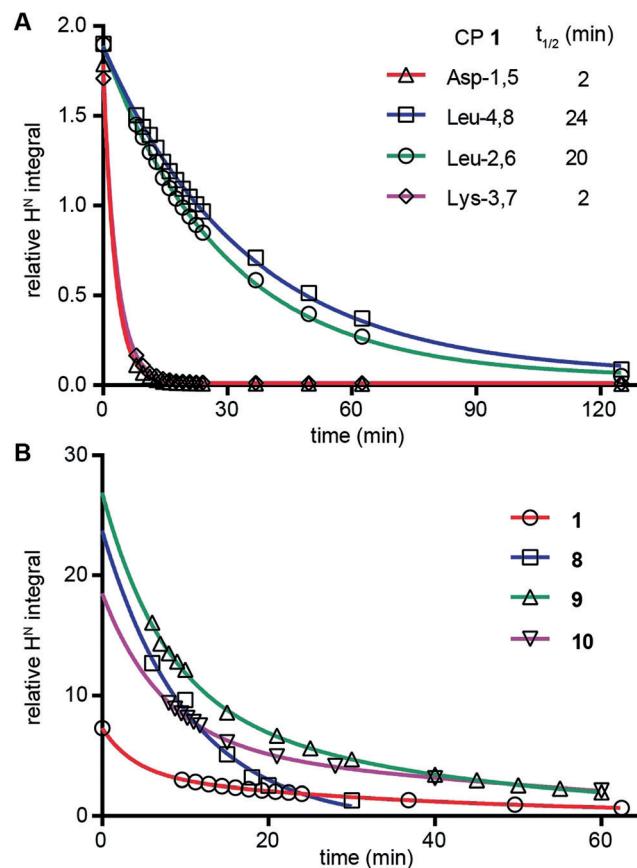


Figure 5. ^1H -D exchange measurements of backbone amides in D_2O . A) Individual amide protons in compound **1** at 8 mM. Half-lives are calculated from the fitted exponential function. B) Total integral of all amide protons. Two-component exponential fits are shown as a guide. See Figures S18–S20 in the Supporting Information for sample spectra.

stable Leu-Leu H-bond interactions form between two of the three peptide interfaces and likely result in the folding arrangement shown in Figure 6B, where the central interface is formed via weaker Asp-Lys H-bonding. In contrast, the backbone H^{N} groups of **8** exchange at an intermediate rate, faster than observed for **9**, but slower than the fast exchanging Asp and Lys H^{N} groups observed in compound **1**. This indicates that **9** forms the more stable folded structure with symmetry that is consistent with an antiparallel H-bonded conformation. Third, the *N*-methylated tetramer **10** clearly adopts an asymmetric folded structure in solution, which is distinctly different from **8** and **9**. The *N*-Me-L-Leu residues prevent Leu-Leu H-bond interactions in the outer CP interfaces, as for **1** and **9**, and disrupt the nanotube structure. Finally, we observe that, although the NMR studies clearly show freely diffusing tetramers at concentrations of 0.25–2 mM, at high concentrations, solutions of the CP monomers and tetramers are turbid, which suggests the presence of large aggregates that are not expected to be observable by NMR, but can be seen by cryo-TEM or DLS. This suggests that NMR provides only a partial view of the species present in solution.

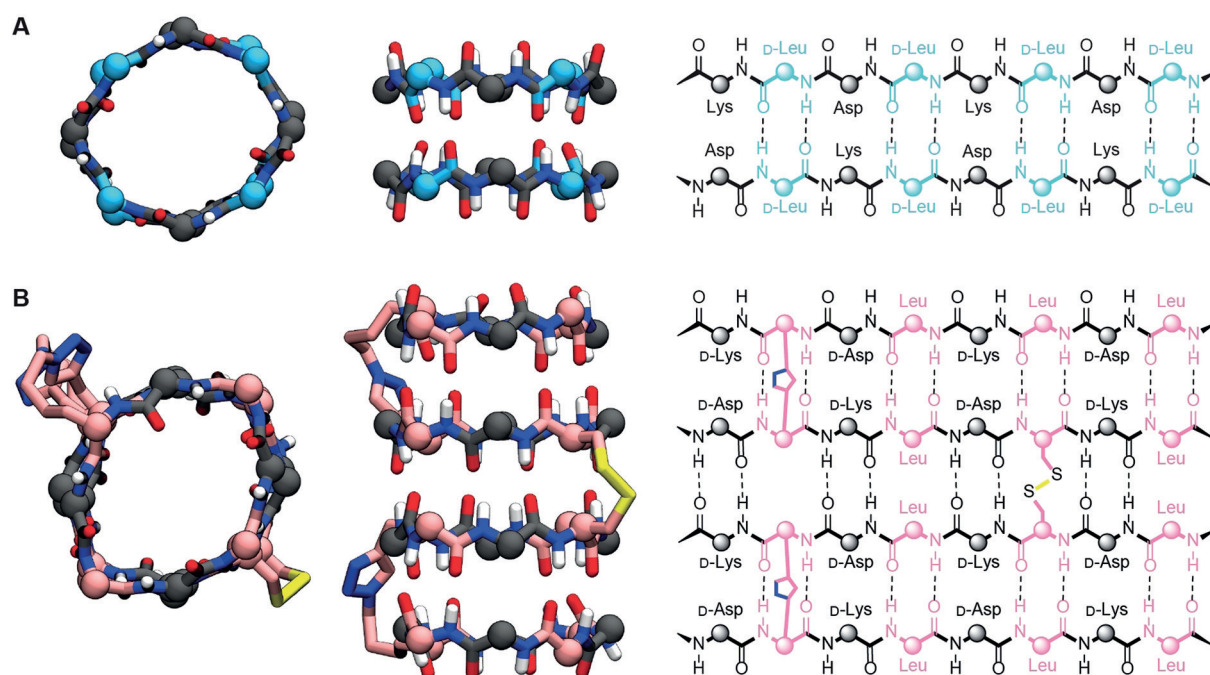


Figure 6. A) Model of an antiparallel H-bonded CP 1 dimer where D-Leu residues (blue) are H-bonded to one another and the L-Asp and L-Lys residue (black) backbone H^N and C=O are projecting into the solvent. The Leu-Leu H-bond interface is substantially stronger than the alternative Asp-Lys H-bond interface, as determined by ¹H-D exchange experiments. B) Model of an antiparallel H-bonded CP tetramer 9 folded such that L-Leu residues (pink) are H-bonded to one another between outer peptides, while the inner peptides are H-bonded between D-Asp and D-Lys residues (black). Side-chains are omitted and spheres used to indicate C α atoms.

In conclusion, side-chain-tethered cyclic D/L peptide tetramers that can be prepared on the multi-milligram scale have been developed. Herein, it has been shown that the tetramers form extended nanotubes and can also exist as isolated structures in solution. Of the structures investigated here, the Leu tetramer (9) adopts a symmetrical structure and forms some long-lived backbone H-bonds. The Ala analogue also folds, but is less stable and NMR spectroscopy shows the presence of multiple conformations. The attempt to use backbone methylation to prevent higher-order tetramer assembly was unsuccessful. Incorporation of Leu backbone *N*-methyl groups (10) disrupted nanotube formation. Overall, this work supports CP tethering as a versatile approach that, when compared to undirected self-assembly, will provide better control over the chemical and physical properties of designed CP nanotubes and enable the development of precisely functionalized or “decorated” peptide nanostructures. This approach should ultimately provide a route to the development of complex designed nanomaterials or discrete pseudo-proteins. We are working towards these goals.

Acknowledgements

M.R.S. acknowledges an RTP scholarship provided by the Australian Government. J.B.S. acknowledges the Leverhulme Trust for a Study Abroad Studentship. The authors acknowledge use of the facilities and the assistance of Adam Costin and Simon Crawford at the Monash Ramaciotti Centre for Cryo-Electron Microscopy.

Conflict of interest

The authors declare no conflict of interest.

Keywords: cyclic peptides · nanotubes · self-assembly

How to cite: *Angew. Chem. Int. Ed.* **2019**, *58*, 596–601
Angew. Chem. **2019**, *131*, 606–611

- [1] a) M. R. Ghadiri, J. R. Granja, R. A. Milligan, D. E. McRee, N. Khazanovich, *Nature* **1993**, *366*, 324–327; b) M. R. Ghadiri, K. Kobayashi, J. R. Granja, R. K. Chadha, D. E. McRee, *Angew. Chem. Int. Ed. Engl.* **1995**, *34*, 93–95; *Angew. Chem.* **1995**, *107*, 76–78.
- [2] a) N. Rodríguez-Vázquez, M. Amorin, J. R. Granja, *Org. Biomol. Chem.* **2017**, *15*, 4490–4505; b) R. Chapman, M. Danial, M. L. Koh, K. A. Jolliffe, S. Perrier, *Chem. Soc. Rev.* **2012**, *41*, 6023–6041.
- [3] J. T. Fletcher, J. A. Finlay, M. E. Callow, J. A. Callow, M. R. Ghadiri, *Chem. Eur. J.* **2007**, *13*, 4008–4013.
- [4] a) W. S. Horne, C. D. Stout, M. R. Ghadiri, *J. Am. Chem. Soc.* **2003**, *125*, 9372–9376; b) M. Amorin, L. Castedo, J. R. Granja, *J. Am. Chem. Soc.* **2003**, *125*, 2844–2845; c) R. J. Brea, M. Amorin, L. Castedo, J. R. Granja, *Angew. Chem. Int. Ed.* **2005**, *44*, 5710–5713; *Angew. Chem.* **2005**, *117*, 5856–5859; d) W. S. Horne, N. Ashkenasy, M. R. Ghadiri, *Chem. Eur. J.* **2005**, *11*, 1137–1144; e) M. Amorin, L. Castedo, J. R. Granja, *Chem. Eur. J.* **2005**, *11*, 6543–6551; f) N. Ashkenasy, W. S. Horne, M. R. Ghadiri, *Small* **2006**, *2*, 99–102; g) R. J. Brea, L. Castedo, J. R. Granja, *Chem. Commun.* **2007**, 3267–3269; h) M. Amorin, L. Castedo, J. R. Granja, *Chem. Eur. J.* **2008**, *14*, 2100–2111; i) C. Reiriz, L. Castedo, J. R. Granja, *J. Pept. Sci.* **2008**, *14*, 241–249; j) R. Hourani, C. Zhang, R. van der Weegen, L. Ruiz, C. Li, S. Keten,

- B. A. Helms, T. Xu, *J. Am. Chem. Soc.* **2011**, *133*, 15296–15299; k) L. Li, H. Zhan, P. Duan, J. Liao, J. Quan, Y. Hu, Z. Chen, J. Zhu, M. Liu, Y.-D. Wu, J. Deng, *Adv. Funct. Mater.* **2012**, *22*, 3051–3056; l) J. Montenegro, M. R. Ghadiri, J. R. Granja, *Acc. Chem. Res.* **2013**, *46*, 2955–2965.
- [5] a) R. Chapman, K. A. Jolliffe, S. Perrier, *Aust. J. Chem.* **2010**, *63*, 1169–1172; b) R. Chapman, K. A. Jolliffe, S. Perrier, *Polym. Chem.* **2011**, *2*, 1956; c) R. Chapman, K. A. Jolliffe, S. Perrier, *Adv. Mater.* **2013**, *25*, 1170–1172; d) R. Chapman, G. G. Warr, S. Perrier, K. A. Jolliffe, *Chem. Eur. J.* **2013**, *19*, 1955–1961; e) M. Danial, C. M. Tran, P. G. Young, S. Perrier, K. A. Jolliffe, *Nat. Commun.* **2013**, *4*, 2780; f) J. Couet, J. D. Samuel, A. Kopyshv, S. Santer, M. Biesalski, *Angew. Chem. Int. Ed.* **2005**, *44*, 3297–3301; *Angew. Chem.* **2005**, *117*, 3361–3365; g) J. Couet, M. Biesalski, *Macromolecules* **2006**, *39*, 7258–7268; h) J. Couet, M. Biesalski, *Small* **2008**, *4*, 1008–1016; i) S. Loschonsky, J. Couet, M. Biesalski, *Macromol. Rapid Commun.* **2008**, *29*, 309–315; j) J. Y. Rho, J. C. Brendel, L. R. MacFarlane, E. D. H. Mansfield, R. Peltier, S. Rogers, M. Hartlieb, S. Perrier, *Adv. Funct. Mater.* **2018**, *28*, 1704569.
- [6] M. Mizrahi, A. Zakrassov, J. Lerner-Yardeni, N. Ashkenasy, *Nanoscale* **2012**, *4*, 518–524.
- [7] A. Montero, P. Gastaminza, M. Law, G. Cheng, F. V. Chisari, M. R. Ghadiri, *Chem. Biol.* **2011**, *18*, 1453–1462.
- [8] T. D. Clark, K. Kobayashi, M. R. Ghadiri, *Chem. Eur. J.* **1999**, *5*, 782–792.
- [9] T. D. Clark, M. R. Ghadiri, *J. Am. Chem. Soc.* **1995**, *117*, 12364–12365.
- [10] J. H. van Maarseveen, W. S. Horne, M. R. Ghadiri, *Org. Lett.* **2005**, *7*, 4503–4506.
- [11] a) C. Steinem, A. Janshoff, M. S. Vollmer, M. R. Ghadiri, *Langmuir* **1999**, *15*, 3956–3964; b) M. S. Vollmer, T. D. Clark, C. Steinem, M. R. Ghadiri, *Angew. Chem. Int. Ed.* **1999**, *38*, 1598–1601; *Angew. Chem.* **1999**, *111*, 1703–1706.
- [12] R. Gokhale, J. Couet, M. Biesalski, *Phys. Status Solidi A* **2010**, *207*, 878–883.
- [13] A. Fuertes, H. L. Ozores, M. Amorin, J. R. Granja, *Nanoscale* **2017**, *9*, 748–753.
- [14] M. R. Silk, J. Newman, J. C. Ratcliffe, J. F. White, T. Caradoc-Davies, J. R. Price, S. Perrier, P. E. Thompson, D. K. Chalmers, *Chem. Commun.* **2017**, *53*, 6613–6616.

Manuscript received: October 17, 2018

Accepted manuscript online: November 19, 2018

Version of record online: December 5, 2018

Chapter 3 – Appendix

Controlled construction of cyclic D/L peptide nanorods
– Supplementary Information

Supporting Information

Controlled Construction of Cyclic D/L Peptide Nanorods

*Mitchell R. Silk, Biswaranjan Mohanty, Joanne B. Sampson, Martin J. Scanlon,
Philip E. Thompson, and David K. Chalmers**

Supporting Information

Table of Contents

Experimental Procedures	3
Cyclic Peptide Monomer Synthesis	3
CP Tetramer Synthesis.....	3
Peptide Products	4
LCMS and NMR Spectroscopy.....	5
Cryo-TEM	5
Results and Discussion	6
CP Tetramer MALDI Analysis.....	6
1D ¹ H NMR Studies	7
2D NMR Studies & Assignments	9
NMR Studies of Disulfide Reduction.....	13
Diffusion NMR (DOSY) Studies	20
H-D Exchange NMR Studies	22
References	24

SUPPORTING INFORMATION

Experimental Procedures

Side-chain protected linear peptides were synthesised by automated methods using Fmoc chemistry on acid-labile 2-chlorotrityl chloride resin. Head-to-tail cyclisation was performed on side chain-protected peptide over 2 days in DMF solution using PyClock/DIPEA as the coupling agent. Following side-chain deprotection, the crude peptides were purified by preparative reverse-phase HPLC. Tethering of the CPs was achieved through a two-step procedure involving copper-activated azide-alkyne cycloaddition followed by oxidation, with purification by prep. HPLC after each coupling was performed. General synthetic methods are described below.

Cyclic Peptide Monomer Synthesis:

Coupling of the first amino acid: 2-chlorotrityl chloride resin (83 mg, resin loading 1.2 mmol g⁻¹, 0.1 mmol) was swelled in 5 mL of CH₂Cl₂ for 30 minutes in a sinter-fitted syringe. The resin was then drained and treated with 1 equivalent (relative to resin capacity) of Fmoc-amino acid dissolved in CH₂Cl₂ (4 mL). To the resin mixture was added 6 equivalents of DIPEA relative to amino acid and the resulting mixture was agitated at room temperature overnight. The resin was drained and washed with DMF (3 x 3 mL) and treated with MeOH (2 x 3 mL) to cap any unreacted sites. The resin was then washed with DMF (3 x 3 mL) and transferred to an SPPS reaction vessel.

Automated synthesis of linear peptides: The linear peptides were prepared using an automated solid-phase peptide-synthesiser (Protein Technologies Inc. PS3). On each coupling cycle, the resin was first washed with DMF (3 x 30 s). Fmoc deprotection was achieved using 20% piperidine in DMF (2 x 5 min) followed by washing with DMF (6 x 30 s) to provide the resin-bound free amino-terminal of the peptide. Couplings used three equivalents of Fmoc amino acid and 2-(6-chloro-1H-benzotriazole-1-yl)-1,1,3,3-tetramethylammonium hexafluorophosphate (HCTU), relative to resin loading. The amino acid and HCTU was dissolved in a solution of 7% DIPEA in DMF. The solution was added to the resin which was agitated at room temperature for 1 h, drained and washed with DMF (3 x 30 s). After coupling the final amino acid, a further Fmoc deprotection was performed to obtain the resin-bound peptide with free amino terminal. The resin was transferred to a sinter-fitted syringe and washed with DMF (3 x 3 mL), MeOH (3 x 3 mL) and Et₂O (3 x 3 mL).

Peptide cleavage from resin: The resin-bound linear peptide was treated with a solution of 20% 1,1,1,3,3,3-hexafluoroisopropanol (HFIP) in CH₂Cl₂ (3 x 3 mL x 10 min) and the HFIP washings were collected by filtration. The resin was then washed with CH₂Cl₂ (3 x 3 mL). The combined HFIP and CH₂Cl₂ washings were concentrated under reduced pressure and freeze-dried from 1:1 ACN/H₂O to yield the side-chain-protected linear peptide as a white powder. A sample of the peptide was deprotected and analysed by LCMS to confirm the linear sequence.

Cyclisation: The linear peptide was added to DMF (7 mg/mL) and treated with 3 equivalents of PyClock and 6 equivalents of DIPEA. The solution was stirred at room temperature for 2 days before being concentrated under reduced pressure to yield a thick oil. The oil was freeze-dried from 1:1 ACN/H₂O to yield the crude side-chain-protected cyclic peptide as an off-white solid.

Deprotection: The side chain protecting groups of the cyclic peptide were removed by treatment with a solution of TFA/TIPS/H₂O (95:2.5:2.5 v/v, 2 mL) for 3 h. The TFA was evaporated using a stream of N₂ gas and the remaining oil was then treated with ice-cold Et₂O to precipitate the peptide. The precipitate was collected by centrifugation and freeze-dried from 1:1 ACN/H₂O to yield the crude cyclic deprotected peptide as a white solid.

Purification: Peptides were purified by preparative reverse-phase HPLC using a Waters Associates liquid chromatography system (Model 600 Controller and Waters 486 Tunable Absorbance Detector) with a Phenomenex Luna C8(2) 100 Å, 10 µm, 250 x 21.2 mm column with 0.1% TFA/H₂O as buffer A and 0.1% TFA in 90% ACN/H₂O as buffer B with a flow rate of 15 mL/min.

CP Tetramer Synthesis through Monomer Tethering

Heterodimerisation by CuAAC (A + B = AB): An azide-peptide (**3**, **4** or **5**, 10 mg, ~0.01 mmol) and alkyne-peptide (**6** or **7**, 10 mg, ~0.01 mmol) were added to KH₂PO₄/K₂HPO₄ buffer (0.1 M, pH 7.1, 8.85 mL) and treated with premixed CuSO₄ and THPTA (150 µL, final conc. 0.1 and 0.5 mM respectively), amino guanidine (500 µL, 0.1 M) and sodium ascorbate (500 µL, 0.1M). Solution was stirred gently for 30 sec and left to stand for 3 to 4 hrs at room temp. Reaction progress was tracked by LCMS and the solution purified directly by prep. HPLC as per CP monomers above with a gradient of 0 to 60% buffer B over 60 mins. Purified intermediate CP dimer was then lyophilised to produce a white solid for subsequent oxidative coupling with consistent yields close to 50%.

SUPPORTING INFORMATION

Homodimerisation by Oxidation (AB + BA = ABBA): To glacial AcOH (1 mL) was added Acm-protected peptide dimer (10 mg, ~0.05 mmol). The mixture was treated with I₂ in AcOH (0.1 M, 350 µL), blanketed with N₂ gas and stirred vigorously for 3 hrs at room temp. The reaction mixture was then quenched until colourless with 0.1M sodium ascorbate, diluted to 100 mL with 0.1% TFA/H₂O and purified by prep. HPLC as per CP monomers above, with a gradient of 0 to 60% buffer B over 60 mins. CP tetramer was then isolated by lyophilisation as a white solid.

Peptide Products

3: *cyclo*[d-A-k-A-d-K(N₃)-k-A]. Purification gradient: 0-60% buffer B over 60 mins, R_T = 28.2 mins (28.2% B). Yield: 33.2 mg (38.9%) as a white solid on 0.1 mmol scale synthesis. ¹H NMR (400 MHz, DMSO-d₆) δ 12.32 (s, 2H), 8.29 (m, 2H), 8.20 (d, J = 7.1 Hz, 1H), 8.16 (d, J = 7.4 Hz, 1H), 7.99 (m, 4H), 7.63 (s, 5H), 4.59 (ddd, J = 15.6, 14.0, 7.5 Hz, 2H), 4.41 – 4.24 (m, 5H), 2.84 – 2.61 (m, 7H), 1.70 – 1.41 (m, 10H), 1.35 – 1.13 (m, 12H). HRMS [M+H]⁺ calculated: 854.4479, found: 854.4496. [M+2H]²⁺ calculated: 427.7276, found: 427.7292. [2M +H]⁺ calculated: 1707.8885, found: 1707.8912.

4: *cyclo*[d-L-k-L-d-K(N₃)-k-L]. Purification gradient: 0-60% buffer B over 90 mins, R_T = 55.5 mins (37.0% B). Yield: 41.7 mg (42.5%) as a white solid on 0.1 mmol scale synthesis. ¹H NMR (400 MHz, DMSO-d₆) δ 12.35 (s, 1H), 8.31 (m, 1H), 8.23 (m, 1H), 8.05 (m, 1H), 7.96 (m, 1H), 7.66 (s, 3H), 4.60 (dd, J = 13.6, 7.3 Hz, 1H), 4.35 (m, 3H), 3.28 (t, J = 7.0 Hz, 1H), 2.82 – 2.60 (m, 3H), 2.56 (d, J = 7.3 Hz, 1H), 1.72 – 1.17 (m, 13H), 0.95 – 0.77 (m, 9H). HRMS [M+H]⁺ calculated: 980.5887, found: 980.5896. [M+2H]²⁺ calculated: 490.7980, found: 490.7992. [2M+H]⁺ calculated: 1960.1702, found: 1960.1719.

5: *cyclo*[d-NMeL-k-NMeL-d-K(N₃)-k-NMeL]. Purification gradient: 0-60% buffer B over 90 mins, R_T = 55.8 mins (37.2% B). Yield: 16.0 mg (15.7%) as a white solid on 0.1 mmol scale synthesis. ¹H NMR (400 MHz, DMSO-d₆) δ 12.30 (s, 2H), 8.68 (m, 1H), 8.46 – 8.04 (m, 4H), 7.65 (m, 6H), 7.43 (d, J = 18.9 Hz, 1H), 6.87 (d, J = 7.7 Hz, 1H), 5.28 – 4.30 (m, 10H), 3.10 (s, 1H), 3.03 (s, 2H), 2.95 (m, 3H), 2.88 (m, 3H), 2.82 – 2.64 (m, 6H), 2.41 (dd, J = 16.0, 6.2 Hz, 1H), 1.90 – 1.09 (m, 26H), 1.02 – 0.64 (m, 18H). HRMS [M+H]⁺ calculated: 1022.6357, found: 1022.6364. [M+2H]²⁺ calculated: 511.8215, found: 511.8227. [M+Na]⁺ calculated: 1044.6176, found: 1044.6176.

6: *cyclo*[d-G(allyl)-k-A-d-C(Acm)-k-A]. Purification gradient: 0-30% buffer B over 60 mins, R_T = 32.0 mins (16.0% B). Yield: 41.8 mg (46.5%) as a white solid on 0.1 mmol scale synthesis. ¹H NMR (400 MHz, DMSO-d₆) δ 12.29 (s, 2H), 8.49 (t, J = 6.4 Hz, 1H), 8.33 – 8.24 (m, 3H), 8.13 (m, 5H), 7.63 (s, 6H), 4.66 (ddd, J = 14.2, 8.1, 6.2 Hz, 2H), 4.58 (dd, J = 14.7, 8.3 Hz, 1H), 4.49 (dd, J = 14.3, 7.3 Hz, 1H), 4.37 (m, 4H), 4.23 (ddd, J = 31.7, 13.4, 6.3 Hz, 3H), 2.87 – 2.64 (m, 11H), 1.86 (s, 3H), 1.68 – 1.20 (m, 14H), 1.15 (m, 6H). HRMS [M+H]⁺ calculated: 898.4087, found: 898.4094. [M+2H]²⁺ calculated: 449.708, found: 449.7091. [2M+H]⁺ calculated: 1795.8102, found: 1795.8085.

7: *cyclo*[d-G(allyl)-k-L-d-C(Acm)-k-L]. Purification gradient: 0-60% buffer B over 60 mins, R_T = 31.8 mins (31.8% B). Yield: 53.0 mg (54.0%) as a white solid on 0.1 mmol scale synthesis. ¹H NMR (400 MHz, DMSO-d₆) δ 12.26 (s, 2H), 8.49 (t, J = 6.3 Hz, 1H), 8.39 – 8.28 (m, 3H), 8.24 – 8.14 (m, 4H), 8.06 (d, J = 8.6 Hz, 1H), 7.63 (s, 6H), 4.76 – 4.57 (m, 4H), 4.57 – 4.37 (m, 6H), 4.23 (ddd, J = 19.5, 13.6, 6.4 Hz, 3H), 2.91 – 2.59 (m, 12H), 1.86 (s, 3H), 1.68 – 1.21 (m, 20H), 0.84 (m, 12H). HRMS [M+H]⁺ calculated: 982.5026, found: 982.5032. [M+2H]²⁺ calculated: 491.7550, found: 491.7561. [2M+H]⁺ calculated: 1963.9930, found: 1963.9974.

8: [*cyclo*(d-A-k-A-d-K(N₃)-k-A)*cyclo*(d-G(allyl)-k-A-d-C-k-A)]₂. Purification gradient: 0-60% buffer B over 30 mins, R_T = 22.0 mins (44.0% B). Yield: 12.3 mg (38.4%) over two steps as a white solid. Scale: 16 mg of each peptide monomer. ¹H NMR (600 MHz, 10% D₂O/H₂O) δ 8.42 (d, J = 7.6 Hz, 1H), 8.37 (d, J = 7.6 Hz, 1H), 8.33 (m, 2H), 8.29 – 8.07 (m, 13H), 7.89 (d, J = 8.0 Hz, 1H), 7.83 (m, 2H), 7.75 (m, 1H), 7.44 (s, 8H), 4.35 – 4.13 (m, 10H), 3.22 – 3.01 (m, 4H), 2.95 – 2.68 (m, 28H), 1.92 – 1.48 (m, 29H), 1.32 – 1.23 (m, 30H). HRMS (ESI) [M+2H]²⁺ calculated: 1679.8044, found: 1679.8082. [M+3H]³⁺ calculated: 1120.2054, found: 1120.2098. [M+4H]⁴⁺ calculated: 840.4058, found: 840.4106.

9: [*cyclo*(d-L-k-L-d-K(N₃)-k-L)*cyclo*(d-G(allyl)-k-L-d-C-k-L)]₂. Purification gradient: 0-60% buffer B over 60 mins, R_T = 37.8 mins (37.8% B). Yield: 5.3 mg (25.2%) over two steps as a white solid. Scale: 10 mg of each peptide monomer. ¹H NMR (600 MHz, 10% D₂O/H₂O) δ 8.30 (m, 4H), 8.23 – 8.05 (m, 7H), 7.95 (d, J = 8.2 Hz, 1H), 7.90 (d, J = 8.1 Hz, 1H), 7.74 (s, 1H), 7.45 (s, 5H), 4.39 – 4.10 (m, 7H), 3.17 (ddd, J = 23.4, 15.0, 7.4 Hz, 2H), 2.95 – 2.66 (m, 16H), 1.88 – 1.12 (m, 44H), 0.91 – 0.72 (m, 31H). HRMS (ESI) [M+2H]²⁺ calculated: 1890.0340, found: 1890.0409. [M+3H]³⁺ calculated: 1260.3619, found: 1260.3632. [M+3Na]³⁺ calculated: 1283.0122, found: 1283.0039.

10: [*cyclo*(d-NMeL-k-NMeL-d-K(N₃)-k-NMeL)*cyclo*(d-G(allyl)-k-L-d-C-k-L)]₂. Purification gradient: 0-60% buffer B over 60 mins, R_T = 48.0 mins (48.0% B). Yield: 5.2 mg (26.0%) over two steps as a white solid. Scale: 10 mg of each peptide monomer. ¹H NMR (600 MHz, 10% D₂O/H₂O) δ 9.49 – 8.57 (m, 2H), 8.53 – 7.79 (m, 16H), 7.74 (s, 1H), 7.73 (s, 1H), 7.68 – 7.20 (m, 13H), 5.82 – 4.84 (m, 3H), 4.53 – 3.92 (m, 8H), 3.27 – 3.03 (m, 12H), 3.02 – 2.53 (m, 39H), 2.02 – 1.10 (m, 80H), 0.94 – 0.67 (m, 60H). HRMS (ESI) [M+2H]²⁺ calculated: 1932.0809, found: 1932.0837. [M+3H]³⁺ calculated: 1288.3932, found: 1288.3947. [M+4H]⁴⁺ calculated: 966.5467, found: 966.5495.

SUPPORTING INFORMATION

LCMS:

Liquid chromatographic analysis was conducted with a Phenomenex Luna C8(2) 100 Å, 3 µm, 100 x 2.0 mm reverse-phase column. Running buffer consisted of solvent A with 0.05% TFA/H₂O and solvent B with 0.05% TFA/ACN.

NMR spectroscopy:

Monomeric peptide NMR spectra were recorded on a 400 MHz Bruker Avance III Nanobay spectrometer. 1D ¹H and 2D [¹H, ¹H]-NOESY (NOE mixing time = 600 ms), TOCSY (TOCSY mixing time = 70 ms), [¹⁵N, ¹H]-SOFAS-HMQC, ¹³C-multiplicity edited [¹³C, ¹H]-HSQC NMR as well as 2D DOSY (diffusion time = 50 ms and length of gradient = 3 ms) NMR spectra of final tetrameric products were recorded on a 600 MHz Bruker Avance III HD spectrometer with CryoProbe, at 298 K. Samples were dissolved in 10% D₂O in H₂O or 100% D₂O for ¹H-D exchange experiments. The pH of samples was measured to be 3.0 ± 0.3. All of the NMR spectra were processed using TopSpin 3.0 (Bruker BioSpin GmbH).

2D DOSY experiments were performed using the standard Bruker pulse program *ledbpgppr2s* with a gradient ramp from 5% up to 95% in 16 squared steps (TD1) calculated with AU program *dosy*. The gradient calibration value was 53.5 G/cm. DOSY data were analysed using the TopSpin T1/T2 routine with a standard equation as described previously by Wang et al.^[1] During the T1/T2 routine analysis, the integral of the aliphatic proton region was manually defined for the first FID slice. Figure S18 provides a typical DOSY plot acquired and Table S1 contains all extracted translational diffusion constants (D_T).

Cryo-TEM:

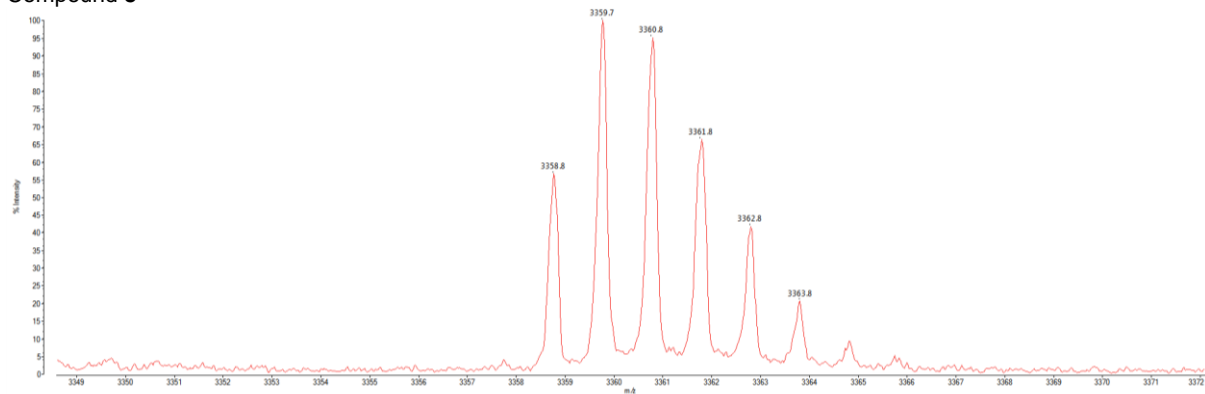
CP tetramers were dissolved at 2 mM in deionised water 30 minutes prior to preparation for cryo-TEM. A Vitrobot Mark IV (FEI, Eindhoven, the Netherlands) vitrification system was used to prepare the samples for Cryo-TEM. Humidity was kept close to 70% for all experiments, and ambient temperature was 4°C. Aliquots of each sample (3 µl) were pipetted onto a 200-mesh copper grid with R 1.2/1.3, over a holey carbon support (Quantifoil Micro Tools GmbH, Germany), glow-discharged with a Peelco Easyglow device. After 10 seconds adsorption time, the grid was blotted using filter paper for 3.5 to 4 seconds with pressure of -3 psi. The grid was then plunged into liquid ethane cooled by liquid nitrogen. Frozen grids were stored in liquid nitrogen until required. The samples were examined using a Gatan 626 cryoholder (Gatan, Pleasanton, CA, USA) and Tecnai G2 Spirit TWIN Transmission Electron Microscope (FEI, Eindhoven, The Netherlands) at an operating voltage of 120kV. Images were recorded using an Eagle 4k HS camera.

SUPPORTING INFORMATION

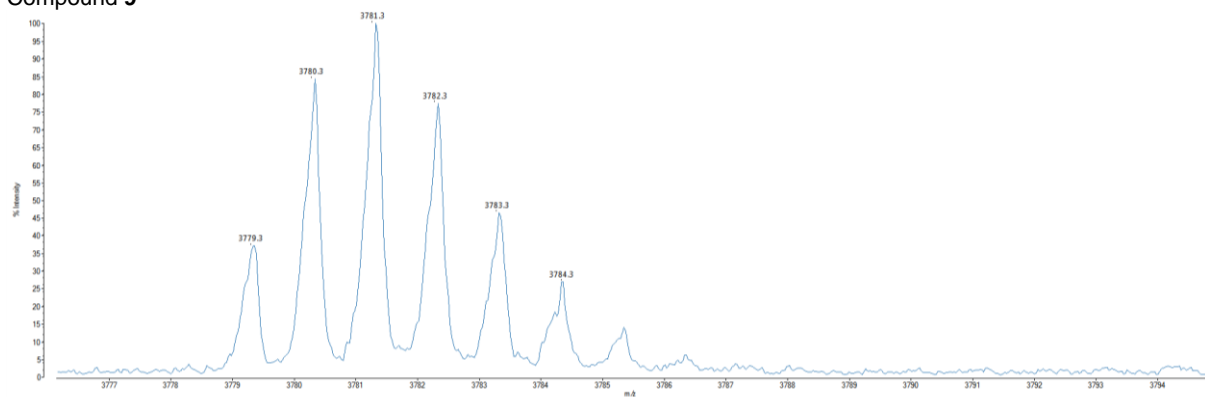
Results and Discussion

CP Tetramer MALDI Analysis:

Compound 8



Compound 9



Compound 10

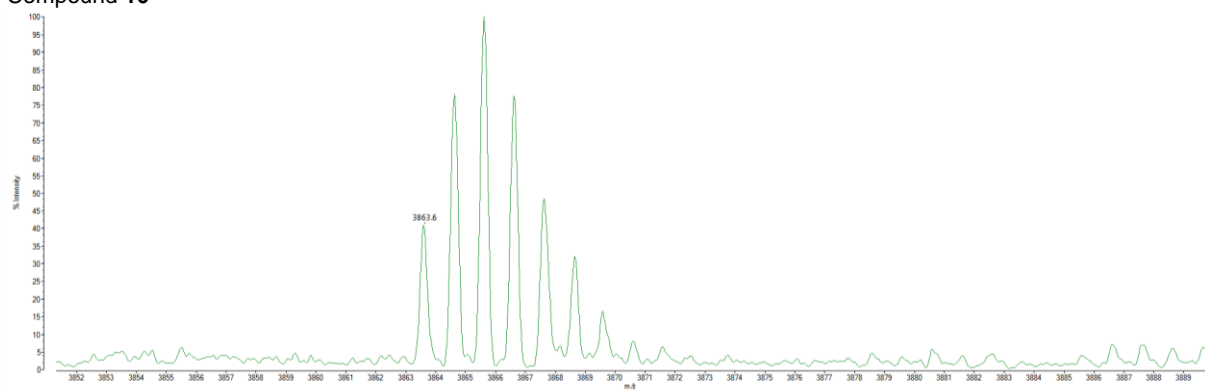


Figure S1. MALDI analysis for **8**, **9** and **10** showing isotopic masses consistent with the predicted molecular weights of 3359.7040, 3780.5140 and 3864.6760 g mol⁻¹ respectively.

SUPPORTING INFORMATION

1D ^1H NMR studies:

$1\text{D } ^1\text{H}$ spectra of the compound low field regions recorded at concentrations of 0.25-2 mM are shown in Figure S2. CP **1** is studied at 4-fold higher concentrations than the tetramers to give an equivalent concentration of CP subunits in solution. The spectrum of CP **1** contains four sharp H^{N} peaks, as expected for a symmetrical octapeptide (assignments are shown in Figure S14-16). Significantly, the spectra of tetramers **8** and **9** are sharp, with well-dispersed amide resonances, suggesting that they form well-organized, folded structures. In contrast, the low field region of **10** contains many more H^{N} signals, implying that this compound is less symmetrical and/or exists in multiple conformational forms. The $1\text{D } ^1\text{H}$ spectra of **1**, **8** and **9** all exhibit concentration-dependent changes in backbone H^{N} dispersion, suggesting a degree of concentration-dependent assembly. Concentration has little effect on the spectra of **10**, indicating that the hydrogen bonding of the backbone amides does not change greatly with peptide concentration. Multiple signals from the single triazole hydrogen atom are also present (~ 7.7 ppm).

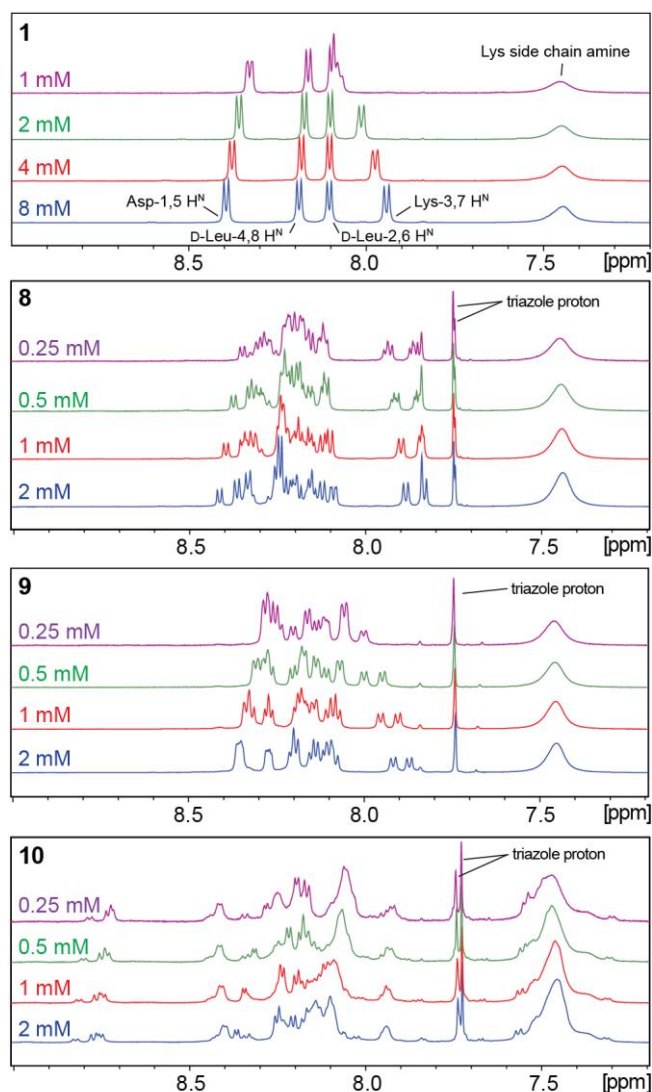


Figure S2: Concentration-dependent changes in ^1H NMR chemical shifts of signals in the low field region of monomer **1** and tetramers **8-10**. Intensities are scaled based on dilution.

SUPPORTING INFORMATION

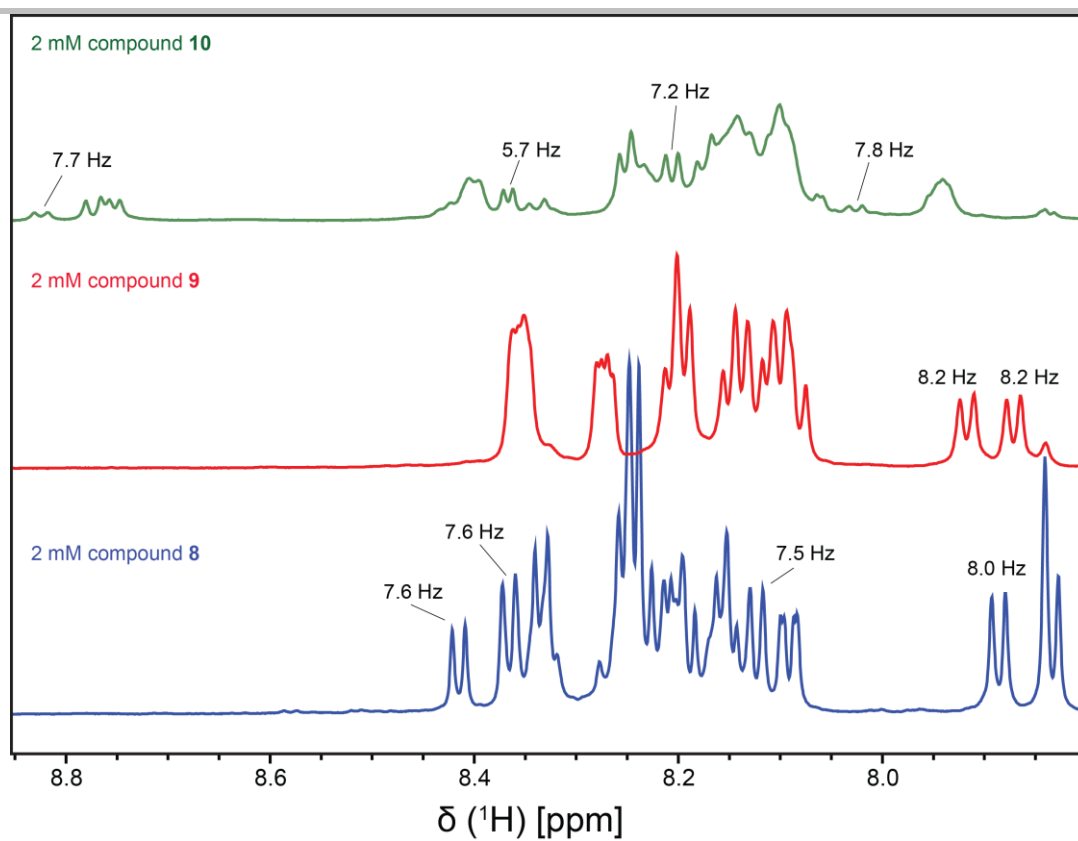


Figure S3. Amide region of the 1D ^1H NMR spectra for compounds **8**, **9** and **10** in 10% D_2O and 90% H_2O . $^3J_{\text{HN-HN}}$ coupling constants for the well-resolved backbone amide proton signals of **8** and **9** are highlighted.

SUPPORTING INFORMATION

2D NMR Studies & Assignments:

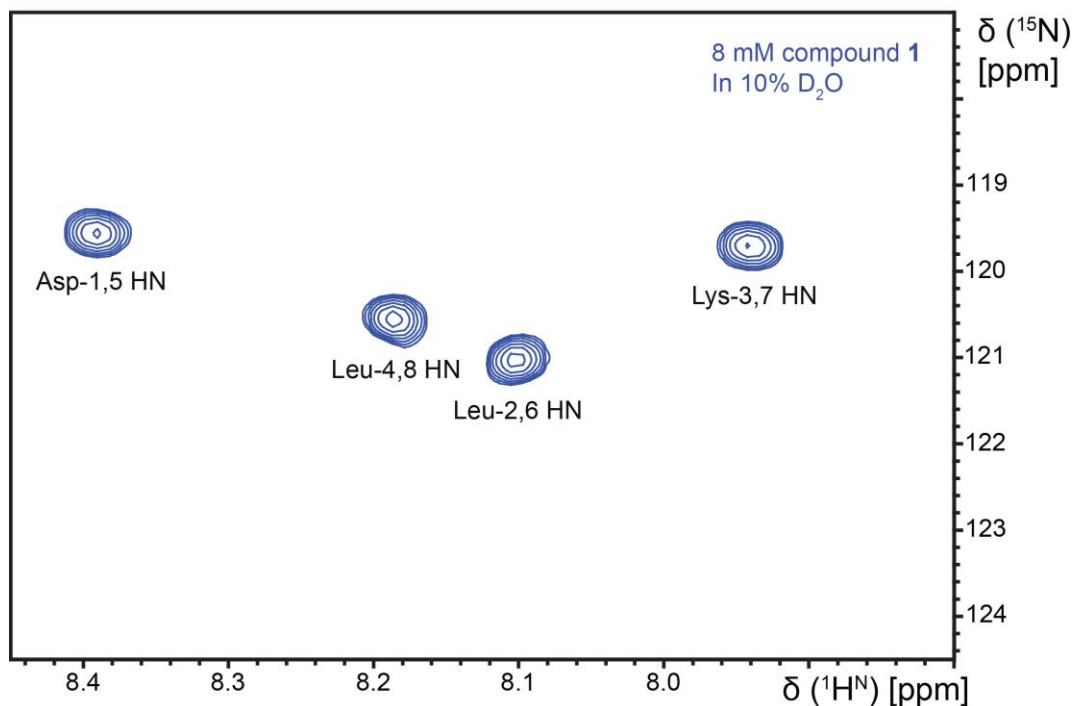


Figure S4. 2D SOFAST [^{15}N , ^1H]-HMQC study of compound 1. The structure has 4 amide proton environments each of which corresponds to two amino acids, consistent with the presence of 2-fold symmetry in the 8-residue cyclic peptide.

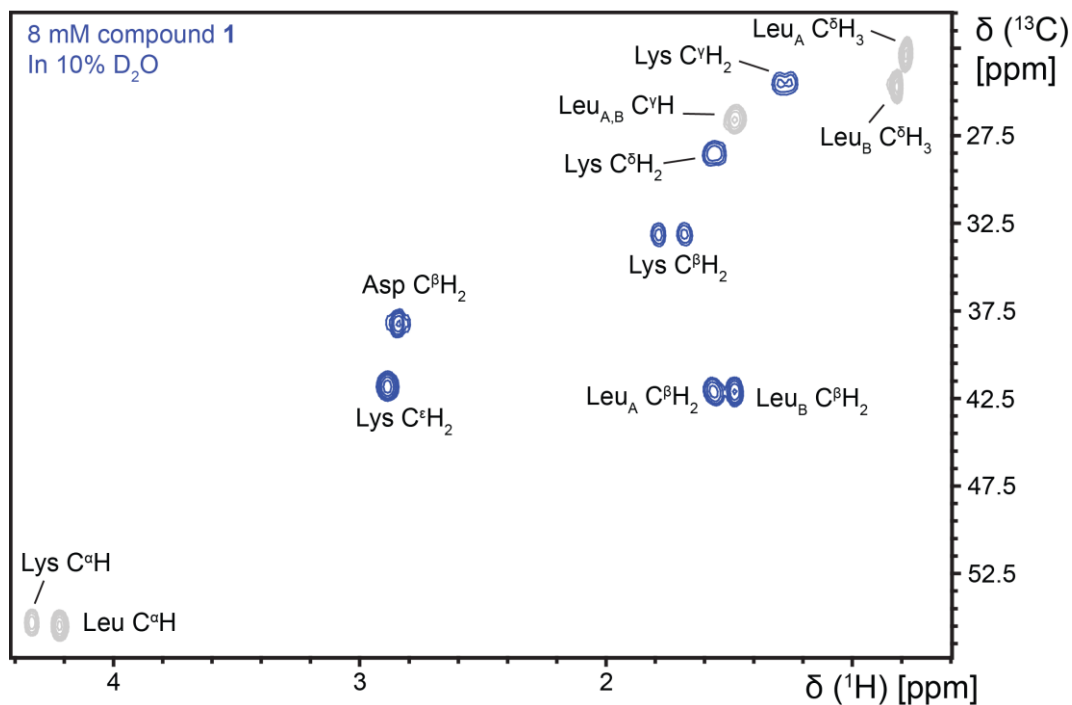


Figure S5. 2D multiplicity edited [^{13}C , ^1H]-HSQC for compound 1. The Asp C^αH signal at ~ 4.7 ppm are obscured by water suppression and is not shown.

SUPPORTING INFORMATION

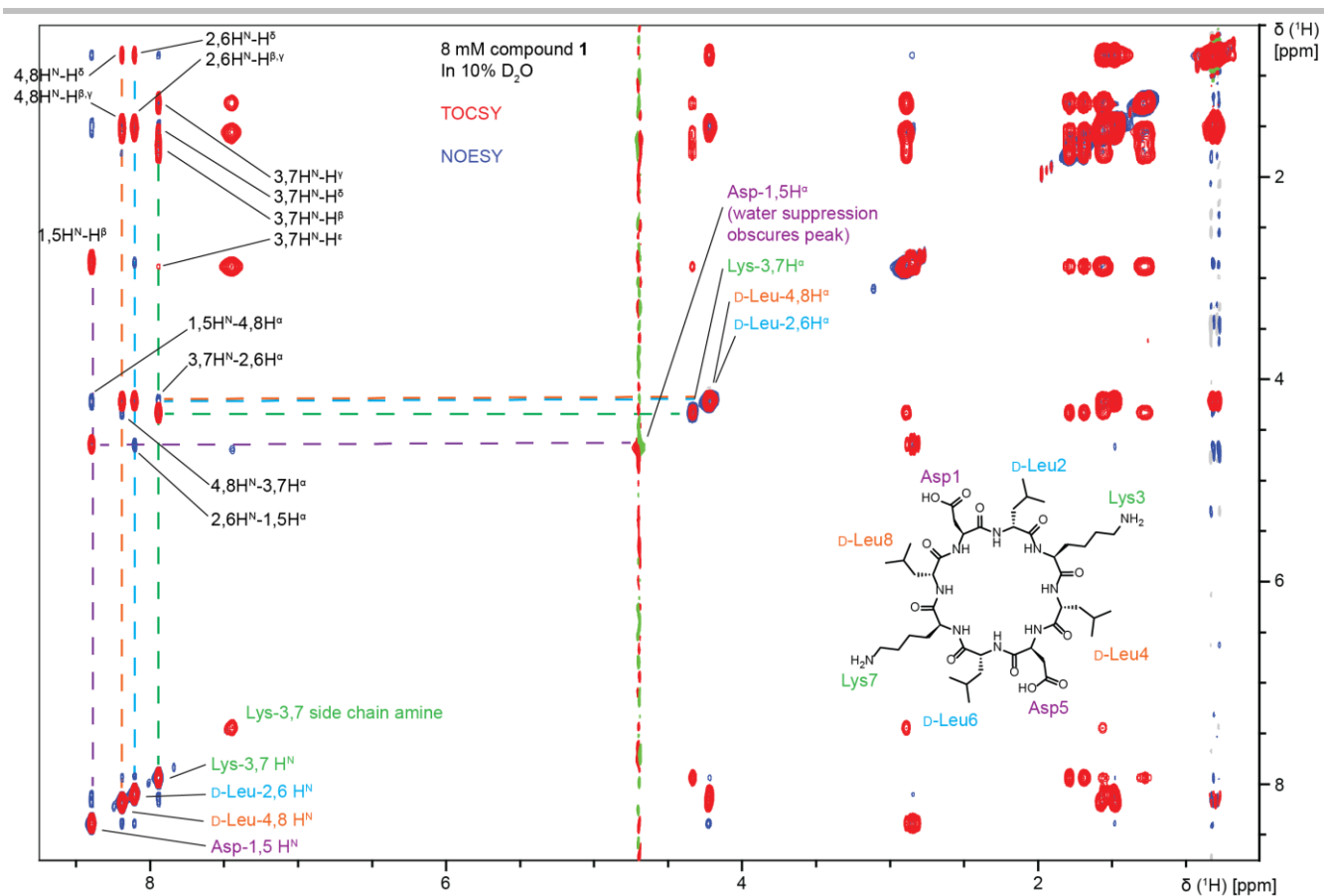


Figure S6. 2D [¹H, ¹H]-NOESY (blue) with TOCSY (red) overlay for CP 1. Coloured dashed lines show H^N-H^C TOCSY correlations. TOCSY correlations and key H^N-H^α NOESY correlations allowing residue assignments are labelled according to residues involved.

SUPPORTING INFORMATION

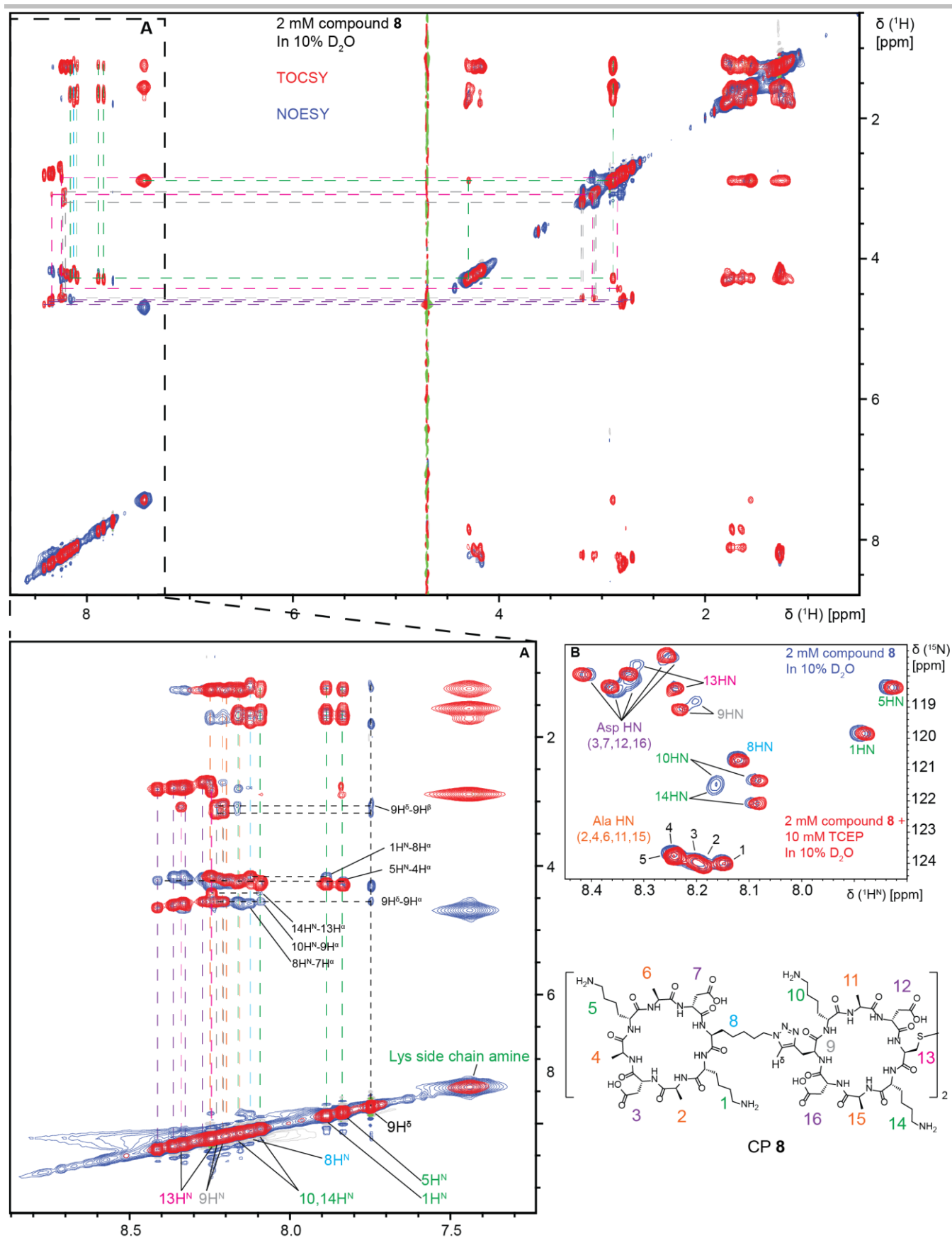


Figure S7. 2D [¹H, ¹H]-NOESY (blue) with TOCSY (red) overlay for CP **8**. Due to overlapping signals, only the residue type could be assigned for some resonances. (A) Expansion of low-field region showing backbone H^N assignments. Coloured dashed lines show H^N-H ^{α} TOCSY correlations. Key NOESY correlations are labelled according to residues involved and shown with black dashed lines. (B) 2D SOFAST [¹⁵N, ¹H]-HMQC of compound **8** with H^N assignments.

SUPPORTING INFORMATION

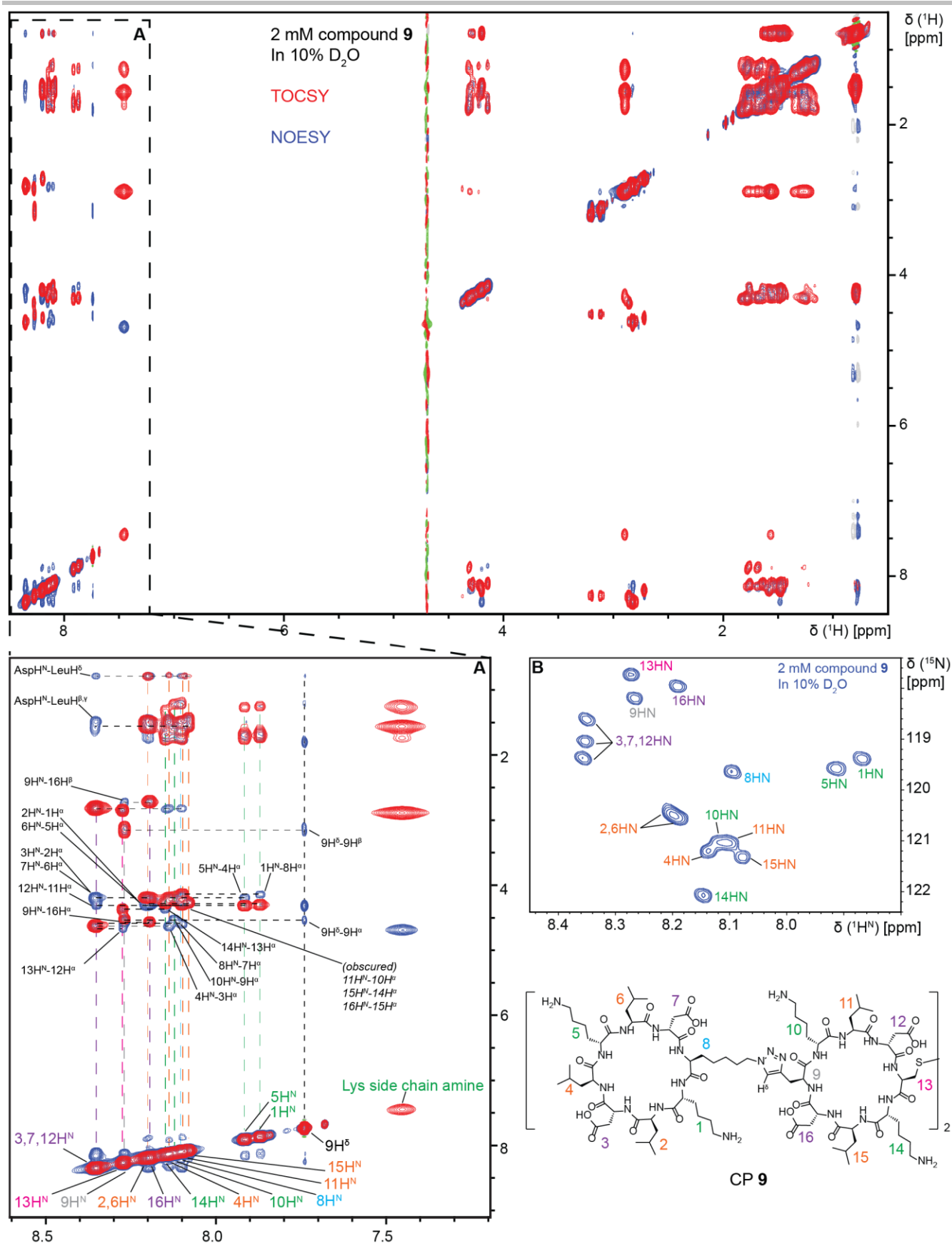


Figure S8. 2D [¹H, ¹H]-NOESY (blue) with TOCSY (red) overlay for CP **9**. (A) Expansion of low-field region showing backbone H^N assignments. Coloured dashed lines show H^N-H^C TOCSY correlations. Key NOESY correlations allowing residue assignments are labelled according to residues involved and shown with black dashed lines. (B) 2D SOFAST [¹⁵N, ¹H]-HMQC of compound **9** with H^N assignments. Overlap within similar residues prevents specific assignment (Asp-3,7,12 and Leu-2,6).

SUPPORTING INFORMATION

NMR Studies of Disulfide Reduction:

The influence of the disulfide linkage on the tetramer structure was tested by reducing the bridge using TCEP. In compound **8**, reduction results in sharp H^N signals, greatly simplified 2D [^{15}N , 1H] spectra that contain only 16 H^N signals (one for each residue in the dimer) and a single triazole proton signal in the 1D 1H spectra (Figure S9). Therefore, reduction of the disulfide in **8** removes the conformational asymmetry caused by the disulfide bridge. In contrast, reduction of tetramer **9** causes all the peaks to broaden (Figure S10, S13), suggesting that the resulting species are in intermediate exchange on the NMR timescale, which may be caused by conformational changes or dimer-dimer association. Reduction of the disulfide in **10** causes a number of peaks to appear and disappear and sharpens peak line shape but does not change the signal resolution (Figures S11 and S15).

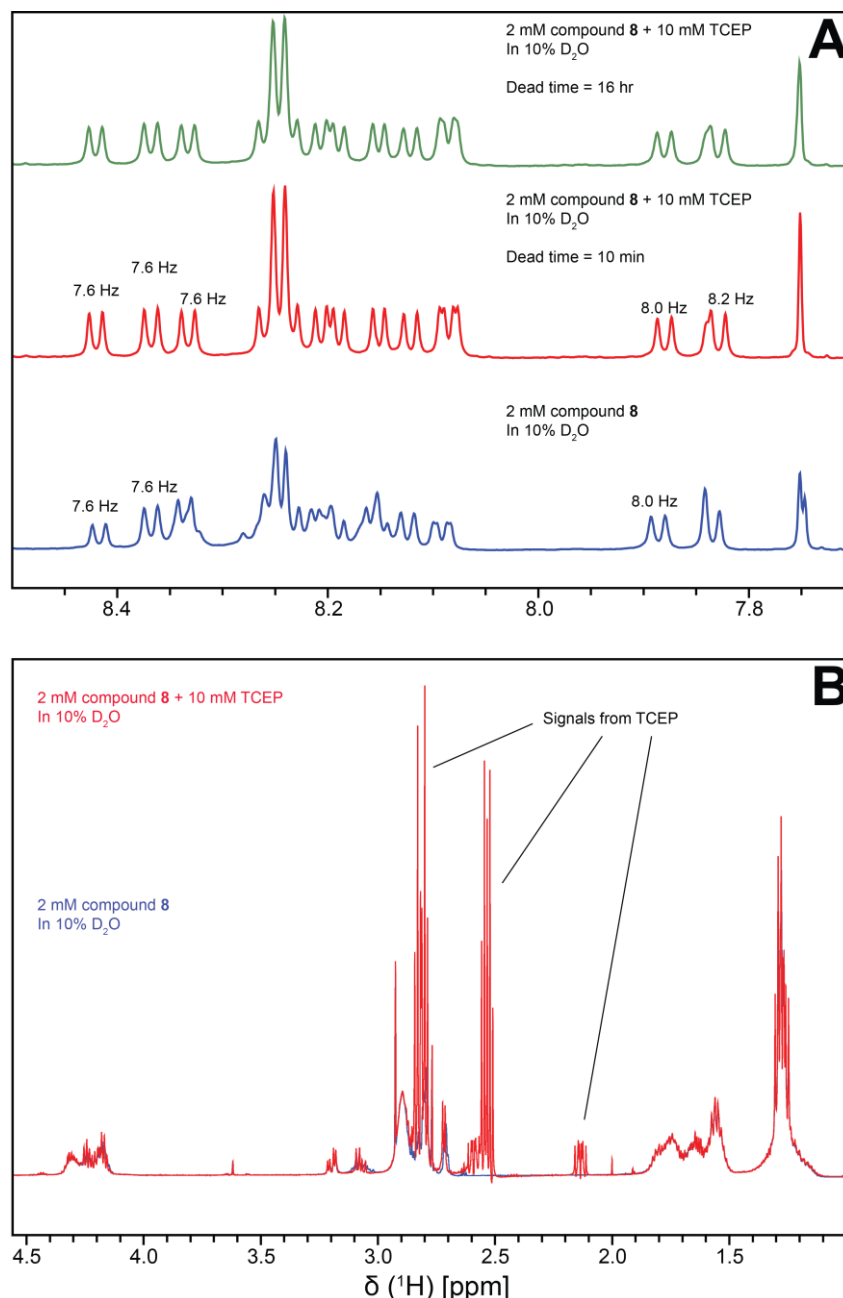


Figure S9. Overlay of 1D 1H NMR spectra of compound **8** before (A) and after (B) reduction of the disulfide bridge by addition of TCEP to generate the tethered peptide dimer. The amide proton region increases in signal resolution upon reduction (red) and no change after 16hr (green). An increase in symmetry is apparent from the convergence of triazole CH signals at 7.75 ppm upon reduction. Proton signals in the aliphatic region do not change upon reduction of disulfide bridge (except for Cys- C^{β} as shown in Figure S12), suggesting supramolecular structure may be independent of the disulfide linkage. $^3J_{HN-HN}$ coupling constants for well-resolved backbone amide proton signals are highlighted.

SUPPORTING INFORMATION

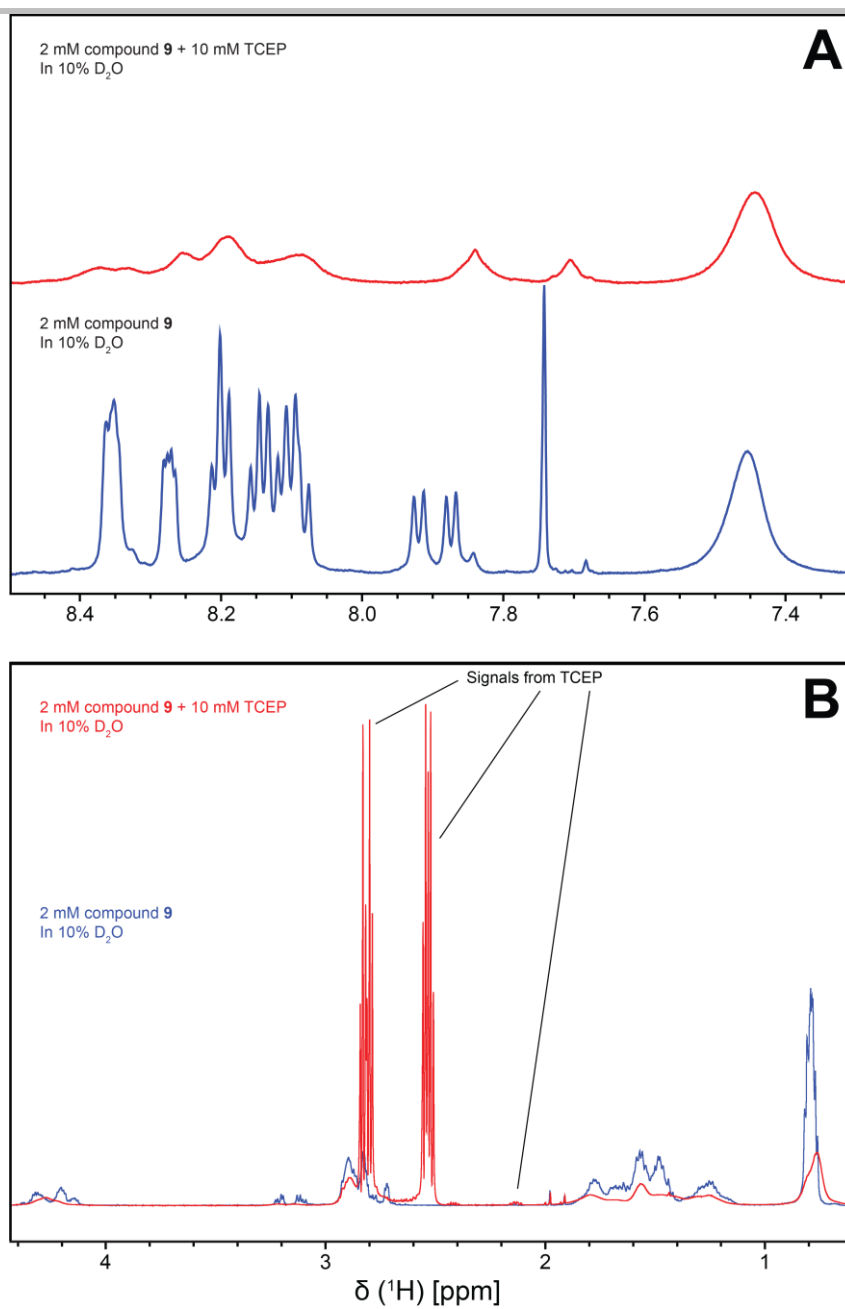


Figure S10. Overlay of 1D ^1H NMR spectra of compound **9** before (A) and after (B) reduction of the disulfide bridge by addition of TCEP to generate the tethered peptide dimer. All amide, aromatic and aliphatic signals broaden substantially upon reduction, suggesting the disulfide bridge may be directly involved in maintaining the ordered structure of compound **9**.

SUPPORTING INFORMATION

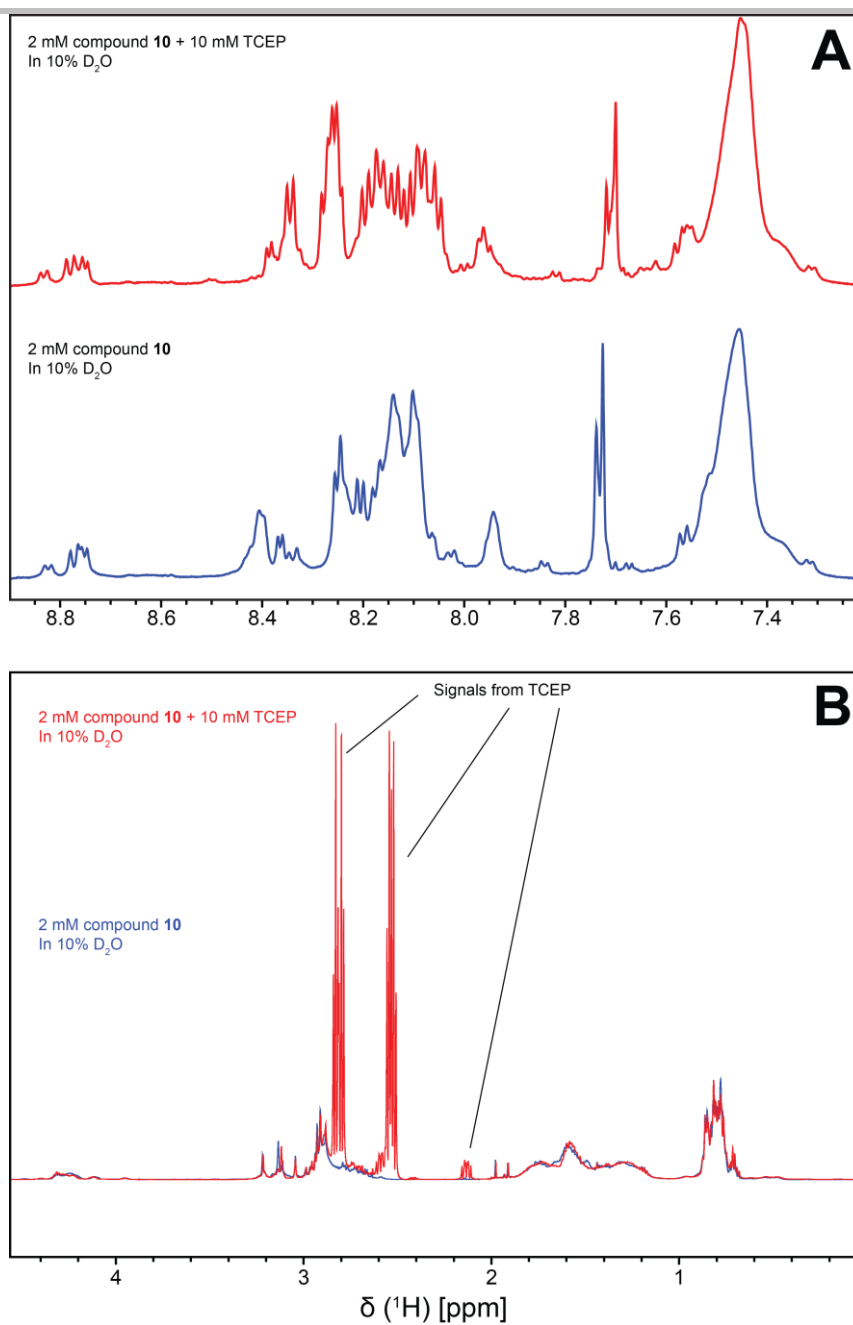


Figure S11. Overlay of 1D ^1H NMR spectra of compound **10** before (A) and after (B) reduction of the disulfide bridge by addition of TCEP to generate the tethered peptide dimer. Amide proton signals undergo moderate change in chemical shift and appearance with an increase in resolution and line sharpness. Triazole CH signals at 7.75 ppm remain separate upon reduction, indicating asymmetry in the structure of the reduced dimer. Signals in the aliphatic region undergo a moderate change in appearance upon reduction.

SUPPORTING INFORMATION

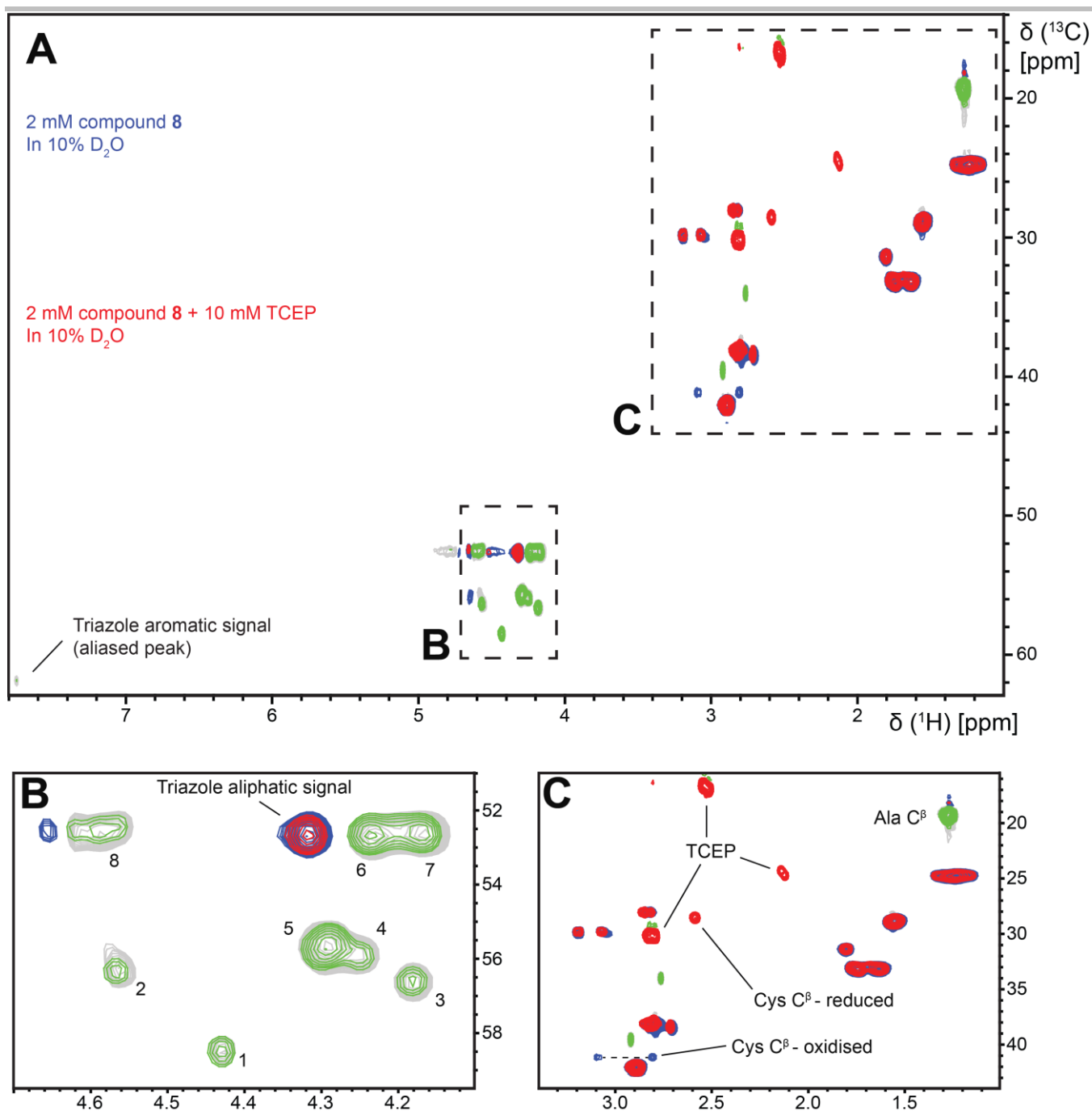


Figure S12. (A) Overlay of 2D multiplicity edited [¹³C, ¹H]-HSQC for compound **8** before (blue, grey) and after (red, green) reduction by TCEP with expansion of (B) C^α region and (C) C^β region. C^α and C^β signals are highly conserved after reduction with the exception of the Cys-C^β signal convergence as a result of unrestricted rotation about the side-chain upon reduction. No changes in appearance of aliphatic proton signals upon reduction suggests backbone conformation and side-chains may be unaffected by reduction of the disulfide bridge.

SUPPORTING INFORMATION

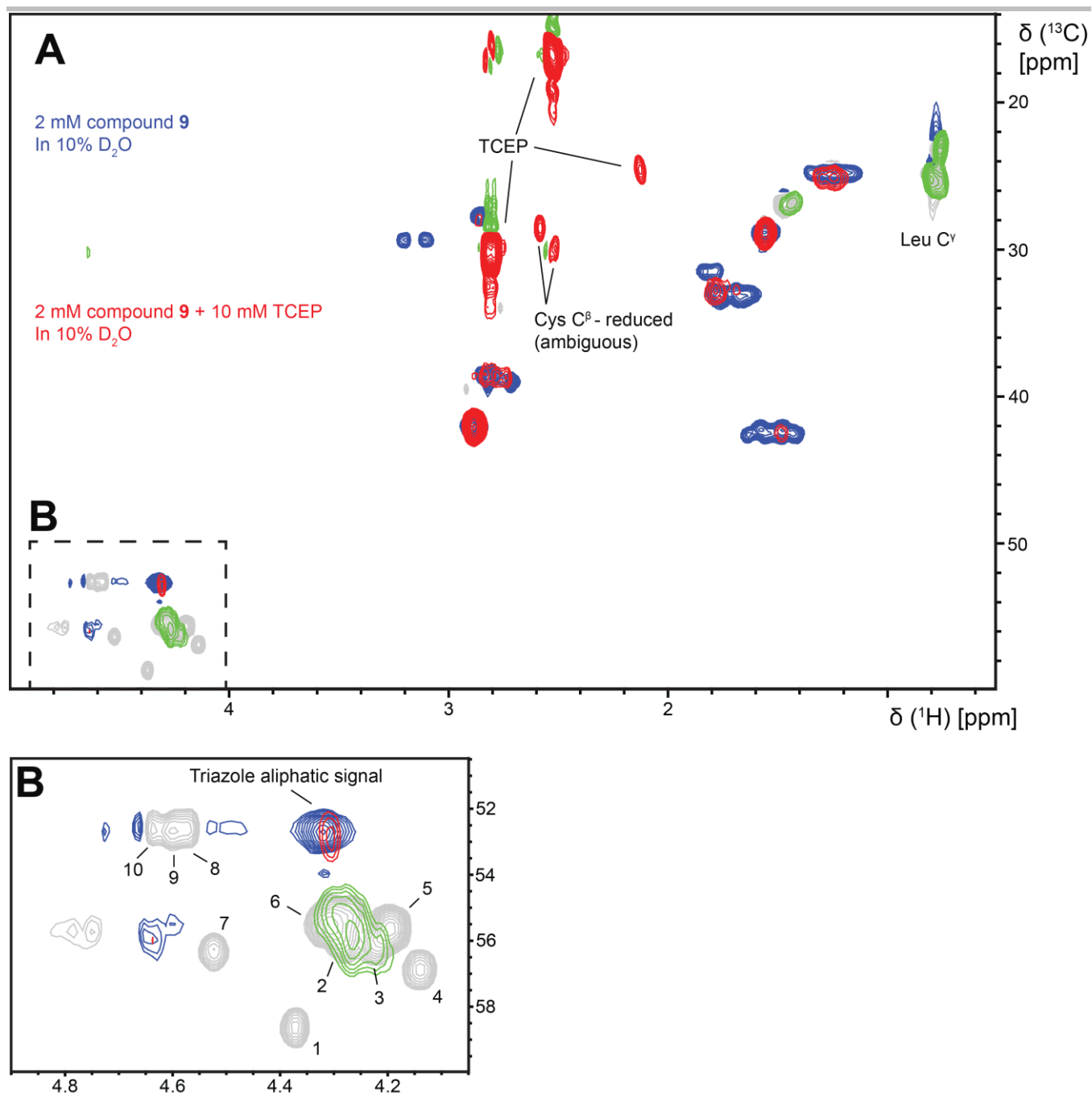


Figure S13. (A) Overlay of 2D multiplicity edited [¹³C, ¹H]-HSQC for compound **9** before (blue, grey) and after (red, green) reduction by TCEP with (B) expansion of C^β region. Low signal resolution for reduced compound **9** and apparent disappearance of multiple signals prevents unambiguous assignment of Cys-C^β resonances for both states.

SUPPORTING INFORMATION

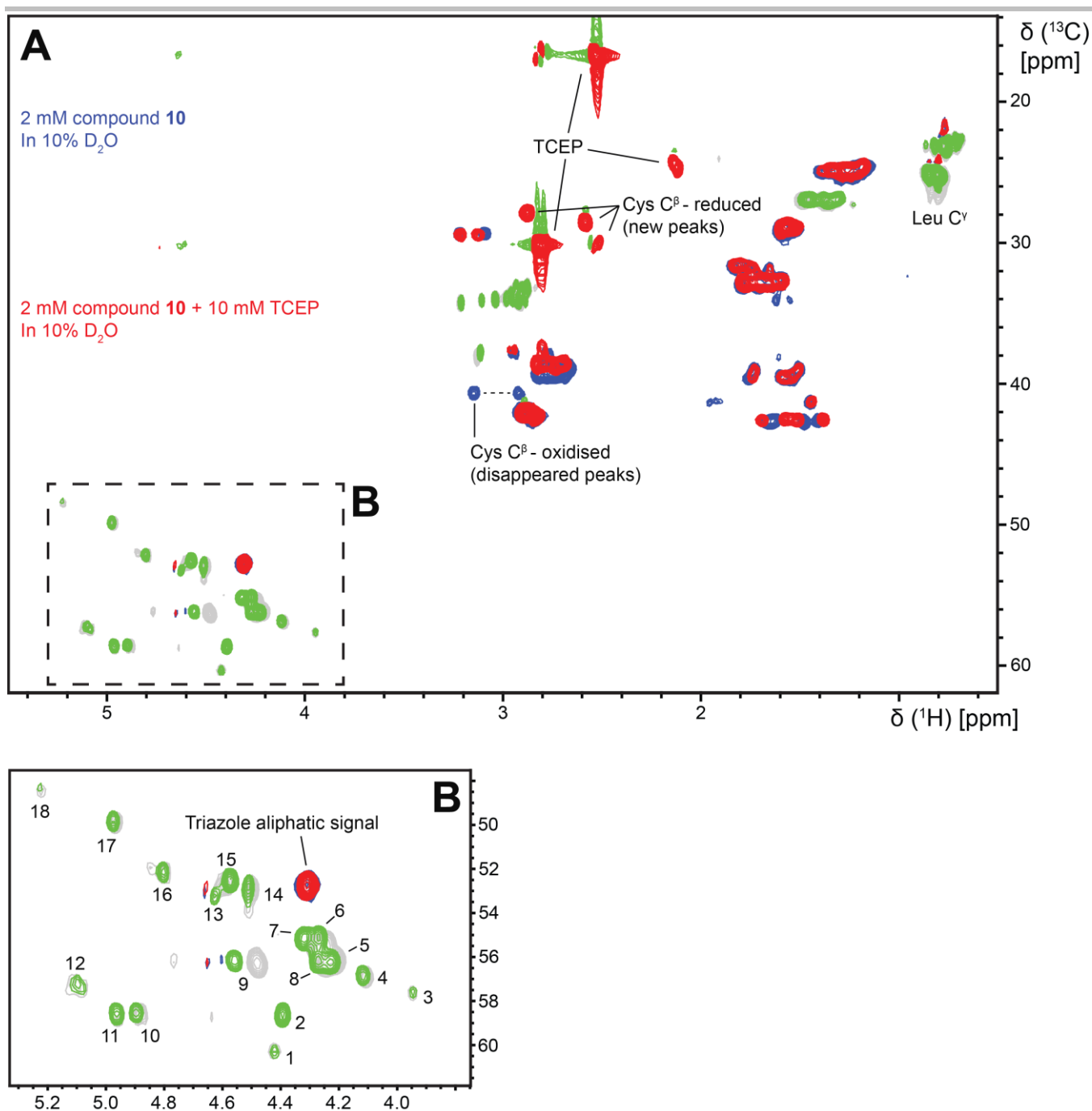


Figure S14. (A) Overlay of 2D multiplicity edited [¹³C, ¹H]-HSQC for compound **10** before (blue, grey) and after (red, green) reduction by TCEP with (B) expansion of C^α region. All aliphatic signals are highly conserved after reduction with the exception of C^α-9 which undergoes a slight increase in ¹H chemical shift. 18 signals in the C^α region suggests alternate conformations for some residues as there are only 16 chemically distinct C^α in the structure of **10**. C^β-reduced could only be ambiguously assigned due to the appearance of several new signals upon reduction. The minor change in signal appearance after reduction indicates that the side-chain conformations of residues in compound **10** do not undergo any substantial changes.

SUPPORTING INFORMATION

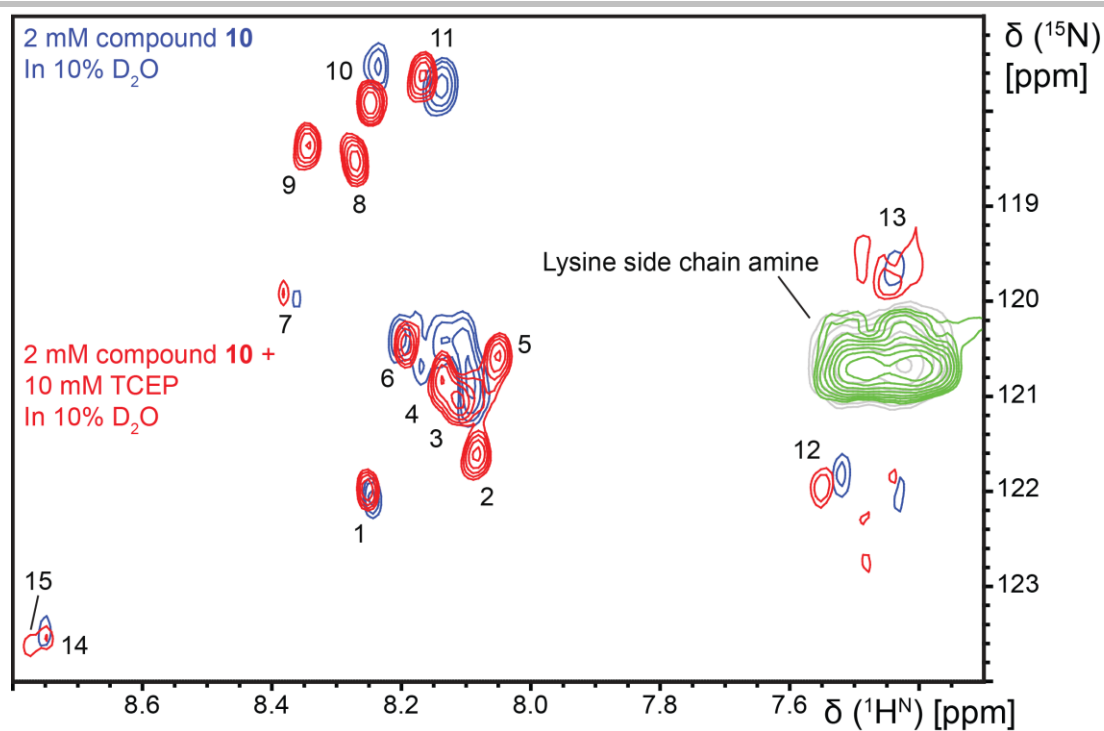


Figure S15. 2D SOFAST [^{15}N , ^1H]-HMQC study of compound **10** before (blue) and after (red) reduction by addition of TCEP. Moderate changes in chemical shifts, improved signal resolution and/or appearance of some new signals indicates reduction of compound **10** causes moderate change in backbone structure.

SUPPORTING INFORMATION

Diffusion NMR (DOSY) studies:

The diffusion properties of the CP materials, including the disulfide-reduced tetramers, were investigated using DOSY NMR (S16-17, Table S1). The translational diffusion constants (D_T) of CP **1** and tetramers **8**, **9** and **10** were measured to be 4.6, 3.0, 3.1 and $2.2 \times 10^{-10} \text{ m}^2/\text{s}$, respectively. Compound **8** diffused the fastest of the tetramers whilst **10** diffused slowest. In addition, DOSY studies of reduced compounds **8** and **10** indicate that there is no significant disassembly upon removal of the disulfide link, with only slightly larger D_T values of 3.4 and $2.9 \times 10^{-10} \text{ m}^2/\text{s}$ respectively. Reduction of the disulfide bridge in tetramers **8** and **10** increases the mobility of the molecular species, which would be expected if the reduced compounds behave as dimers. The diffusion of reduced compound **9** could not be accurately measured due to substantial broadening of the signals.

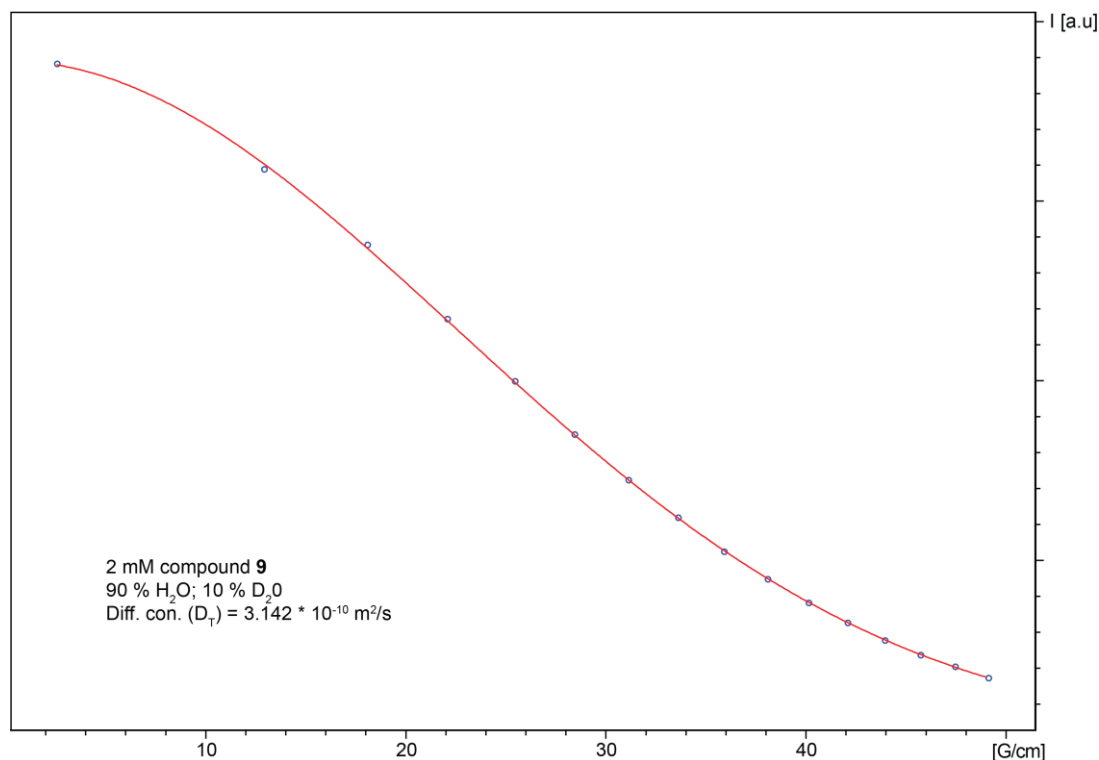


Figure S16. DOSY diffusion study for compound **9** at 2 mM with calculated translational diffusion constant (D_T) = $3.142 \times 10^{-10} \text{ m}^2/\text{s}$ based on integration of peaks in the methyl proton region (1.004 to 0.663 ppm).

Table S1. DOSY D_T measurements. DOSY experiments for **8**, **9** and **10** were performed at 2 mM. Substantial broadening of the 1D ^1H spectra for compound **9** in the reduced state prevents accurate D_T measurement. Values are plotted in Figure S17.

Compound	D_T ($10^{-10} \text{ m}^2\text{s}^{-1}$)
1 (1 mM)	5.462
1 (8 mM)	4.609
8 (ox)	3.009
8 (red)	3.433
9 (ox)	3.142
10 (ox)	2.238
10 (red)	2.912

SUPPORTING INFORMATION

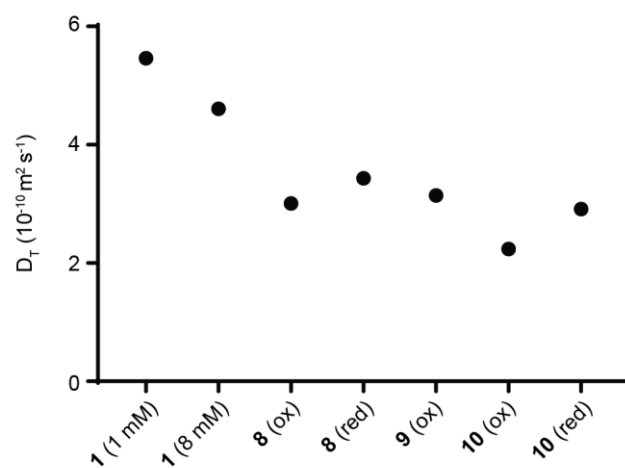


Figure S17: Translational diffusion constants (D_T) from DOSY NMR: 'ox' = disulfide present, 'red' = reduced with TCEP. The diffusion of **9** (red) could not be measured due to signal broadening.

SUPPORTING INFORMATION

H-D Exchange NMR studies:

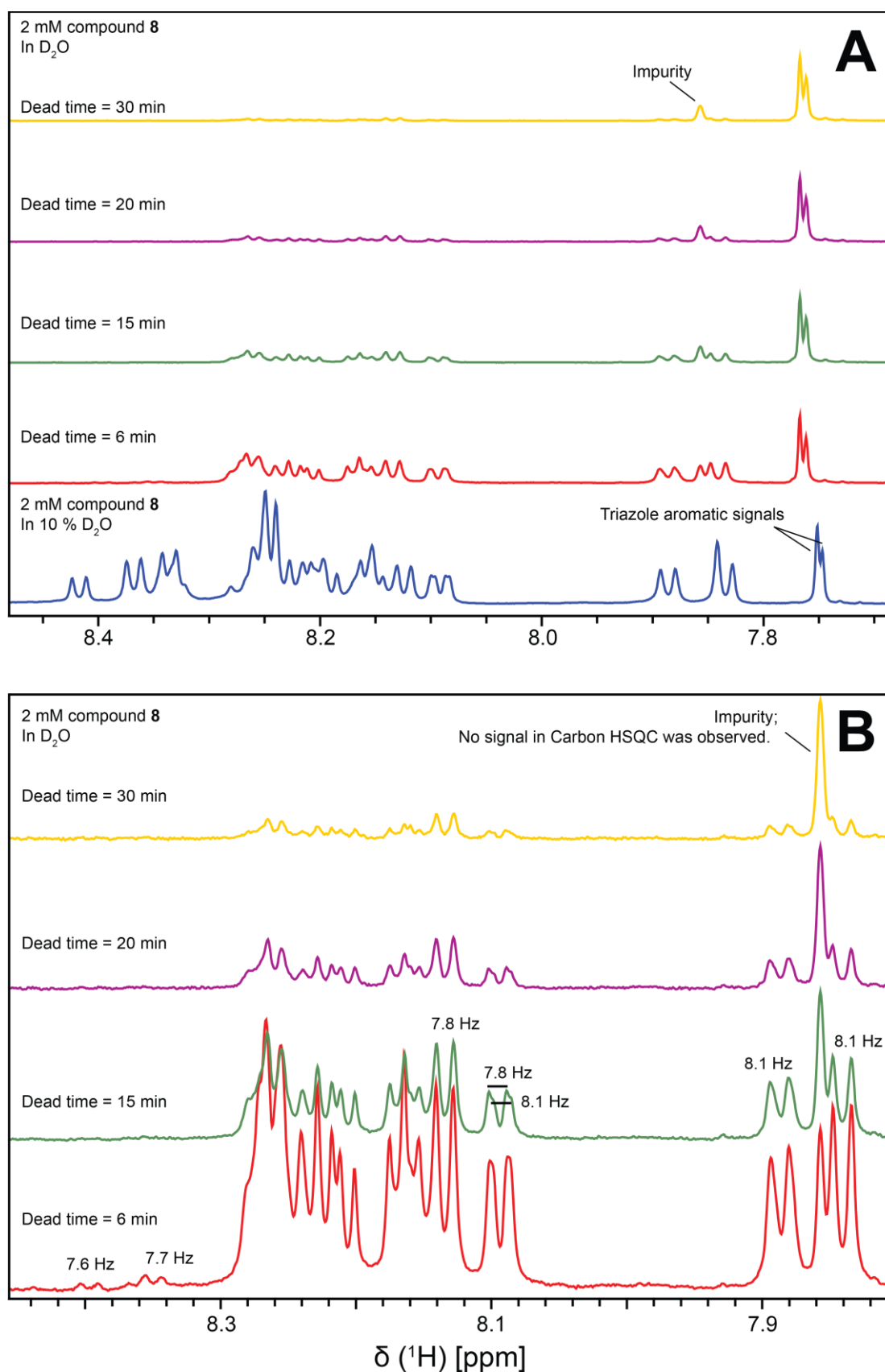


Figure S18. ^1H -D exchange study of compound **8**. (A) The disappearance of the exchangeable backbone amide protons over a period of 30 minutes. (B) An expansion of the 7.8 to 8.4 ppm region for spectra in D_2O with signals scaled up 9-fold. The signals at 7.75 ppm are the non-exchangeable aromatic protons of the triazole linker in alternate conformations. $^3J_{\text{HN-HN}}$ coupling constants for the well-resolved backbone amide proton signals are highlighted.

SUPPORTING INFORMATION

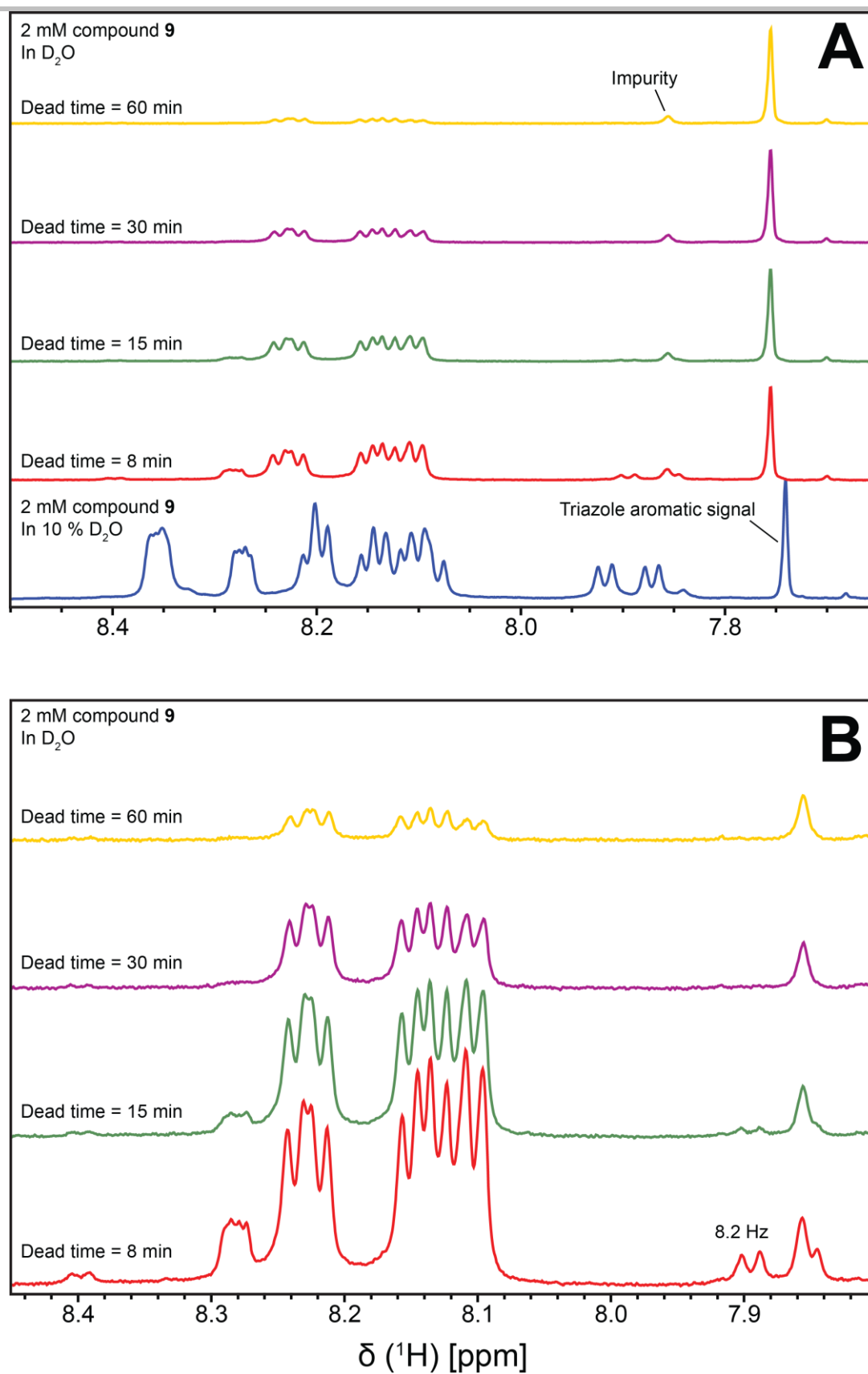


Figure S19. ^1H -D exchange study of compound **9**. (A) The disappearance of the exchangeable backbone amide protons over a period of 60 minutes. (B) An expansion of the 7.8 to 8.4 ppm region for spectra in D_2O with signals scaled up 6-fold. The signal at 7.75 ppm is the non-exchangeable aromatic protons of the triazole linker. $^3J_{\text{HN-HN}}$ coupling constant for a well-resolved backbone amide proton signal is highlighted.

SUPPORTING INFORMATION

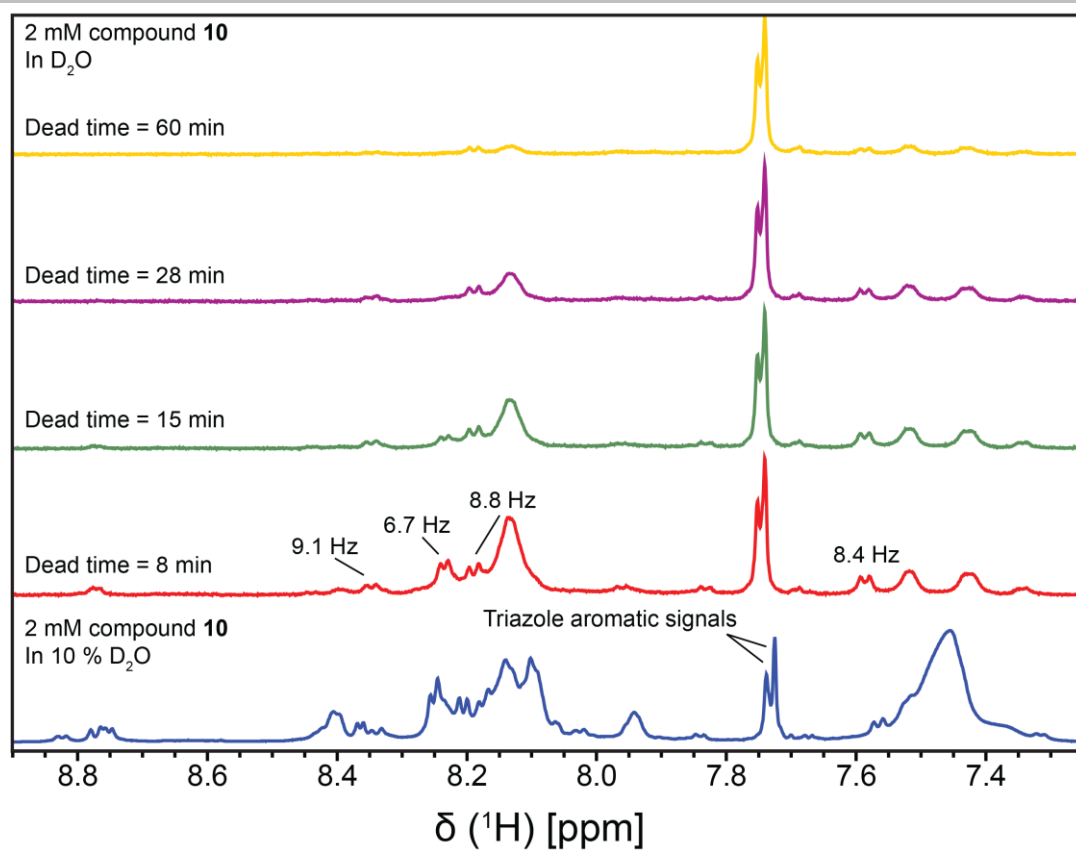


Figure S20. ¹H-D exchange study of compound **10** tracking the disappearance of the exchangeable backbone amide protons over a period of 60 minutes. The signals at 7.75 ppm are the non-exchangeable aromatic protons of the triazole linker in alternate conformations. ³J_{HN-HN} coupling constants for well-resolved backbone amide proton signals are highlighted.

References

- [1] C. K. Wang, S. E. Northfield, J. E. Swedberg, P. J. Harvey, A. M. Mathiowetz, D. A. Price, S. Liras, D. J. Craik, *J Phys Chem B* **2014**, *118*, 11129-11136.

Chapter 4

Studies of cyclic D/L peptide nanotube stability

We were excited to see that covalent tethering did not interfere with the self-assembly process and was effective in generating ordered, water-soluble material as discussed in Chapter 3. However, there were substantial differences in the stability and folded structures of the nanorods. Due to the complexity of CPN assembly, there are a broad range of features that work in unison to control their stability, and we were interested to investigate whether they could be identified and manipulated to improve our CPN designs. By improving our understanding of these features, we could potentially engineer highly stable CPN material and in future develop these towards biomedical applications.

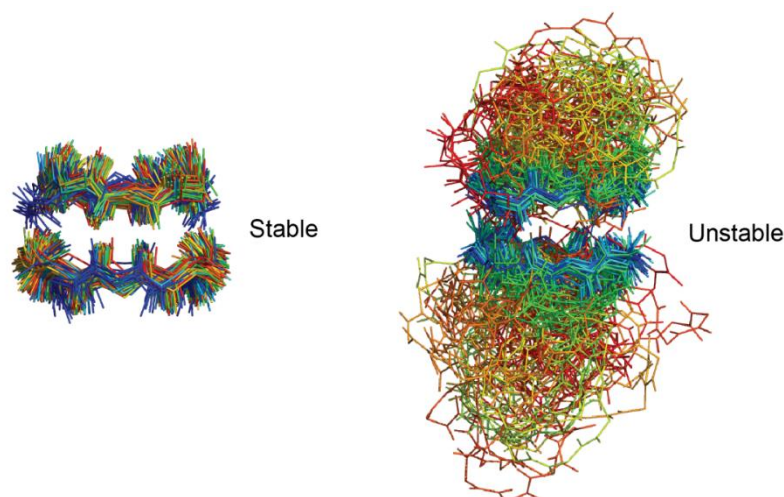


Figure i. CP dimer stability is influenced by the different H-bond alignments and not just the composition of side-chains. Shown in the figure is an overlay of the frames from two MD simulations of the same CP but in different H-bonded alignments. CP backbones are coloured from blue (simulation time = 0 ns) through the colour spectrum to red (100 ns).

Chapter 4 describes our combined experimental and theoretical analyses of CPNs in order to examine the features critical to CPN structure and stability. A range of CPs were designed and synthesised based on our successfully crystallised CPs described in Chapter 2. The CPs varied in hydrophobicity and in the number, position and length of ionisable amino acid side-chains. The impact of these variations on the stability of CP systems was studied by crystallography, NMR spectroscopy and MD simulations. Side-chain interactions such as hydrophobic and ionic interactions significantly improved CPN stability both experimentally and computationally, although all systems were highly dependent on the specific H-bond arrangements (or alignments) between CPs (**Figure i**). We found that there was good correlation between the experimental and theoretical analyses which supports the use of MD simulations as a predictive tool when engineering CPN stability in our future work.

To our knowledge, this is the first study which considers the combined effects of side-chain composition, relative CP orientations and distinct H-bond interfaces on CPN structure and stability. Understanding these features is critical to the advancement of CP-based nanomaterials.

This chapter contains the unpublished manuscript: M. R. Silk, J. R. Price, B. Mohanty, M. J. Scanlon, P. E. Thompson, D. K. Chalmers, Studies of cyclic D/L peptide nanotube stability by NMR, crystallography and molecular dynamics. Supplementary information is included after the manuscript and contains additional MD data and experimental data.

Studies of cyclic D/L peptide nanotube stability by crystallography, NMR and molecular dynamics

Mitchell R. Silk, Jason R. Price, Biswaranjan Mohanty, Martin J. Scanlon, Philip E. Thompson, David K. Chalmers

Abstract: Cyclic peptides with alternating D/L residues (CPs) self-assemble to form nanotubes (CPNs). These CPNs have potential diverse applications as molecular scaffolds, synthetic membrane channels or as bioactive compounds in their own right. However, our understanding of the factors that control the assembly of CPNs remains underdeveloped. In this work, we investigate the structure-property relationships of CPNs through X-ray crystallography, NMR spectroscopy and molecular dynamics (MD) simulations. Minor changes in sequence resulted in substantial changes in CP dimer stability by NMR spectroscopy and MD studies. H-bonding half-lives of the synthesized CP dimers were determined using H-D exchange experiments. Stable and unstable CP dimers were identified by MD simulations with their stability dependent on the amino acid side-chains. Hydrophobic amino acids were found to increase CP dimer stability but experimentally reduce nanotube solubility. Charged amino acids promoted nanotube stability when opposing charges in adjacent CP monomers were aligned while alignment of negative charges destabilised CP dimers. Comparison of the MD predictions with the experimental measurements showed the theoretical models to be consistent with experiment which demonstrates the advantage of modelling CPN systems prior to synthesis and experimental analysis. Ultimately this work will assist the educated design of stable tubular structures for potential applications in biomedicine.

Introduction

Self-assembling cyclic peptides built from alternating D and L amino acids (CPs) assemble to create unique tubular, supramolecular assemblies.¹⁻³ The assembly process is mediated by β -sheet-like hydrogen bonding between CP backbones.^{1, 4, 5} The alternating chirality of the amino acids means that all the side-chains project outwards from the nanotube, providing the potential for the control of CP nanotube (CPN) surface properties simply by modifying the amino acids in the sequence during synthesis.⁶ CP nanostructures have exciting potential applications as biomolecular mimetics, for example as pseudoproteins or artificial membrane channels. However, despite the fact that CP systems have been known for more than 25 years, there have to date been few demonstrated applications of these systems. There have been some studies of methods to improve our control of CPN structure and composition, particularly through covalent tethering of CPs to one-another. CPs have been tethered to one-another to control the relative CP orientations in dimers,⁷⁻¹² or to generate heterogeneous structures of controlled composition.¹³⁻¹⁵ However, a primary limitation to the development of CP-based nanostructures is a lack of detailed knowledge about the factors that govern the stability of CPs constructed from different amino acid sequences. For example, there is little available information about the extent to which the incorporation of ionic or nonpolar side chain interactions can improve CPN stability (**Figure 1**). Improving our structural understanding of CP nanotubes and the key factors driving self-assembly will enable us to better predict and control their assembly and ultimately enable the development functional CP-based nanomaterials.

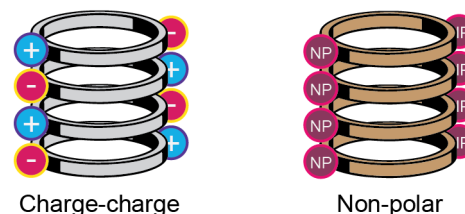


Figure 1. To what extent do side chain interactions, such as polar charge-charge interactions or non-polar hydrophobic interactions, increase nanotube stability?

Analysis of CP structure can be done experimentally using a variety of methods including crystallography, NMR, IR, electron microscopy and theoretically through energy calculations or MD simulation.

Crystallography has been used to investigate CP-CP interactions. Extensive studies have been performed on CPs where the backbone amides on one face are blocked with methyl groups allowing only CP dimers to form.^{2, 16-20} CPs have also been crystallised in folded conformations that make intramolecular backbone H-bonds rather than forming tubular assemblies.²¹ We have previously reported that CPs **1** and **2** (**Table 1**) crystallise in parallel and antiparallel nanotube forms.²² In each case, the crystal lattice is reinforced by a network of charge-charge interactions between Asp and Lys side-chains.

NMR methods also provide significant insight into aspects of CP structure in solution. 1D ¹H NMR has been used to characterise the concentration-dependent assembly of CPs,^{16, 23, 24} the existence of multiple conformations^{21, 25, 26} and to determine association constants.^{2, 16, 25, 26} Inter-CP interactions have been measured by ROESY and NOESY NMR. This has been used to identify the relative orientations of CPs to one-another^{2, 14, 27, 28} or the encapsulation of guest-molecules within CP cavities.¹⁵ The strength of H-bond interactions within CPN materials has been measured by 1D ¹H NMR using H-D exchange experiments.¹³ DOSY analysis provides an estimate of CP size and aggregation in solution based on the diffusion properties of the dissolved material.¹³⁻¹⁵

Molecular dynamics (MD) simulations have been used to investigate the properties of CP nanotubes, particularly for CPN structure and molecular partitioning across lipid bilayers.²⁹⁻³⁶ The overall structural stability of assembled CPNs was investigated by Vijayaraj *et al.*, who used MD and quantum chemistry calculations to probe the effects of the number of CP subunits within a CPN. They found that CPs located at the tube termini were weakly associated, regardless of the number of subunits present and, as such, the overall stability of a CPN is determined by the length of the core-region³⁷ and the nature of the solvent.³⁸ Garcia-Fandino *et al.* used MD methods to show that α,γ -CPs can be designed to favour heterogeneous dimer assembly over homogeneous assembly. α,γ -CPs contain alternating α - and γ -amino acids rather than D- α / L- α , but achieve a similar conformation allowing the formation of backbone H-bonded, hollow nanotubes. *Cis*-3-

aminocyclohexanecarboxylic acid (γ -Ach) and *cis*-3-aminocyclopentanecarboxylic acid (γ -Acp) incorporated into different α,γ -CPs were more stable as heterogeneous H-bonded dimers than as homodimers.³⁹ Liu *et al.* have studied the mechanisms behind CPN-mediated transport of the antitumor drug 5-fluorouracil, describing how the drug alternately makes hydrophobic and H-bonding interactions as it passes from CP-plane to CP-CP junction regions within the nanotube pore.³² These distinct environments within the CPN channel have an impact on the diffusion of water, which requires a driving force to

enable diffusion through the antiparallel-stacked environment of a CPN channel, as shown by Zhu *et al.*⁴⁰

The factors that contribute to CPN stability are as diverse as they are complex, and not all of them are known or understood. In this work, we investigate the factors that control the stability of CP nanotube assemblies in order to understand how to design stable CP nanostructures. The structure and stability of a range of ionisable CPs are studied by X-ray crystallography, NMR spectroscopy and molecular dynamics simulation.

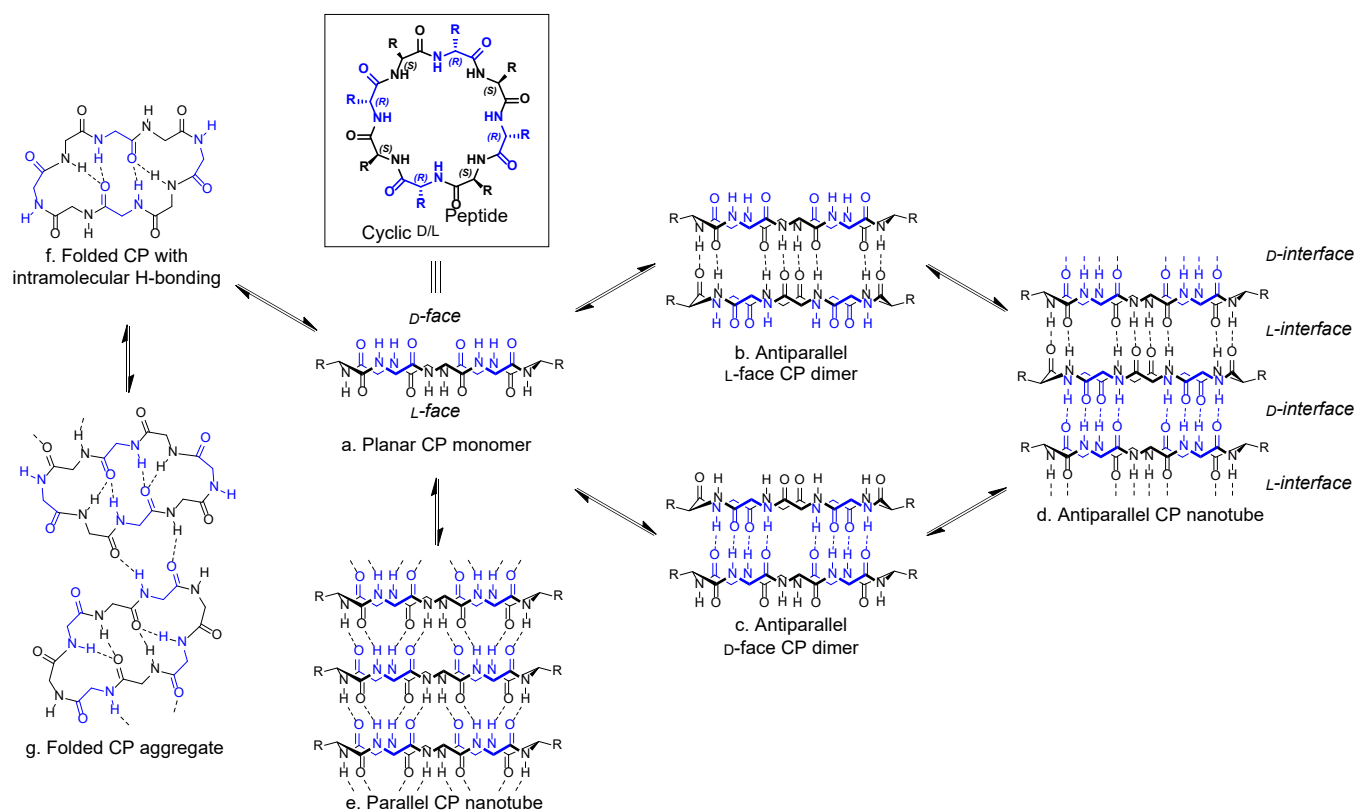


Figure 2. Backbone arrangements for potential supramolecular structures of cyclic D/L octapeptides. L-amino acids are shown in black and D-amino acids are in blue. a) The planar monomer has two faces (L-face and D-face). b, c) Monomers can assemble through the L- or D- faces to form antiparallel dimers. d) Dimers can further assemble to make antiparallel CP nanotubes. e) Self-assembly can alternatively result in parallel CP nanotubes. f) CP monomers can fold into non-planar conformations stabilized by internal H-bonding. g) Larger (possibly regular) aggregates of nonplanar monomers can form.

The self-assembly of CP nanotubes is a complex process that is influenced both by the conformational preferences of individual CP monomers and by interactions between CP monomers within the supramolecular nanotube assembly. **Figure 2** illustrates potential species that may form in a solution of CP monomers. For a planar CP (**Figure 2a**), the backbone atoms of all L-amino acids project in the same direction while the D-amino acids project in the opposite direction, giving rise to two distinct faces (the L-face and the D-face). As a result, there are two different antiparallel arrangements that can form depending on whether L or D-amino acid H-bonding is involved (**Figure 2b, 2c**). Extended antiparallel H-bonded nanotubes that then assemble are comprised of alternating L and D H-bond interfaces (**Figure 2d**) whose stability is directly determined by the amino acid composition of the CP. Additionally, intermolecular backbone-backbone H-bonding can produce parallel H-bonded nanotubes comprised of a consistent H-bond interface (**Figure 2e**) or even undergo intramolecular

backbone H-bonding to form folded CPs (**Figure 2f**) and CP-aggregates (**Figure 2g**). While parallel H-bonded nanotubes are known to exist, antiparallel H-bonding is often proposed to be the more stable arrangement.^{23, 25}

Results

Peptide design

We designed and analysed a series of CPs to investigate the interactions important for CPN stability, particularly regarding side-chain interactions and H-bond networks. The peptides used in this study are based on the water-soluble CPs **1** and **2** that have been described previously by our group. Compounds **1** and **2** contain equal numbers of aspartic acid and lysine residues and therefore have an overall neutral charge at moderate pH. They have good water solubility and were shown to assemble into fibres by cryo-EM and crystallography. Their general composition of

alternating hydrophobic and charged amino acids forms the basis of this structural study.

Table 1. Cyclic D/L peptides synthesised. Lower case denotes L-amino acids. O indicates ornithine.

CP	Sequence	CP	Sequence
1	<i>cyclo</i> [(DaKa) ₂]	9	<i>cyclo</i> [(EIOI) ₂]
2	<i>cyclo</i> [(DIKI) ₂]	10	<i>cyclo</i> (DIDIKIKI)
3	<i>cyclo</i> (DIKIDIKf)	11	<i>cyclo</i> (DIKIKIKI)
4	<i>cyclo</i> [(DfKf) ₂]	12	<i>cyclo</i> (DIDIDIKI)
5	<i>cyclo</i> [(HIKI) ₂]	13	<i>cyclo</i> (DILIKILI)
6	<i>cyclo</i> [(HhLI) ₂]	14	<i>cyclo</i> [(KdLI) ₂]
7	<i>cyclo</i> [(EIKI) ₂]	15	<i>cyclo</i> [(DIKI) ₃]
8	<i>cyclo</i> [(DIOI) ₂]		

CPs **3** and **4** are analogues of leucine-containing compound **2** where 1 or 2 D-Leu residues have been replaced with D-Phe. These are more hydrophobic variants of **1** and **2**, with a predicted hydrophobicity ranking of **2** < **3** < **4**.⁴¹ CPs **5** and **6** investigate the incorporation of His residues and are not charge-neutral. CPs **7-9** were designed to compare the effects of changing the lengths of the sidechains in the charged residues. Ornithine and lysine were used to vary the length of basic side-chains and aspartic acid and glutamic acid were used to vary the length of acidic side-chains. CPs **10-14** vary the numbers and arrangements of Asp, Lys and Leu residues to generate compositionally similar but structurally distinct CPs. CP **15** is a cyclic dodecapptide that was designed to investigate the assembly of larger CPs. This peptide is similar to CP **2** but contains an additional DIKI segment

Peptide synthesis

All CPs were synthesised using standard Fmoc solid-phase peptide synthesis methodology. Linear peptide precursors were synthesised on 2-CTC resin before cleavage with the side-chain protecting groups intact. Head-to-tail cyclisation was then performed in solution. Deprotection of the amino acid side-chains and purification by preparative HPLC gave the cyclic peptides in moderate to good yields and in high purity. All the sequence variations prepared are shown in **Table 1**.

Peptide crystallisation

We aimed to determine the effects of amino acid composition on the molecular packing of CPs within larger assemblies using X-ray crystallography. Hanging and sitting-drop vapour diffusion experiments were conducted for CPs **1-15** in an effort to generate crystals that were suitable for X-ray diffraction studies. Initial screens used the 'Shotgun' screen⁴² before optimization of crystal morphology using additive screens (Hampton Research, USA). Diffraction data was then collected for promising crystalline material using the MX2 micro-focus beamline at the Australian Synchrotron.

We have previously crystallised CPs **1** and **2**.²² CPs **10**, **11** and **12** crystallised as needle-like crystals of up to 100 x 8 x 8 μm, while **8** crystallised as larger needles of up to 1000 x 15 x 15 μm. An additional crystal form of **2** was obtained from novel growth conditions (1.44M trisodium citrate with 2-5% HFIP) producing

diamond-shaped crystals with approximate widths of 100 x 100 x 100 μm. Growth conditions are reported in the supplementary information (**Table S1**). CPs **7** and **9** did not produce any crystalline material but instead, consistently generated highly viscous solutions. All remaining CPs formed amorphous non-crystalline aggregates and precipitates.

Minor differences in CP sequence were found to produce marked variations in the crystallization results. Substitution of Asp by Glu (**2** versus **7** and **8** versus **9**) resulted in the formation of highly viscous solutions rather than crystals. Replacement of Leu residues in CP **2** with Phe (CPs **3** and **4**) or incorporation of many Leu residues (**13**) caused the CPs to produce turbid solutions, likely due to poor solubility and/or CP aggregation. CP **14** also gave highly turbid solutions despite having the same amino acid composition as the more soluble CPs **2** and **10**.

Peptide crystallography

Of the CPs that were successfully crystallised, structures could be solved for CPs **2** and **8**. Crystals of **8** diffracted to 1.5 Å with a unit cell of dimensions $a = 12.9$ Å, $b = 17.7$ Å, $c = 26.4$ Å, $\alpha = \beta = \gamma = 90^\circ$ and the structure was solved by dual space methods using SHELXT⁴³ and refined with SHELXL.⁴⁴ Crystals of **2** diffracted to 1.1 Å, but could not be solved by direct methods. The structure of **2** was ultimately solved by molecular replacement using the crystal-structure backbone of **8** as a search model (unit cell dimensions of $a = 17.8$ Å, $b = 32.6$ Å, $c = 58.0$ Å, $\alpha = \beta = \gamma = 90^\circ$). Molecular replacement was performed in the CCP4 suite⁴⁵ using Phaser⁴⁶ for initial model fitting and iterated refinement using Refmac.⁴⁷

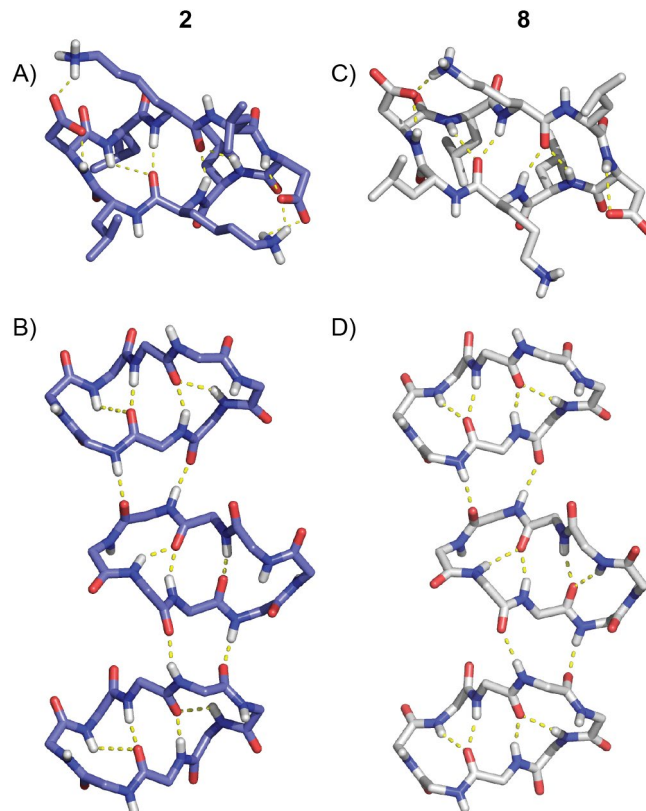


Figure 3. Crystal structures of CPs **2** and **8**. A) CP **2** adopts a folded conformation that is stabilised by three or four intramolecular H-bonds. B) Two intermolecular H-bonds form between each CP subunit for **2**. C & D) CP **8** contains almost identical intra and intermolecular H-bond interactions to **2**.

Both CP **2** (in the new form) and CP **8** were found to crystallise not as nanotubes but in an approximately symmetrical, folded conformation that is stabilised by inter- and intramolecular H-bonds. This conformation is quite similar to that reported for some α,γ -CPs.^{21, 39} In this form, the backbone of CP **2** is twisted to accommodate a total of four intramolecular H-bonds (**Figure 3a**) formed between the carbonyl of each Lys residue and the backbone NH of the Lys and Leu residues on the opposite side of the CP. Four conformations of **2** exist within the asymmetric unit and 16 CP molecules are contained in the unit cell. All conformations have almost identical backbone conformations with slight variations in the sidechain conformations. One of the conformations has only three intramolecular H-bonds although it is quite similar to the other conformations (**Figure 3b**, middle CP). In addition to intramolecular H-bonds, there are two intermolecular H-bonds between each CP (**Figure 3b**). The crystal structure of **8** is very similar to **2**. The backbone of CP **8** adopts an almost identical conformation to that of **2** with the same four intramolecular H-bonds being present (**Figure 3c**). For CP **8** the asymmetric unit contains only one peptide and four in the unit cell, although each CP forms the same two intermolecular H-bonds between adjacent CPs as seen for **2**.

NMR spectroscopy

The stability of CP assemblies in solution was investigated by NMR spectroscopy. The half-lives of the backbone H-bonds were measured using H-D exchange at 298 K and pH 3.0. On dissolution in D₂O, the backbone H^N signals exchange with deuterium and decay over time. This decay can be quantified to derive half-life values, providing information about the solvent exposure of the H^N groups and the stability of the H-bonding within the assembly. In addition, the sample turbidity was assessed visually as an indication of CPN assembly and aggregation.

Peptides were dissolved in 100% D₂O at a concentration of 8 mM and 1D ¹H NMR spectra were acquired over 60 minutes. For CPs that gave spectra with well-dispersed backbone H^N signals, the H-bond half-lives were calculated for each individual residue in the peptide. For CPs with overlapping H^N signals, half-lives were determined for the amide region as a whole. In all cases, half-lives were averaged to provide an estimate of overall stability (half-lives were summed and divided by 4 for CPs with two-fold symmetry or divided by 8 for asymmetric CPs).

The exchange experiments show that changes in CP sequence strongly influence CPN stability. The backbone amide protons of the His-containing CPs **5** and **6** were completely unprotected from the solvent and exchanged with deuterium within 8 minutes, before the first spectrum could be acquired. CPs **1**, **12** and **15** had short half-lives while CPs **2**, **7**, **10**, **11** and **14** had the longest half-lives. CP **14** was poorly soluble at 8 mM and was studied at 4 mM. The single substitution of Leu by Phe in CP **3** resulted in an almost 2-fold decrease in H^N half-life when compared with **2**. Lys to Orn substitution in CP **8** reduced H^N half-lives while the introduction Glu and Orn residues in CP **9** induced substantial turbidity and poor aqueous solubility. CPs **4** and **13** could not be analysed due to poor aqueous solubility caused by the presence of hydrophobic Phe residues in CP **4** and high Leu content in **13**.

The turbidity of CP solutions gave further insight into the degree of aggregation within different samples. Turbidity was assessed by eye and classified as low, medium or high (**Figure S1**), and was consistent with our measurements of H-bond half-lives. The

more turbid samples (CPs **7** and **14**) had longer half-lives while CPs **1**, **5-8** and **15** had short half-lives and low turbidity.

Assembly of CP dimers

CPs can assemble through parallel or antiparallel H-bonding in a β -sheet-like manner. In both parallel and antiparallel systems the amino acid side-chains of each CP align with the neighbouring monomer. Each amino acid forms two hydrogen bonds (C=O-HN and NH-O=C) to the adjacent CP (**Figure 4**). In parallel CP systems, each H-bond is to the residues on either side of the residue with which it is aligned. In antiparallel CP systems, the two H-bonds form between only the aligned residues.

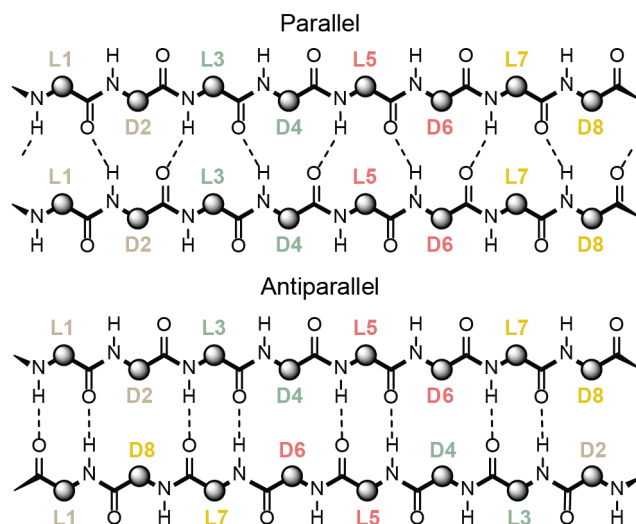


Figure 4. 'Unwrapped' representation of the backbone H-bonding in parallel and antiparallel CP dimers. There are two H-bonds per residue. In both cases, amino acid side-chains are aligned. In the parallel arrangement H-bonds are made to the residues on either side of the aligned residue. In antiparallel H-bonding, H-bonds are made directly between the aligned residues.

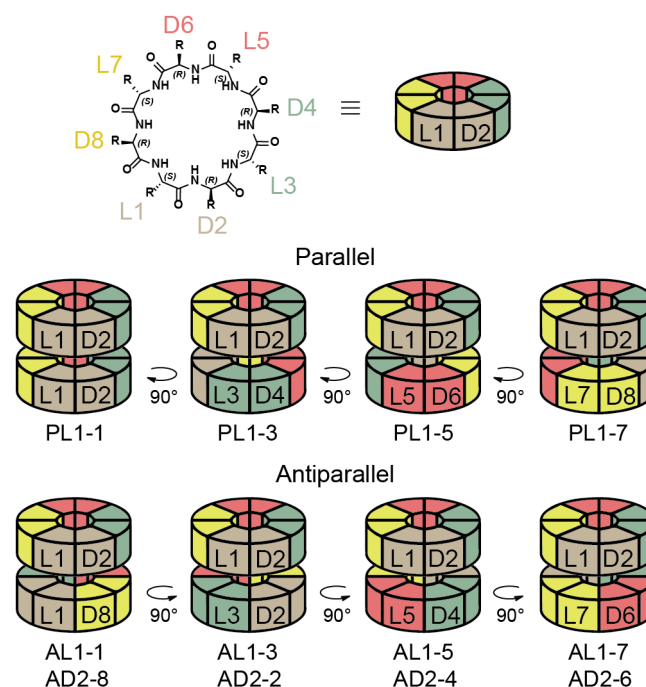


Figure 5. There are four distinct alignments of amino acids within an 8-AA CP homodimer. Successive 90° rotations of one monomer generate all possible alignments. Antiparallel dimers can form through the L-face or the D-face giving a total of 8 distinct antiparallel alignments.

Examination of the CP dimer structure reveals that multiple distinct H-bonded alignments are possible (**Figure 5**) and that these all need to be considered when analysing CP dimer stability. We will use the term ‘alignments’ to denote different hydrogen bonded pairings of amino acids. The total number of possible CP dimer alignments depends on: 1) the number of residues in the CP, 2) whether the dimer is parallel or antiparallel, 3) whether the dimer is homogeneous or heterogeneous and 4) any symmetry within the individual CP monomers. Here we consider asymmetric octapeptide homodimers. We refer to residues by their sequence number and stereochemistry. For example, an 8-AA CP can be represented *cyclo*(L1-D2-L3-D4-L5-D6-L7-D8). In an 8-AA CP, successive 90° rotations of one peptide relative to the other create four different ways to align amino acids. In a parallel dimer, we denote the four alignments as PL1-1, PL1-3, PL1-5 and PL1-7. As an example, alignment ‘PL1-3’ indicates a parallel dimer aligned with residue L3 of one CP adjacent to L1 of the other. In antiparallel dimers, the interactions can be made through the L-face or the D-face of the CP. Four rotations per face give a total of 8 possible alignments for an antiparallel cyclic D/L octapeptide. These alignments are denoted AL1-1, AL1-3, AL1-5 and AL1-7 for an antiparallel L-face dimer and AD2-2, AD2-4, AD2-6 and AD2-8 for a D-face CP dimer. For symmetrical peptides where residues 1 to 4 are the same as residues 5 to 8, only two possible alignments exist for each L or D-face where AL1-1, AD2-2, AL1-3 and AD2-4 are equivalent to AL1-5, AD2-6, AL1-7, AD2-8 respectively. **Figure 5** summarises the various distinct alignments of CPs within an 8-AA antiparallel dimer.

Molecular dynamics simulations of CP dimers

MD simulations of CP homodimers in explicit solvent (water) were used to investigate the influence of the AA sidechains on CP assembly and to gain additional insight into the experimental measurements of CP assembly. The solvated dimers were modelled using the Desmond MD software (D. E. Shaw Research, version 4.3). Systems were built in 35 × 35 × 35 Å orthorhombic cells with periodic boundary conditions and solvated with explicit water containing 0.15 M NaCl to more closely model a biological system (**Figure 6a**). Ionisable side-chains (His, Orn, Lys, Asp and Glu) were considered to be charged. Simulations were run at 300 K and 1.01 bar for 100 ns. Multiple individual simulations were run for each CP dimer, testing all possible parallel and antiparallel alignments. The average number of intermolecular backbone-backbone H-bonds was calculated for each simulation and used as a measure of dimer stability. In stable CP dimers, the CPs remained associated to one-another throughout the 100 ns simulation, while the CPs of an unstable dimer dissociated and fell apart.

Figure 6 illustrates a set of simulations performed on the antiparallel CP 2 dimer. The dimer was modelled in its four possible H-bonded alignments (**Figure 6b**). The AD2-2 alignment was found to be the most stable (**Figure 6c**), with no dissociation of the dimer for the full duration of the simulation (**Figure 6d, 6e**). The most stable alignments of CP 2 arose from Leu-Leu H-bonding in the D-interface of CP dimers (alignments AD2-2, AD2-4), while the AL1-1 and AL1-3 alignments caused the dimer to fall apart.

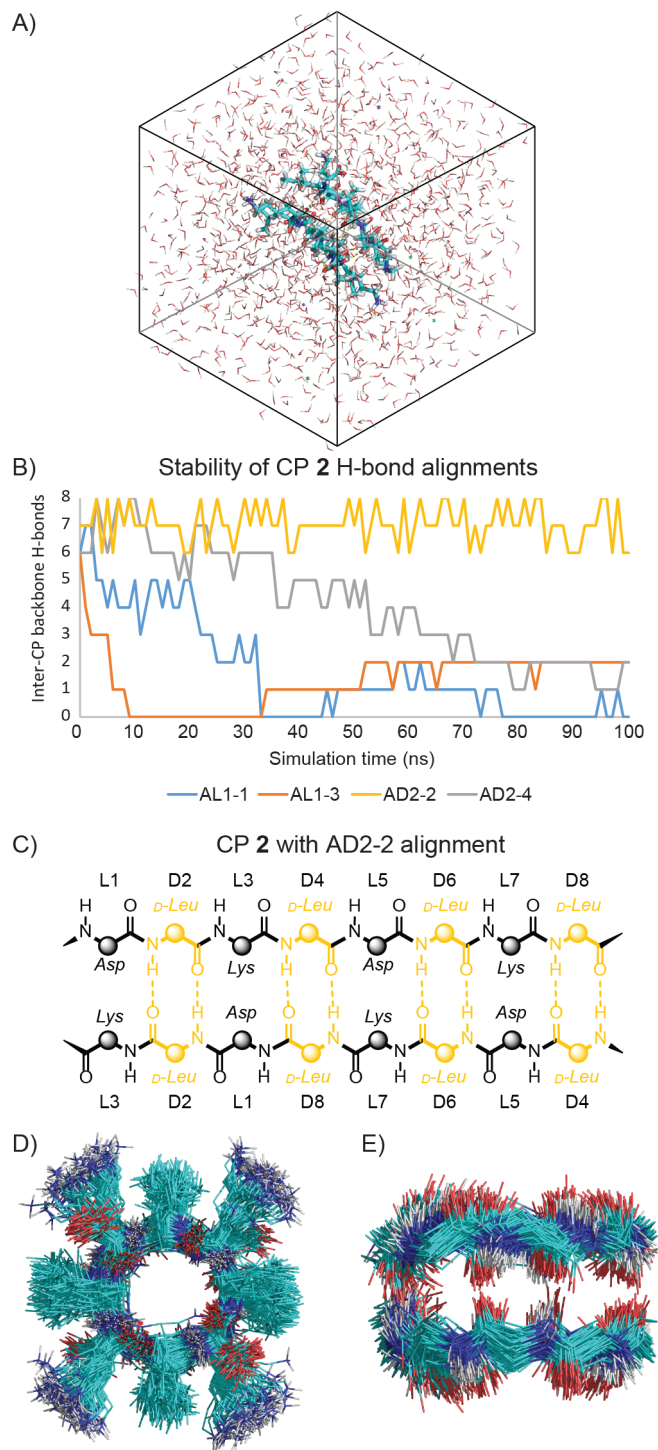


Figure 6. A) MD simulation system of a CP 2 dimer in explicit water containing 0.15M NaCl. B) The number of intermolecular backbone H-bonds (Y-axis) present over the course of 100 ns MD simulations of each of the four possible antiparallel alignments of the CP 2 dimer. C) AD2-2 was the most stable dimer alignment for CP 2 and was entirely comprised of Leu-Leu H-bonds. D) Overlay of all frames from the simulation of CP 2 showing the structural stability of this arrangement. E) Side-view of CP 2 (AD2-2) showing the peptide backbone only.

All parallel CP dimers investigated were found to be unstable (**Table S3**) with dissociation occurring within 1 ns. In contrast, the antiparallel dimers varied between being stable during the 100 ns simulation and rapidly dissociating. Dimer stability was dependent on the particular alignment of amino acids and no CP dimer was

stable in all of its possible antiparallel alignments. The average number of backbone intermolecular H-bonds over the course of a 100 ns MD simulation for each CP in each antiparallel alignment is presented in **Table 2**. Most of the CPs were found to have at least one antiparallel alignment that remained stable for the full 100 ns. CPs **1**, **6** and **12** were found to be very unstable, with all alignments resulting in disassembly of the CP dimers. CPs **7**, **11** and **14** had stable alignments in both the L and D interfaces, indicating these CPs may form highly stable nanotube assemblies.

A number of interesting observations can be made from our simulations of this set of CP analogues, particularly regarding side-chain hydrophobicity, opposing or matching charge-charge interactions and the backbone H-bonding interfaces.

Side-chain hydrophobicity had a strong impact on CP dimer stability. More hydrophobic CPs, containing phenylalanine (CPs **3** and **4**) or many leucine residues (CP **13**), were generally more stable. CP **3** was stable in all D-interface alignments with a single D-Phe, while **4** with four D-Phe's was more stable in the L-interface in addition to being stable in all D-interface alignments. However, **13** was only stable in two D-interface alignments despite high Leu-content, suggesting that increasing side-chain hydrophobicity does not necessarily improve H-bond stability.

CP dimers with oppositely-charged side-chains aligned were stable in many cases, but were highly dependent on the side-chain lengths. Asp, Orn and His have short side-chains while Glu and Lys have longer side-chains. The most stable alignments of opposing charge were Glu-Orn, Glu-Lys and Asp-Orn (CPs **7-9**,

alignments AL1-3 / AL1-7). Asp-Lys alignment was only stable in D-interface dimers (geometries AD2-2, AD2-6 of CPs **2-4** and **15**). CP dimers of **7-9** were more stable than **2**, possibly due to the closer matching of side-chain length in **7-9** facilitating ionic interactions. The shorter, polar Asp side-chain terminal lies near the non-polar mid-section of the longer Lys side-chain and may contribute to the instability of dimers with such an alignment.

All cases where negative charges were aligned were unstable, with the exception of CP **14**. All CP dimer alignments with Asp-Asp or Glu-Glu H-bonding were unstable regardless of the other amino acids in the CP sequence. This is likely a result of unfavourable interactions of like-charge causing dissociation of the CP dimer. CP **14** in the AD2-2 / AD2-6 alignment was the only exception, where favourable Leu-Leu interactions counteracted against the unstable effects of the Asp-Asp interactions. Alignment of positively-charged lysines was not as detrimental to stability as Asp-Asp alignment, possibly due to greater flexibility of the Lys side-chains allowing distance between like-charges without forcing dimer dissociation. This was reflected by Lys-based **11** having 4 stable alignments while Asp-based **12** had none. Charge-matching of histidine residues had interesting effects on CP dimer stability. It produced a stable geometry in CP **5** when histidine residues were aligned and H-bonded (AL1-1 / AL1-3) but was very unstable when histidines were aligned and not H-bonded (AD2-4, AD2-8). High numbers of Histidine in CP **6** resulted in complete instability in all geometries, all of which suggests Histidine is particularly sensitive to inter and intramolecular side-chain distances and alignments.

Table 2. MD study of the average number of intermolecular backbone H-bonds for CP dimers in antiparallel alignments

CP	Sequence	Dimer alignments								Total of stable simulations		
		AL1-1	AL1-3	AL1-5	AL1-7	AD2-8	AD2-2	AD2-4	AD2-6	L	D	All
1 ^[a]	<i>cyclo</i> [(DaKa) ₂]	3.1	1.4	3.1	1.4	2.8	3.7	2.8	3.7	-	-	0
2 ^[a]	<i>cyclo</i> [(DIKl) ₂]	3.3	1.8	3.3	1.8	5.8	7.0	5.8	7.0	-	2	2
3	<i>cyclo</i> [(DIKIDIKf)]	3.5	1.1	4.6	1.0	6.9	7.1	7.0	7.0	-	4	4
4 ^[a]	<i>cyclo</i> [(DfKf) ₂]	4.5	1.3	4.5	1.3	7.4	7.6	7.4	7.6	-	4	4
5 ^[a]	<i>cyclo</i> [(HIKl) ₂]	7.3	4.3	7.3	4.3	0.4	5.0	0.4	5.0	2	-	2
6 ^[a]	<i>cyclo</i> [(HhLI) ₂]	0.2	1.5	0.2	1.5	2.2	1.4	2.2	1.4	-	-	0
7 ^[a]	<i>cyclo</i> [(EIKl) ₂]	4.1	7.4	4.1	7.4	6.7	2.7	6.7	2.7	2	2	4
8 ^[a]	<i>cyclo</i> [(DIOl) ₂]	2.8	7.6	2.8	7.6	5.4	1.2	5.4	1.2	2	-	2
9 ^[a]	<i>cyclo</i> [(EIOl) ₂]	3.0	7.2	3.0	7.2	4.2	5.5	4.2	5.5	2	-	2
10	<i>cyclo</i> [(DIDIKIKI)]	1.9	1.5	2.1	0.8	3.7	6.7	6.6	6.2	-	2	2
11	<i>cyclo</i> [(DIKIKIKI)]	2.2	3.4	6.9	6.0	7.0	7.1	3.5	4.6	2	2	4
12	<i>cyclo</i> [(DIDIDIKI)]	0.2	0.8	0.4	0.3	1.4	6.0	5.9	6.1	-	-	0
13	<i>cyclo</i> [(DILIKILI)]	3.6	3.5	2.2	6.1	7.3	5.0	7.2	2.0	-	2	2
14 ^[a]	<i>cyclo</i> [(KdLI) ₂]	4.1	7.0	4.1	7.0	0.7	5.9	0.7	5.9	2	2	4
15 ^[a,b]	<i>cyclo</i> [(DIKl) ₃]	0.7	1.9	0.7	1.9	4.8	7.0	4.8	7.0	-	2	2

[a] In these peptides, the alignments AL1-1, AD2-2, AL1-3, AD2-4 are equivalent to AL1-5, AD2-6, AL1-7 and AD2-8 respectively.

[b] To enable comparison with 8-AA CPs, the number of H-bonds is adjusted by a factor of 2/3. CP **15** has 3-fold symmetry and has only 4 unique dimer alignments.

The L-interface and D-interface of the CP dimers had significantly different stabilities and were not just affected by amino acid alignment alone. This behaviour was seen for many of the CPs where specific side-chain alignments were only stable in one interface (L or D). For example, **7-9** were completely stable when opposing side-chains were aligned with backbone H-bonding in the L-interface (geometries AL1-3 / AL1-7) but unstable with the exact same side-chain alignments but with H-bonding through the D-interface (geometries AD2-2 / AD2-6).

When comparing the experimental and computational data of CPN stability, it is clear that the MD studies provide predictive power. A comparison of the NMR, turbidity and MD data is given in **Table 3**, which has been organized according to NMR-derived half-lives. CP dimers with stable H-bond alignments by MD simulation had longer H-bond half-lives as determined experimentally by NMR spectroscopy. Likewise, dimers with no stable alignments by MD had shorter half-lives. Furthermore, a CP dimer with stable geometries in both D and L interfaces by MD study would potentially form an extended nanotube with stable H-bond interfaces throughout the entire structure. This was evident for CPs **7**, **11** and **14** which had stable arrangements in both the D and L interfaces by MD and long half-lives with high turbidity. We note that the MD simulations only model CP dimers which are just one of the potential species that assemble from a solution of CP monomers (**Figure 2**). However, theoretical studies of dimers are simpler than extended nanostructures which allows for in-depth analysis of the features critical to CP-CP stability.

Table 3. Stability of CP assemblies by different measures, arranged by average $t_{1/2}$.

CP	Sequence	$t_{1/2}$ avg (min)	Turbidity	Stable MD ^[a]
4	<i>cyclo</i> [(DfKf) ₂]	- ^[b]	High	4/8
9	<i>cyclo</i> [(EIOI) ₂]	- ^[b]	High	2/8
13	<i>cyclo</i> [(DILIKILI)]	- ^[b]	High	2/8
2	<i>cyclo</i> [(DIKI) ₂]	12.5	Med	2/8
14	<i>cyclo</i> [(KdLI) ₂]	12.0 ^[c]	High	4/8
10	<i>cyclo</i> [(DIDIKIKI)]	11.4	Med	2/8
11	<i>cyclo</i> [(DIKIKIKI)]	10.1	Med	4/8
7	<i>cyclo</i> [(EIKI) ₂]	10.0	High	4/8
8	<i>cyclo</i> [(DIOI) ₂]	8.7	Low	2/8
3	<i>cyclo</i> [(DIKIDIKf)]	6.0	Med	4/8
12	<i>cyclo</i> [(DIDIDIKI)]	4.4	Med	0/8
15	<i>cyclo</i> [(DIKI) ₃]	4.1	Low	3/12
1	<i>cyclo</i> [(DaKa) ₂]	3.2	Low	0/8
5	<i>cyclo</i> [(HIKI) ₂]	0.5	Low	2/8
6	<i>cyclo</i> [(HhLI) ₂]	~0.0	Low	0/8

[a] Number of dimer alignments stable after 100 ns

[b] Not measured due to very poor solubility

[c] Measured at 4 mM due to poor solubility

Discussion

As outlined in **Figure 2**, CPs have the potential to form a variety of distinct supramolecular assemblies including CP dimers, nanotubes and disordered aggregates. The preference of a particular CP for each type of assembly will depend on the relative strengths of the inter-CP interactions present in each type of supramolecular assembly. Among those were the parallel H-bonded alignments which were completely unstable for all CP dimers studied. Although we have a crystal structure of a parallel H-bonded CPN, its stability is likely due to a combination of inter-nanotube and solvent interactions. As a result, we considered antiparallel dimers to be the likely geometrical arrangements.

Through a combination of experimental and theoretical methods, we have analysed the impact of relative CP geometry, sidechain hydrophobicity and charge on CPN stability. We found that the amino acid side-chain composition had a large influence on the stability of CPNs as measured by NMR and MD analysis. This was particularly evident for hydrophobic and charge-based interactions but was dependent on the relative H-bond interfaces.

We found that inter-sidechain hydrophobic interactions were particularly beneficial for dimer stability. For example, CP **4** contains four Phe residues and was stable in all D-interface dimer alignments in the MD simulations. A disadvantage, however, of increasing the sidechain hydrophobicity is poor aqueous solubility as seen for CP **4**. CP **1** contained less hydrophobic alanine in the place of phenylalanine which significantly improved aqueous solubility but completely reduced the H-bond stability as measured by both MD simulations and NMR spectroscopy.

The incorporation of charged residues within the CP sequence greatly improved aqueous solubility. Additionally, inter-CP charge interactions played a key role in the stability of CPN assemblies. The MD studies showed that alignments of opposing charge stabilised antiparallel CP dimers while aligned like-charges often caused complete dimer dissociation. Although our crystal structures of **1** and **2** have aligned like-charges in their extended CPN forms, they are stabilized by opposing charge interactions of adjacent nanotubes.

The crystallography studies performed here also highlight the importance of sidechain interactions in CPN stability. Relatively small changes in amino acid composition produced distinctly different crystal morphologies. We have found folded CP aggregates (**2** and **8**), parallel H-bonded nanotubes (**1**) and antiparallel H-bonded nanotubes (**2**) despite quite similar sequences between the CPs. The dominant geometry of a CP depends on subtle differences in the side-chain composition combined with solvent composition, either promoting the formation of nanotubes stabilized by a lattice of ionic interactions or a collapse into non-porous CP aggregates with intra and intermolecular H-bonding. These principles may apply in solution, where CPs could be driven towards different assemblies depending on the solvent conditions and side-chain composition.

There is good correlation between the theoretical MD studies and experimental NMR analysis. CP dimers with stable H-bond alignments by MD had longer H-bond half-lives by NMR, while unstable CPs by MD had much shorter half-lives. Although we only applied our MD studies to CP dimers, the good correlation between the MD and experimental findings indicates that this information could be applied to extended nanostructures.

Conclusions

We investigated the factors governing the stability of CPN assemblies by crystallography, NMR and computational methods.

Crystallography studies of the peptides produced folded conformations for 2 of the CPs. These folded conformations are alternate conformations that can be expected to compete with nanotube formation in solution.

CP dimer stability is highly dependent on the amino acid configuration and is susceptible to minor changes in sequence. Furthermore, there is a significant difference in the stabilities of the L and D-interfaces in any given antiparallel H-bonded dimer.

Incorporation of hydrophobic amino acids improved CP dimer stability through inter-CP side-chain interactions, but alone was not enough to stabilize all H-bond alignments. Alignment of opposing side-chain charges improved overall dimer stability provided that the side-chains were of similar length, while alignments of negative charges were detrimental to CPN stability. Hydrophobicity should be mitigated to promote aqueous solubility and should not be sought as the sole contributor to CPN stability. Nanostructures that are stable in water will most likely require a mix of charged and hydrophobic residues.

Although we simplified these complex CPN structures by modelling dimers, we found useful correlation between the MD results and experimentally-obtained NMR data. Overall, the approach described herein will allow us to engineer the stability of CP H-bond interfaces and direct the pattern of assembly. In the future, we will apply this information to extended nanostructures to aid in the manipulation of CPN stability and assembly control.

Experimental Section

Cyclic peptide synthesis: *Coupling of the first amino acid:* 2-chlorotriyl chloride resin (83 mg, resin loading 1.2 mmol g⁻¹, 0.1 mmol) was swelled in 5 mL of CH₂Cl₂ for 30 minutes in a sinter-fitted syringe. The resin was then drained and treated with 1 equivalent (relative to resin capacity) of Fmoc-amino acid dissolved in CH₂Cl₂ (4 mL). To the resin mixture was added 6 equivalents of DIPEA relative to amino acid and the resulting mixture was agitated at room temperature overnight. The resin was drained and washed with DMF (3 x 3 mL) and treated with MeOH (2 x 3 mL) to cap any unreacted sites. The resin was then washed with DMF (3 x 3 mL) and transferred to an SPPS reaction vessel. *Automated synthesis of linear peptides:* The linear peptides were prepared using an automated solid-phase peptide-synthesiser (Protein Technologies Inc. PS3). On each coupling cycle, the resin was first washed with DMF (3 x 30 s). Fmoc deprotection was achieved using 20% piperidine in DMF (2 x 5 min) followed by washing with DMF (6 x 30 s) to provide the resin-bound free amino-terminal of the peptide. Amino acid couplings used three equivalents of Fmoc amino acid and 2-(6-chloro-1H-benzotriazole-1-yl)-1,1,3,3-tetramethylammonium hexafluorophosphate (HCTU), relative to resin loading. The amino acid and HCTU was dissolved in a solution of 7% DIPEA in DMF. The solution was added to the resin which was agitated at room temperature for 1 h, drained and washed with DMF (3 x 30 s). After coupling the final amino acid, a further Fmoc deprotection was performed to obtain the resin-bound peptide with free amino terminal. The resin was transferred to a sinter-fitted syringe and washed with DMF (3 x 3 mL), MeOH (3 x 3 mL) and Et₂O (3 x 3 mL). *Peptide cleavage from resin:* The resin-bound linear peptide was treated with a solution of 20% 1,1,1,3,3,3-hexafluoroisopropanol (HFIP) in CH₂Cl₂ (3 x 3 mL x 10 min) and the HFIP washings were collected by filtration. The resin was then washed with CH₂Cl₂ (3 x 3 mL). The combined HFIP and CH₂Cl₂ washings were concentrated under reduced pressure and freeze-dried from 1:1

ACN/H₂O to yield the side-chain-protected linear peptide as a white powder. A sample of the peptide was deprotected and analysed by LCMS to confirm the linear sequence. *Cyclisation:* The linear peptide was added to DMF (7 mg/mL) and treated with 3 equivalents of PyCLOCK and 6 equivalents of DIPEA. The solution was stirred at room temperature for 2 days before being concentrated under reduced pressure to yield a thick oil. The oil was freeze-dried from 1:1 ACN/H₂O to yield the crude side-chain-protected cyclic peptide as an off-white solid. *Deprotection:* The side chain protecting groups of the cyclic peptide were removed by treatment with a solution of TFA/TIPS/H₂O (95:2.5:2.5 v/v, 2 mL) for 3 h. The TFA was evaporated using a stream of N₂ gas and the remaining oil was then treated with ice-cold Et₂O to precipitate the peptide. The precipitate was collected by centrifugation and freeze-dried from 1:1 ACN/H₂O to yield the crude cyclic deprotected peptide as a white solid. *Purification:* Peptides were purified by preparative reverse-phase HPLC using a Waters Associates liquid chromatography system (Model 600 Controller and Waters 486 Tunable Absorbance Detector) with a Phenomenex Luna C8(2) 100 Å, 10 µm, 250 x 21.2 mm column with 0.1% TFA/H₂O as buffer A and 0.1% TFA/ACN as buffer B with a flow rate of 10 mL/min.

(CPs 1, 2, 5): Synthesis and characterisation previously reported.²²

(CP3): *Linear:* HOOC-D-Leu-Lys(Boc)-D-Leu-Asp(tBu)-D-Leu-Lys(Boc)-D-Phe-Asp(tBu)-NH₂. White powder, 53.7% yield, MS-ESI (deprotected): [M + H]⁺ 991.95, [M + 2H]²⁺ 496.80. *Cyclic:* *cyclo*(D-Leu-Lys-D-Leu-Asp-D-Leu-Lys-D-Phe-Asp). Purification gradient: 20-60% buffer B over 60 min, R_T = 25.5 min (37.0% B). Yield: 14.7 mg (27.5%) as a white solid. ¹H NMR (400 MHz, DMSO-*d*₆) δ 12.28 (s, 2H), 8.37 – 8.16 (m, 5H), 8.11 (d, *J* = 7.1 Hz, 1H), 8.04 – 7.94 (m, 2H), 7.63 (s, 6H), 7.29 – 7.15 (m, 5H), 4.66 – 4.53 (m, 3H), 4.46 – 4.27 (m, 5H), 2.92 (d, *J* = 15.7 Hz, 2H), 2.79 – 2.60 (m, 7H), 2.39 – 2.27 (m, 2H), 1.65 – 1.32 (m, 16H), 1.28 – 1.08 (m, 5H), 0.96 – 0.73 (m, 17H). HRMS (ESI) [M + Na]⁺ calculated: 995.5536, found: 995.5537, [M + H]⁺ calculated: 973.5717, found: 973.5727, [M + 2H]²⁺ calculated: 487.2895, found: 487.2913.

(CP4): *Linear:* HOOC-D-Phe-Lys(Boc)-D-Phe-Asp(tBu)-D-Phe-Lys(Boc)-D-Phe-Asp(tBu)-NH₂. White powder, 58.5% yield, MS-ESI (deprotected): [M + H]⁺ 1094.00, [M + 2H]²⁺ 547.80. *Cyclic:* *cyclo*[(Asp-D-Phe-Lys-D-Phe)₂]. Purification gradient: 0-50% buffer B over 60 min, R_T = 50.4 min (41.9% B). Yield: 9.9 mg (18.1%) as a white solid. ¹H NMR (400 MHz, DMSO-*d*₆) δ 12.13 (s, 2H), 8.29 (d, *J* = 8.3 Hz, 2H), 8.21 (t, *J* = 9.1 Hz, 4H), 7.98 (d, *J* = 8.4 Hz, 2H), 7.53 (s, 6H), 7.20 – 7.04 (m, 20H), 4.67 – 4.52 (m, 6H), 4.25 (dd, *J* = 13.9, 7.6 Hz, 2H), 2.88 – 2.72 (m, 5H), 2.68 – 2.59 (m, 3H), 2.57 – 2.48 (m, 6H), 2.17 – 2.00 (m, 5H), 1.25 – 1.13 (m, 6H), 0.98 (dd, *J* = 13.5, 7.8 Hz, 4H), 0.81 – 0.57 (m, 5H). HRMS (ESI) [M + Na]⁺ calculated: 1097.5067, found: 1097.5048, [M + H]⁺ calculated: 1075.5247, found: 1075.5258, [M + 2H]²⁺ calculated: 538.2660, found: 538.2679.

(CP6): *Linear:* HOOC-D-Leu-Leu-D-His(Trt)-His(Trt)-D-Leu-Leu-D-His(Trt)-His(Trt)-NH₂. White powder, 70.4% yield, MS-ESI (deprotected): [M + H]⁺ 1019.85, [M + 2H]²⁺ 510.70. *Cyclic:* *cyclo*[(His-D-His-Leu-D-Leu)₂]. Purification gradient: 0-60% buffer B (0.1% TFA in 90% ACN/H₂O) over 60 min, R_T = 33.5 min (30.1% ACN/H₂O). Yield: 13.1 mg (37.4%) as a white solid from half of the linear precursor. ¹H NMR (400 MHz, DMSO-*d*₆) δ 8.96 (s, 1H), 8.94 (s, 1H), 8.50 (d, *J* = 9.3 Hz, 1H), 8.37 (t, *J* = 8.4 Hz, 2H), 8.25 (d, *J* = 8.8 Hz, 1H), 7.33 (s, 1H), 7.24 (s, 1H), 4.86 – 4.74 (m, 2H), 4.49 (td, *J* = 9.2, 4.9 Hz, 1H), 4.41 – 4.33 (m, 1H), 3.04 – 2.82 (m, 4H), 2.74 (dd, *J* = 15.1, 9.2 Hz, 2H), 1.39 – 1.02 (m, 6H), 0.88 – 0.65 (m, 12H). HRMS (ESI) [M + H]⁺ calculated: 1001.5792, found: 1001.5796, [M + 2H]²⁺ calculated: 501.2932, found: 501.2948, [M + 3H]³⁺ calculated: 334.5312, found: 334.5330.

(CP7): *Linear:* HOOC-D-Leu-Lys(Boc)-D-Leu-Glu(tBu)-D-Leu-Lys(Boc)-D-Leu-Glu(tBu)-NH₂. White powder, 50.4% yield, MS-ESI (deprotected): [M + H]⁺ 986.05, [M + 2H]²⁺ 493.85. *Cyclic:* *cyclo*[(Glu-D-Leu-Lys-D-Leu)₂]. Purification gradient: 20-60% buffer B over 60 min, R_T = 21.1 min (34.1% B). Yield: 7.4 mg (15.3%) as a white solid. ¹H NMR (400 MHz, DMSO-*d*₆) δ 12.03 (s, 1H), 8.23 – 8.00 (m, 4H), 7.54 (s, 3H), 4.46 – 4.25 (m, 4H), 2.66 (dt, *J* = 12.7, 6.3 Hz, 2H), 2.10 (dt, *J* = 10.0, 7.2 Hz, 2H), 1.86 – 1.72 (m,

2H), 1.72 – 1.09 (m, 18H), 0.86 – 0.71 (m, 12H). HRMS (ESI) $[M + Na]^+$ calculated: 989.6006, found: 989.5985, $[M + H]^+$ calculated: 967.6186, found: 967.6192, $[M + 2H]^{2+}$ calculated: 484.313, found: 484.3146.

(CP8): Linear: HOOC-D-Leu-Orn(Boc)-D-Leu-Asp(tBu)-D-Leu-Orn(Boc)-D-Leu-Asp(tBu)-NH₂. White powder, 59.6% yield, MS-ESI (deprotected): $[M + H]^+$ 929.95, $[M + 2H]^{2+}$ 465.75. *Cyclic:* *cyclo*[(Asp-D-Leu-Orn-D-Leu)₂]. Purification gradient: 20-60% buffer B over 60 min, R_T = 25.5 min (37.0% B). Yield: 11.3 mg (31.3%) as a white solid. ¹H NMR (400 MHz, DMSO-*d*₆) δ 12.35 (s, 1H), 8.29 (d, *J* = 6.9 Hz, 2H), 8.02 (dd, *J* = 27.5, 6.8 Hz, 2H), 7.66 (s, 3H), 4.60 (dd, *J* = 12.6, 6.5 Hz, 1H), 4.50 – 4.27 (m, 3H), 2.76 (d, *J* = 19.5 Hz, 2H), 2.63 (ddd, *J* = 24.6, 10.1, 5.5 Hz, 2H), 1.73 – 1.23 (m, 11H), 0.94 – 0.70 (m, 12H). HRMS (ESI) $[M + Na]^+$ calculated: 933.5380, found: 933.5366, $[M + H]^+$ calculated: 911.5560, found: 911.5568, $[M + 2H]^{2+}$ calculated: 455.2738, found: 455.2780.

(CP9): Linear: HOOC-D-Leu-Orn(Boc)-D-Leu-Glu(tBu)-D-Leu-Orn(Boc)-D-Leu-Glu(tBu)-NH₂. White powder, 47.9% yield, MS-ESI (deprotected): $[M + H]^+$ 958.00, $[M + 2H]^{2+}$ 479.80. *Cyclic:* *cyclo*[(Glu-D-Leu-Orn-D-Leu)₂]. Purification gradient: 20-60% buffer B over 60 min, R_T = 21.0 min (34.0% B). Yield: 10.5 mg (22.6%) as a white solid. ¹H NMR (400 MHz, DMSO-*d*₆) δ 12.10 (s, 1H), 8.28 – 8.19 (m, 3H), 8.16 (d, *J* = 8.8 Hz, 1H), 7.65 (s, 3H), 4.56 – 4.40 (m, 4H), 2.84 – 2.73 (m, 2H), 2.16 (dd, *J* = 15.3, 9.4 Hz, 2H), 1.91 – 1.20 (m, 14H), 0.97 – 0.77 (m, 12H). HRMS (ESI) $[M + Na]^+$ calculated: 961.5693, found: 961.5689, $[M + H]^+$ calculated: 939.5873, found: 939.5883, $[M + 2H]^{2+}$ calculated: 470.2973, found: 470.2988.

(CP10): Linear: HOOC-D-Leu-Lys(Boc)-D-Leu-Asp(tBu)-D-Leu-Asp(tBu)-D-Leu-Lys(Boc)-NH₂. White powder, 61.4% yield, MS-ESI (deprotected): $[M + H]^+$ 958.00, $[M + 2H]^{2+}$ 479.85. *Cyclic:* *cyclo*(D-Leu-Lys-D-Leu-Asp-D-Leu-Asp-D-Leu-Lys). Purification gradient: 20-60% buffer B over 60 min, R_T = 24.8 min (36.5% B). Yield: 14.2 mg (41.4%) as a white solid. ¹H NMR (400 MHz, DMSO-*d*₆) δ 12.37 (s, 2H), 8.28 – 8.06 (m, 6H), 7.98 (d, *J* = 7.9 Hz, 1H), 7.86 (d, *J* = 8.7 Hz, 1H), 7.64 (s, 6H), 4.61 (qd, *J* = 7.9, 2.4 Hz, 2H), 4.41 – 4.20 (m, 6H), 2.80 – 2.55 (m, 8H), 1.71 – 1.17 (m, 26H), 0.93 – 0.75 (m, 24H). HRMS (ESI) $[M + Na]^+$ calculated: 961.5693, found: 961.5681, $[M + H]^+$ calculated: 939.5873, found: 939.5884, $[M + 2H]^{2+}$ calculated: 470.2973, found: 470.2990.

(CP11): Linear: HOOC-D-Leu-Lys(Boc)-D-Leu-Lys(Boc)-D-Leu-Lys(Boc)-D-Leu-Asp(tBu)-NH₂. White powder, 54.2% yield, MS-ESI (deprotected): $[M + H]^+$ 971.05, $[M + 2H]^{2+}$ 486.25. *Cyclic:* *cyclo*(D-Leu-Lys-D-Leu-Lys-D-Leu-Lys-D-Leu-Asp). Purification gradient: 20-60% buffer B over 60 min, R_T = 24.0 min (36.0% B). Yield: 12.4 mg (36.1%) as a white solid on 0.1 mmol scale synthesis. ¹H NMR (400 MHz, DMSO-*d*₆) δ 12.36 (s, 1H), 8.28 (d, *J* = 7.9 Hz, 1H), 8.20 (dd, *J* = 10.9, 9.0 Hz, 2H), 8.16 – 7.95 (m, 5H), 7.68 (s, 8H), 4.63 (dd, *J* = 13.7, 7.8 Hz, 1H), 4.46 – 4.32 (m, 7H), 2.82 – 2.54 (m, 10H), 1.69 – 1.19 (m, 36H), 0.94 – 0.77 (m, 24H). HRMS (ESI) $[M + H]^+$ calculated: 952.6554, found: 952.6561, $[M + 2H]^{2+}$ calculated: 476.8313, found: 476.8327, $[M + 3H]^{3+}$ calculated: 318.2233, found: 318.2245.

(CP12): Linear: HOOC-D-Leu-Lys(Boc)-D-Leu-Asp(tBu)-D-Leu-Asp(tBu)-D-Leu-Asp(tBu)-NH₂. White powder, 53.1% yield, MS-ESI (deprotected): $[M + H]^+$ 944.90, $[M + 2H]^{2+}$ 473.25. *Cyclic:* *cyclo*(D-Leu-Lys-D-Leu-Asp-D-Leu-Asp-D-Leu-Asp). Purification gradient: 20-60% buffer B over 60 min, R_T = 34.9 min (43.3% B). Yield: 10.6 mg (20.8%) as a white solid. ¹H NMR (400 MHz, DMSO-*d*₆) δ 12.35 (s, 3H), 8.31 – 8.17 (m, 3H), 8.08 (d, *J* = 6.9 Hz, 1H), 8.04 – 7.93 (m, 3H), 7.70 (d, *J* = 8.2 Hz, 1H), 7.62 (s, 3H), 4.66 – 4.52 (m, 3H), 4.44 – 4.35 (m, 1H), 4.31 – 4.20 (m, 3H), 4.19 – 4.11 (m, 1H), 2.80 – 2.54 (m, 9H), 1.71 – 1.20 (m, 20H), 0.95 – 0.72 (m, 24H). HRMS (ESI) $[M + Na]^+$ calculated: 948.5013, found: 948.5019, $[M + H]^+$ calculated: 926.5193, found: 926.5206, $[M + 2H]^{2+}$ calculated: 463.7633, found: 463.7650.

(CP13): Linear: HOOC-D-Leu-Leu-D-Leu-Asp(tBu)-D-Leu-Leu-D-Leu-Lys(Boc)-NH₂. White powder, 65.7% yield, MS-ESI (deprotected): $[M + H]^+$ 941.05, $[M + 2H]^{2+}$ 471.35. *Cyclic:* *cyclo*(D-Leu-Leu-D-Leu-Asp-D-Leu-Leu-

D-Leu-Lys). Yield: 63.0 mg of crude peptide at 41.8% purity as a white solid. MS-ESI: $[M + H]^+$ 923.05, $[M + 2H]^{2+}$ 462.35.

(CP14): Linear: HOOC-Leu-D-sp(tBu)-Lys(Boc)-D-Leu-Leu-D-Asp(tBu)-Lys(Boc)-D-Leu-NH₂. White powder, 69.3% yield, MS-ESI (deprotected): $[M + H]^+$ 957.75, $[M + 2H]^{2+}$ 479.60. *Cyclic:* *cyclo*[(Lys-D-Asp-Leu-D-Leu)₂]. Purification gradient: 0-60% buffer B over 60 min, R_T = 28.2 min (28.2% B). Yield: 6.5 mg (10.0%) as a white solid. ¹H NMR (400 MHz, DMSO-*d*₆) δ 8.31 (d, *J* = 6.5 Hz, 1H), 8.27 (d, *J* = 8.1 Hz, 1H), 7.93 (d, *J* = 8.7 Hz, 1H), 7.88 (d, *J* = 8.3 Hz, 1H), 7.62 (s, 3H), 4.59 (dd, *J* = 13.1, 7.7 Hz, 1H), 4.50 – 4.40 (m, 1H), 4.38 – 4.27 (m, 1H), 4.12 (dd, *J* = 13.7, 7.7 Hz, 1H), 2.80 – 2.70 (m, 3H), 1.44 (m, 12H), 0.83 (m, 12H). HRMS (ESI) $[M + Na]^+$ calculated: 961.5693, found: 961.5667, $[M + H]^+$ calculated: 939.5873, found: 939.5885, $[M + 2H]^{2+}$ calculated: 470.2973, found: 470.2986.

(CP15): Linear: HOOC-D-Leu-Lys(Boc)-D-Leu-Asp(tBu)-D-Leu-Lys(Boc)-D-Leu-Asp(tBu)-D-Leu-Lys(Boc)-D-Leu-Asp(tBu)-NH₂. White powder, 51.7% yield, MS-ESI (deprotected): $[M + H]^+$ 1428.30, $[M + 2H]^{2+}$ 714.60. *Cyclic:* *cyclo*[(Asp-D-Leu-Lys-D-Leu)₃]. Purification gradient: 20-60% buffer B over 60 min, R_T = 22.5 min (35.0% B). Yield: 5.8 mg (8.9%). ¹H NMR (400 MHz, DMSO-*d*₆) δ 12.38 (s, 1H), 8.28 (d, *J* = 4.0 Hz, 1H), 8.14 – 7.93 (m, 3H), 7.63 (s, 3H), 4.57 (dd, *J* = 13.6, 6.9 Hz, 1H), 4.39 – 4.26 (m, 3H), 2.79 – 2.55 (m, 5H), 1.73 – 1.37 (m, 11H), 1.30 – 1.20 (m, 2H), 0.90 – 0.79 (m, 12H). HRMS (ESI) $[M + H]^+$ calculated: 1408.8774, found: 1408.8768, $[M + 2H]^{2+}$ calculated: 704.9423, found: 704.9440, $[M + 3H]^{3+}$ calculated: 470.2973, found: 470.2988.

Crystallisation: Crystal screening was performed at the CSIRO C3 crystallisation centre using sitting drop vapour-diffusion in 96 well plates with droplets of 150 nL peptide and 150 nL of reservoir solution, equilibrated against a reservoir of 50 μL. Initial screens were set up using the 'shotgun' screen⁴⁸ at 20°C and each well was imaged by robot 15 times over a period of 80 days. Conditions that provided initial crystal hits were selected for further additive optimisation, using the Additive Screen HT (Hampton Research, USA) mixed with the original hit condition (90:10 v/v original condition:additive). Crystals were often seen after 1 day and grew to final size within 7 days. Peptides were found to crystallise best at concentrations of 5 mg/mL, as 10 mg/mL often caused precipitation and <2 mg/mL provided little to no supersaturation (precipitation or crystal growth).

Crystallography: Diffraction data was collected using the MX2 micro-focus beamline at the Australian Synchrotron on an ADSC Quantum 315r CCD detector at 100(2) K using Si(111) monochromated synchrotron radiation. Bluice control software⁴⁹ was used for data-collection and integration was carried out with XDS.⁵⁰ Structure of CP 8 was solved by dual space methods using SHELXT⁴³ and refined with SHELXL.⁴⁴ The structure of CP 2 was solved by molecular replacement in the CCP4 suite⁴⁵ using Phaser⁴⁶ for initial model fitting and iterated refinement using Refmac.⁴⁷ Crystal data for 2 and 8 are given in Table S2.

NMR spectroscopy: 1D ¹H NMR spectra of peptide products were recorded on a 600 MHz Bruker Avance III HD spectrometer with CryoProbe, at 298 K. Samples were dissolved in 10% D₂O in H₂O for initial analysis and 100% D₂O for ¹H-D exchange experiments. The pH of samples was measured to be 3.0 ± 0.3. All of the NMR spectra were processed using TopSpin 3.0 (Bruker BioSpin GmbH). ¹H-D exchange studies were performed immediately following dissolution of CP tetramers at 2 mM in 100% D₂O. The first spectrum was acquired within 8 min of dissolution and up to 13 spectra in total were acquired over 60 to 90 min, depending on the rate of H^N signal exchange. CP half-lives were averaged according to the number of unique H^N signals.

Turbidity assessment: Samples were assessed by eye for turbidity and ranked as low, medium or highly turbid samples. Examples of turbidity are provided in the supplementary information (Figure S1).

Molecular Dynamics simulations: Model building and molecular dynamics studies were conducted in Maestro (Schrödinger version 10.3) using the integrated Desmond MD software (D. E. Shaw Research, version 4.3).⁵¹ CP subunits were built manually using the crystal structure of CP 2²² as a backbone scaffold for antiparallel backbone-backbone hydrogen bonded dimers. Dimers were minimised in water for 2500 iterations using the OPLS 2005 forcefield^{52, 53} prior to preparation of the system for simulation. Systems were prepared as orthorhombic cells of 35 x 35 x 35 Å³ and were solvated by SPC water with 0.15M NaCl and additional Na⁺/Cl⁻ counterions to neutralise the system. Simulations were conducted under the OPLS 2005 forcefield with NPT ensemble class at 300 K and 1.01325 bar with a 2 fs timestep. Nose-Hoover chain was employed for the thermostat method and Martyna-Tobias-Klein for the barostat method. Simulations used periodic boundary conditions and the particle-mesh Ewald method for long range electrostatics. Simulations were run for 100 ns and evaluated for stability according to the number of intermolecular backbone-backbone H-bonds.

Acknowledgements

MRS acknowledges an RTP scholarship provided by the Australian Government. X-ray diffraction data was acquired using the MX2 beamline at the Australian Synchrotron.

Keywords: cyclic peptide • nanotube • self-assembly • molecular dynamics • NMR

- Ghadiri, M. R.; Granja, J. R.; Milligan, R. A.; McRee, D. E.; Khazanovich, N. Self-assembling organic nanotubes based on a cyclic peptide architecture. *Nature* **1993**, 366, 324-327.
- Ghadiri, M. R.; Kobayashi, K.; Granja, J. R.; Chadha, R. K.; McRee, D. E. The Structural and Thermodynamic Basis of the Formation of Self-Assembled Peptide Nanotubes. *Angew. Chem. Int. Ed.* **1995**, 34, 93-95.
- Hartgerink, J. D.; Granja, J. R.; Milligan, R. A.; Ghadiri, M. R. Self-Assembling Peptide Nanotubes. *J. Am. Chem. Soc.* **1996**, 118, 43-50.
- Santis, P. D.; Morosetti, S.; Rizzo, R. Conformational Analysis of Regular Enantiomeric Sequences. *Macromolecules* **1973**, 7, 52-58.
- Tomasich, L.; Lorenzi, G. P. Some Cyclic Oligopeptides with S₂N Symmetry. *Helvetica Chimica Acta* **1987**, 70, 1012 - 1016.
- Pavone, V.; Benedetti, E.; Di Blasio, B.; Lombardi, A.; Pedone, C.; Tomasich, L.; Lorenzi, G. P. Regularly Alternating L,D-Peptides. III. Hexacyclic Peptides from Valine or Phenylalanine. *Biopolymers* **1989**, 28, 215-223.
- Steinem, C.; Janshoff, A.; Vollmer, M. S.; Ghadiri, M. R. Reversible Photoisomerization of Self-Organized Cylindrical Peptide Assemblies at Air-Water and Solid Interfaces. *Langmuir* **1999**, 15, 3956-3964.
- Vollmer, M. S.; Clark, T. D.; Steinem, C.; Ghadiri, M. R. Photoswitchable Hydrogen-Bonding in Self-Organized Cylindrical Peptide Systems. *Angew. Chem. Int. Ed.* **1999**, 38, 1598-1601.
- Gokhale, R.; Couet, J.; Biesalski, M. In situ cross-linking of the shell of self-assembled peptide nanotubes. *Phys. Status Solidi A* **2010**, 207, 878-883.
- Maarseveen, J. H. V.; Horne, W. S.; Ghadiri, M. R. Efficient Route to C₂ Symmetric Heterocyclic Backbone Modified Cyclic Peptides. *Org. Lett.* **2005**, 7, 4503-4506.
- Clark, T. D.; Ghadiri, M. R. Supramolecular Design by Covalent Capture. Design of a Peptide Cylinder via Hydrogen-Bond-Promoted Intermolecular Olefin Metathesis. *J. Am. Chem. Soc.* **1995**, 117, 12364-12365.
- Clark, T. D.; Kobayashi, K.; Ghadiri, M. R. Covalent capture and stabilization of cylindrical beta-sheet peptide assemblies. *Chem. Eur. J.* **1999**, 5, 782-792.
- Silk, M. R.; Mohanty, B.; Sampson, J. B.; Scanlon, M. J.; Thompson, P. E.; Chalmers, D. K. Controlled Construction of Cyclic D/L Peptide Nanorods. *Angewandte Chemie* **2019**, 58, 596-601.
- Fuertes, A.; Ozores, H. L.; Amarin, M.; Granja, J. R. Self-assembling Venturi-like peptide nanotubes. *Nanoscale* **2017**, 9, 748-753.
- Ozores, H. L.; Amarin, M.; Granja, J. R. Self-Assembling Molecular Capsules Based on alpha,gamma-Cyclic Peptides. *J. Am. Chem. Soc.* **2017**.
- Amarin, M.; Castedo, L.; Granja, J. R. New Cyclic Peptide Assemblies with Hydrophobic Cavities: The Structural and Thermodynamic Basis of a New Class of Peptide Nanotubes. *J. Am. Chem. Soc.* **2003**, 125, 2844-2845.
- Amarin, M.; Castedo, L.; Granja, J. R. Self-assembled peptide tubelets with 7 Å pores. *Chemistry* **2005**, 11, 6543-51.
- Bong, D. T.; Ghadiri, M. R. Self-Assembling Cyclic Peptide Cylinders as Nuclei for Crystal Engineering. *Angewandte Chemie* **2001**, 40, 2163-2166.
- Brea, R. J.; Amarin, M.; Castedo, L.; Granja, J. R. Methyl-blocked dimeric alpha,gamma-peptide nanotube segments: formation of a peptide heterodimer through backbone-backbone interactions. *Angew. Chem. Int. Ed.* **2005**, 44, 5710-3.
- Brea, R. J.; Castedo, L.; Granja, J. R. Large-diameter self-assembled dimers of alpha,gamma-cyclic peptides, with the nanotubular solid-state structure of cyclo-[(L-Leu-D-(Me)N-gamma-Acp)₄]-4CHCl₂COOH. *Chemical communications* **2007**, 3267-9.
- Amarin, M.; Castedo, L.; Granja, J. R. Folding control in cyclic peptides through N-methylation pattern selection: formation of antiparallel beta-sheet dimers, double reverse turns and supramolecular helices by 3alpha,gamma cyclic peptides. *Chemistry* **2008**, 14, 2100-11.
- Silk, M. R.; Newman, J.; Ratcliffe, J. C.; White, J. F.; Caradoc-Davies, T.; Price, J. R.; Perrier, S.; Thompson, P. E.; Chalmers, D. K. Parallel and antiparallel cyclic D/L peptide nanotubes. *Chem. Commun.* **2017**, 53, 6613-6616.
- Sun, X.; Lorenzi, G. P. On the Stacking of β-Rings: The Solution Self-Association Behaviour of Two Partially N-Methylated Cyclo(hexaleucines). *Helvetica Chimica Acta* **1994**, 77, 1520-1526.
- Reiriz, C.; Castedo, L.; Granja, J. R. New alpha,gamma-cyclic peptides-nanotube molecular caps using alpha,alpha-dialkylated alpha-amino acids. *J. Pept. Sci.* **2008**, 14, 241-9.
- Kobayashi, K.; Granja, J. R.; Ghadiri, M. R. β-Sheet Peptide Architecture: Measuring the Relative Stability of Parallel vs. Antiparallel β-Sheets. *Angew. Chem. Int. Ed.* **1995**, 34, 95-98.
- Horne, W. S.; Ashkenasy, N.; Ghadiri, M. R. Modulating charge transfer through cyclic D,L-alpha-peptide self-assembly. *Chem. Eur. J.* **2005**, 11, 1137-1144.
- Rodriguez-Vazquez, N.; Garcia-Fandino, R.; Aldegunde, M. J.; Brea, J.; Loza, M. I.; Amarin, M.; Granja, J. R. cis-Platinum Complex Encapsulated in Self-Assembling Cyclic Peptide Dimers. *Org. Lett.* **2017**.
- Hourani, R.; Zhang, C.; van der Weegen, R.; Ruiz, L.; Li, C.; Keten, S.; Helms, B. A.; Xu, T. Processable cyclic peptide nanotubes with tunable interiors. *J. Am. Chem. Soc.* **2011**, 133, 15296-9.
- Asthagiri, D.; Bashford, D. Continuum and Atomistic Modeling of Ion Partitioning into a Peptide Nanotube. *Biophysical journal* **2002**, 82, 1176-1189.
- Hwang, H.; Schatz, G. C.; Ratner, M. A. Ion Current Calculations Based on Three Dimensional Poisson-Nernst-Planck Theory for a Cyclic Peptide Nanotube. *J. Phys. Chem. B* **2006**, 110, 6999-7008.
- Garcia-Fandino, R.; Granja, J. R.; D'Abramo, M.; Orozco, M. Theoretical Characterization of the Dynamical Behaviour and Transport Properties of α,γ-peptide Nanotubes in Solution. *J. Am. Chem. Soc.* **2009**, 131, 15678-15686.
- Liu, H.; Chen, J.; Shen, Q.; Fu, W.; Wu, W. Molecular Insights on the Cyclic Peptide Nanotube-Mediated Transportation of Antitumor Drug 5-Fluorouracil. *Molecular Pharmaceutics* **2010**, 7, 1985-1994.
- Liu, J.; Fan, J.; Tang, M.; Cen, M.; Yan, J.; Liu, Z.; Zhou, W. Water Diffusion Behaviours and Transportation Properties in Transmembrane Cyclic Hexa-, Octa and Decapeptide Nanotubes. *J. Phys. Chem. B* **2010**, 114, 12183-12192.
- Li, R.; Fan, J.; Li, H.; Yan, X.; Yu, Y. Exploring the dynamic behaviors and transport properties of gas molecules in a transmembrane cyclic peptide nanotube. *J. Phys. Chem. B* **2013**, 117, 14916-27.
- Montenegro, J.; Ghadiri, M. R.; Granja, J. R. Ion Channel Models Based on Self-Assembling Cyclic Peptide Nanotubes. *Accounts of Chemical Research* **2013**, 46, 2955-2965.
- Alsina, M. A.; Gaillard, J. F.; Keten, S. Conformational changes during permeation of Na⁺ through a modified cyclic peptide nanotube promote energy landscape roughness. *Phys. Chem. Chem. Phys.* **2016**, 18, 31698-31710.
- Vijayaraj, R.; Raman, S. S.; Kumar, R. M.; Subramanian, V. Studies on the Structure and Stability of Cyclic Peptide Based Nanotubes Using Oligomeric Approach: A Computational Chemistry Investigation. *J. Phys. Chem. B* **2010**, 114, 16574-16583.
- Vijayaraj, R.; Van Damme, S.; Bultinck, P.; Subramanian, V. Molecular dynamics and umbrella sampling study of stabilizing factors in cyclic peptide-based nanotubes. *J. Phys. Chem. B* **2012**, 116, 9922-33.
- Garcia-Fandino, R.; Castedo, L.; Granja, J. R.; Vazquez, S. A. Interaction and Dimerization Energies in Methyl-Blocked α,γ-Peptide Nanotube Segments. *J. Phys. Chem. B* **2010**, 114, 4973-4983.
- Zhu, J.; Cheng, J.; Liao, Z.; Lai, Z.; Liu, B. Investigation of structures and properties of cyclic peptide nanotubes by experiment and molecular dynamics. *J. Comput. Aided Mol. Des.* **2008**, 22, 773-81.

41. Mant, C. T.; Kovacs, J. M.; Kim, H.-M.; Pollock, D. D.; Hodges, R. S. Intrinsic amino acid side-chain hydrophilicity/hydrophobicity coefficients determined by reversed-phase high-performance liquid chromatography of model peptides: comparison with other hydrophilicity/hydrophobicity scales. *Biopolymers* **2009**, *92*, 573-595.
42. Fazio, V. J.; Peat, T. S.; Newman, J. A drunken search in crystallization space. *Acta Crystallographica Section F* **2014**, *70*, 1303-1311.
43. Sheldrick, G. M. SHELXT - Integrated space-group and crystal-structure determination. *Acta Crystallographica Section A* **2015**, *71*, 3-8.
44. Sheldrick, G. M. A short history of SHELX. *Acta Crystallographica Section A* **2008**, *64*, 112-122.
45. Winn, M. D.; Ballard, C. C.; Cowtan, K. D.; Dodson, E. J.; Emsley, P.; Evans, P. R.; Keegan, R. M.; Krissinel, E. B.; Leslie, A. G.; McCoy, A.; McNicholas, S. J.; Murshudov, G. N.; Pannu, N. S.; Potterton, E. A.; Powell, H. R.; Read, R. J.; Vagin, A.; Wilson, K. S. Overview of the CCP4 suite and current developments. *Acta Cryst.* **2011**, D67, 235-242.
46. McCoy, A. J.; Grosse-Kunstleve, R. W.; Adams, P. D.; Winn, M. D.; Storoni, L. C.; Read, R. J. Phaser crystallographic software. *Journal of Applied Crystallography* **2007**, *40*, 658-674.
47. Murshudov, G. N.; Vagin, A. A.; Dodson, E. J. Refinement of Macromolecular Structures by the Maximum-Likelihood Method. *Acta Cryst.* **1997**, D53, 240-255.
48. Fazio, V. J.; Peat, T. S.; Newman, J. A drunken search in crystallization space. *Acta crystallographica. Section F, Structural biology communications* **2014**, *70*, 1303-11.
49. McPhillips, T. M.; McPhillips, S. E.; Chiu, H. J.; Cohen, A. E.; Deacon, A. M.; Ellis, P. J.; Garman, E.; Gonzalez, A.; Sauter, N. K.; Phizackerley, R. P.; Soltis, S. M.; Kuhn, P. Blu-Ice and the Distributed Control System : software for data acquisition and instrument control at macromolecular crystallography beamlines. *Journal of Synchrotron Radiation* **2002**, *9*, 401-406.
50. Kabsch, W. Automatic processing of rotation diffraction data from crystals of initially unknown symmetry and cell constants. *J. Appl. Cryst.* **1993**, *26*, 795-800.
51. Bowers, K. J.; Chow, E.; Xu, H.; Dror, R. O.; Eastwood, M. P.; Gregersen, B. A.; Klepeis, J. L.; Kolossvary, I.; Moraes, M. A.; Sacerdoti, F. D.; Salmon, J. K.; Shan, Y.; Shaw, D. E. Scalable algorithms for molecular dynamics simulations on commodity clusters. *Proceedings of the ACM/IEEE Conference on Supercomputing (SC06), Tampa, Florida* **2006**.
52. Jorgensen, W. L.; Maxwell, D. S.; Tirado-Rives, J. Development and Testing of the OPLS All-Atom Force Field on Conformational Energetics and Properties of Organic Liquids. *Journal of the American Chemical Society* **1996**, *118*, 11225-11236.
53. Kaminski, G. A.; Friesner, R. A.; Tirado-Rives, J.; Jorgensen, W. L. Evaluation and Reparametrization of the OPLS-AA Force Field for Proteins via Comparison with Accurate Quantum Chemical Calculations on Peptides. *The Journal of Physical Chemistry B* **2001**, *105*, 6474-6487.

Chapter 4 – Appendix

Studies of cyclic D/L peptide nanotube stability – Supplementary Information

Crystallisation

Table S1. Most effective crystallisation conditions for the CPs that formed crystals.

CP	Sequence	Optimised conditions	Crystal Habit	Max. Dimensions
2	<i>cyclo</i> [(DIKI) ₂]	1.44M trisodium citrate, 4% HFIP	Diamond/prism	~100 x 50 x 50 μm
8	<i>cyclo</i> [(DIOI) ₂]	3.6M sodium formate, 3% TFE	Thick needle	~1000 x 15 x 15 μm
10	<i>cyclo</i> (DIDIKIKI)	0.2M MgCl, 30% PEG400, 0.1M sodium HEPES pH 7.5	Needles	~100 x 8 x 8 μm
11	<i>cyclo</i> (DIKIKIKI)	0.2M MgCl, 30% PEG400, 0.1M sodium HEPES pH 7.5	Needles	~100 x 8 x 8 μm
12	<i>cyclo</i> (DIDIDIKI)	0.2M MgCl, 30% PEG400, 0.1M sodium HEPES pH 7.5	Needles	~100 x 8 x 8 μm
		1.44M trisodium citrate, 4% TFE		
		3.6M sodium formate, 4% HFIP		

Crystallography

Table S2. X-ray crystallography table of data collection and refinement.

Compound (molecules in ASU)	CP 2 (4)	CP 8 (1)
Method	Molecular replacement (Phaser)	Direct methods (SHELX)
Other molecules in ASU	H ₂ O (8), HFIP (21)	H ₂ O (3), TFE (2)
Formula	C ₂₃₉ H ₃₃₄ F ₁₂₆ N ₄₀ O ₇₇	C ₄₆ H ₇₈ F ₆ N ₁₀ O ₁₇
Model Molecular Weight	7447.649 g/mol	1185.405 g/mol
Crystal System	Orthorhombic	Orthorhombic
Space Group	(#19) <i>P</i> ₂ ₁ ₂ ₁ ₂ ₁	(#19) <i>P</i> ₂ ₁ ₂ ₁ ₂ ₁
<i>a</i>	17.791 Å	12.856(3) Å
<i>b</i>	32.628 Å	17.664(4) Å
<i>c</i>	58.015 Å	26.446(5) Å
<i>V</i>	33677 Å ³	6006(2) Å ³
<i>D</i> _c	1.458 g cm ⁻³	1.276 g cm ⁻³
<i>Z</i>	16	4
Crystal Size	0.1 x 0.05 x 0.05 mm	0.4 x 0.004 x 0.002 mm
Crystal Colour	Colourless	Colourless
Crystal Habit	Prism	Needle
Temperature	100(2) Kelvin	100(2) Kelvin
<i>λ</i> (synchrotron)	0.71073 Å	0.71073 Å
<i>μ</i> (synchrotron)	0.109 mm ⁻¹	0.109 mm ⁻¹
2 θ _{max}	-	49.44°
<i>hkl</i> range	-16 16, -29 29, -52 52	-15 15, -20 20, -31 31
<i>N</i> _{ind}	13642	10070
<i>N</i> _{obs}	9238 (<i>I</i> > 3 σ (<i>I</i>))	7274 (<i>I</i> > 2 σ (<i>I</i>))
R value (working set)	0.20431	-
R-free value (test set)	0.21682	-
GoF	-	1.100

Table S3. MD study of the average intermolecular backbone H-bonds for CP dimers in parallel geometries.

CP	Sequence	PL1-1	PL1-3	PL1-5	PL1-7
1 ^[a]	c[(DaKa) ₂]	0.9	2.5	0.9	2.5
2 ^[a]	c[(DIKl) ₂]	0.3	1.2	0.3	1.2
3	c(DIKIDIKf)	0.8	2.2	1.8	1.0
4 ^[a]	c[(DfKf) ₂]	0.2	1.7	0.2	1.7
5 ^[a]	c[(HIKl) ₂]	0.4	0.8	0.4	0.8
6 ^[a]	c[(HhLl) ₂]	0.5	0.8	0.5	0.8
7 ^[a]	c[(EIKl) ₂]	0.7	0.8	0.7	0.8
8 ^[a]	c[(DIOl) ₂]	0.1	1.2	0.1	1.2
9 ^[a]	c[(EIOl) ₂]	0.6	1.4	0.6	1.4
10	c(DIDIKIKl)	1.5	0.6	0.5	1.3
11	c(DIKIKIKl)	1.2	1.0	1.7	2.4
12	c(DIDIDIKl)	0.4	1.5	0.4	0.3
13	c(DILIKILl)	1.6	2.2	1.5	0.8
14 ^[a]	c[(KdLl) ₂]	1.8	2.0	1.8	2.0
15 ^[a,b]	c[(DIKl) ₃]	0.1	0.8	0.1	0.8

[a] For CPs with symmetry, alignment PL1-1 = PL1-5 and PL1-3 = PL1-7

[b] For comparison to 8-AA CPs, the number of H-bonds is adjusted by a factor of 2/3

Turbidity



Figure S1. From left to right; example images of low (CP 8), medium (CP 3) and high (CP 7) sample turbidity for CPs at 2 mM in 10% D₂O/H₂O.

Chapter 5

Developing the structure, stability and function of tethered cyclic D/L peptide nanorods

Our investigations into the factors contributing to CPN stability discussed in Chapter 4 highlighted the importance of side-chain interactions and the subtle differences in H-bonding arrangements for CPN stability. To expand on our investigations, we applied our stability investigations to tethered CP nanorods. Combining covalent tethering with favourable side-chain interactions could produce highly-stable, well-ordered heterogeneous CP-based material suitable for the development of functional nanomaterials. The modular design of the tethered nanorods would allow for a series of different monomeric CP-subunits to be tethered in different combinations to generate nanorods of different properties and stabilities. Furthermore, we wanted to explore the conjugation of polymers to the nanorod exterior as a means of diversifying nanorod function, post-synthesis.

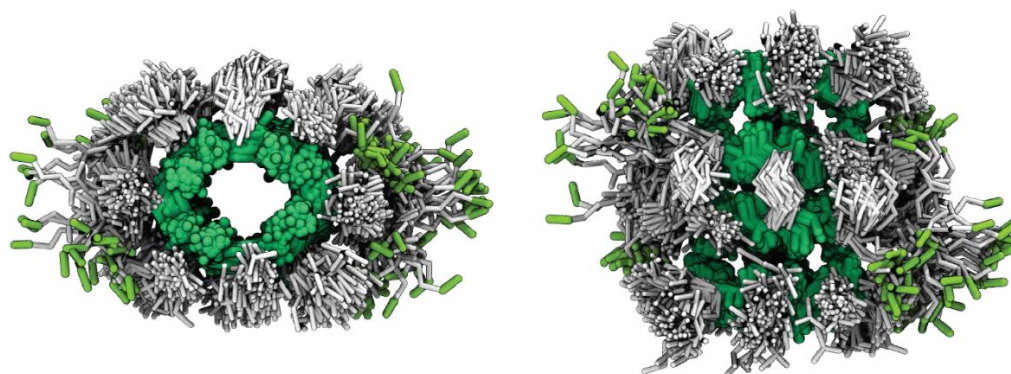


Figure i. CP nanorods are highly-modular and can be built from a variety of distinct subunits, creating nanorods of different stabilities and behaviours. This CP tetramer is shown as an overlay of the frames from an MD simulation as viewed from the top and side. The overlay highlights the stable H-bonded backbone (dark green) with a consistent conformation, shielded by the amino acid side-chains (silver). By design, this tetramer contains alkene functional groups (light green) which allows for the conjugation of other moieties such as polymers and enables post-synthetic modification of tetramer behaviour and function.

Chapter 5 explores the stability of tethered CP nanorods through the design, synthesis and analysis of a series of different CP nanorods. The nanorods were analysed experimentally by 1D and 2D NMR and theoretically by computational analysis. In addition, we investigated backbone *N*-methylation and the conjugation of polymers as a means of further modulating the structure and function of CP nanorods. Specific amino acid combinations were found to greatly enhance nanorod stability such as Leu-Ala and Leu-Lys(Alloc) side-chain alignments (**Figure i**). Several compounds were found to be stable by MD simulation and well-ordered by NMR as a result of favourable backbone H-bonding interactions. Backbone *N*-methylation had

different effects on nanorod structure depending on the position of *N*-methylation, although it induced conformational disorder in all cases. A hydrophilic polymer was effectively conjugated to the exterior of a CP tetramer, inducing further assembly and stabilising the structure to dilution-triggered disassembly.

This chapter contains the unpublished manuscript: M. R. Silk, B. Mohanty, J. Y. Rho, S. E. Ellacott, S. Perrier, M. J. Scanlon, P. E. Thompson, D. K. Chalmers, Developing the stability and function of modular nanorods built from cyclic D/L peptides. Supplementary information is included after the manuscript and contains experimental methods and analytical data.

Developing the stability and function of modular nanorods built from tetramers of cyclic octapeptides

Mitchell R. Silk, Biswaranjan Mohanty, Julia Y. Rho, Sean H. Ellacott, Sébastien Perrier, Martin J. Scanlon, Philip E. Thompson, David K. Chalmers.

Abstract: Nanorods built from tethered cyclic D/L peptides (CPs) are modular, tunable scaffolds with potential applications in biomedicine as protein-like channels or encapsulation devices. In this work, we investigate the structure-stability relationships of tetramers built from various cyclic octapeptides using NMR spectroscopy and molecular dynamics (MD) simulations in order to develop our control of their functionality. Further structural modulation was explored by backbone *N*-methylation and side-chain polymer conjugation. Assembly behaviour and H-bond stability was explored experimentally by NMR spectroscopy, revealing sequence-dependent differences in tetramer stability. A range of possible H-bonding arrangements were identified for each of the tetramer analogues and their stabilities explored by MD studies for comparison to the experimental findings. Well-ordered tetramers by NMR analysis were found to have a particular H-bonded foldamer in which they were highly stable by MD simulation. *N*-methylation was found to create conformational disorder within the CP tetramers although it was effective in blocking further H-bonding interactions. Conjugation of a hydrophilic polymer to the tetramer exterior was found to stabilize the CP material to dilution-induced disassembly. This work represents a significant advancement in tethered tetramer development and highlights their suitability for the development of functional, CP-based nanomaterials.

Introduction

Cyclic peptides with alternating D and L amino acids (CPs) have great potential for the construction of complex organic nanostructures. CPs undergo spontaneous self-assembly by stacking with one-another to form extended nanotubes (CPNs). CPNs can form parallel or antiparallel β -sheet assemblies driven by backbone H-bonding,^{1,2} although the antiparallel form is often regarded as the more stable arrangement.³ CPN structures are tuneable, where many of their chemical and physical properties can be engineered synthetically.⁴ The amino acid side-chains project outwards from an internal channel, the size of which depends on the number of residues in the peptide.⁵ The chemical properties of the nanotube surface are governed by the side-chains of the amino acids, which is not limited to natural amino acids alone. The scope for CP customization is nearly limitless. This customizability, combined with their high biological compatibility, makes CP nanostructures ideal candidates for the development of synthetic, biomimetic nanomaterials that can be developed for molecular transport and encapsulation or as synthetic proteins and channels.

CPs and CP assemblies have been studied using an array of analytical approaches, including static and dynamic light scattering, infrared spectroscopy, electron microscopy, X-ray crystallography, NMR spectroscopy and by computational calculations including molecular dynamics (MD) simulations. Of these methods, we have found NMR and MD to provide particularly useful insights and complement each-other in their findings.

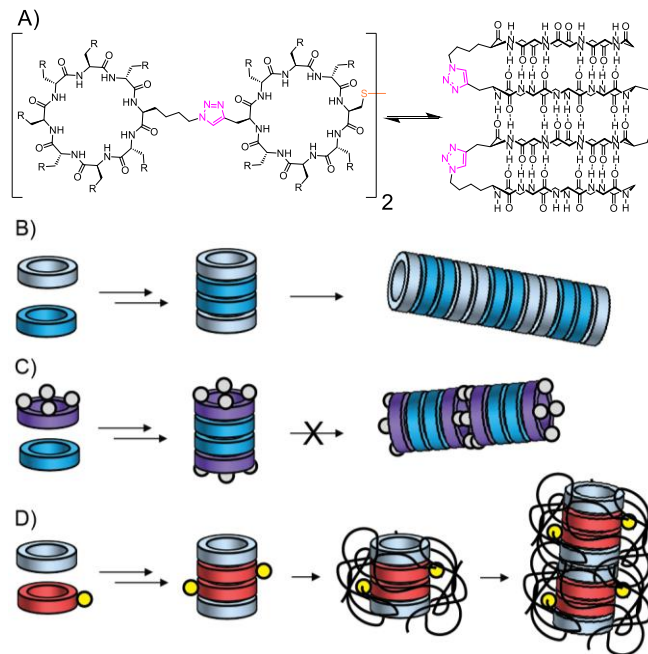


Figure 1. Tethered CP tetramers are modular, tuneable, versatile structures. CP subunits can be combined in different combinations to generate nanorods of different behaviour and function. A) Chemical structure of a tethered CP tetramer backbone. B) Tethering controls the short-range order within nanorods and long-range order upon further self-assembly. C) Backbone *N*-methylation prevents further self-assembly of nanorods. D) Post-synthetic modification of nanorod properties through polymer conjugation.

NMR provides detailed information of CP structure and behaviour in solution. 1D ^1H NMR can be used to characterise the concentration-dependent assembly of CPs,^{1, 6, 7} the existence of distinct conformations^{3, 8, 9} and to determine their association constants.^{3, 7, 9, 10} Intermolecular interactions within CP assemblies can be measured by ROESY and NOESY NMR.¹⁰⁻¹⁴ NMR has also been applied to study the encapsulation of guest-molecules within CP cavities.¹⁵ The strength of H-bond interactions within CPN materials can be measured by 1D ^1H NMR using H-D exchange experiments.¹⁶ Diffusion-ordered spectroscopy (DOSY) can provide an estimate of CP size and aggregation in solution based on the diffusion properties of the dissolved material.^{11, 15, 16}

Molecular dynamics studies of CP structures can aid in the design of new compounds and assist in the explanation of CPN properties and behaviour. CP-based systems are significantly complex and MD can provide detailed, atomic scale representations to explain the key interactions and features of their unique structure. In our previous studies of CPNs, we found that side chain hydrophobicity and specific backbone H-bonding interactions are important for the stability of CPN systems.¹⁷ MD studies have been used to probe the association constants of CP systems in a range of solvents,^{18, 19} model the stability of CPNs of different lengths²⁰ and diameters,²¹ and to study the transport properties of CPNs.²¹ A key finding from MD is that the

stability of CPNs is directly related to the number of CPs within the assembly.²⁰ CPs near the core of the nanotube form significantly more stable interactions than those located at the ends of the CPN due to reduced solvent exposure. Furthermore, the inter-CP H-bond strength increases gradually until reaching a maximum at a length of 5 or more CP subunits. MD studies of antiparallel CPNs have explored the transport of ions,²²⁻²⁴ water²⁵ and other organic compounds²⁶ through the internal channel. However, a driving force is needed to allow directional diffusion through the CPN channel due to the antiparallel nature of the structure.^{21, 26, 27}

Despite the unique properties of CPNs, a number of limitations hinder their development as functional materials. The self-assembly of most CPNs reported to date is an uncontrolled, spontaneous process that produces aggregates of a range of sizes and compositions. Further complexity in the self-assembly process arises from the fact that the CPs are in constant dynamic exchange between nanotubes and free in solution.²⁸ With little control over CPN self-assembly, heterogeneous CPNs cannot be reliably accessed, limiting the complexity of the structures that can be developed. We need to be able to understand the factors that contribute to the assembly of stable nanotubes to direct the assembly of complex, heterogeneous structures. By doing so, we will have the means to control the precise composition and properties of CPNs allowing their development into useful materials.

A range of approaches have offered some degree of control over the structure and properties of CPN material. These include control of inter-CP sidechain interactions, backbone *N*-methylation, polymer conjugation and covalent tethering.

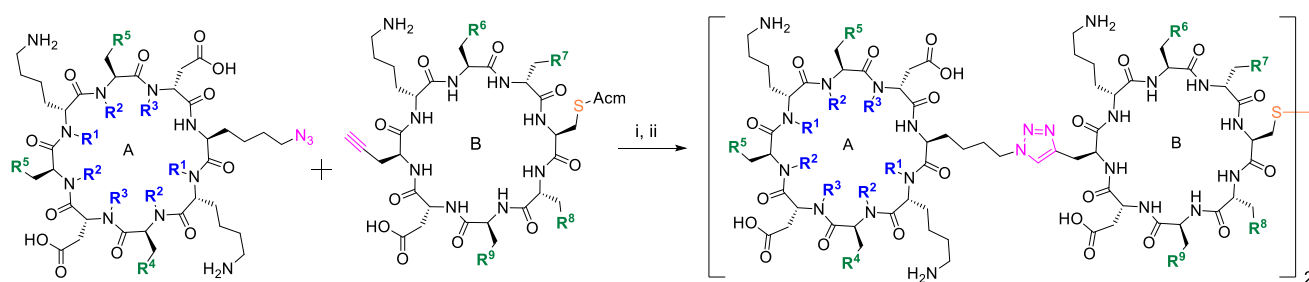
Inter-CP side chain interactions have been used to introduce some order to CPN structure, by rotationally aligning CPs to one-another and directing the packing of CPN bundles. Sidechains with aromatic moieties can rotationally align CPs within a CPN through favourable π -stacking interactions^{9, 29}. Ionic interactions between sidechains of opposite charge have also been used to direct the alignment of CP monomers.³⁰ Ionic interactions between CPNs have been used to direct the assembly of individual nanotubes into extended CPN networks.² Not only have side-chain interactions regulated CP alignment within CPNs, but they can also improve the overall stability of CPNs.¹⁷

Blocking inter-CP hydrogen bonds has been used to prevent CP self-assembly and introduce some control to nanotube formation. *N*-methylation of the CP backbone amide groups inhibits the H-bonding interactions between CPs and limits assembly to the formation of dimers.^{1, 31} Reducing the CP aggregation behaviour has led to a range of crystal structures being solved for *N*-methylated CP dimers.^{7, 10, 14, 31, 32} In some cases, *N*-methylation of the backbone amides favours the formation of folded, rather than planar, conformations, depending on the pattern of *N*-methylation and amino acid composition.⁸

CPN self-assembly has been further regulated through the addition of polymers to the CPN exterior. Polymers have been conjugated to CPs through 'click' chemistry³³⁻³⁶ or polymerisation reactions be performed directly onto initiator sites located on the surface of assembled CPNs.³⁷⁻³⁹ Both approaches have enabled the diversification of CPN properties such as CPN solubility, depending on the nature of the polymer attached.^{33, 40} The conjugation of acrylic acid has been used to promote aqueous solubility of CPNs and introduce pH-mediated assembly/disassembly, as shown by Chapman *et al.*⁴⁰ Combinations of miscible and non-miscible polymers have been used to produce CPNs which cluster according to hydrophobic and hydrophilic polymeric shells.³⁶ CP-polymer conjugation has also been shown to reduce aggregation between nanotubes^{33, 34, 41} as well as limit CPN length by disrupting CP assembly.^{34, 42} Increasing the molecular mass of the polymers overcomes the forces that hold CPNs together and breaks the CP-polymer aggregates into smaller assemblies.⁴²

A more direct approach to controlling CPN self-assembly and structure is covalent tethering. Tethering CPs together through amino acid side-chains or backbone atoms controls the pattern of assembly and allows for control over the short- and long-range order of CPN materials. An additional benefit of CP-tethering is that it enables the controlled construction of heterogeneous CPN systems, i.e. CPNs built from chemically-distinct CPs. Tethered CP homodimers have been prepared by metathesis of alkene-functionalised side-chains,^{43, 44} through the introduction of polymer tethers⁴⁵ and by amide coupling of lysine and glutamic acid side-chains.⁴⁶ Intermolecular tethering of CP backbones has been used to create capsule-type structures¹⁵ or to design extended heterogeneous nanotube structures.¹¹ Tethers have also been used to provide additional functionality to the CP system. For example, CPs have been tethered through an azobenzene moiety that acts as a photoswitchable linker, enabling CPN assembly to be induced under UV irradiation.^{47, 48}

We have previously reported the use of homo and hetero coupling of CP side-chains to generate tethered CP tetramers.¹⁶ The process involves the heterodimerisation of two chemically-distinct CPs using click chemistry before further homodimerisation to create four CP-subunits tethered together (**Figure 1**). These CP tetramers provide control over the chemical and structural composition of CPN materials. However, the structure-stability relationship of these systems has not yet been explored. In this work, we investigate the effects of CP amino acid composition on the stability of tethered CP tetramers. A selection of tetramers are reported and their stabilities studied by NMR and molecular dynamics. We discuss the impact of amino acid composition and the relative structural isomers on tetramer stability. Additionally, selective backbone *N*-methylation and side-chain polymer conjugation were explored as a means for further modulating the behaviour of tethered CP tetramers in aqueous solution.



Note: All stereochemistries shown here are *relative*. The absolute stereochemistries are defined by the chirality of Asp specified in the table below.

No.	Scaffold	Asp enant. ^[a]	R ¹	R ²	R ³	R ⁴	R ⁵	R ⁶	R ⁷	R ⁸	R ⁹
1		D	H	H	H	H	H	-	-	-	-
2		D	H	H	H	CH(CH ₃) ₂	CH(CH ₃) ₂	-	-	-	-
3	A	D	H	H	H	H	CH(CH ₃) ₂	-	-	-	-
4		D	H	CH ₃	H	CH(CH ₃) ₂	CH(CH ₃) ₂	-	-	-	-
5		L	H	H	CH ₃	CH(CH ₃) ₂	CH(CH ₃) ₂	-	-	-	-
6		L	CH ₃	H	H	CH(CH ₃) ₂	CH(CH ₃) ₂	-	-	-	-
7		D	-	-	-	-	-	H	COOH	(CH ₂) ₃ NH ₂	H
8		D	-	-	-	-	-	CH(CH ₃) ₂	COOH	(CH ₂) ₃ NH ₂	CH(CH ₃) ₂
8m	B	L	-	-	-	-	-	CH(CH ₃) ₂	COOH	(CH ₂) ₃ NH ₂	CH(CH ₃) ₂
9		D	-	-	-	-	-	H	COOH	(CH ₂) ₃ NH ₂	CH(CH ₃) ₂
10		D	-	-	-	-	-	CH(CH ₃) ₂	CH(CH ₃) ₂	CH(CH ₃) ₂	CH(CH ₃) ₂
11		D	-	-	-	-	-	CH(CH ₃) ₂	COOH	(CH ₂) ₃ NH ₂	(CH ₂) ₃ NH(Alloc)
12		D	H	H	H	H	H	H	COOH	(CH ₂) ₃ NH ₂	H
13		D	H	H	H	CH(CH ₃) ₂	CH(CH ₃) ₂	CH(CH ₃) ₂	COOH	(CH ₂) ₃ NH ₂	CH(CH ₃) ₂
14		D	H	H	H	H	CH(CH ₃) ₂	H	COOH	(CH ₂) ₃ NH ₂	CH(CH ₃) ₂
15	ABBA	D	H	H	H	CH(CH ₃) ₂	CH(CH ₃) ₂	CH(CH ₃) ₂			
16		D	H	H	H	CH(CH ₃) ₂	CH(CH ₃) ₂	CH(CH ₃) ₂	COOH	(CH ₂) ₃ NH ₂	(CH ₂) ₃ NH(Alloc)
17		D	H	CH ₃	H	CH(CH ₃) ₂	CH(CH ₃) ₂	CH(CH ₃) ₂	COOH	(CH ₂) ₃ NH ₂	CH(CH ₃) ₂
18		L	H	H	CH ₃	CH(CH ₃) ₂	CH(CH ₃) ₂	CH(CH ₃) ₂	COOH	(CH ₂) ₃ NH ₂	CH(CH ₃) ₂
19	L	CH ₃	H	H	CH(CH ₃) ₂	CH(CH ₃) ₂	CH(CH ₃) ₂	COOH	(CH ₂) ₃ NH ₂	CH(CH ₃) ₂	

Figure 2. CP monomers and tetramers prepared by the two-step tethering method. i) CuAAC coupling: Peptide monomers at 1 mg/mL in 1:1 ratio, 0.1 mM CuSO₄, 0.5 mM THPTA and 5 mM sodium ascorbate, 3 h rt at pH 7.1 under N₂. ii) Disulfide formation: Acn-protected peptide at 10 mg/mL in neat AcOH, 10 eq. I₂, 3 h rt under N₂. ^[a] Stereochemistry of aspartic acid in the monomer or tetramer. This defines the absolute stereochemistry of the synthesised material.

Results

CP tetramer design

CP tetramers are completely synthetic and of modular design. Monomeric CP subunits are synthesized before being tethered together into the target CP tetramers through a two-step process (Figure 2). We designed a series of CP tetramers based on the monomeric CP subunits 1-11. Eight chemically-distinct CP tetramers (12-19) were synthesised through coupling of different combinations of CP subunits. The tetramers were designed to investigate the nature of inter-CP side-chain interactions and to determine whether *N*-methylation of backbone amides could be

used to stop assembly of the tetramers into extended nanotubes. We have previously reported tetramers 12, 13 and 17,¹⁶ which have a common framework and substitution pattern of Asp and Lys residues and differ in incorporation of Ala (12) and Leu (13) residues and in backbone *N*-methyl groups (17). We established through NMR analysis that 13 formed the most ordered, stable H-bonded structure and we therefore used 13 as the basis for structural modifications to create an extended series of CP tetramers. Tetramer 14 contains both Ala and Leu residues and was designed to have intermediate hydrophobicity between that of 12 and 13. Additionally, the Leu and Ala residues were arranged to provide a knobs-in-holes type interaction, similar to Crick's description of the packing in coiled-coils.⁴⁹ This

interaction involves a sterically bulky Leu side-chain adjacent to a short Ala sidechain (**Figure S1**). In tetramer **15** additional Leu residues were incorporated within the CP-tetramer core to investigate whether additional hydrophobic contacts improved stability. Compound **16** incorporates two Lys(Alloc) residues to enable the conjugation of functional moieties to the tetramer exterior. Compounds **17-19** were designed to investigate different backbone *N*-methylation positions to determine the structural effects of blocking specific amino acids. Note that for reasons of synthetic accessibility, compounds **18** and **19** have the inverse stereochemistry to **13** although the relative stereochemistry of the hydrophobic and hydrophilic groups are the same.

Synthesis

CP monomers **1-11** were synthesised using standard Fmoc solid-phase peptide synthesis methodology. Linear peptide precursors were synthesised on-resin using an automated peptide synthesizer before cleavage from the resin with side-chain protecting groups intact. Head-to-tail cyclisation was then performed in solution, followed by side-chain deprotection and purification by preparative HPLC. Monomers were obtained in moderate yields and high purities. Some CP monomers retain orthogonal protecting groups such as an acetamidomethyl-protected cysteine (Cys-Acm) in CPs **7-11** and the Alloc-protected lysine of CP **11**.

CP monomers were 'mixed and matched' to make a set of eight tethered CP tetramers (**12-19**) in two steps. First, a heterodimer was synthesised from two CPs ($A + B = AB$) using copper-activated azide-alkyne cycloaddition (CuAAC) in aqueous conditions using THPTA as the copper-coordinating ligand. This reaction achieves ~80% conversion from a 1:1 CP monomer ratio within 3 h. Purification by preparative HPLC afforded all dimers in high purity (>99%) and moderate yields (40-60%). Poor aqueous solubility of CP **10** required the use of 20% DMSO and the coordinating ligand TNBT to achieve 95-100% conversion within 1 h, which has become the preferred method in our lab. Selection of a suitable coordinating ligand and optimization of the CuAAC conditions was achieved according to the study by Stanislav *et al.*⁵⁰ In the second step, the AB heterodimer was dimerised into the tetrameric ABBA product by the formation of a disulfide bridge. This was achieved by oxidation of Cys(Acm) using I_2 in AcOH, which simultaneously removes the acetamidomethyl protecting group and generates the intermolecular disulfide bridge. The oxidation proceeded to 95-100% completion within 3 h and afforded the desired tetrameric products **12-19** in high purities (>99%) and moderate yields (15-40% after CuAAC and oxidation) following purification by preparative HPLC.

NMR analysis of tetramer structure

The solution behaviour of tetramers **12-19** was studied by 1D and 2D NMR in 10% D_2O/H_2O at 298K and pH 3.0 \pm 0.3. The concentration dependent assembly of tetramers was investigated by 1H NMR (**Figure S2-6**), while 2D heteronuclear SOFAST [^{15}N , 1H]-HMQC (**Figure S7-11**) and [^{13}C , 1H]-HSQC (**Figure S12-16**) were used to study the detailed structural differences between tetramers **12-19**. Complete H^N assignment of all tetramers was not possible due to signal overlap, but residue types were identified using the [1H , 1H]-NOESY and TOCSY spectra (**Figure S7-11**).

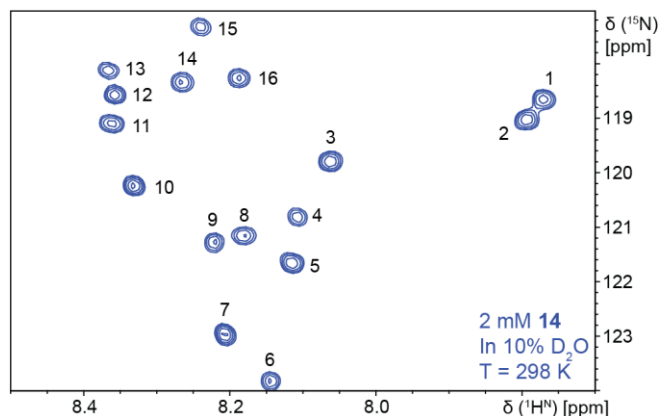


Figure 3. 2D SOFAST [^{15}N , 1H]-HMQC of tetramer **14**. The tetramer is symmetrical, with 16 unique HN signals. Numbers indicate peak-count only.

The assembly and aggregation behaviour of tetramers **12-19** was studied by 1D 1H NMR across a range of concentrations (0.25, 0.5, 1 and 2 mM, **Figure S2-6**). Much information could be obtained by analysing changes in H^N chemical shift in addition to the appearance of the triazole proton. We found that the H^N resonances of all the non-*N*-methylated tetramers (**12-16**) became more dispersed with increasing concentration, suggesting increased structural ordering. Tetramer **14** gave the most dispersed H^N signals (range 8.40-7.75 ppm at 2 mM) while tetramer **13** was the most variable (0.2 ppm increase in overall dispersion from 0.25 to 2 mM). All of the *N*-methylated tetramers (**17-19**) contained a minor population appearing as a distinct set of signals with substantially weaker intensity. These minor populations had a significantly greater chemical shift dispersion than the major population in **17-19**. In the case of **19**, the minor population increases moderately in H^N chemical shift dispersion with increasing concentration. In contrast to the observations for the non-*N*-methylated tetramers, the H^N chemical shift of the methylated tetramers (**17-19**) showed little concentration dependency overall. There are two triazole protons within a tetramer and their appearance as a single or multiple signals can be used as an indicator of symmetry. The spectra of compounds **13**, **15** and **16** contained a single triazole proton signal (~7.75 ppm) while **12** and **14** had an additional, smaller signal separated by ~0.005 ppm and appearing as a shoulder. Backbone *N*-methylated tetramers **18** and **19** gave a single signal for the triazole proton at ~7.75 ppm while **17** had several signals. There are six *N*-methyl groups in compound **17** and four in **18** and **19**. Due to symmetry across the disulfide bridge, only three signals are expected for **17** and two signals for each of **18** and **19**. The backbone *N*-methyl groups of compound **18** had one major signal at 2 mM which separated into two singlets at 0.25 mM. These *N*-methyl groups had additional minor singlets from 2.6 to 3.0 ppm.

The symmetry of the structures in solution was determined by the number of HN signals within heteronuclear 2D NMR spectra. The spectrum of a symmetrical 32-residue CP-tetramer is expected to contain 16 unique HN signals. Of the non-*N*-methylated tetramers, compounds **13-16** gave spectra containing 16 distinct HN signals (although there is some signal overlap in **15**), indicating that they are symmetrical in solution. The HN signals of the knobs-in-holes tetramer **14** were the most dispersed (shown in **Figure 3**). Spectra of the Ala-containing

tetramer **12** contained many more than 16 HN signals, indicating a lack of symmetry or the existence of multiple conformations. Backbone *N*-methylation reduces the number of expected signals to 13 for tetramer **17** (3 × *N*-Me Leu) and 14 for both tetramers **18** and **19** (2 × *N*-Me Asp or Lys). However, spectra of all the methylated tetramers all contained more than their expected number of signals, consistent with the presence of multiple distinct signal subsets observed in the 1D ¹H spectra.

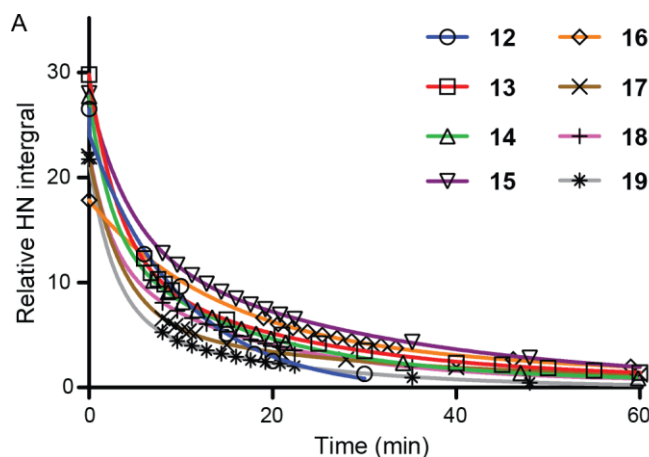
Backbone H-bonding of CP tetramers

The stability of backbone H-bonds within the CP tetramers was investigated by 1D ¹H NMR using ¹H-D exchange experiments. The decay of H^N signals as a result of exchange with deuterium was used as a measure of solvent accessibility and H-bond strength of the exchangeable backbone amide protons of the CP tetramers. Tetramers **12-19** were dissolved in 100% D₂O at 2 mM and 1D ¹H spectra were recorded over 1-2 h (Figure S17-21). The signals from solvent-exposed amides, such as those within terminal CPs, are expected to decay quickly, while buried, H-bonded H^Ns will decay more slowly. Although exchange rates of individual H^N signals could not be obtained due to overlap between signals, analysis of the amide region as a whole provides insight into the relative stability of each tetramer. A two component exponential function was fitted to estimate the fast and slow components of the decay of the total H^N signal versus time (Figure 4a). Here we will just consider the slow decay component as it is directly relevant to the H^N signals involved in tetramer stability. Tetramer **15** was found to have the longest half-life while **12** had the shortest half-life. Compound **14** had a short half-life of 11 min, which was between **12** (7 min) and **13** (15 min). Tetramer **16** contains two Lys(Alloc) residues which resulted in a moderately longer half-life (18 min) compared to **13** which contains Leu residues in the same positions. Of the *N*-methylated tetramers, compound **17** had the longest half-life while **18** and **19** had similar half-lives to each-other. For all tetramers **12-19**, the lysine side-chain H₃N⁺ signals were completely exchanged before acquisition of the first spectrum (within 8 min), including the Lys(Alloc) side-chain amide of **16**.

We found that the behaviour of the *N*-methylated tetramers was dependent on which CP face was *N*-methylated. Tetramers **18** and **19** are *N*-methylated on the Asp and Lys residues respectively which are located in the same face of the CP and had similar half-lives. Tetramer **17** was quite different from **18** and **19** despite all three being *N*-methylated analogues of **13** with the same side-chain compositions. The *N*-methylations of **17** lie on the opposite face of the CP to those of **18** and **19**. The *N*-methylations of the Leu residues in **17** inhibit the formation of stable Leu-Leu H-bonding interactions that are otherwise possible for tetramers **13**, **18** and **19**. However, it resulted in longer half-lives than **13**, **18** and **19** for the slow and fast components.

The diffusion of tetramers **12-19** was measured by diffusion-ordered spectroscopy (DOSY). The diffusion rates and derived hydrodynamic radii are shown in Figure 4. A typical DOSY experiment is shown in Figure S22. The diffusion constants of the non-*N*-methylated compounds (**12-16**) ranged from 2.5-3.1 × 10⁻¹⁰ m²s⁻¹ where tetramer **15** had the slowest diffusion. The *N*-methylated tetramers **17-19** had the slowest diffusion overall,

ranging from 2.2-2.4 × 10⁻¹⁰ m²s⁻¹. Assuming spherical structures, diffusion constants (*D*_T) can be related to hydrodynamic radii (*R*_h) following the Stokes-Einstein relationship.⁵¹ *D*_T values across the range of 2.2-3.1 × 10⁻¹⁰ m²s⁻¹ correlate to *R*_h values of 11.1 Å to 7.9 Å, consistent with the dimensions of a folded CP tetramer (Figure 4b). The *N*-methylated tetramers **17-19** were less-ordered by 1D and 2D NMR analysis. Unfolded conformations of these less-ordered structures may contribute to their slower diffusion and larger *R*_h values.



No.	t _{1/2} fast (min)	t _{1/2} slow (min)	Diff. const. (× 10 ⁻¹⁰ m ² s ⁻¹)	Hydrodynamic radius (Å)
12	< 1	7	3.0	8.2
13	2	15	3.1	7.9
14	2	11	2.9	8.5
15	10	113	2.5	9.8
16	3	19	2.9	8.5
17	3	18	2.2	11.1
18	2	12	2.3	10.7
19	2	13	2.4	10.2

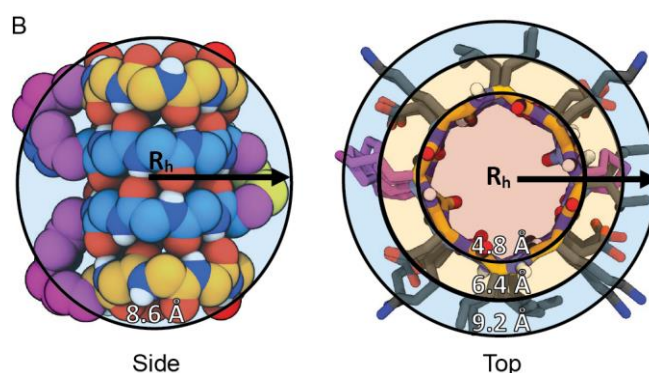


Figure 4. A) The change in total backbone H^N integral over time from 1D ¹H NMR spectra of CP tetramers **12-19** upon dissolution at 2 mM in 100% D₂O. Table contains half-lives, diffusion constants and hydrodynamic radii (*R*_h) of tetramers **12-19**. B) Approximate radius of a folded CP tetramer (viewed from the side and top) is consistent with measured *R*_h values.

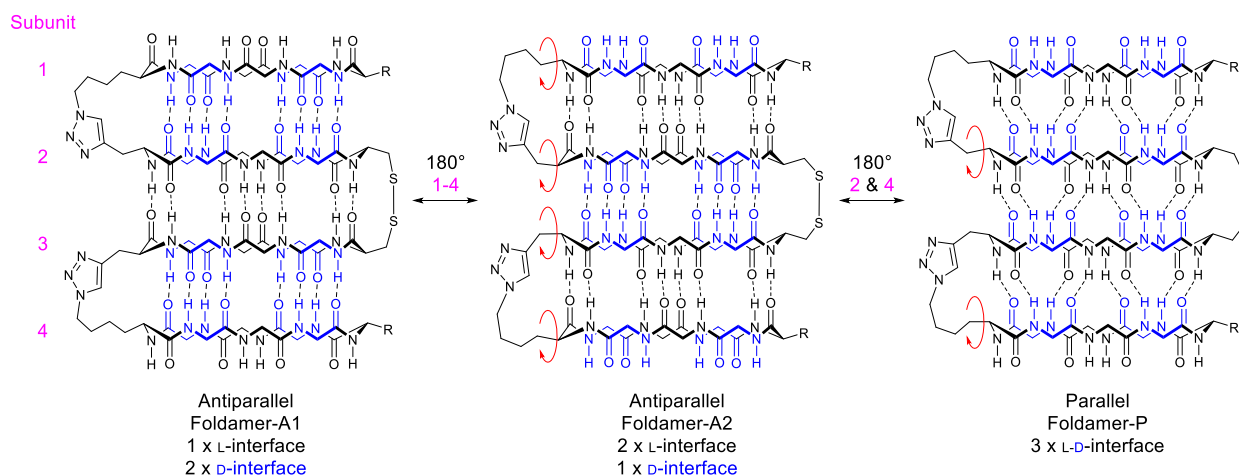


Figure 6. A CP tetramer has 3 possible fully H-bonded foldamers; two with antiparallel H-bonding and one with parallel. L-AA backbones are shown in black and D-AAs in blue, with pink numbers designating CP subunits. The two possible antiparallel foldamers (A1 and A2) are related through 180° rotations of each CP subunit, where the arrangements differ in whether the L or D-interface dominates H-bonding interactions. In the parallel arrangement (Foldamer-P), all CP interfaces involve H-bonding between the L and D-amino acid backbones.

Molecular dynamics studies of CP tetramer stability

MD simulations were used to further investigate stability of different CP tetramer conformations and to provide insight into the most likely foldamer. As shown in **Figure 6**, a fully H-bonded CP tetramer can fold into three possible conformations; two antiparallel H-bond foldamers (denoted A1 and A2) and one parallel foldamer (denoted P). The antiparallel foldamers differ in whether the H-bonding is dominated by the L or D-interface (please see our earlier paper¹⁷ for a discussion of these interfaces). Foldamer-A1 has an L-interface between the middle CPs and two D-interfaces between the outer subunits. Foldamer-A2 is the inverse of A1, with a D-interface in the middle and two L-interfaces between the outer subunits. The two foldamers are related to one-another through a 180° rotation of each CP subunit at the tethering positions. It is important to note that side-chain tethering fixes the rotation of each CP subunit relative to one another which enforces only a single possibility for amino acid alignments. Conversely, an untethered 8-AA CP can adopt as many as four different alignments per CP-CP interface. The parallel H-bonding arrangement involves H-bonding between L and D amino acids in each interface throughout the structure. Calculations have suggested that antiparallel H-bonding is more favourable, but we have observed the parallel arrangement in the crystalline state and considered it in our MD studies here.

The stability of each CP tetramer was evaluated by MD simulation using Desmond MD software at 300 K and 1.01 bar. Aspartic acid and lysine side-chains were ionised. Each tetramer was simulated for 100 ns in each of the two possible antiparallel foldamers and the parallel foldamer. The stability of each foldamer was assessed by counting the number of inter-CP H-bonds where a total of $8 + 8 + 8 = 24$ intermolecular backbone H-bonds are possible.

The number of backbone H-bonds within tetramers **12-16** during the 100 ns simulations are shown in **Figure 7a**. The most stable tetramers displayed no dissociation of CP subunits, such as **15** (**Figure 7b, 7c**), while unstable tetramers suffered varying degrees of dissociation between CP subunits, such as **13** (**Figure 7d**). The average number of backbone H-bonds within each CP interface for all tetramers **12-19** are shown in **Table 1**.

The MD simulations show that several factors contribute to tetramer stability. The specific backbone H-bonding arrangement (antiparallel foldamers A1 and A2, or the parallel foldamer), the interactions between CP side chains and the positions of backbone N-methylation.

The different backbone H-bonding arrangements of the foldamers had a significant impact on CP-tetramer stability. Most foldamers were, in fact, completely unstable and no tetramers were stable as foldamer-A1. The parallel foldamers of the non-N-methylated CP tetramers (**12-16**) were found to be completely unstable and immediately dissociated within 1 ns of simulation (data not shown). However, foldamer-A2 of tetramers **14, 15** and **16** were completely stable for the full 100 ns simulation.

Side-chain hydrophobicity affected CP-tetramer stability. The high alanine content of **12** resulted in the lowest average stability between both of its antiparallel foldamers. Ala-Ala H-bonding in **12** provided the most stable of all its interfaces but low steric size of the side-chains facilitated disruption by water of the backbone H-bonds. **15** was one of the most stable tetramers on average and this may be attributed to its high Leu content. Hydrophobic Leu's shield the backbone from disruption by water in a more effective manner than alanine, exemplified by the difference in overall stability by MD. In foldamer-A2, **15** forms Leu-Leu H-bonding between all three CP interfaces as it contains both L and D-leucine throughout the structure, promoting high overall stability.

Specific amino acid combinations were found to have a dramatic effect on CP tetramer stability, particularly for **14** and **16**. The addition of Leu-Ala H-bonding in **14** provided significantly high stability for the structure in foldamer-A2 (higher than **13** despite containing more alanines). As a H-bonded pair in foldamer-A2, they improved the stability of all interfaces relative to **12** or **13**, even between subunits 2-3 for which there were no Leu-Ala H-bonds. However, complete dissociation occurred almost immediately in foldamer-A1. The amino acid composition can indirectly stabilize the overall structure as seen for **16** which was one of the most stable structures in foldamer-A2. The Lys(Alloc) side-chains are quite large and can shield the backbone of other amino acids in addition to its own.

Backbone *N*-methylation of Leu in tetramer **17** and Asp or Lys in **18** and **19** blocks foldamer-A2 and P. As a result, H-bonding between all CP interfaces can only occur in foldamer-A1. In this arrangement, tetramers **18** and **19** were more stable than **17** and very similar in stability to their non-*N*-methylated mirror image; tetramer **13**. Tetramers **18** and **19** were more stable than **17**, likely due to Leu-Leu H-bonding between interfaces 1-2 and 3-4, while **17** contains the less-stable Asp-Lys H-bonding.

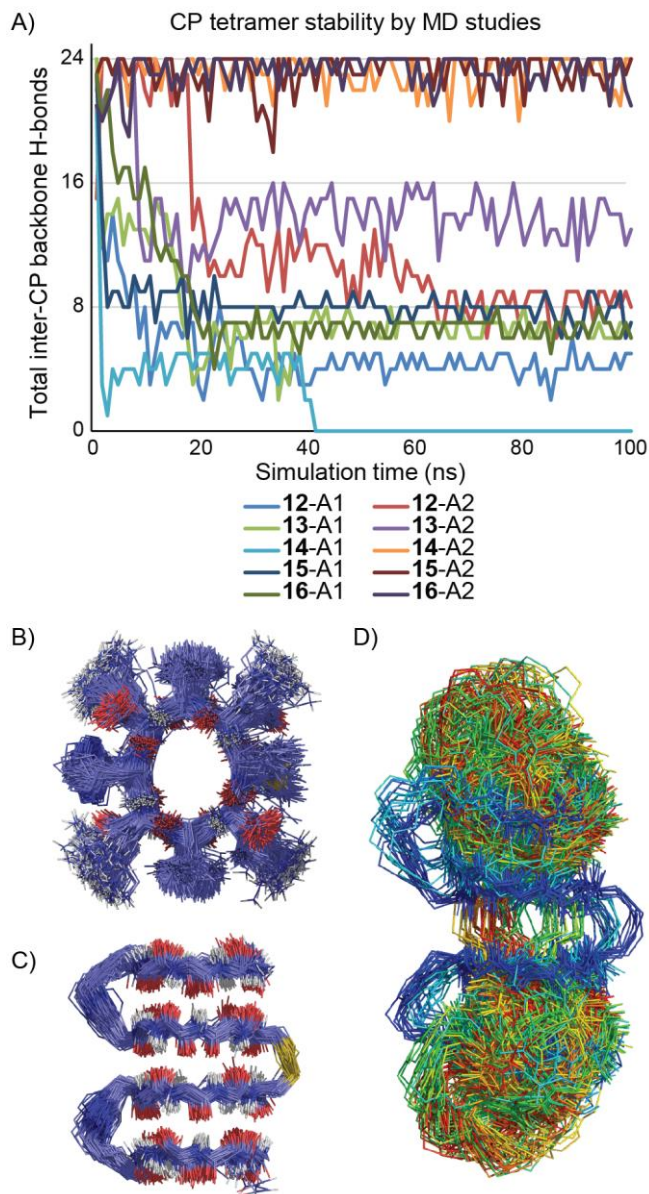


Figure 7. A) The average number of intermolecular backbone H-bonds over time for tetramers **12-16**. Each tetramer was simulated in each of the two possible antiparallel H-bonding foldamers (A1 and A2) and parallel foldamer-P. Conformers **14**-A2, **15**-A2 and **16**-A2 were stable during the full 100 ns. B) Overlay of frames from the MD simulation of CP tetramer **15** in foldamer-A2, viewed from the top. This structure was completely stable in foldamer-A2 with no CP-dissociation after 100 ns. C) Side view of the overlay of **15**-A2 with only the backbone and tethering moieties shown. D) Overlay of frames from the MD simulation of **13** in foldamer-A2, which is unstable. The starting geometry is shown in dark blue and the colouring of structures progresses through the colour spectrum to the final state in red.

Table 1. Average number of backbone H-bonds within each CP interface for **12-19** in antiparallel foldamers A1 and A2 by MD simulation.

No.	Foldamer-A1 CP interfaces			Foldamer-A2 CP interfaces		
	1-2	2-3	3-4	1-2	2-3	3-4
12	0.1	4.4	0.6	3.4	1.5	7.1
13	1.1	6.5	0.1	6.9	0.6	6.8
14	0.1	1.7	0.1	7.6	8.0	7.6
15	1.9	4.7	1.7	7.6	8.0	7.6
16	0.9	6.7	0.5	7.5	8.0	7.7
17	2.7	1.1	1.1	0.1 ^[a]	3.3	1.7 ^[a]
18	7.1	0.1	7.0	0.1 ^[a]	1.0	0.0 ^[a]
19	7.1	2.8	7.2	0.0 ^[a]	2.5	0.0 ^[a]

^[a] The backbone *N*-methyl groups in CP subunits 1 and 4 inhibit H-bonding in these interfaces for this foldamer.

Polymer conjugation: Development of functionalised tetramers

Polymer conjugation was explored to demonstrate further functionalization of the nanorods and enable further complexity in our heterogeneous CP-tetramer designs. Thiol-ene click chemistry was used to attach poly(2-ethylloxazoline), a hydrophilic polymer, to tetramer **16** through the Lys(Alloc) residues which are present in the 'B' peptide. When folded in an antiparallel manner the Lys(Alloc) residues project in opposite directions from the centre of the structure. Poly(2-ethylloxazoline)₅₀ (PEtOx) was synthesized by cationic ring-opening polymerization of ethyl oxazoline using potassium xanthogenate to cap the polymer (**Figure 8**). The xanthogenate was then removed to reveal the free thiol in two steps. Firstly, treatment with diethylamine generated the disulfide-bridged polymer (PEtOx-S)₂. This was followed by reduction with dithiothreitol to form the thiol-terminated PEtOx-SH polymer immediately prior to conjugation. PEtOx-SH was then conjugated to the Alloc-protected Lys residues of tetramer **16** using UV-activated thiol-ene click chemistry. A two-fold excess of PEtOx-SH relative to the Lys(Alloc) alkenes was used to ensure good conversion to the peptide-polymer conjugate.

The unfunctionalised tetramer **16** and the polymer-conjugated **16**-(PEtOx)₂ were studied by static light scattering (SLS) to determine the effects of polymer-conjugation on CP self-assembly and aggregation in water (**Figure 9**). Compound **16** was studied at concentrations 1, 2, 5 and 10 mg/mL while **16**-(PEtOx)₂ was studied at lower concentrations of 0.1, 0.25, 0.5 and 2 mg/mL, as it generated significantly turbid solutions. CP tetramer **16** had an average number of aggregates of 5, 24, 56 and 2125 at 1, 2, 5 and 10 mg/mL respectively. Compound **16**-(PEtOx)₂ had an average number of aggregates of 1435, 1837, 1747 and 1791 at 0.1, 0.25, 0.5 and 2 mg/mL respectively.

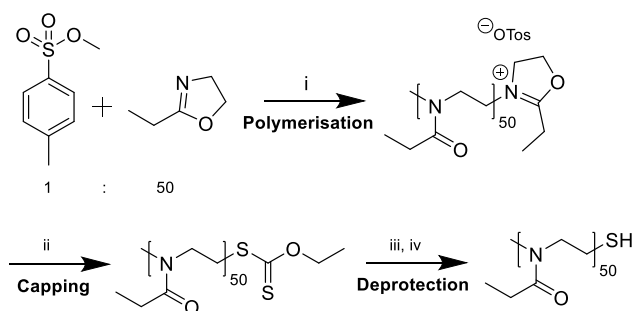


Figure 8. Synthesis of thiol-functionalised poly(2-ethylloxazoline)₅₀-SH. i) Dry ACN, 140°C, 15 bar, N₂, 8.5 min. ii) Potassium ethylxanthate, rt, N₂, stirred overnight. iii) Diethylamine, 40°C, 3 hr. iv) Triethylamine, dithiothreitol, DCM, N₂, 2 hr.

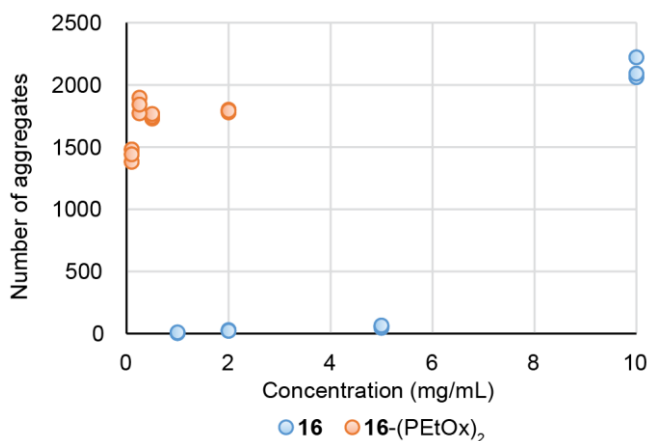


Figure 9. Static light scattering analysis of **16** and **16-(PEtOx)₂** in water with increasing concentration, in triplicate. The number of aggregates corresponds to the approximate number of molecules of **16** or **16-(PEtOx)₂** within the average aggregate. **16** demonstrated concentration-dependent aggregation while **16-(PEtOx)₂** formed large aggregates at low concentrations. PEtOx conjugation stabilized the CPN aggregate to dilution-induced disassembly.

The conjugation of both polar and non-polar polymers to CPs has been shown to reduce CPN length and aggregation between nanotubes depending on the nature of the solvent,⁵² where the shortest nanotubes are induced by larger polymers.^{34, 42} Chapman *et al* demonstrated that PEtOx-conjugated CP monomers form relatively short nanotubes as observed by DLS.⁵³ Tetramer **16** was found to have concentration-dependent aggregation that is typical of CP-based systems.^{2, 28} At concentrations greater than 10 mg/mL, CP aggregation began to detrimentally impact aqueous solubility. However, **16-(PEtOx)₂** did not exhibit concentration-dependent aggregation but rather formed large aggregates at 0.1 to 2 mg/mL of similar size to **16** at 10 mg/mL. Conjugation of **16** with PEtOx stabilized the tetramer to the dilution-based disassembly seen for most CPs and promoted significant self-assembly and aggregation at low concentration. Furthermore, this characteristic is quite the opposite of what has previously been found for monomeric CP-polymer conjugation. The conjugation of polymers to CP monomers has often been shown to reduce the overall aggregation of CP systems by interfering with lateral aggregation of assembled CPNs.^{34, 42} For CP-polymer monomers, the minimum ratio of polymer:CP is 1:1 which is still sufficient to generate CPNs with a polymer density high enough to reduce aggregation and assembly. For CP-tetramers such as **16**, conjugation sites can be reduced to ratios below 1:1 for

polymers to individual CPs. This is a direct result of tethering granting control over the pattern of CPs within heterogeneous CPN systems. **16-(PEtOx)₂** has a 1:2 ratio of polymer to CP, two-fold lower than the minimum density achievable for homogeneous CP monomers.

Discussion

We have developed an efficient route for the synthesis of tethered CP tetramers. We have shown that poorly-soluble CP subunits can be tethered to more soluble counterparts through the CuAAC coupling reaction in 20% DMSO with TNBT as the copper-coordinating ligand. Both tethering stages are compatible with the unprotected CP subunits during the CuAAC step. Furthermore, this tetramer-construction method is modular and allows various combinations of CP subunits to be combined to make chemically distinct, heterogeneous CP tetramers.

This work provides new information about factors that influence tetramer assembly. The NMR and MD studies show that the stability of tethered CP tetramers is governed by: the overall amino acid composition and amino acid side chain contacts between residues in adjacent CP monomers, the specific arrangement of H-bonds (antiparallel-A, antiparallel-B or parallel) and the *N*-methylation positions. We show that CP tetramer stability is susceptible to minor changes in amino acid sequence. Tetramers with as few as two residue substitutions have marked differences in dispersion of H^N resonances and H-bond half-lives, as measured by NMR. We found that combinations of Ala-Leu, Leu-Leu and Leu-Lys within tetramer sequences produced particularly stable structures by NMR. The MD studies strongly suggest that these amino acid combinations stabilise tetramers when H-bonded to one-another in foldamer-A2, as seen for **14-16**. No structure was stable in both antiparallel H-bonded arrangements, further highlighting the dependence of tetramer stability on the amino acids involved in H-bonding. Incorporation of more hydrophobic residues improved the stability of CP tetramers. Increasing the number of Leu residues in the tetramer improved overall stability by experimental and computational measurements. Compound **15**, which contains a total of 14 Leu residues, was one of the most stable tetramers by all measurements. However, in practical terms, the increased hydrophobicity of this compound made handling difficult due to reduced solubility and an increased tendency to aggregate. The knobs-in-holes tetramer (**14**), which packs Ala residues against Leu residues, was one of the more superior tetramer designs in this regard, as it was seen to be stable by MD and had well-dispersed amide signals in NMR spectra, implying that the structure is well-folded. This compound also maintains good aqueous solubility.

We proposed that *N*-methylation could be used to block the higher-order assembly of tetramers and create discrete nanorods. Of the tetramers studied, we found that *N*-methylation was most effective for the Asp or Lys residues as shown by the improved order of H^N signals by NMR. Further analysis by MD indicated that Leu-Leu H-bonding interfaces were crucial to tetramer stability, which are inhibited when the Leu's are *N*-methylated. However, all of the *N*-methylation positions explored appeared to induce alternate conformations and arrangements as detected by NMR and their diffusion properties suggested no significant reduction in supramolecular size.

Finally, we investigated whether the CP tetramers could be functionalised post-synthesis by attaching two molecules of the

hydrophilic PEOx polymer to each tetramer. SLS studies showed that addition of the polymer created water-soluble CPN assemblies that were stable to dilution-induced disassembly. This was most likely due to the lower ratio of polymer to CP monomer that tethered CP systems can achieve (1:2 of polymer:CP in this case) when compared with monomeric CP-polymer conjugates,^{34, 42} which have a minimum 1:1 of polymer:CP. A lower ratio may allow favourable aggregation interactions between polymers of adjacent nanotubes rather than preventing aggregation through steric effects between polymers. In addition, tethering controls the relative positions of the polymers which project from opposite faces of the CP and further disperses the polymers. Exploring the conjugation of other polymers through a combinatorial approach is expected to yield interesting and functional tetramers with unique properties.

Conclusions

We have identified some key factors in the stability of these water-soluble CP nanomaterials. Amino acid composition had a significant effect on the relative stability of tetramers and may induce specific H-bond arrangements within assemblies. Of the tetramers reported, side-chain hydrophobicity promoted stability but should be mitigated to maintain decent aqueous solubility. High-alanine content produced the least stable tetramer while a combination of alanine and leucine was highly stable with good aqueous solubility. CPN properties could be further tuned through polymer conjugation and backbone *N*-methylation, although care should be taken to avoid blocking potentially stable H-bond interfaces and reducing stability. The modular synthesis of our tetramers grants access to heterogeneous CPN structures and indeed an extensive library of analogues could be developed through a combinatorial approach. Our group is working on the conjugation of chromophores, fluorophores, bioactive compounds, light-activated moieties and more to create nanotubes of diverse function.

Experimental Section

Detailed peptide and polymer synthesis, NMR characterisation and MD methods are provided in the supplementary information.

Acknowledgements

MRS gratefully acknowledges an RTP scholarship provided by the Australian Government.

Keywords: Cyclic Peptides, Self-assembly, Nanotubes, Molecular Dynamics, NMR

Abbreviations: THPTA; Tris(3-hydroxypropyltriazolylmethyl)amine, TNBT; Triethyl 5,5',5''-[2,2',2''-nitrilotris(methylene)tris(1*H*-benzo[*d*]imidazole-2,1-diyl)]tripentanoate

1. Sun, X.; Lorenzi, G. P. On the Stacking of β -Rings: The Solution Self-Association Behaviour of Two Partially *N*-Methylated Cyclo(hexaleucines). *Helvetica Chimica Acta* **1994**, *77*, 1520-1526.

- Silk, M. R.; Newman, J.; Ratcliffe, J. C.; White, J. F.; Caradoc-Davies, T.; Price, J. R.; Perrier, S.; Thompson, P. E.; Chalmers, D. K. Parallel and antiparallel cyclic D/L peptide nanotubes. *Chem. Commun.* **2017**, *53*, 6613-6616.
- Kobayashi, K.; Granja, J. R.; Ghadiri, M. R. β -Sheet Peptide Architecture: Measuring the Relative Stability of Parallel vs. Antiparallel β -Sheets. *Angew. Chem. Int. Ed.* **1995**, *34*, 95-98.
- Chapman, R.; Danial, M.; Koh, M. L.; Jolliffe, K. A.; Perrier, S. Design and properties of functional nanotubes from the self-assembly of cyclic peptide templates. *Chem. Soc. Rev.* **2012**, *41*, 6023-41.
- Brea, R. J.; Castedo, L.; Granja, J. R. Large-diameter self-assembled dimers of alpha,gamma-cyclic peptides, with the nanotubular solid-state structure of cyclo-[(L-Leu-D-(Me)N-gamma-Acp)₄]-4CHCl₂COOH. *Chem. Commun.* **2007**, 3267-9.
- Reiriz, C.; Castedo, L.; Granja, J. R. New alpha,gamma-cyclic peptides-nanotube molecular caps using alpha,alpha-dialkylated alpha-amino acids. *J. Pept. Sci.* **2008**, *14*, 241-9.
- Amorin, M.; Castedo, L.; Granja, J. R. New Cyclic Peptide Assemblies with Hydrophobic Cavities: The Structural and Thermodynamic Basis of a New Class of Peptide Nanotubes. *J. Am. Chem. Soc.* **2003**, *125*, 2844-2845.
- Amorin, M.; Castedo, L.; Granja, J. R. Folding control in cyclic peptides through *N*-methylation pattern selection: formation of antiparallel beta-sheet dimers, double reverse turns and supramolecular helices by 3alpha,gamma cyclic peptides. *Chemistry* **2008**, *14*, 2100-11.
- Horne, W. S.; Ashkenasy, N.; Ghadiri, M. R. Modulating charge transfer through cyclic D,L-alpha-peptide self-assembly. *Chem. Eur. J.* **2005**, *11*, 1137-1144.
- Ghadiri, M. R.; Kobayashi, K.; Granja, J. R.; Chadha, R. K.; McRee, D. E. The Structural and Thermodynamic Basis of the Formation of Self-Assembled Peptide Nanotubes. *Angew. Chem. Int. Ed.* **1995**, *34*, 93-95.
- Fuertes, A.; Ozores, H. L.; Amorin, M.; Granja, J. R. Self-assembling Venturi-like peptide nanotubes. *Nanoscale* **2017**, *9*, 748-753.
- Rodriguez-Vazquez, N.; Garcia-Fandino, R.; Aldegunde, M. J.; Brea, J.; Loza, M. I.; Amorin, M.; Granja, J. R. cis-Platinum Complex Encapsulated in Self-Assembling Cyclic Peptide Dimers. *Org. Lett.* **2017**.
- Hourani, R.; Zhang, C.; van der Weegen, R.; Ruiz, L.; Li, C.; Keten, S.; Helms, B. A.; Xu, T. Processable cyclic peptide nanotubes with tunable interiors. *J. Am. Chem. Soc.* **2011**, *133*, 15296-9.
- Amorin, M.; Castedo, L.; Granja, J. R. Self-assembled peptide tubelets with 7 Å pores. *Chemistry* **2005**, *11*, 6543-51.
- Ozores, H. L.; Amorin, M.; Granja, J. R. Self-Assembling Molecular Capsules Based on alpha,gamma-Cyclic Peptides. *J. Am. Chem. Soc.* **2017**.
- Silk, M. R.; Mohanty, B.; Sampson, J. B.; Scanlon, M. J.; Thompson, P. E.; Chalmers, D. K. Controlled Construction of Cyclic D/L Peptide Nanorods. *Angewandte Chemie* **2019**, *58*, 596-601.
- Silk, M. R.; Price, J. R.; Mohanty, B.; Scanlon, M. J.; Thompson, P. E.; Chalmers, D. K. Chapter 4. *This thesis*.
- Vijayaraj, R.; Van Damme, S.; Bultinck, P.; Subramanian, V. Molecular dynamics and umbrella sampling study of stabilizing factors in cyclic peptide-based nanotubes. *J. Phys. Chem. B* **2012**, *116*, 9922-33.
- Garcia-Fandino, R.; Castedo, L.; Granja, J. R.; Vazquez, S. A. Interaction and Dimerization Energies in Methyl-Blocked α,γ -Peptide Nanotube Segments. *J. Phys. Chem. B* **2010**, *114*, 4973-4983.
- Vijayaraj, R.; Raman, S. S.; Kumar, R. M.; Subramanian, V. Studies on the Structure and Stability of Cyclic Peptide Based Nanotubes Using Oligomeric Approach: A Computational Chemistry Investigation. *J. Phys. Chem. B* **2010**, *114*, 16574-16583.
- Zhu, J.; Cheng, J.; Liao, Z.; Lai, Z.; Liu, B. Investigation of structures and properties of cyclic peptide nanotubes by experiment and molecular dynamics. *J. Comput. Aided Mol. Des.* **2008**, *22*, 773-81.
- Asthaqiri, D.; Bashford, D. Continuum and Atomistic Modeling of Ion Partitioning into a Peptide Nanotube. *Biophysical Journal* **2002**, *82*, 1176-1189.
- Hwang, H.; Schatz, G. C.; Ratner, M. A. Ion Current Calculations Based on Three Dimensional Poisson-Nernst-Planck Theory for a Cyclic Peptide Nanotube. *J. Phys. Chem. B* **2006**, *110*, 6999-7008.
- Alsina, M. A.; Gaillard, J. F.; Keten, S. Conformational changes during permeation of Na⁺ through a modified cyclic peptide nanotube promote energy landscape roughness. *Phys. Chem. Chem. Phys.* **2016**, *18*, 31698-31710.
- Liu, J.; Fan, J.; Tang, M.; Cen, M.; Yan, J.; Liu, Z.; Zhou, W. Water Diffusion Behaviours and Transportation Properties in Transmembrane Cyclic Hexa-, Octa and Decapeptide Nanotubes. *J. Phys. Chem. B* **2010**, *114*, 12183-12192.
- Liu, H.; Chen, J.; Shen, Q.; Fu, W.; Wu, W. Molecular Insights on the Cyclic Peptide Nanotube-Mediated Transportation of Antitumor Drug 5-Fluorouracil. *Molecular Pharmaceutics* **2010**, *7*, 1985-1994.
- Garcia-Fandino, R.; Granja, J. R.; D'Abramo, M.; Orozco, M. Theoretical Characterization of the Dynamical Behaviour and Transport Properties of α,γ -peptide Nanotubes in Solution. *J. Am. Chem. Soc.* **2009**, *131*, 15678-15686.
- Rho, J. Y.; Brendel, J. C.; MacFarlane, L. R.; Mansfield, E. D. H.; Peltier, R.; Rogers, S.; Hartlieb, M.; Perrier, S. Probing the Dynamic Nature of Self-Assembling Cyclic Peptide-Polymer Nanotubes in Solution and in Mammalian Cells. *Adv. Funct. Mat.* **2018**, *28*, 1704569.
- Ashkenasy, N.; Horne, W. S.; Ghadiri, M. R. Design of self-assembling peptide nanotubes with delocalized electronic states. *Small* **2006**, *2*, 99-102.

30. Mizrahi, M.; Zakrassov, A.; Lerner-Yardeni, J.; Ashkenasy, N. Charge transport in vertically aligned, self-assembled peptide nanotube junctions. *Nanoscale* **2012**, *4*, 518-24.
31. Saviano, M.; Zaccaro, L.; Lombardi, A.; Pedone, C.; Blasio, B. D.; Sun, X.; Lorzenzi, G. P. A structural two-ring version of a tubular stack of β -rings in crystals of a cyclic D,L-hexapeptide. *J. Incl. Phenom.* **1994**, *18*, 27-36.
32. Horne, W. S.; Stout, C. D.; Ghadiri, M. R. A Heterocyclic Peptide Nanotube. *J. Am. Chem. Soc.* **2003**, *125*, 9372-9376.
33. Chapman, R.; Jolliffe, K. A.; Perrier, S. Synthesis of Self-assembling Cyclic Peptide-polymer Conjugates using Click Chemistry. *Aust. J. Chem.* **2010**, *63*, 1169-1172.
34. Chapman, R.; Jolliffe, K. A.; Perrier, S. Modular design for the controlled production of polymeric nanotubes from polymer/peptide conjugates. *Polymer Chemistry* **2011**, *2*, 1956.
35. Chapman, R.; Jolliffe, K. A.; Perrier, S. Multi-shell soft nanotubes from cyclic peptide templates. *Adv. Mater.* **2013**, *25*, 1170-2.
36. Danial, M.; Tran, C. M.; Young, P. G.; Perrier, S.; Jolliffe, K. A. Janus cyclic peptide-polymer nanotubes. *Nat. Commun.* **2013**, *4*, 2780.
37. Couet, J.; Samuel, J. D.; Kopyshv, A.; Santer, S.; Biesalski, M. Peptide-Polymer Hybrid Nanotubes. *Angew. Chem. Int. Ed.* **2005**, *44*, 3297-3301.
38. Couet, J.; Biesalski, M. Surface-Initiated ATRP of *N*-Isopropylacrylamide from Initiator-Modified Self-Assembled Peptide Nanotubes. *Macromolecules* **2006**, *39*, 7258-7268.
39. Loschonsky, S.; Couet, J.; Biesalski, M. Synthesis of Peptide/Polymer Conjugates by Solution ATRP of Butylacrylate Using an Initiator-Modified Cyclic D-alt-L-Peptide. *Macromol. Rapid Commun.* **2008**, *29*, 309-315.
40. Chapman, R.; Warr, G. G.; Perrier, S.; Jolliffe, K. A. Water-soluble and pH-responsive polymeric nanotubes from cyclic peptide templates. *Chemistry* **2013**, *19*, 1955-61.
41. Sun, L.; Fan, Z.; Wang, Y.; Huang, Y.; Schmidt, M.; Zhang, M. Tunable synthesis of self-assembled cyclic peptide nanotubes and nanoparticles. *Soft matter* **2015**, *11*, 3822-32.
42. Couet, J.; Biesalski, M. Polymer-Wrapped Peptide Nanotubes: Peptide-Grafted Polymer Mass Impacts Length and Diameter. *Small* **2008**, *4*, 1008-1016.
43. Clark, T. D.; Ghadiri, M. R. Supramolecular Design by Covalent Capture. Design of a Peptide Cylinder via Hydrogen-Bond-Promoted Intermolecular Olefin Metathesis. *J. Am. Chem. Soc.* **1995**, *117*, 12364-12365.
44. Clark, T. D.; Kobayashi, K.; Ghadiri, M. R. Covalent capture and stabilization of cylindrical beta-sheet peptide assemblies. *Chem. Eur. J.* **1999**, *5*, 782-792.
45. Gokhale, R.; Couet, J.; Biesalski, M. In situ cross-linking of the shell of self-assembled peptide nanotubes. *Phys. Status Solidi A* **2010**, *207*, 878-883.
46. Maarseveen, J. H. V.; Horne, W. S.; Ghadiri, M. R. Efficient Route to C₂ Symmetric Heterocyclic Backbone Modified Cyclic Peptides. *Org. Lett.* **2005**, *7*, 4503-4506.
47. Steinem, C.; Janshoff, A.; Vollmer, M. S.; Ghadiri, M. R. Reversible Photoisomerization of Self-Organized Cylindrical Peptide Assemblies at Air-Water and Solid Interfaces. *Langmuir* **1999**, *15*, 3956-3964.
48. Vollmer, M. S.; Clark, T. D.; Steinem, C.; Ghadiri, M. R. Photoswitchable Hydrogen-Bonding in Self-Organized Cylindrical Peptide Systems. *Angew. Chem. Int. Ed.* **1999**, *38*, 1598-1601.
49. Crick, F. H. C. The packing of α -helices: Simple coiled-coils. *Acta Cryst.* **1953**, *6*, 689-697.
50. Presolski, S. I.; Hong, V.; Cho, S.-H.; Finn, M. G. Tailored Ligand Acceleration of the Cu-Catalyzed Azide-Alkyne Cycloaddition Reaction: Practical and Mechanistic Implications. *Journal of the American Chemical Society* **2010**, *132*, 14570-14576.
51. Jones, J. A.; Wilkins, D. K.; Smith, L. J.; Dobson, C. M. Characterisation of protein unfolding by NMR diffusion measurements. *J. Biomol. NMR* **1997**, *10*, 199-203.
52. Chapman, R.; Koh, M. L.; Warr, G. G.; Jolliffe, K. A.; Perrier, S. Structure elucidation and control of cyclic peptide-derived nanotube assemblies in solution. *Chemical Science* **2013**, *4*, 2581-2589.
53. Chapman, R.; Bouten, P. J.; Hoogenboom, R.; Jolliffe, K. A.; Perrier, S. Thermoresponsive cyclic peptide - poly(2-ethyl-2-oxazoline) conjugate nanotubes. *Chem. Commun.* **2013**, *49*, 6522-6524.

Chapter 5 – Appendix

Developing the structure, stability and function of tethered cyclic D/L peptide nanorods – Supplementary information

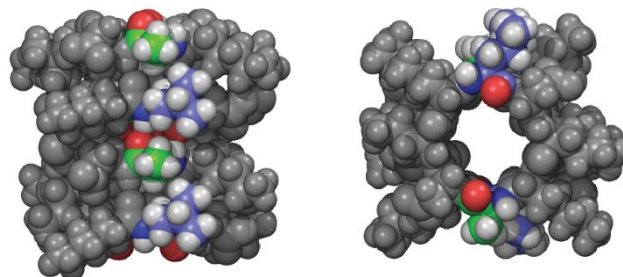


Figure S1. Model of compound **14** with antiparallel H-bonding, forming knobs-in-holes-type favourable interactions between sterically bulky Leu side-chains (blue) and short Ala side-chains (Green), viewed from the side and top.

CP monomer synthesis

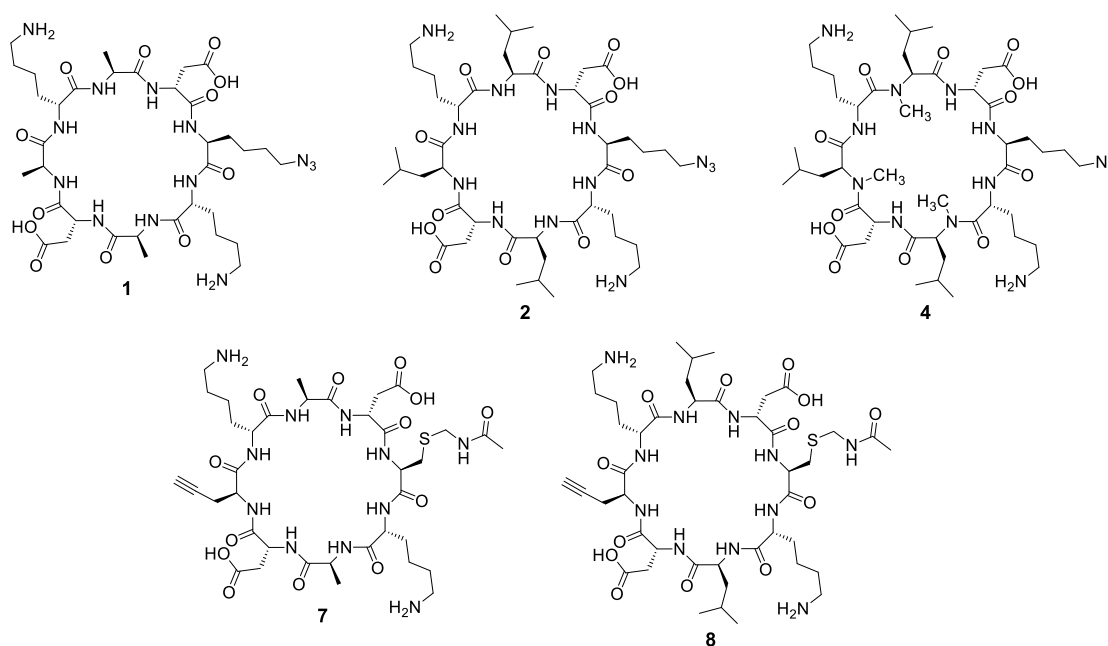
Coupling of the first amino acid: 2-chlorotrityl chloride resin (83 mg, resin loading 1.2 mmol/g, 0.1 mmol) was swelled in 5 mL of CH_2Cl_2 for 30 minutes in a sinter-fitted syringe. The resin was then drained and treated with 1 equivalent (relative to resin capacity) of Fmoc-amino acid dissolved in CH_2Cl_2 (4 mL). To the resin mixture was added 6 equivalents of DIPEA relative to amino acid and the resulting mixture was agitated at room temperature overnight. The resin was drained and washed with DMF (3×3 mL) and treated with MeOH (2×3 mL) to cap any unreacted sites. The resin was then washed with DMF (3×3 mL) and transferred to an SPPS reaction vessel.

Automated synthesis of linear peptides: The linear peptides were prepared using an automated solid-phase peptide-synthesiser (Protein Technologies Inc. PS3). On each coupling cycle, the resin was first washed with DMF (3×30 s). Fmoc deprotection was achieved using 20% piperidine in DMF (2×5 min) followed by washing with DMF (6×30 s) to provide the resin-bound free amino-terminal of the peptide. Amino acid couplings used three equivalents of Fmoc amino acid and 2-(6-chloro-1H-benzotriazole-1-yl)-1,1,3,3-tetramethylammonium hexafluorophosphate (HCTU), relative to resin loading. The amino acid and HCTU was dissolved in a solution of 7% DIPEA in DMF. The solution was added to the resin which was agitated at room temperature for 1 h, drained and washed with DMF (3×30 s). After coupling the final amino acid, a further Fmoc deprotection was performed to obtain the resin-bound peptide with free amino terminal. The resin was transferred to a sinter-fitted syringe and washed with DMF (3×3 mL), MeOH (3×3 mL) and Et_2O (3×3 mL).

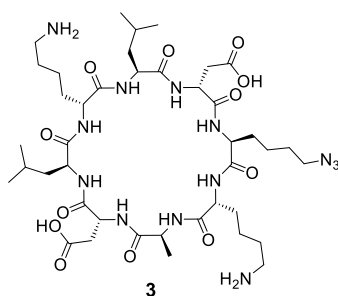
Peptide cleavage from resin: The resin-bound linear peptide was treated with a solution of 20% 1,1,1,3,3,3-hexafluoroisopropanol (HFIP) in CH_2Cl_2 ($3 \times 3 \text{ mL} \times 10 \text{ min}$) and the HFIP washings were collected by filtration. The resin was then washed with CH_2Cl_2 ($3 \times 3 \text{ mL}$). The combined HFIP and CH_2Cl_2 washings were concentrated under reduced pressure and freeze-dried from 1:1 ACN/ H_2O to yield the side-chain-protected linear peptide as a white powder. A sample of the peptide was deprotected and analysed by LCMS to confirm the linear sequence.

Cyclisation: The linear peptide was added to DMF (7 mg/mL) and treated with 3 equivalents of PyClock and 6 equivalents of DIPEA. The solution was stirred at room temperature for 2 days before being concentrated under reduced pressure to yield a thick oil. The oil was freeze-dried from 1:1 ACN/ H_2O to yield the crude side-chain-protected cyclic peptide as an off-white solid. *Deprotection:* The side chain protecting groups of the cyclic peptide were removed by treatment with a solution of TFA/TIPS/ H_2O (95:2.5:2.5 v/v, 2 mL) for 3 h. The TFA was evaporated using a stream of N_2 gas and the remaining oil was then treated with ice-cold Et_2O to precipitate the peptide. The precipitate was collected by centrifugation and freeze-dried from 1:1 ACN/ H_2O to yield the crude cyclic deprotected peptide as a white solid.

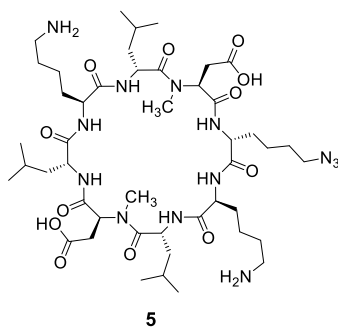
Purification: Peptides were purified by preparative reverse-phase HPLC using a Waters Associates liquid chromatography system (Model 600 Controller and Waters 486 Tunable Absorbance Detector) with a Phenomenex Luna C8(2) 100 Å, 10 μm , 250 \times 21.2 mm column with 0.1% TFA/ H_2O as buffer A and 0.1% TFA/ACN as buffer B with a flow rate of 10 mL/min.



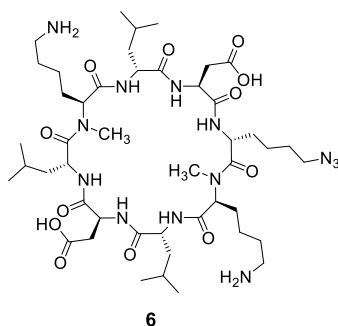
1, 2, 4, 7 and 8: Synthesis and characterization have been previously reported.¹



3: Linear: HOOC-Leu-D-Lys(Boc)-Leu-D-Asp(tBu)-Ala-D-Lys(Boc)-Lys(N₃)-D-Asp(tBu)-NH₂. White powder, 77.0% yield, MS-ESI (deprotected): m/z 956.70 [M + H]⁺, 479.05 [M + 2H]²⁺. Cyclic: *cyclo*[d-K(N₃)-k-A-d-L-k-L]. Purification gradient: 0-60% buffer B over 60 min, R_T = 33.2 min (33.2% B). Yield: 34.8 mg (37.1%) as a white solid. HRMS (ESI) [M + Na]⁺ calculated: 960.5237, found: 960.5302, [M + H]⁺ calculated: 938.5418, found: 938.5425, [M + 2H]²⁺ calculated: 469.7745, found: 469.7760.

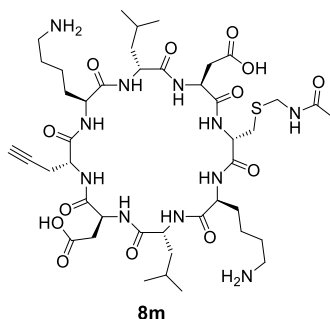


5: Linear: HOOC-NMeAsp(tBu)-D-Leu-Lys(Boc)-D-Lys(N₃)-NMeAsp(tBu)-D-Leu-Lys(Boc)-D-Leu-NH₂. White powder, 53.0% yield, MS-ESI (deprotected): m/z 1026.75 [M + H]⁺, 514.10 [M + 2H]²⁺. Cyclic: *cyclo*[NMeD-k(N₃)-K-I-NMeD-I-K-I]. Purification gradient: 20-60% buffer B over 60 min, R_T = 21.4 min (34.3% B). Yield: 14.5 mg (14.4%) as a white solid. HRMS (ESI) [M + Na]⁺ calculated: 1030.6020, found: 1030.6010, [M + H]⁺ calculated: 1008.6200, found: 1008.6206, [M + 2H]²⁺ calculated: 504.8137, found: 504.8151.

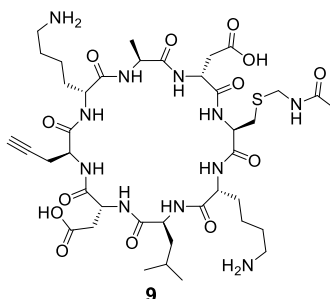


6: Linear: HOOC-NMeLys(Boc)-D-Lys(N₃)-Asp(tBu)-D-Leu-NMeLys(Boc)-D-Leu-Asp(tBu)-D-Leu-NH₂. White powder, 65.0% yield, MS-ESI (deprotected): m/z 1026.70 [M + H]⁺, 514.10 [M

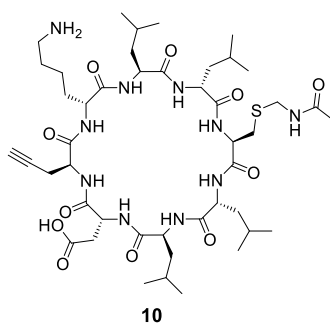
+ 2H]²⁺. Cyclic: *cyclo*[D-k(N₃)-NMeK-I-D-I-NMeK-I]. Purification gradient: 0-60% buffer B over 60 min, R_T = 33.0 min (33.0% B). Yield: 12.9 mg (12.8%) as a white solid. HRMS (ESI) [M + H]⁺ calculated: 1008.6200, found: 1008.6092, [M + 2H]²⁺ calculated: 504.8137, found: 504.8143.



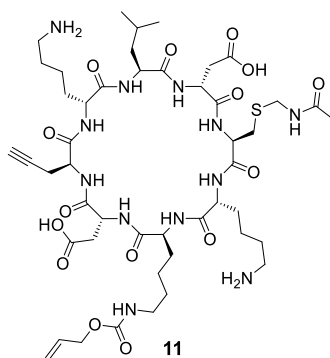
8m: Linear: HOOC-D-Leu-Lys(Boc)-D-Gly(Pra)-Asp(tBu)-D-Leu-Lys(Boc)-D-Cys(Acm)-Asp(tBu)-NH₂. White powder, 92.8% yield, MS-ESI (deprotected): m/z 1000.60 [M + H]⁺, 501.05 [M + 2H]²⁺. Cyclic: *cyclo*[D-c(Acm)-K-I-D-g(Pra)-K-I]. Purification gradient: 0-60% buffer B over 60 min, R_T = 37.5 min (25.0% B). Yield: 62.0 mg (42.1%) as a white solid on 0.15 mmol scale synthesis. HRMS (ESI) [M + Na]⁺ calculated: 1004.4846, found: 1004.4821, [M + H]⁺ calculated: 982.5026, found: 982.5031, [M + 2H]²⁺ calculated: 491.7550, found: 491.7566



9: Linear: HOOC-Leu-D-Lys(Boc)-Cys(Acm)-D-Asp(tBu)-Ala-D-Lys(Boc)-Gly(Pra)-D-Asp(tBu)-NH₂. White powder, 80.6% yield, MS-ESI (deprotected): m/z 958.60 [M + H]⁺, 480.00 [M + 2H]²⁺. Cyclic: *cyclo*[d-C(Acm)-k-L-d-G(Pra)-k-A]. Purification gradient: 0-60% buffer B over 60 min, R_T = 24.1 min (24.1% B). Yield: 51.6 mg (54.9%) as a white solid. HRMS (ESI) [M + Na]⁺ calculated: 962.4376, found: 962.4353, [M + H]⁺ calculated: 940.4557, found: 940.4561, [M + 2H]²⁺ calculated: 470.7315, found: 470.7328.



10: Linear: HOOC-Leu-D-Leu-Cys(Acm)-D-Leu-Leu-D-Lys(Boc)-Gly(Pra)-D-Asp(tBu)-NH₂. White powder, 71.2% yield, MS-ESI (deprotected): m/z 983.65 [M + H]⁺, 492.60 [M + 2H]²⁺. Cyclic: *cyclo*[l-C(Acm)-l-L-d-G(Pra)-k-L]. Purification gradient: 20-80% buffer B over 60 min, 30 mg of crude per 10 mL injection. R_T = 26.2 min (46.2% B). Yield: 25.3 mg (26.2%) as a white solid. HRMS (ESI) [M + Na]⁺ calculated: 987.5308, found: 987.5274, [M + H]⁺ calculated: 965.5489, found: 965.5485, [M + 2H]²⁺ calculated: 483.2781, found: 483.2805.



11: Linear: HOOC-Leu-D-Lys(Boc)-Gly(Pra)-D-Asp(tBu)-Lys(Alloc)-D-Lys(Boc)-Cys(Acm)-D-Asp(tBu)-NH₂. White powder, 93.5% yield, MS-ESI (deprotected): m/z 1099.70 [M + H]⁺, 550.65 [M + 2H]²⁺. Cyclic: *cyclo*[d-C(Acm)-k-K(Alloc)-d-G(Pra)-k-L]. Purification gradient: 0-60% buffer B over 90 min, R_T = 37.5 min (25.0% B). Yield: 52.0 mg (32.1%) as a white solid on 0.15 mmol scale synthesis. HRMS (ESI) [M + Na]⁺ calculated: 1103.5166, found: 1103.5144, [M + H]⁺ calculated: 1081.5347, found: 1081.5350, [M + 2H]²⁺ calculated: 541.2710, found: 541.2725.

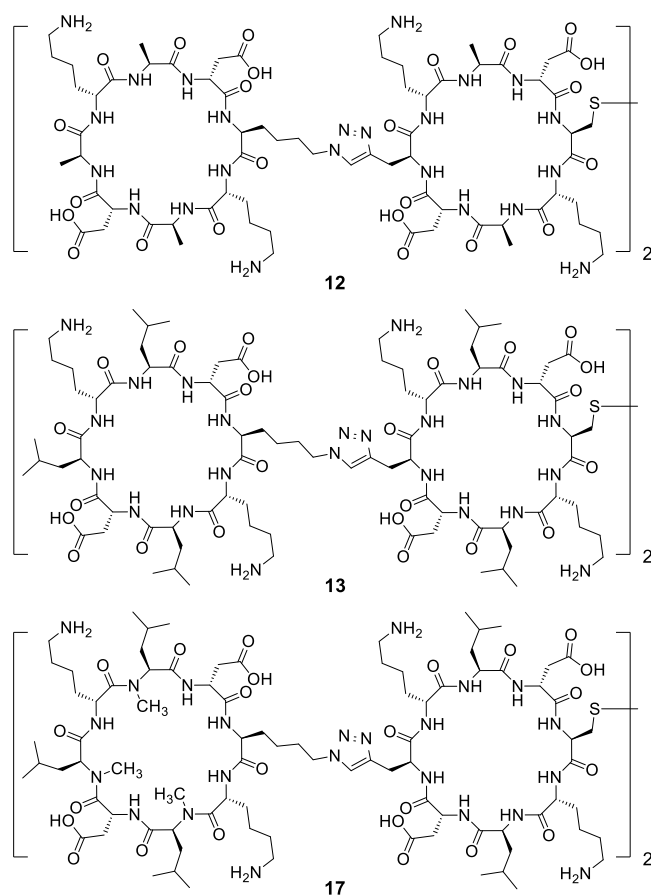
CP tetramer synthesis

CuAAC ($A + B = AB$): An azide-peptide (CPs **1-6**, 10 mg, ~0.01 mmol) and alkyne-peptide (CPs **7-11**, 10 mg, ~0.01 mmol) were added to KH₂PO₄/K₂HPO₄ buffer (0.1 M, pH 7.1, 8.85 mL) and treated with premixed CuSO₄ and THPTA (150 μL, final conc. 0.1 and 0.5 mM respectively), and sodium ascorbate (500 μL, 0.1M). Solution was stirred gently for 30 sec and left to stand for 3 h rt. Reaction progress was tracked by LCMS and the solution purified directly by prep. HPLC as per CP monomers above with a gradient of 0 to 60% buffer B over 60-90

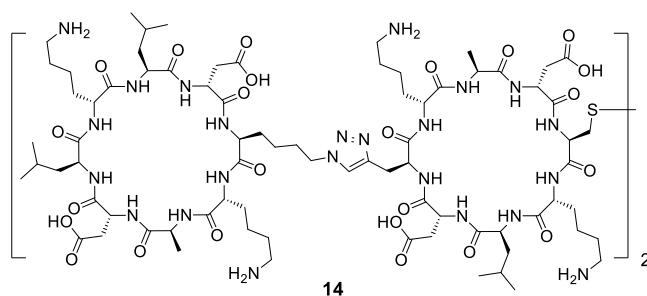
min. The purified intermediate CP dimer was then lyophilised to yield a white solid for subsequent oxidative coupling with yields 50-60%.

Alternative CuAAC: The CuAAC procedure for CPs with poor aqueous solubility was as stated above but with the following adjustments. TNBT (triethyl 5,5',5''-[2,2',2''-nitrilotris(methylene)tris(1*H*-benzo[*d*]imidazole-2,1-diyl)]tripentanoate) was used as the ligand in a 2:1 ratio to CuSO₄ (final concentrations of 0.2 and 0.1 mM for TNBT:CuSO₄).² Reaction mixture contained 20% DMSO with 80% KH₂PO₄/K₂HPO₄ buffer (0.1 M, pH 7.1). The reaction proceeded to ~100% conversion in under 60 min followed by dilution and purification by prep. HPLC.

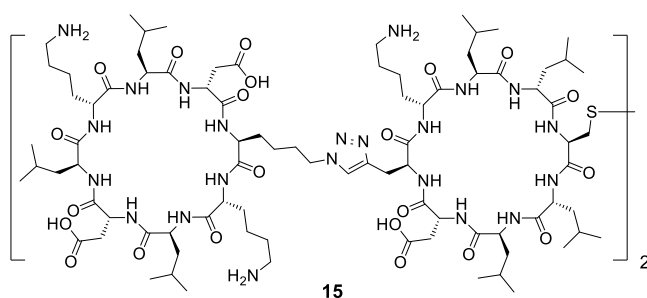
Oxidation (2AB = ABBA): To glacial AcOH (1 mL) was added Acm-protected intermediate CP dimer (10 mg, ~0.05 mmol). The mixture was treated with I₂ in AcOH (0.1 M, 350 μL), blanketed with N₂ gas and stirred vigorously for 3 h rt. The reaction mixture was then quenched until colourless with 0.1M sodium ascorbate, diluted to 100 mL with 0.1% TFA/H₂O and purified by prep. HPLC as per CP monomers above, with a gradient of 0 to 60% buffer B over 60 min. CP tetramer was then isolated by lyophilisation as a white solid.



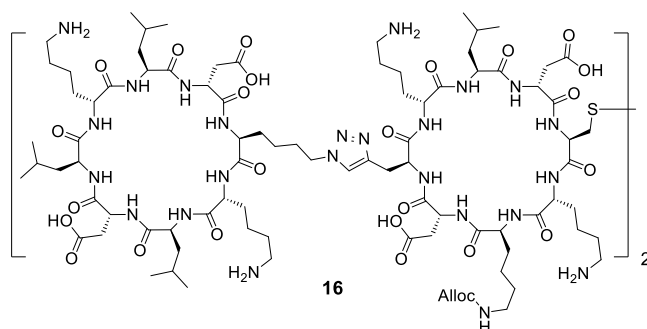
12, 13 and 17: Synthesis and characterization previously reported.¹



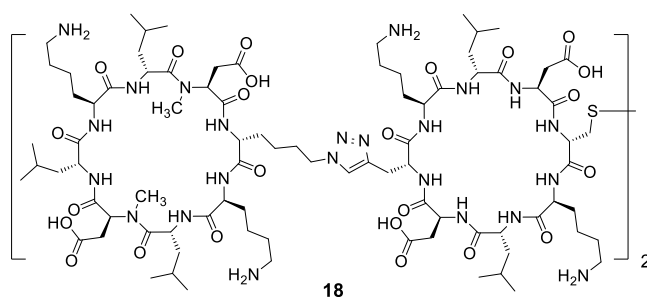
14: [*cyclo*(d-L-k-L-d-K(N₃)-k-A)*cyclo*(d-G(Pra)-k-A-d-C-k-L)]₂. Purification gradient: 0-60% buffer B over 60 min, R_T = 26.9 min (26.9% B). Yield: 14.0 mg (29.1%) over two steps as a white solid. Scale: 25 mg of each peptide monomer. ¹H NMR (600 MHz, 10% D₂O/H₂O) δ 8.37 (d, *J* = 7.3 Hz, 2H), 8.34 (d, *J* = 6.7 Hz, 1H), 8.31 – 8.16 (m, 5H), 8.15 (d, *J* = 6.1 Hz, 1H), 8.11 (m, 2H), 8.06 (d, *J* = 7.6 Hz, 1H), 7.81 – 7.74 (m, 2H), 7.73 (s, 1H), 7.44 (s, 8H), 4.37 – 4.01 (m, 7H), 3.21 (dd, *J* = 15.1, 5.3 Hz, 1H), 3.16 – 3.00 (m, 2H), 3.00 – 2.50 (m, 19H), 1.88 – 1.00 (m, 49H), 1.00 – 0.60 (m, 21H), 0.49 (s, 1H). HRMS (ESI) [M+3H]³⁺ calculated: 1204.2993, found: 1204.3016. [M+4H]⁴⁺ calculated: 903.4763, found: 903.4799. [M+5H]⁵⁺ calculated: 722.9825, found: 722.9866.



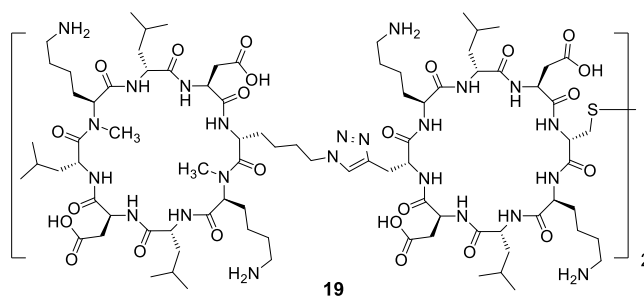
15: [*cyclo*(d-L-k-L-d-K(N₃)-k-L)*cyclo*(d-G(Pra)-k-L-l-C-l-L)]₂. Purification gradient: 20-60% buffer B over 80 min, R_T = 40.3 min (40.1% B). Yield: 6.0 mg (14.3%) over two steps as a white solid. Scale: 21 mg of each peptide monomer. ¹H NMR (600 MHz, 10% D₂O/H₂O) δ 8.46 (d, *J* = 7.2 Hz, 1H), 8.35 (d, *J* = 5.7 Hz, 1H), 8.33 – 8.25 (m, 2H), 8.20 (d, *J* = 7.0 Hz, 1H), 8.18 – 8.08 (m, 5H), 8.04 (d, *J* = 5.4 Hz, 2H), 7.93 (d, *J* = 8.4 Hz, 2H), 7.86 (d, *J* = 8.0 Hz, 1H), 7.71 (s, 2H), 7.46 (s, 6H), 4.48 – 3.99 (m, 11H), 3.24 – 2.54 (m, 18H), 1.89 – 1.11 (m, 53H), 1.00 – 0.63 (m, 54H). HRMS (ESI) [M+3H]³⁺ calculated: 1249.0593, found: 1249.0591. [M+3K]³⁺ calculated: 1287.3494, found: 1287.3513.



16: [*cyclo*(d-L-k-L-d-K(N₃)-k-L)*cyclo*(d-G(Pra)-k-L-d-C-k-K(Alloc))]₂. Purification gradient: 0-60% buffer B over 90 min, R_T = 45.0 min (30.0% B). Yield: 32.1 mg (31.6%) over two steps as a white solid. Scale: 52 mg of each peptide monomer. ¹H NMR (600 MHz, 10% D₂O/H₂O) δ 8.38 – 8.28 (m, 6H), 8.25 – 8.18 (m, 6H), 8.14 (d, *J* = 6.9 Hz, 3H), 8.09 (mp, 4H), 8.02 (d, *J* = 7.5 Hz, 2H), 7.89 (d, *J* = 8.2 Hz, 2H), 7.84 (d, *J* = 8.0 Hz, 2H), 7.73 (s, 2H), 7.45 (s, 13H), 6.74 (s, 1H), 5.85 (ddd, *J* = 16.5, 10.5, 5.0 Hz, 1H), 5.21 (d, *J* = 19.0 Hz, 1H), 5.15 (d, *J* = 11.5 Hz, 1H), 4.41 – 4.10 (m, 14H), 3.21 (dd, *J* = 15.2, 5.6 Hz, 2H), 3.10 (dd, *J* = 15.2, 8.2 Hz, 2H), 3.06 – 2.65 (m, 36H), 1.89 – 1.09 (m, 88H), 0.91 – 0.69 (m, 48H). [M+3H]³⁺ calculated: 1326.3832, found: 1326.3814. [M+4Na]⁴⁺ calculated: 1017.0212, found: 1017.0326. [M+5H]⁵⁺ calculated: 796.2328, found: 796.2353.



18: [*cyclo*(NMeD-l-K-l-NMeD-k(N₃)-K-l)*cyclo*(D-g(Pra)-K-l-D-c-K-l)]₂. Purification gradient: 0-60% buffer B over 60 min, R_T = 35.8 min (35.8% B). Yield: 8.9 mg (38.9%) over two steps as a white solid. Scale: 12 mg of each peptide monomer. ¹H NMR (600 MHz, 10% D₂O/H₂O) δ 8.55 – 8.38 (m, 1H), 8.35 – 8.05 (m, 6H), 7.95 (dd, *J* = 12.8, 7.9 Hz, 1H), 7.84 (d, *J* = 9.5 Hz, 1H), 7.78 – 7.70 (m, 1H), 7.47 (s, 6H), 5.24 (s, 1H), 4.27 (ddd, *J* = 29.9, 18.4, 6.5 Hz, 5H), 3.25 – 3.07 (m, 3H), 3.03 (s, 5H), 2.98 – 2.56 (m, 15H), 1.97 (s, 4H), 1.90 – 1.02 (m, 40H), 0.95 – 0.69 (m, 28H). HRMS (ESI) [M+3H]³⁺ calculated: 1279.0494, found: 1279.0514. [M+4H]⁴⁺ calculated: 959.5389, found: 959.5426. [M+5H]⁵⁺ calculated: 767.8325, found: 767.8365.



19: [*cyclo*(D-I-NMeK-I-D-k(N₃)-NMeK-I)*cyclo*(D-g(Pra)-K-I-D-c-K-I)]₂. Purification gradient: 0-60% buffer B over 90 min, R_T = 48.0 min (32.0% B). Yield: 6.9 mg (30.2%) over two steps as a white solid. Scale: 12 mg of each peptide monomer. ¹H NMR (600 MHz, 10% D₂O/H₂O) δ 8.45 (d, *J* = 34.1 Hz, 1H), 8.36 – 7.99 (m, 5H), 7.82 – 7.66 (m, 2H), 7.59 – 7.32 (m, 5H), 4.45 – 3.98 (m, 3H), 3.29 – 2.52 (m, 16H), 1.97 (s, 2H), 1.89 – 1.01 (m, 28H), 0.81 (m, 21H), 0.44 (dd, *J* = 41.2, 6.9 Hz, 1H). HRMS (ESI) [M+3H]³⁺ calculated: 1279.0494, found: 1279.0504. [M+4H]⁴⁺ calculated: 959.5389, found: 959.5420. [M+5H]⁵⁺ calculated: 767.8325, found: 767.8364.

NMR spectroscopy

1D ¹H and 2D [¹H, ¹H]-TOCSY (TOCSY mixing time = 70 ms), NOESY (NOE mixing time = 600 ms), [¹⁵N, ¹H]-SOFAS-HMQC and ¹³C-multiplicity edited [¹³C, ¹H]-HSQC as well as 2D DOSY (diffusion time = 50 ms and length of gradient = 3 ms) NMR spectra of CP tetramers were recorded on a 600 MHz Bruker Avance III HD spectrometer with CryoProbe, at 298 K. Samples were dissolved in 10% D₂O in H₂O or 100% D₂O for ¹H-D exchange studies. The pH of samples was measured to be 3.0 ± 0.3. All of the NMR spectra were processed using TopSpin 3.0 (Bruker BioSpin GmbH).

¹H NMR

An impurity at ~7.85 ppm of the 1D ¹H spectra is present in the spectra of tetramers 12-19. This signal did not change with concentration, remained unchanged in 100% D₂O and offered no [¹³C, ¹H] or [¹⁵N, ¹H] signal.

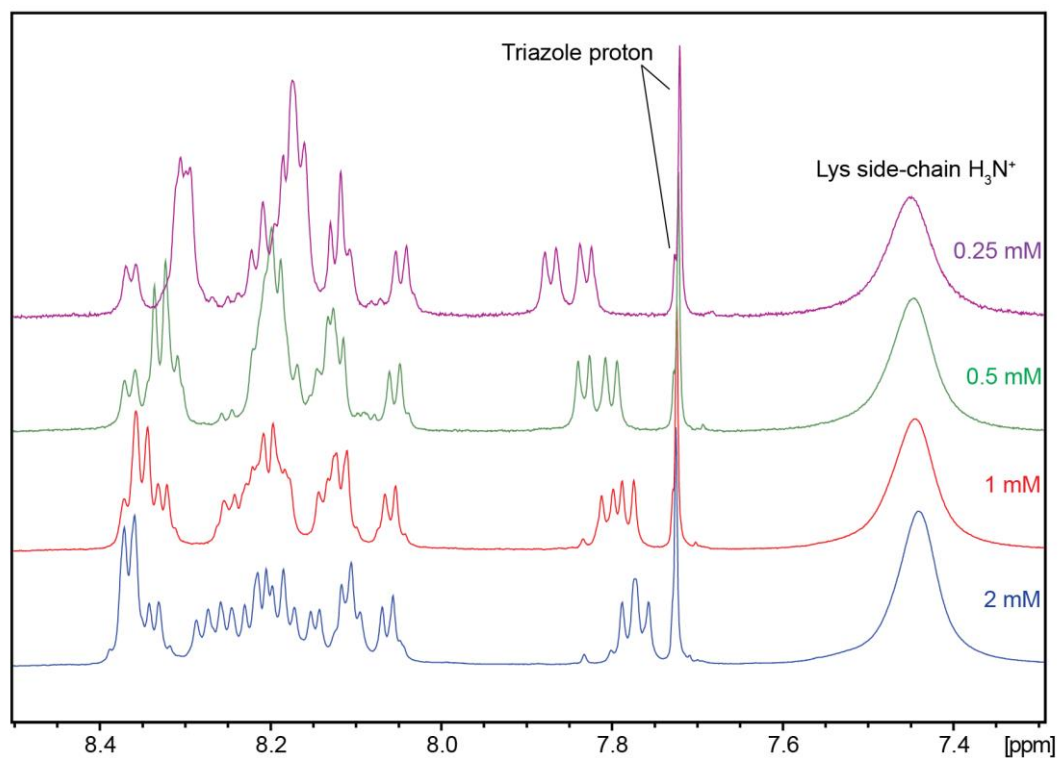


Figure S2. Amide proton region of 1D ^1H NMR spectra for **14** at 0.25, 0.5, 1 and 2 mM in 10% D_2O at 298 K. Overall dispersion of H^{N} signals increases with increasing concentration, indicating concentration-dependent assembly into more ordered structures. Triazole proton signals converge at higher concentration, consistent with the formation of a more ordered structure at high concentration.

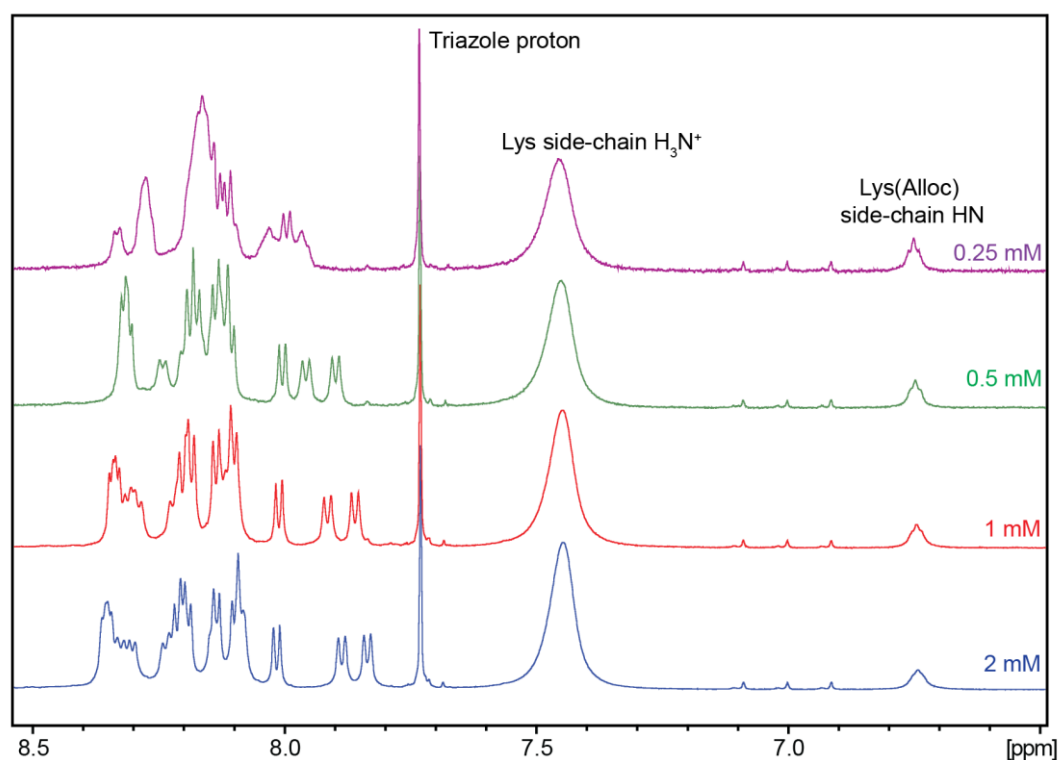


Figure S3. Amide proton region of 1D ^1H NMR spectra for **15** at 0.25, 0.5, 1 and 2 mM in 10% D_2O at 298 K. H^{N} signals become sharper and more dispersed with increasing concentration indicating the formation of ordered structures at high concentration. The triazole proton exists as a single signal, indicating symmetry in the structure at all concentrations.

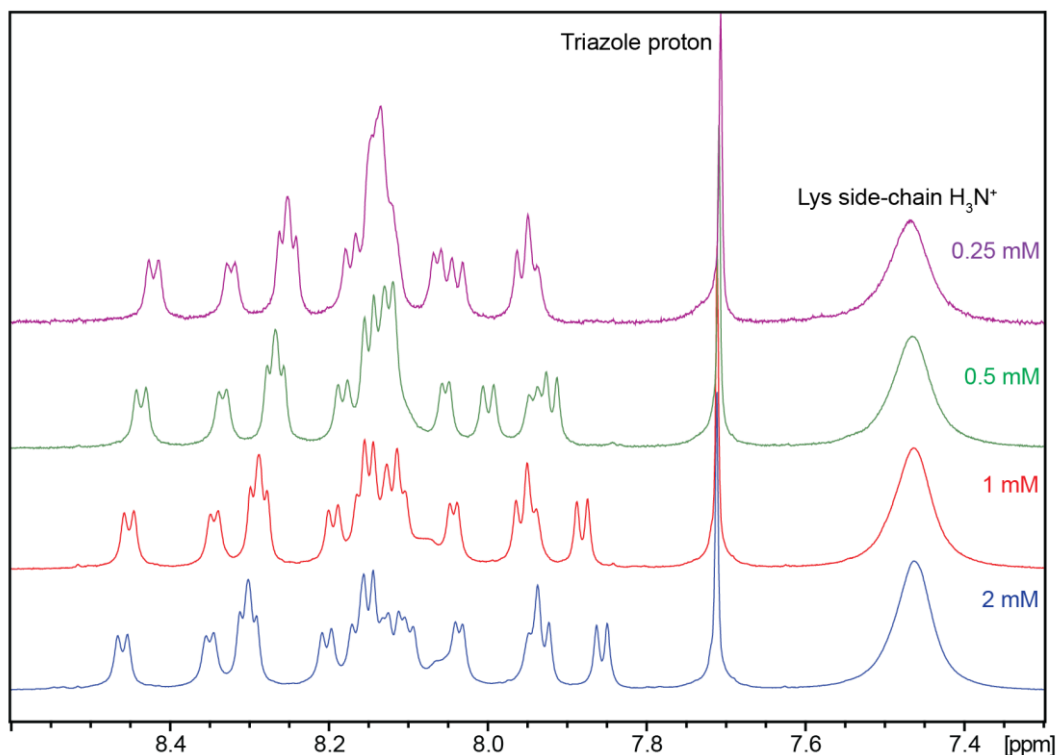


Figure S4. Amide proton region of 1D ^1H NMR spectra for **16** at 0.25, 0.5, 1 and 2 mM in 10% D_2O at 298 K. H^{N} signals are highly-dispersed even at 0.25 mM and become more dispersed with increasing concentration. The triazole proton exists as a single signal even at low concentration, indicating symmetry within the structure and a consistent conformation.

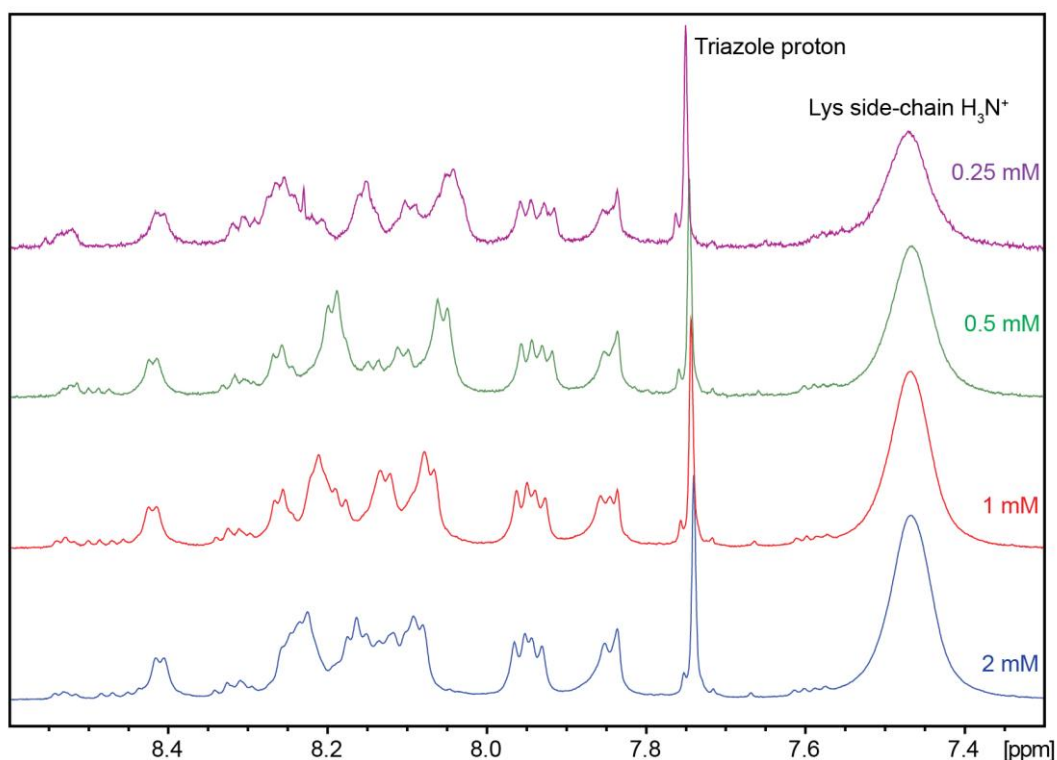


Figure S5. Amide proton region of 1D ^1H NMR spectra for **18** at 0.25, 0.5, 1 and 2 mM in 10% D_2O at 298 K. H^{N} signals do not increase in overall dispersion with increasing concentration. Distinct conformations exist for **18** at all concentrations as seen by the weaker H^{N} signals throughout the spectra. H^{N} signals undergo some changes with concentration, indicating there are some concentration-dependent effects on structure although it does not appear to improve order.

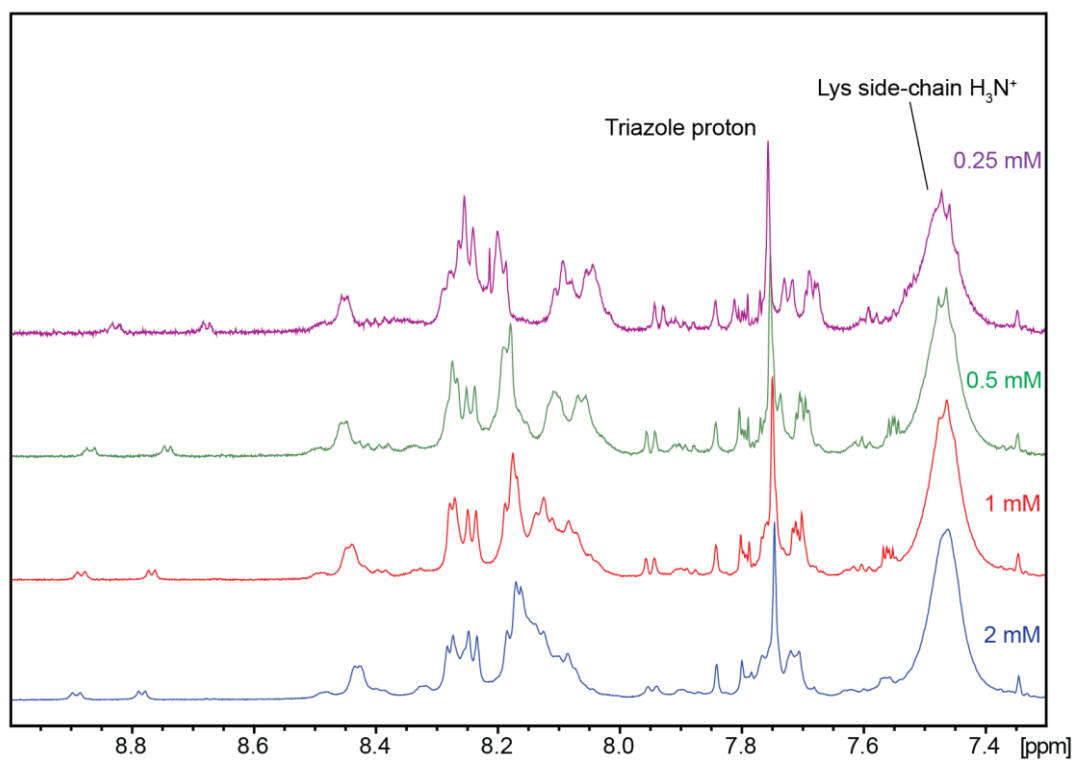


Figure S6. Amide proton region of 1D ^1H NMR spectra for **19** at 0.25, 0.5, 1 and 2 mM in 10% D_2O at 298 K. Multiple conformations exist in solution for **19** as seen by the presence of weaker H^{N} signals throughout the spectra. H^{N} signals for the major species in solution become less dispersed with increasing concentration while H^{N} signals for the minor species increase in overall dispersion with increasing concentration.

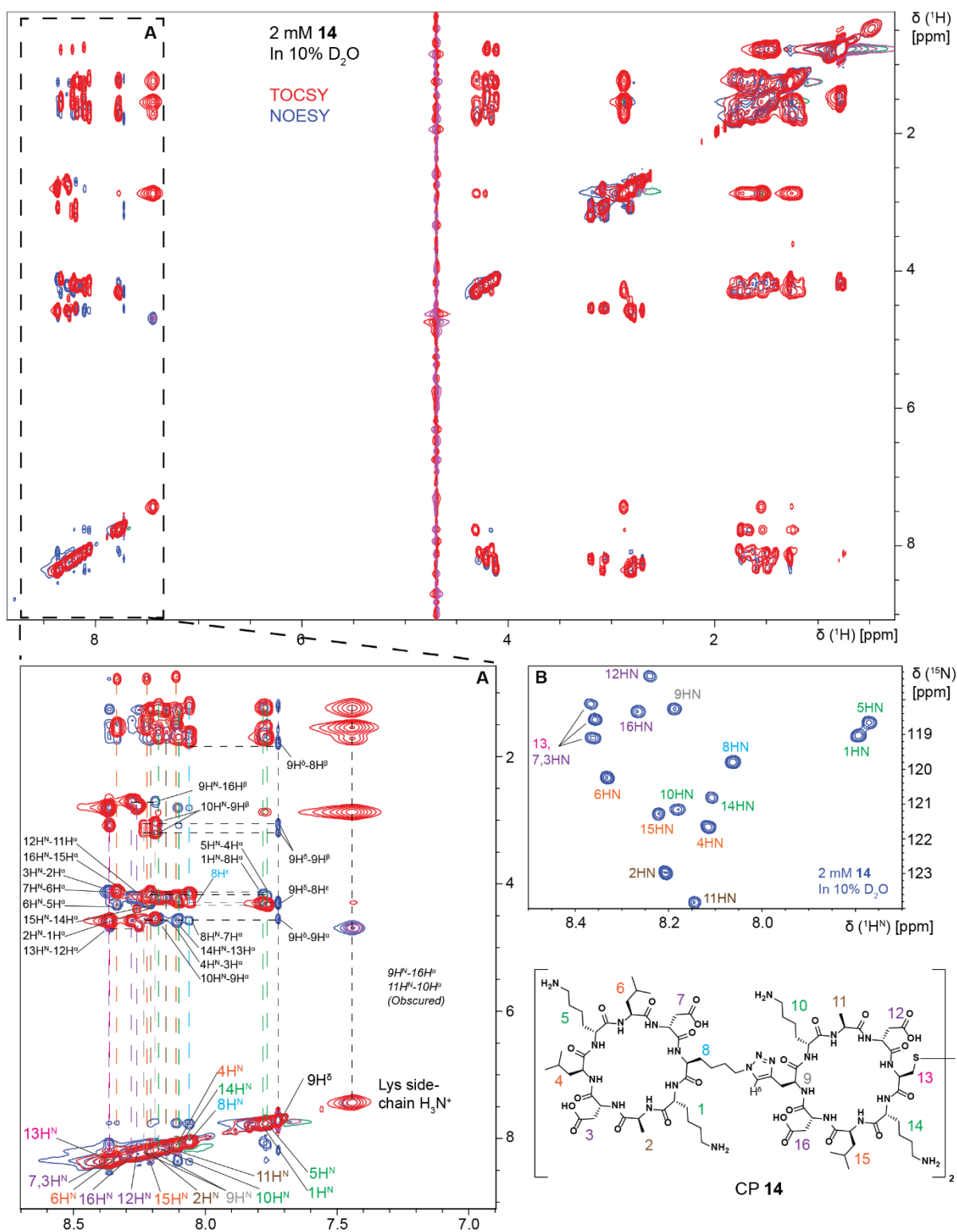
^1H - ^1H NOESY, TOCSY and ^{15}N - ^1H SOFAST HMQC

Figure S7. 2D [^1H , ^1H]-NOESY (blue) and TOCSY (red) overlaid spectra of CP tetramer **14**. A) Expansion of the downfield region containing the backbone H^N signals. Key NOESY interactions are labelled. B) ^1H - ^{15}N SOFAST HMQC spectrum of **14** with HN signals assigned. Residues 3, 7 and 13 could not be unambiguously assigned due to H^N signal overlap.

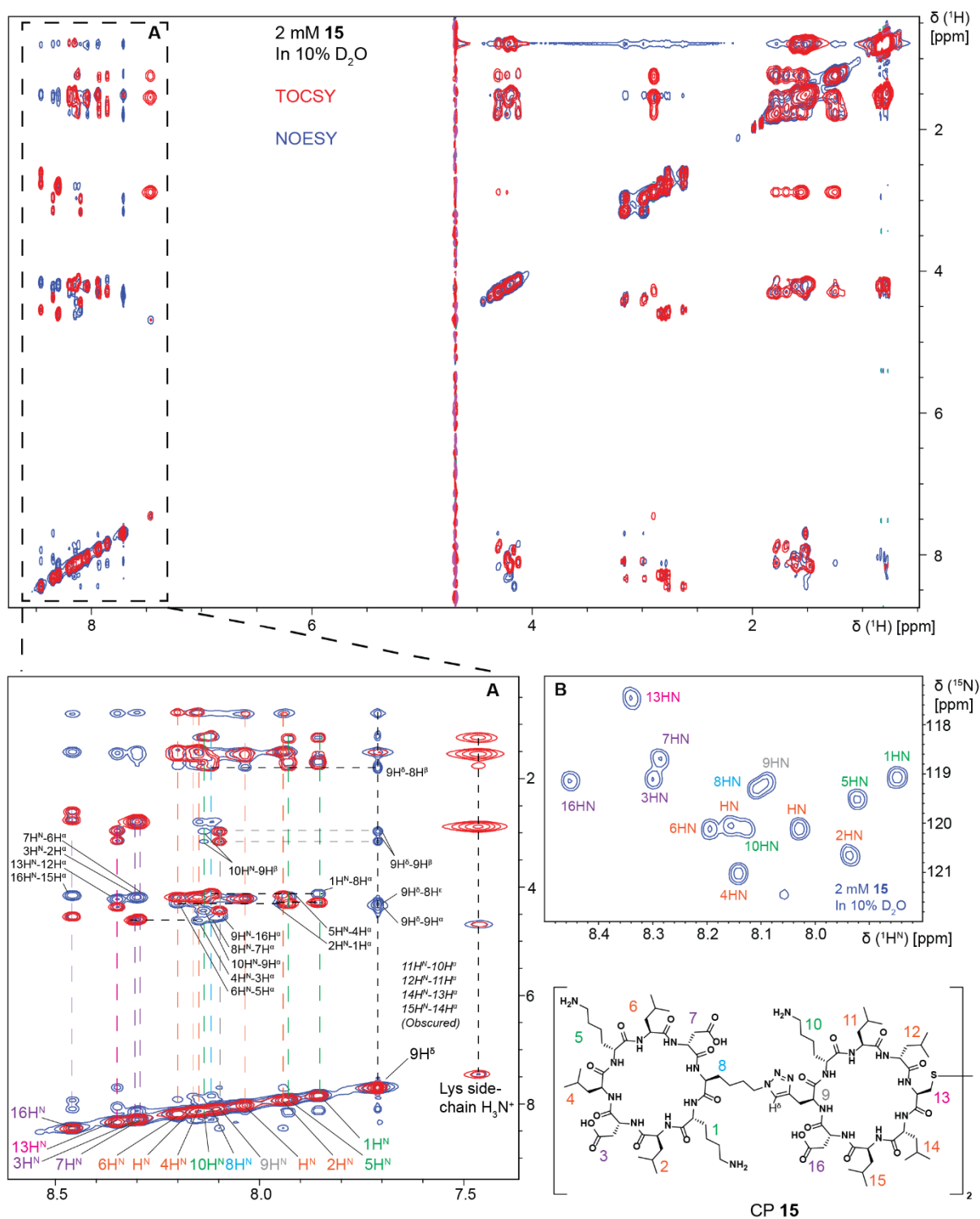


Figure S8. 2D [¹H, ¹H]-NOESY (blue) and TOCSY (red) overlaid spectra of CP tetramer **15**. A) Expansion of the downfield region containing the backbone H^N signals. Key NOESY interactions are labelled. B) ¹H-¹⁵N SOFAST HMQC spectrum of **15** with HN signals assigned. Residues 11, 12, 14 and 15 could not be unambiguously assigned due to signal overlap throughout the 2D spectra.

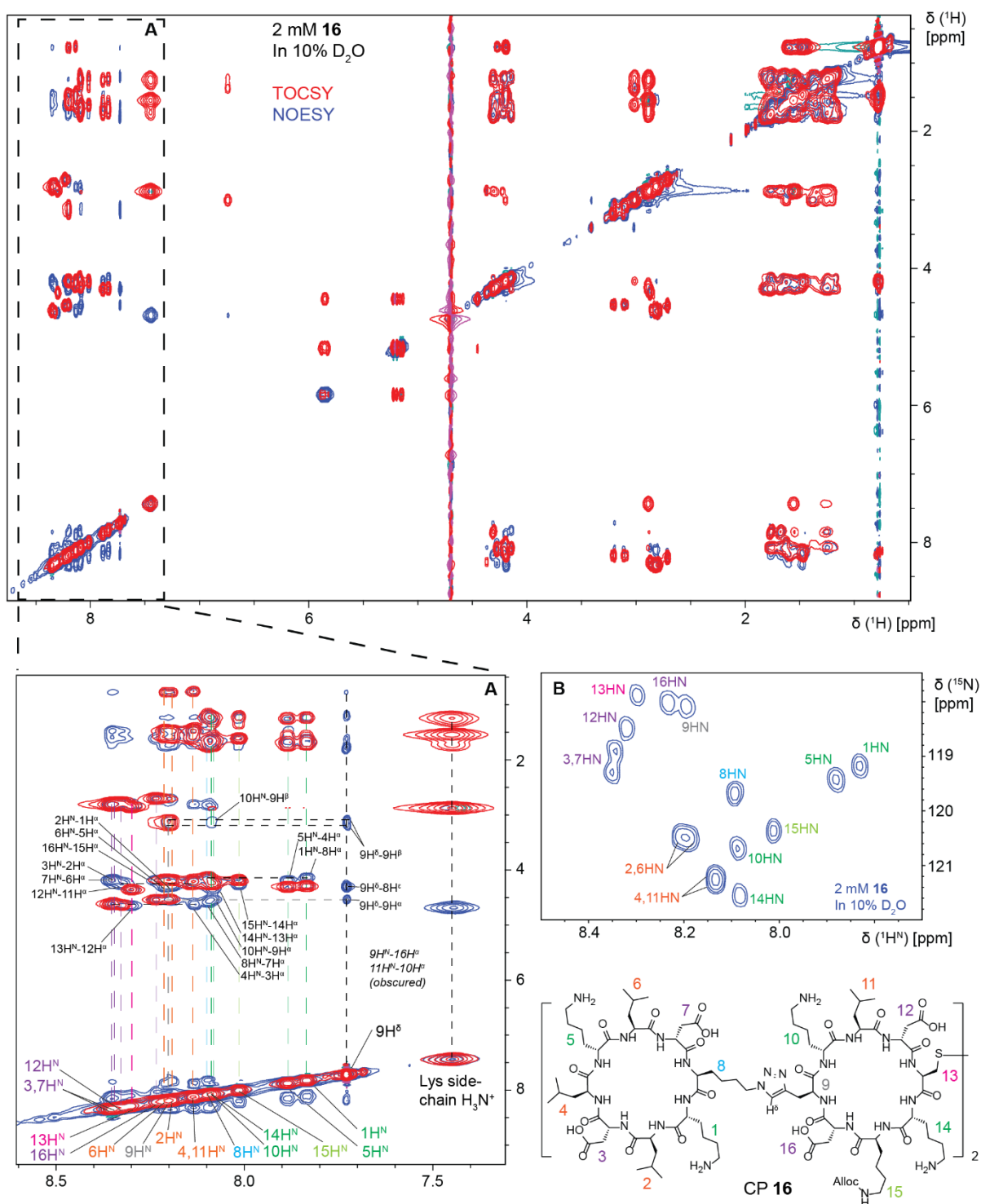


Figure S9. 2D [¹H, ¹H]-NOESY (blue) and TOCSY (red) overlaid spectra of CP tetramer **16**. A) Expansion of the downfield region containing the backbone H^N signals. Key NOESY interactions are labelled. B) ¹H-¹⁵N SOFAST HMQC spectrum of **16** with HN signals assigned. Some residue pairs could not be unambiguously assigned due to signal overlap.

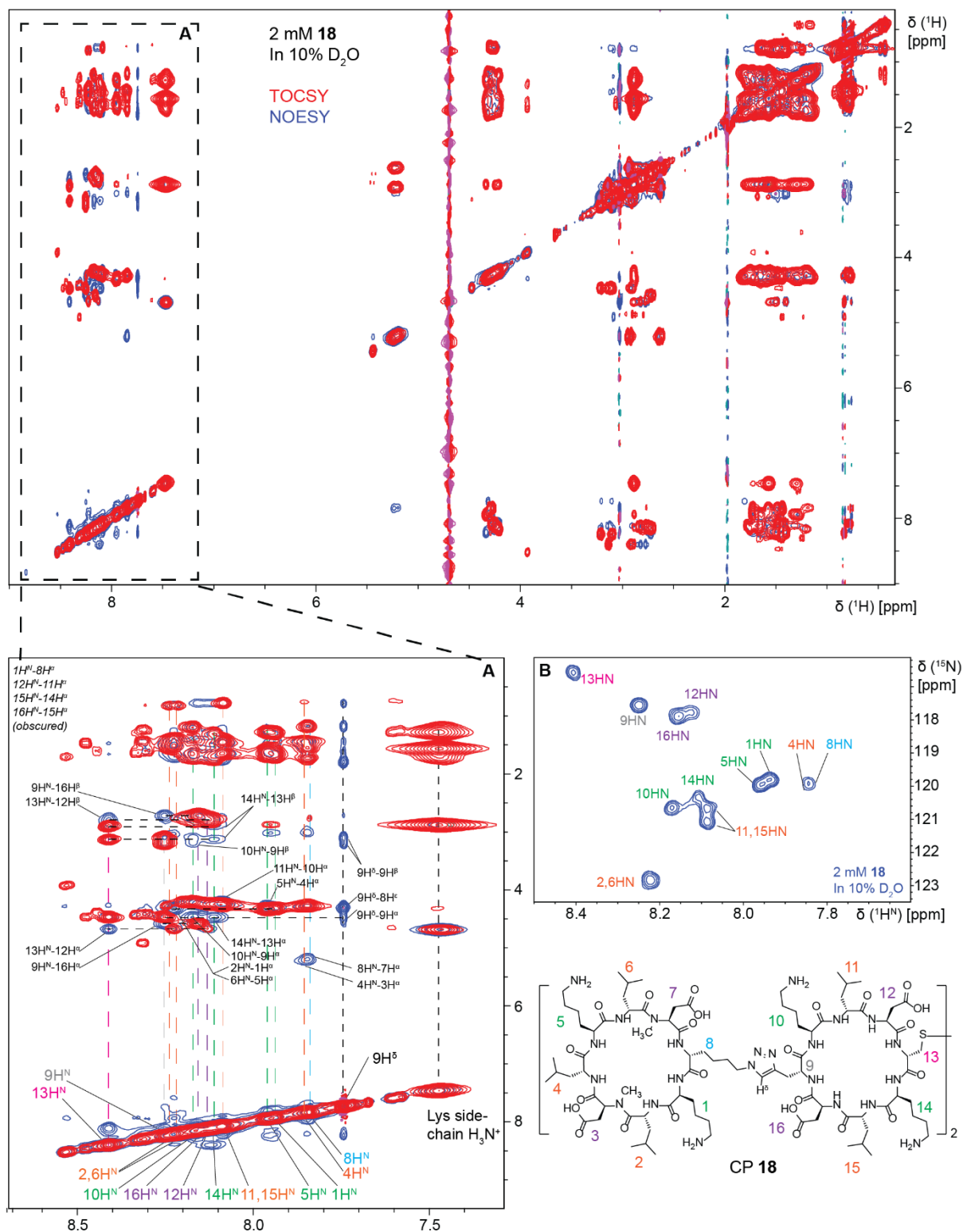


Figure S10. 2D [¹H, ¹H]-NOESY (blue) and TOCSY (red) overlaid spectra of CP tetramer **18**. A) Expansion of the downfield region containing the backbone H^N signals. Key NOESY interactions are labelled. B) ¹H-¹⁵N SOFAST HMQC spectrum of **18** with HN signals assigned. Residues 11 and 15 could not be unambiguously assigned due to H^N signal overlap.

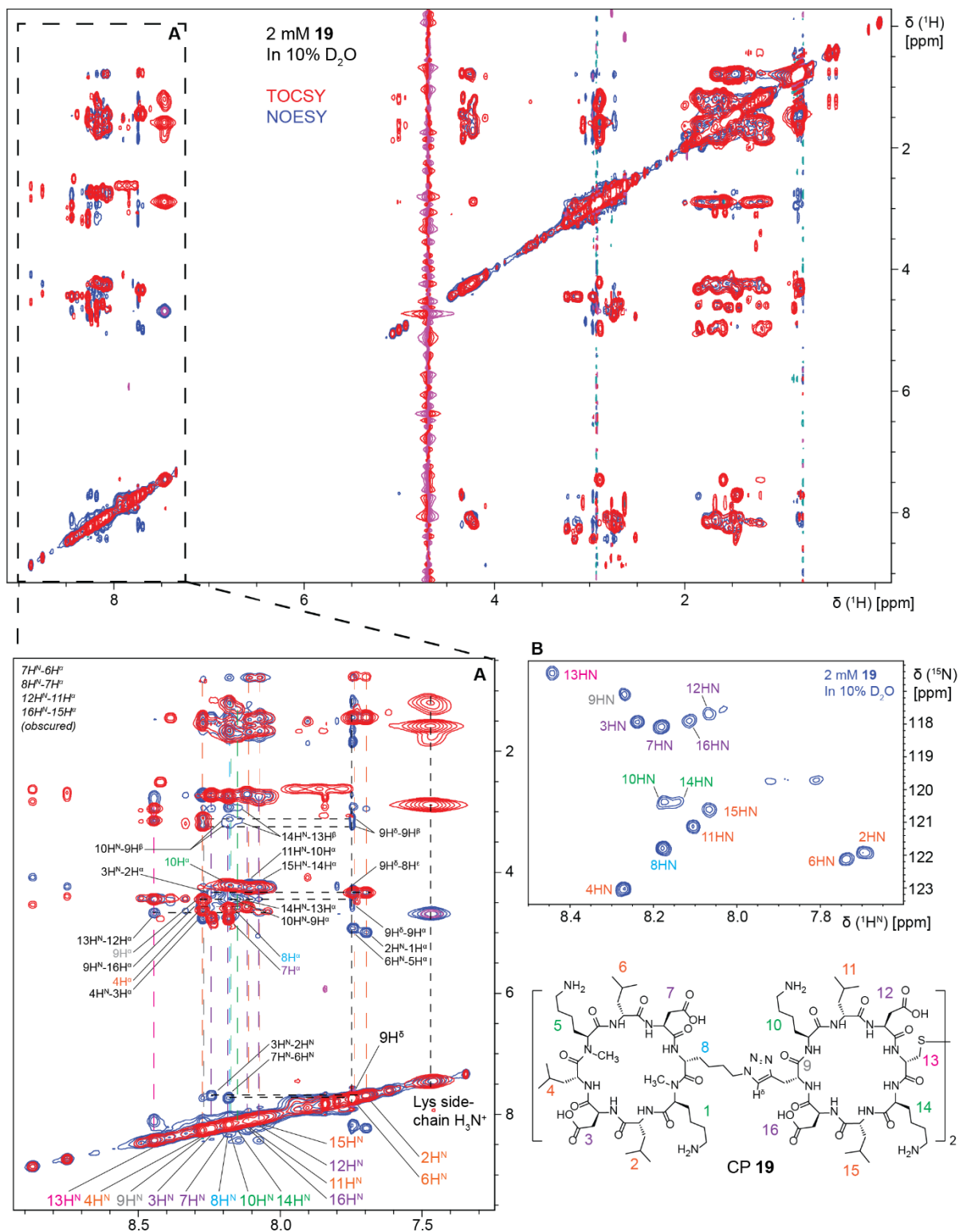


Figure S11. 2D [¹H, ¹H]-NOESY (blue) and TOCSY (red) overlaid spectra of CP tetramer **19**. A) Expansion of the downfield region containing the backbone H^N signals. Key NOESY interactions are labelled. B) ¹H-¹⁵N SOFAST HMQC spectrum of **19** with HN signals assigned. Only the signals associated with the major population have been assigned.

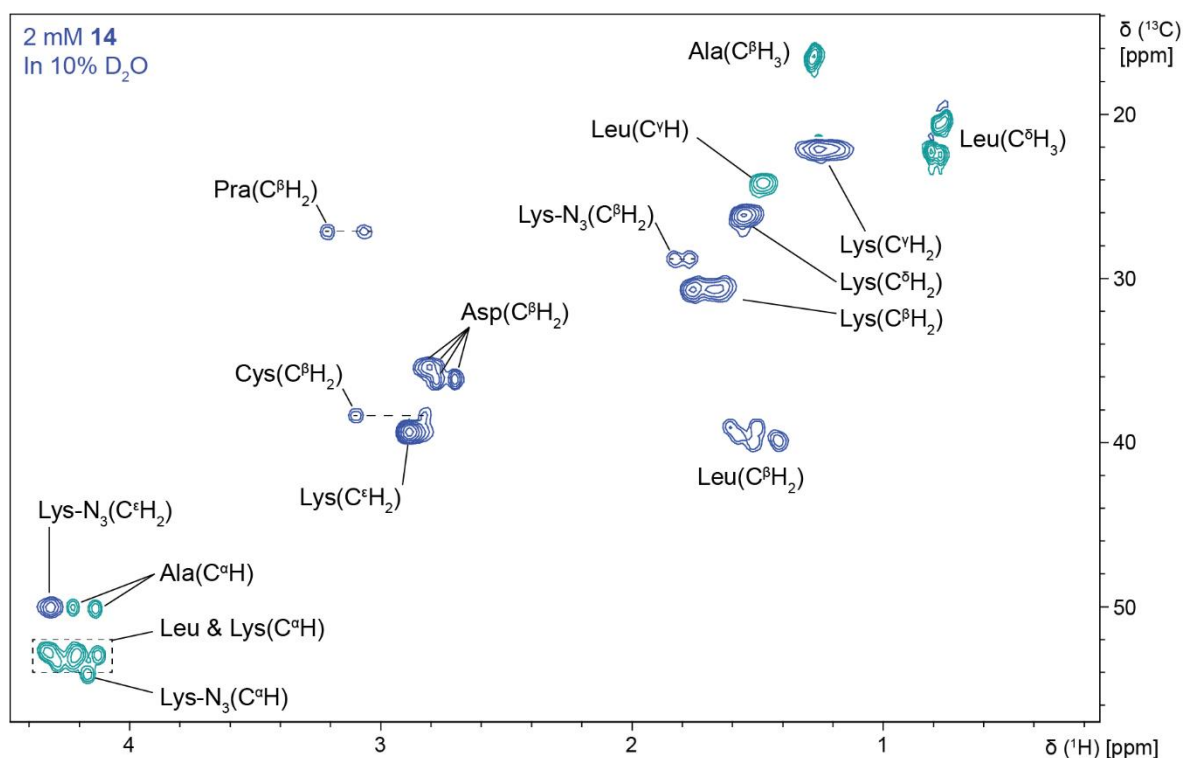
2D multiplicity edited [^{13}C , ^1H]-HSQC

Figure S12. 2D multiplicity edited [^{13}C , ^1H]-HSQC for compound **14**, aliphatic region. Asp, Cys and Pra C^αH signals are obscured by water suppression and are not shown. Triazole CH signal at ~ 7.75 ppm is not shown.

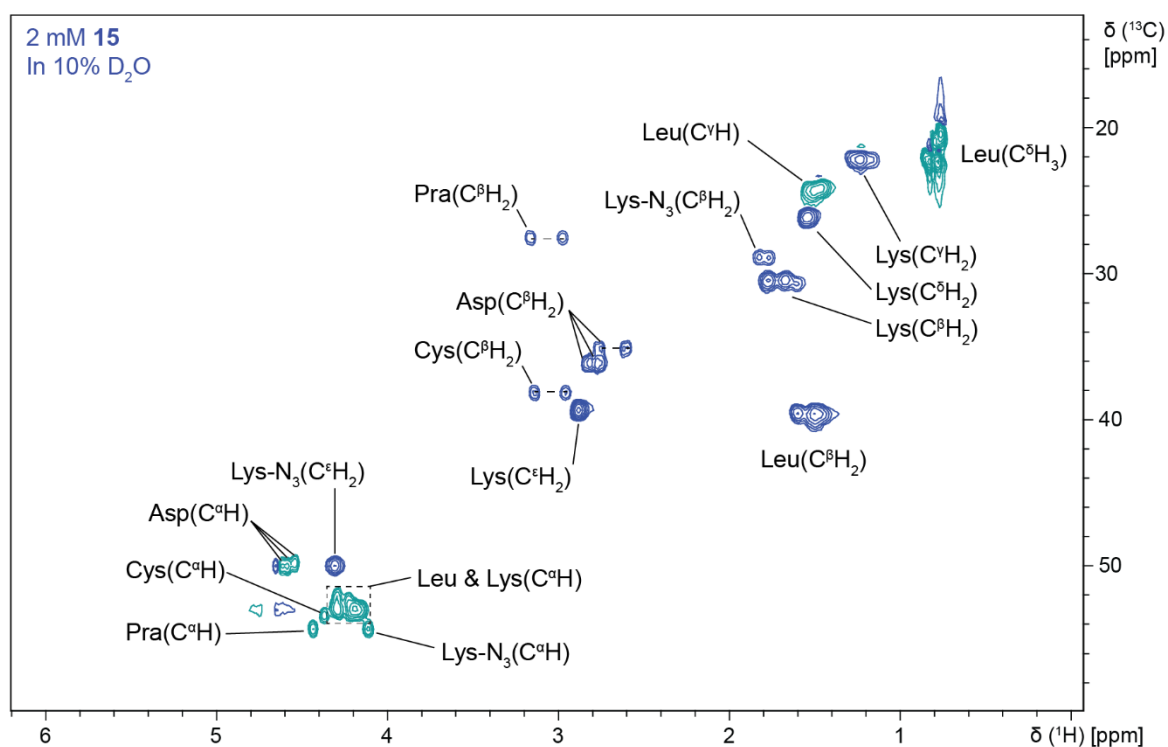


Figure S13. 2D multiplicity edited [^{13}C , ^1H]-HSQC for compound **15**, aliphatic region. Triazole CH signal at ~ 7.75 ppm is not shown.

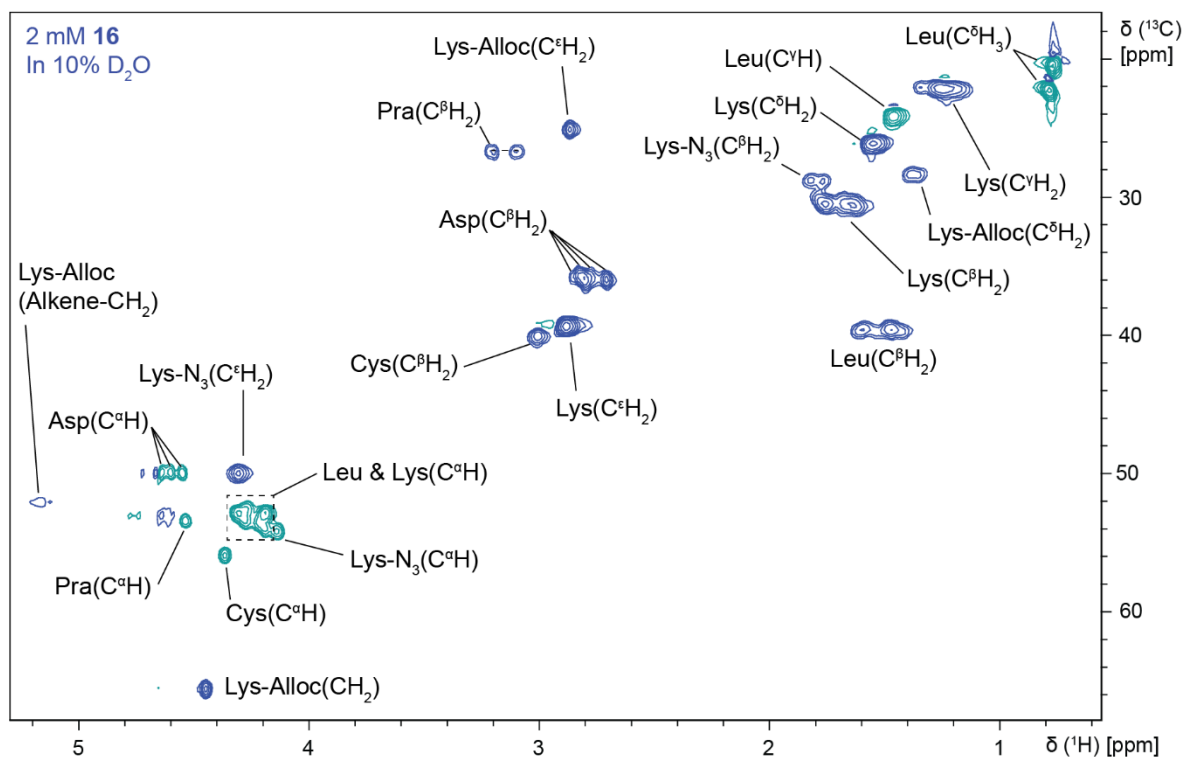


Figure S14. 2D multiplicity edited $[^{13}\text{C}, ^1\text{H}]$ -HSQC for compound **16**, aliphatic region. Alkene CH signal at ~ 5.8 ppm and triazole CH signal at ~ 7.75 ppm are not shown.

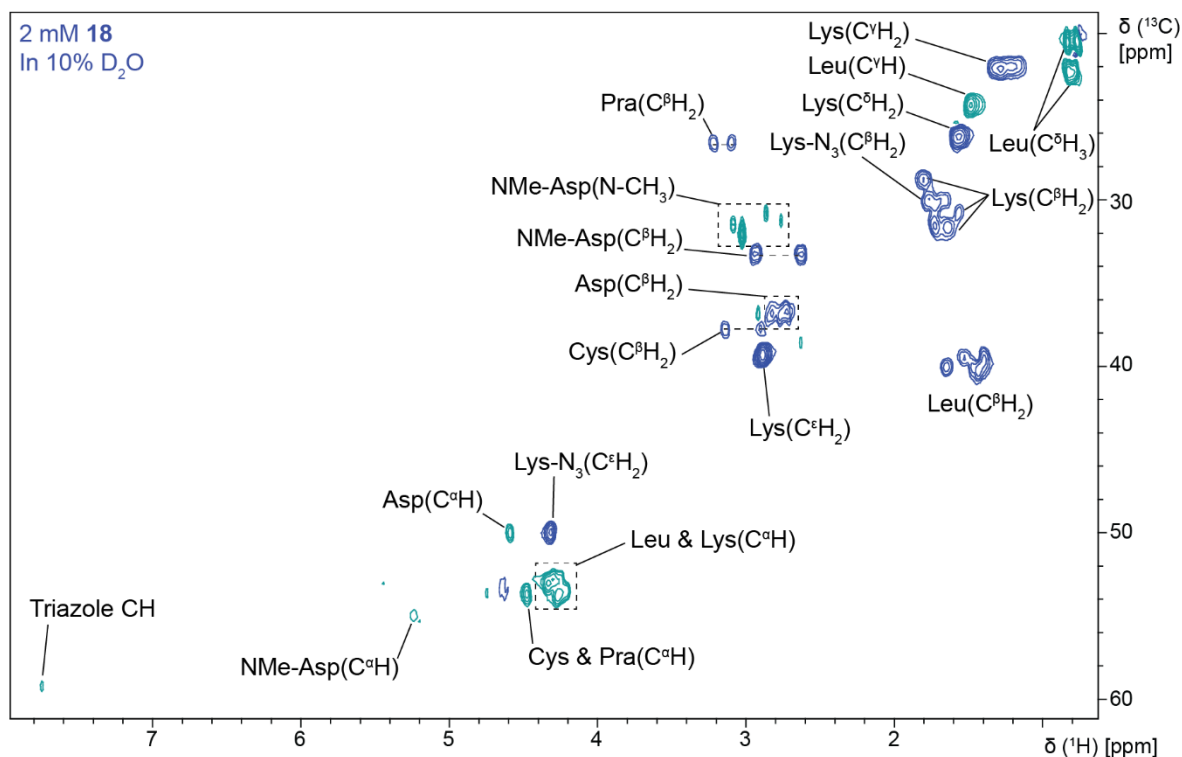


Figure S15. 2D multiplicity edited $[^{13}\text{C}, ^1\text{H}]$ -HSQC for compound **18**. Some Leu and Asp C^αH signals have been obscured due to water suppression.

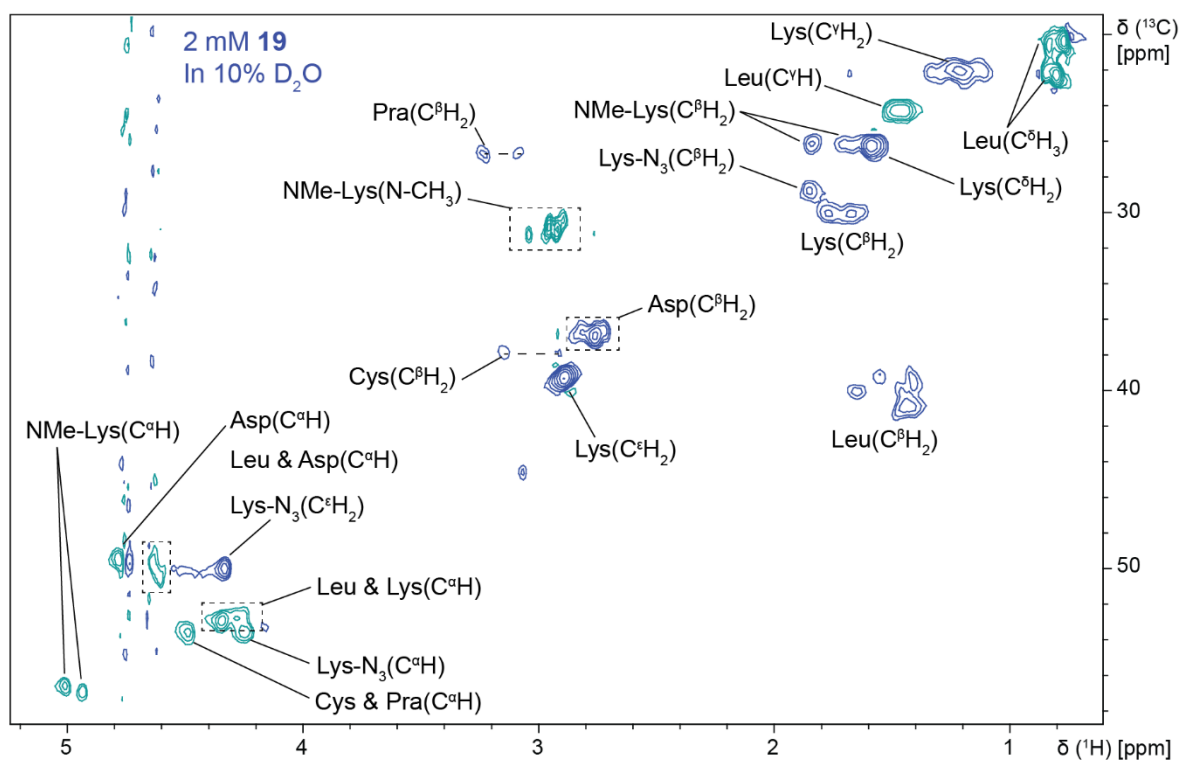


Figure S16. 2D multiplicity edited [^{13}C , ^1H]-HSQC for compound **19**. Some Leu and Asp C^αH signals have been obscured due to water suppression. Triazole CH signal at ~ 7.75 ppm is not shown.

^1H -D exchange studies

^1H -D exchange studies were performed immediately following dissolution of CP tetramers at 2 mM in 100% D_2O . The first spectrum was acquired within 8 min of dissolution and up to 13 spectra in total were acquired over 60 to 120 min, depending on the rate of H^{N} signal exchange. H^{N} integrals at $t = 0$ min were calculated from 2 mM samples in 10% D_2O with an adjustment of /0.9 to account for D_2O exchange.

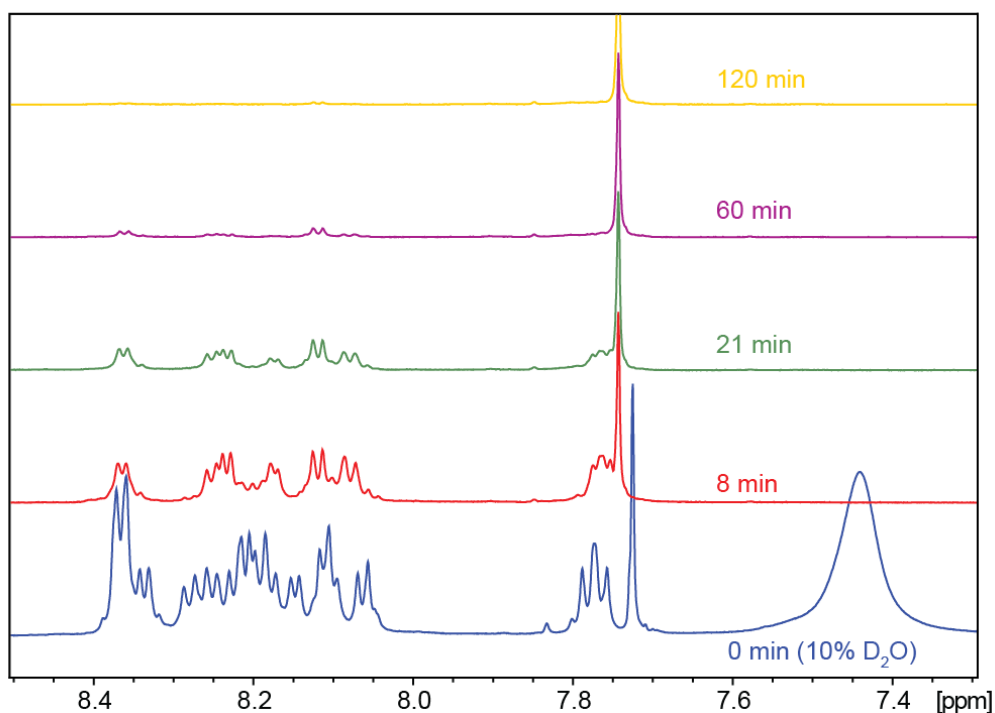


Figure S17. 1D ^1H spectra of the ^1H -D exchange study for **14** at 2 mM and 298 K. 14 spectra were acquired from 8-120 min in 100% D_2O . The spectrum at 0 min was acquired with 10% $\text{D}_2\text{O}/\text{H}_2\text{O}$ causing some solvent-dependent changes to chemical shifts. Lysine side-chain has completely exchanged with deuterium before acquisition of the first spectrum at 8 min.

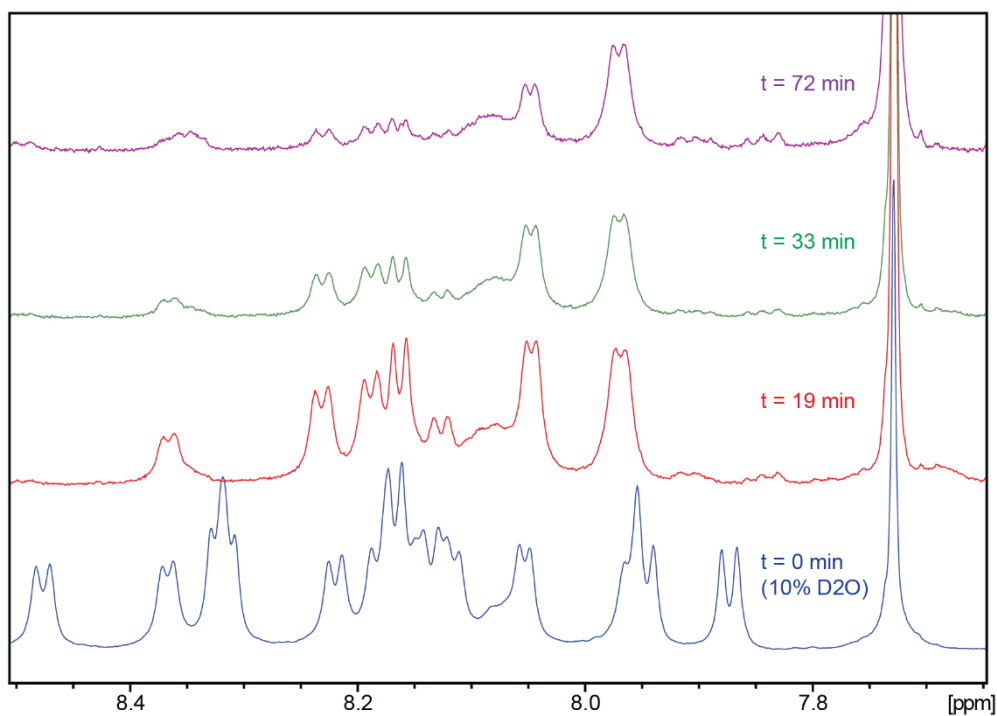


Figure S18. 1D ^1H spectra of the ^1H -D exchange study for **15** at 2 mM and 298 K. 14 spectra were acquired from 19-90 min in 100% D_2O . Spectrum at 0 min was acquired with 10% $\text{D}_2\text{O}/\text{H}_2\text{O}$ causing some solvent-dependent changes to chemical shifts.

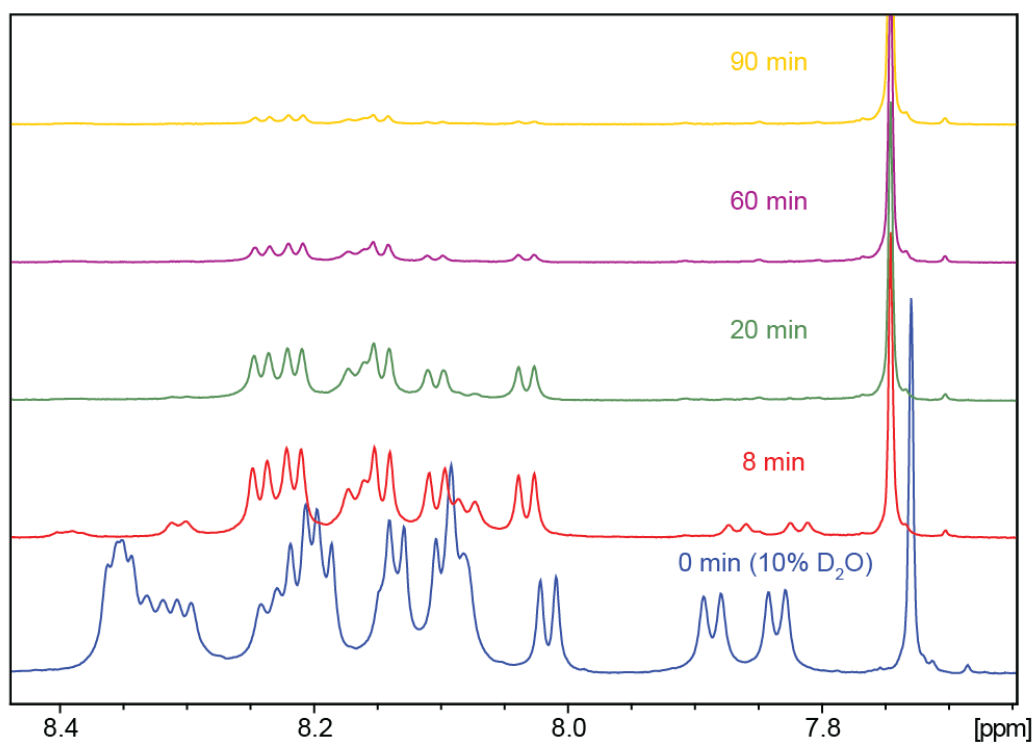


Figure S19. 1D ^1H spectra of the ^1H -D exchange study for **16** at 2 mM and 298 K. 14 spectra were acquired from 8-90 min in 100% D_2O . Spectrum at 0 min was acquired with 10% $\text{D}_2\text{O}/\text{H}_2\text{O}$ causing some solvent-dependent changes to chemical shifts.

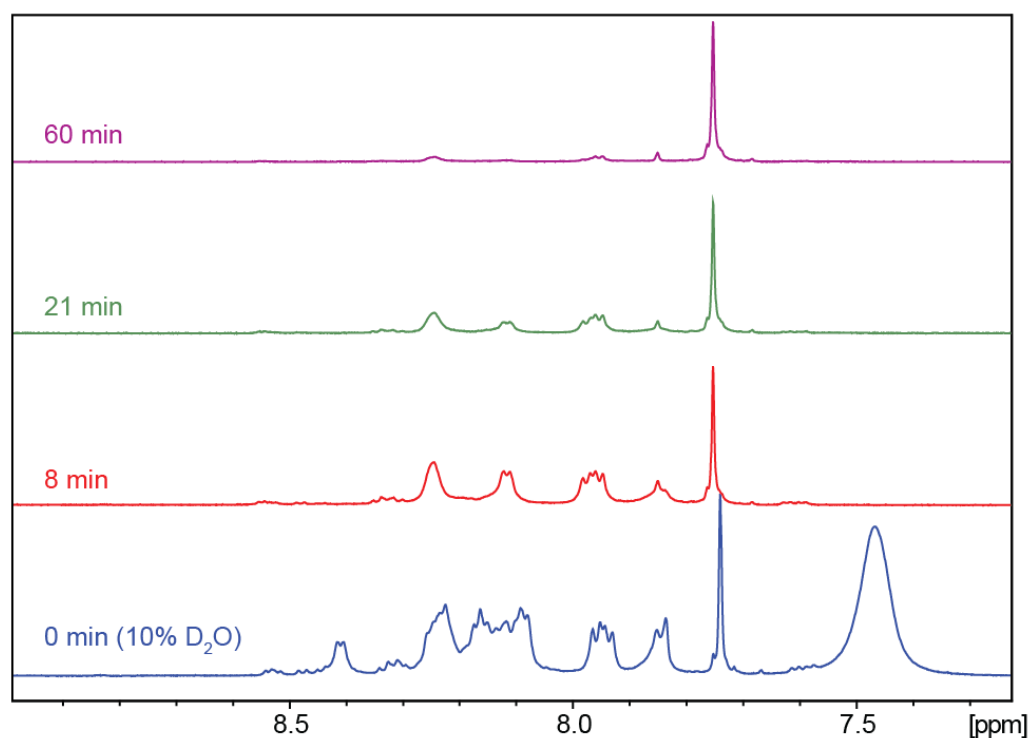


Figure S20. 1D ^1H spectra of the ^1H -D exchange study for **18** at 2 mM and 298 K. 13 spectra were acquired from 8-60 min in 100% D_2O . Spectrum at 0 min was acquired with 10% $\text{D}_2\text{O}/\text{H}_2\text{O}$ causing some solvent-dependent changes to chemical shifts.

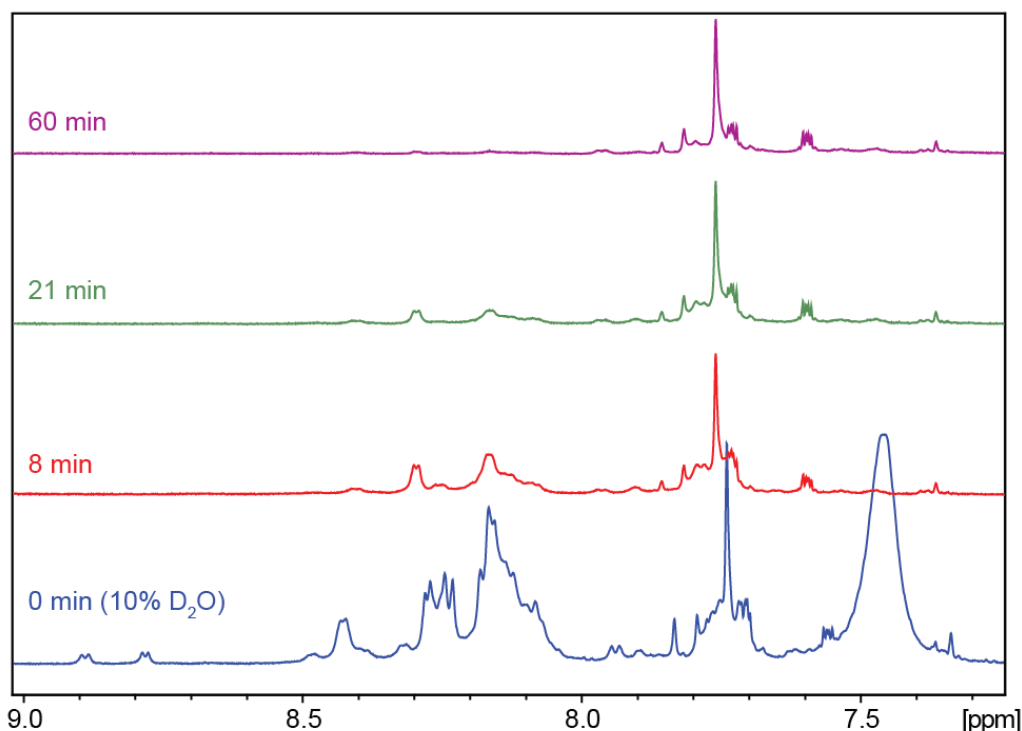


Figure S21. 1D ^1H spectra of the ^1H -D exchange study for **19** at 2 mM and 298 K. 13 spectra were acquired from 8-60 min in 100% D_2O . Spectrum at 0 min was acquired with 10% $\text{D}_2\text{O}/\text{H}_2\text{O}$ causing some solvent-dependent changes to chemical shifts.

DOSY Diffusion NMR

All samples were studied at 2 mM in 10% D_2O , 298 K and pH 3. Diffusion constants were determined according to integrals of the side-chain methyl protons. 2D DOSY experiments were performed using the standard Bruker pulse program *ledbpgppr2s* with a gradient ramp from 5% to 95% in 16 squared steps (TD1) calculated with AU program *dosy*. The gradient calibration value was 53.5 G/cm. DOSY data were analysed using the TopSpin T1/T2 routine with a standard equation as described previously by Wang *et al.*³ During the T1/T2 routine analysis, the integral of the aliphatic proton region was manually defined for the first FID slice. **Figure S22** provides a typical DOSY plot acquired and **Figure 4** contains all extracted translational diffusion constants (D_T).

Assuming spherical structures, diffusion constants (D_T) can be related to hydrodynamic radii (R_h) following the Stokes-Einstein relationship.⁴

$$D_T = \frac{k_B T}{6\pi\eta R_h}$$

T is temperature (K), k_B is Boltzmann's constant and η is the sample viscosity. The viscosity of water at 298 K (0.89 cP) was used as the solvent viscosity, as samples were in 90%

water/D₂O. R_h values for tetramers **12-19** are provided in **Figure 4** with approximate dimensions of a folded CP tetramer in **Figure 4b**.

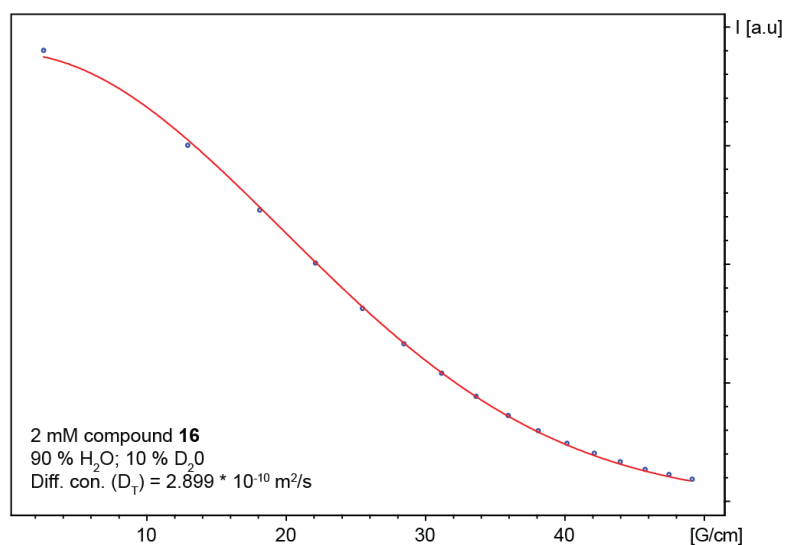


Figure S22. The DOSY determined diffusion constant for **16** was $2.899 \times 10^{-10} \text{ m}^2 \text{ s}^{-1}$.

Molecular dynamics

Model building and molecular dynamics studies were conducted in Maestro (Schrödinger version 10.3) using the integrated Desmond MD software (D. E. Shaw Research, version 4.3).⁵ Tetramers were built manually using the crystal structure of *cyclo*[(Asp-D-Leu-Lys-D-Leu)₂]⁶ as a scaffold for an antiparallel H-bonded backbone before addition of the side-chain tethers. Each tetramer was built in the two possible antiparallel H-bonding arrangements by rotation of each CP by 180° about the tethering bonds. Tetramers were minimised in water for 2500 iterations using the OPLS 2005 forcefield prior to preparation of the system for simulation. Systems were prepared as orthorhombic cells of $35 \times 35 \times 35 \text{ \AA}$ and were solvated by explicit water (SPC) containing 0.15M NaCl. Tetramer **16** was prepared in a cell of dimensions $45 \times 45 \times 45 \text{ \AA}$ to accommodate the long Lys(Alloc) side-chains. All simulations using the OPLS 2005 forcefield in the NPT ensemble at 300 K and 1.01325 bar with a 2 fs timestep. The Nose-Hoover chain method was employed for the thermostat method and Martyna-Tobias-Klein method for the barostat. Simulations used periodic boundary conditions and the particle-mesh Ewald method for long range electrostatics. Simulations were run for 100 ns. and evaluated for stability according to the number of intermolecular backbone-backbone H-bonds between each CP interface (between CP-subunits 1-2, 2-3 and 3-4, maximum of 8 H-bonds for each interface) in addition to the tetramer as a whole (maximum of 24 H-bonds).

Synthesis of Poly(2-ethyl-2-oxazoline)₅₀-SH

Distilled initiator (methyltosylate, 0.24 mmol, 36.22 μ L), distilled monomer (2-ethyloxazoline, 12 mmol, 1211 μ L) and dry ACN were added to a microwave vial (2-5 mL, preheated, under N₂). The total reaction mixture was 3 mL with a monomer:initiator ratio of 50. The vial was sealed and stirred at 140°C for 8.32 min under microwave conditions to achieve 95% conversion. Potassium ethylxanthate (0.288 mmol) in 2 mL dry ACN was added to the reaction mixture and stirred overnight at rt to cap the polymer. The mixture was diluted with 30 mL CHCl₃, washed with 2 \times 30 mL sat. NaHCO₃ and 2 \times 30 mL brine before concentration to approx. 3 mL by rotovap. The capped polymer was precipitated upon addition to ice-cold Et₂O (40 mL), isolated by centrifugation and repeated, before oven-drying (40°C) to afford PEtOx-ethylxanthate as a white solid (1.024 g, 82.9% yield).

494.4 mg of PEtOx-ethylxanthate in 7.5 mL of 33% diethylamine/EtOH was stirred for 3 h at 40°C. The mixture was poured over 7 mL H₂SO₄ in 70 mL ice-water, extracted with 3 \times 20 mL CHCl₃ and washed with 3 \times 30 mL sat. NaHCO₃ and 3 \times 30 mL brine. The CHCl₃ mixture was dried over MgSO₄ before separation and concentration by rotovap to yield a yellow oil of the disulfide-bridged (PEtOX-S-)₂ (GPC analysis presented in **Figure S23**, LHS). To the yellow oil was added 10 mL DCM, dithiothreitol (35.6 mg, 0.231 mmol) and triethylamine (37 μ L, 0.265 mmol). The mixture was stirred for 3 h under N₂ then washed with HCl (20 mL, N₂-degassed) and H₂O (20 mL, N₂-degassed) and dried over MgSO₄. The DCM mixture was separated and concentrated under a flow of N₂ gas and dried over the weekend in a vacuum oven to afford PEtOx-SH as a white solid (73.3 mg, 15% yield, GPC analysis presented in **Figure S23**, RHS).

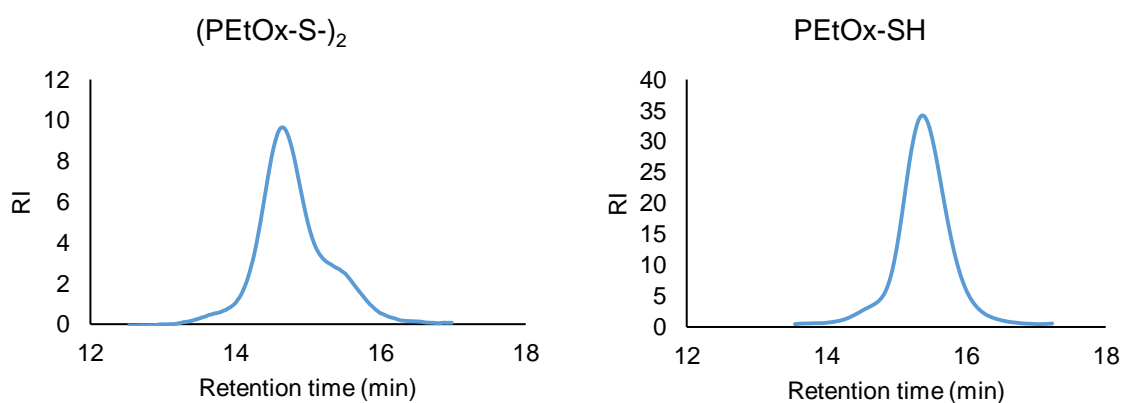


Figure S23. GPC analysis for (PEtOx-S-)₂ after xanthate deprotection, showing mixture of (PEtOx-S-)₂ and PEtOx-SH. After reduction, the major species is PEtOx-SH.

Thiol-ene polymer-peptide conjugation

10 mg of **16** (0.0024 mmol) and 51.1 mg of PEtOx-SH (0.0096 mmol, 2 eq. relative to alkenes of **16**) were added to 2 mL DMF in a glass vial (N_2 -degassed). 1.5 mg of DMPA (0.0049 mmol, 1 eq. relative to alkenes) in DMF (N_2 -degassed) was added to the vial which was stirred overnight under UV light (365 nm, 6 watts, shielded from external light). The mixture was concentrated under N_2 gas flow and added to 40 mL H_2O , followed by dialysis by centrifugation (30 kDa dialysis tube, 3-cycles for the mixture before H_2O dilution and an additional 2-cycles). The separated solid was redissolved in water and freeze-dried to afford the product **16**-(PEtOx)₂ as a white solid (5.6 mg, 15.7% yield, GPC analysis presented in **Figure S24**).

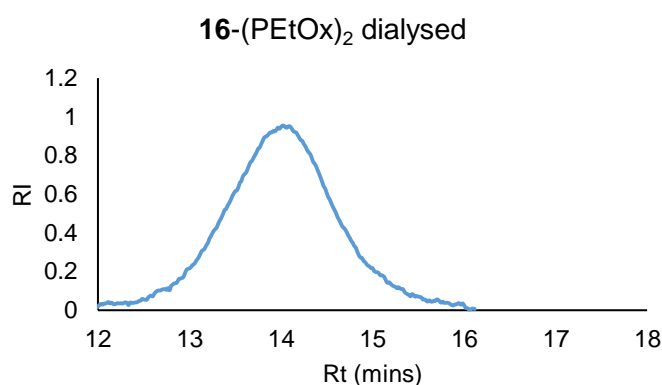


Figure S24. GPC analysis for **16**-(PEtOx)₂ following conjugation and purification by dialysis.

Static light scattering

Samples were prepared individually at each concentration and dissolved in deionized water which had been filtered (0.2 μm GHP filter) prior to use. Samples were left overnight with gentle agitation to allow complete dissolution. Each sample was allowed 10 min to settle upon moving to the SLS sample chamber prior to data acquisition. SLS data was acquired at 25°C and standardized against toluene immediately prior to use. SLS data for each sample/concentration was acquired using 10° intervals for 20-30° scattering angles and 20° intervals for 50-150° scattering angles, with 30 sec acquisition per angle. Each sample was analyzed in triplicate. Samples were then filtered using a 0.45 μm nylon filter and left to stand for 90 min to allow samples to settle. SLS data for filtered samples was then acquired as described for the unfiltered samples. Filtering of the samples significantly improved concordance of the triplicates by removing dust and particulate in addition to possible insoluble aggregates and provided a more accurate analysis of **16** and **16**-(PEtOx)₂ in solution. The average number of molecules within an aggregate was determined according to the molecular mass of the aggregate divided by the molecular weight of the tetramer (~4000 g mol⁻¹) or tetramer-polymer conjugate (~14600 g mol⁻¹).

References

1. Silk, M. R.; Mohanty, B.; Sampson, J. B.; Scanlon, M. J.; Thompson, P. E.; Chalmers, D. K. Controlled Construction of Cyclic D/L Peptide Nanorods. *Angewandte Chemie* **2019**, *58*, 596-601.
2. Presolski, S. I.; Hong, V.; Cho, S.-H.; Finn, M. G. Tailored Ligand Acceleration of the Cu-Catalyzed Azide-Alkyne Cycloaddition Reaction: Practical and Mechanistic Implications. *Journal of the American Chemical Society* **2010**, *132*, 14570-14576.
3. Wang, C. K.; Northfield, S. E.; Swedberg, J. E.; Harvey, P. J.; Mathiowetz, A. M.; Price, D. A.; Liras, S.; Craik, D. J. Translational diffusion of cyclic peptides measured using pulsed-field gradient NMR. *The journal of physical chemistry. B* **2014**, *118*, 11129-36.
4. Jones, J. A.; Wilkins, D. K.; Smith, L. J.; Dobson, C. M. Characterisation of protein unfolding by NMR diffusion measurements. *J. Biomol. NMR* **1997**, *10*, 199-203.
5. Bowers, K. J.; Chow, E.; Xu, H.; Dror, R. O.; Eastwood, M. P.; Gregersen, B. A.; Klepeis, J. L.; Kolossvary, I.; Moraes, M. A.; Sacerdoti, F. D.; Salmon, J. K.; Shan, Y.; Shaw, D. E. Scalable algorithms for molecular dynamics simulations on commodity clusters. *Proceedings of the ACM/IEEE Conference on Supercomputing (SC06), Tampa, Florida* **2006**.
6. Silk, M. R.; Newman, J.; Ratcliffe, J. C.; White, J. F.; Caradoc-Davies, T.; Price, J. R.; Perrier, S.; Thompson, P. E.; Chalmers, D. K. Parallel and antiparallel cyclic D/L peptide nanotubes. *Chem. Commun.* **2017**, *53*, 6613-6616.

Chapter 6

Conclusions

Our goal was to develop methods to direct the self-assembly process to generate complex nanomaterials of heterogeneous composition and, in doing so, improve the structural characterisation of CPN-based materials. The project was very successful to this end, as we obtained the first crystal structures of H-bonded CP nanotubes, developed methods to direct the orientation of CPs, reported the controlled construction of heterogeneous CPNs and demonstrated further functionalisation of our material.

At the time that this work commenced, the only reported crystal structures of CPs were from blocked dimers. This was primarily due to difficulties in generating ordered, crystalline material from assembled CPNs that was suitable for X-ray diffraction experiments. We designed a selection of CPs with ionisable amino acid side-chains in an effort to direct the self-assembly process through charge-charge interactions. Crystallisation screens of the CPs generated μm -long, needle-like crystals, which diffracted under X-ray beam. Solving these structures yielded the first crystal structures of continuously H-bonded CPNs. Fascinatingly, and despite relatively minor differences in sequence, the two structures involve antiparallel or parallel backbone H-bonding networks respectively. These crystal structures provide atomistic insight into the H-bonding networks critical to the assembly of CPNs. Although parallel H-bonding has widely been considered as less stable than antiparallel H-bonding, our structure suggests it requires consideration when studying CPNs whether its formation is solvent-induced or a result of inter-CPN interactions. The key to our successful crystallisation studies seemed to be due to the extended network of inter-tube ionic interactions formed between the Lys and Asp side-chains, encouraging the formation of ordered structures and confirming the importance of ionic interactions in directing the assembly of CPNs.

Our use of ionic interactions between CP side-chains proved to be effective in providing a degree of order to the assembly of CPNs both within and between nanotubes, although the formation of heterogeneous CPNs could not be confirmed. To address our lack of heterogeneity, we studied side-chain tethering as a means of combining different CPs into heterogeneous CPN structures. Tethering allows precise control over the position and orientation of CPs within assembled CPNs, significantly improving our control over CPN properties and composition. We developed a robust, efficient synthetic method for building tethered CP tetramers using chemistry which was orthogonal to the remaining side-chains of a deprotected CP. Analysis by cryo-EM revealed the formation of fibrous structures which confirmed that the tethering of side-chains did not interfere with CPN self-assembly. Further

study of the CP tetramers in solution identified well-ordered structures with concentration dependent assembly for some of the analogues.

The variations in stability we found for our tethered CP tetramers encouraged us to investigate the key interactions involved in CPN assembly and stability. Understanding and controlling these factors would enable us to engineer stable and potentially well-ordered CP-based materials. We applied an in-depth analysis to the features contributing to the stability of homogeneous CPNs using combined experimental and theoretical analyses of a series of CP monomers. After studying a range of properties, charge-charge and hydrophobic side-chain interactions were found to significantly contribute to the stability of CP-CP interactions. Intriguingly, CPN stability was completely dependent on the specific H-bonding interfaces between the different faces of a CP and not simply the intermolecular alignment of residues alone. Molecular dynamics simulations allowed us to identify specific H-bonded geometries with high stability which correlated well with experimental studies of CP assembly, aggregation and H-bond strength by NMR spectroscopy.

We applied our understanding of general CPN stability to improve the stability and order within our tethered CP tetramer designs. In addition, the modification of tetramer behaviour and function was explored through selective backbone *N*-methylation and the conjugation of polymers to CP side-chains. Our tethering methodology was applied to the synthesis of a series of CP tetramer analogues and improved further to achieve >95% coupling conversion within 1 hr for the first coupling step. Due to the modular design of CP tetramers, a range of combinations of CP subunits were explored which generated tetramers with distinct properties and behaviours. Stability of the different tetramers was highly dependent on the amino acid composition, with hydrophobicity playing an important role in the stabilisation of CP-CP interactions. However, some specific combinations of amino acids were found to generate stable tetramers. These tetramers adopted well-ordered conformations by NMR spectroscopy and were found to have particular H-bonding conformations in which they were completely stable by MD analysis. Further modulation of tetramer function and behaviour was demonstrated by the conjugation of a polymer to the CPN exterior. The conjugation was orthogonal to the tetramer side-chains and could be performed on the final, deprotected tetramer product, providing a means of post-synthesis diversification of tetramer properties. Backbone *N*-methylation was sensitive to position and induced conformational disorder within the CP tetramers, although it was effective in blocking H-bonding in all situations.

The research presented within this thesis represents substantial advancements in the structural characterisation for CPN materials and methods for control over CPN composition and self-assembly. Our tethered tetramer designs have demonstrated control over the short

and long-range order within CPNs, including the controlled construction of heterogeneous CPNs. Our synthetic method for tetramers allows for the combinatorial synthesis of a suite of tetramer analogues from CP subunits, followed by further combinatorial diversification by polymer conjugation. In combination, these methodologies could yield an immense library of tethered tetramer products with an immense array of functionality.

As with any project, there will always be unexplored avenues and logical progressions in the research. Among the many, our group is actively exploring alternate approaches to controlling CPN length and aggregation, the interactions between our charged CPs and membranes, and crystallography of tethered CP structures. Predicting the structure and behaviour of our systems is of great importance to the success of the project. Molecular dynamics simulations have granted some insight into the possible behaviour and stabilities of our CPN systems and even correlated well with experimental findings. However, the MD simulations are only a snapshot (100 ns timescale) and does not necessarily explain all features of these CP-based systems. Furthering the MD simulations to cover larger timescales and explore the mechanisms driving the self-assembly process would significantly enhance our understanding of these systems, although we are limited by computational power and resources. We believe an improved approach to backbone *N*-methylation is required for CPN capping, as the current use of *N*-methylation induced some conformational disorder in our tetramer designs. Extending our tethering chemistry to develop 'A-B-C-D' tetramers of complete heterogeneity would further enhance our control of CPN properties. Additional coupling chemistry could enable the creation of tethered octamers which would more closely match the length required of a structure to span a biological membrane. Mixing and matching linkers of different sizes, chemical composition and functionality may have a significant impact on the folded structures of our tetramers and could yield novel approaches to increasing or decreasing the structural stability. In advance of these developments, studies are underway into the behaviour of our current monomeric and tetrameric CP structures with membranes. Preliminary investigations show significant interactions with synthetic liposomes despite the charged nature of our CP designs. The successful crystallography studies of our CP monomers has yet to translate into a structure of a tethered CP tetramer, although crystals from a CP tetramer have indeed been grown and studied for diffraction at the Australian Synchrotron. These crystals did not diffract under X-ray beam but could be further analysed by electron microscopy to provide some detail into their chemical and structural composition. Further optimisation of these crystals to acquire a crystal structure with atomistic evidence of our tethered tetramers is actively underway.